



Publicly Accessible Penn Dissertations

1-1-2012

Identification and Characterization of Small Molecule Antagonists of the Human Papillomavirus Oncoproteins

Daniela Fera

University of Pennsylvania, daniela.fera3@gmail.com

Follow this and additional works at: <http://repository.upenn.edu/edissertations>



Part of the [Biochemistry Commons](#), and the [Chemistry Commons](#)

Recommended Citation

Fera, Daniela, "Identification and Characterization of Small Molecule Antagonists of the Human Papillomavirus Oncoproteins" (2012). *Publicly Accessible Penn Dissertations*. 508.
<http://repository.upenn.edu/edissertations/508>

This paper is posted at ScholarlyCommons. <http://repository.upenn.edu/edissertations/508>
For more information, please contact libraryrepository@pobox.upenn.edu.

Identification and Characterization of Small Molecule Antagonists of the Human Papillomavirus Oncoproteins

Abstract

Human papillomavirus (HPV) is the most common sexually transmitted pathogen, and is associated with almost all cervical cancers, about 20 percent of head and neck cancers and an array of other cancers. Current HPV vaccines offer preventative care, however, long-term benefits are unknown and the vaccines are not effective for therapy. High risk forms of HPV mediate cell transformation via two viral oncoproteins, E6 and E7, which lead to cell cycle disruption and cancer. E7 deregulates the cell cycle and abrogates other pathways mediated by the retinoblastoma protein, pRb. pRb is essential for regulating many cellular activities through its binding and inhibition of E2F transcription activators, and pRb inactivation leads to many cancers. pRb activity can be perturbed by viral oncoproteins, including HPV, that contain an LxCxE motif. E6 mediates cell transformation, in part, by forming a complex with the cellular E3 ligase E6-Association Protein (E6AP) to target p53 for degradation.

To tackle these problems, we performed two high throughput solution screens of ~88,000 compounds to search for (1) compounds that inhibit the ability of HPV-E7 to disrupt pRb/E2F complexes and (2) small molecule inhibitors of the E6/E6AP interaction. The HPV-E7 screen led to the identification of thiadiazolidinedione compounds that bind to pRb with mid-high nanomolar affinity, are competitive with the binding of viral oncoproteins containing an LxCxE motif and are selectively cytotoxic in HPV positive cells alone and in mice. The HPV-E6 screen resulted in 30 inhibitors with in vitro IC50 values in the low-micromolar to mid-nanomolar range. Six of these compounds were shown to associate with HPV-E6, block p53 degradation and promote apoptosis in high risk HPV positive cells. These E6 and E7 inhibitors provide promising scaffolds for the development of therapies to treat HPV-mediated pathologies.

An in silico screen was also done to identify small molecules that bind directly to E7 and prevent its interaction with E2F. This resulted in two compounds that prevented E7-mediated displacement of E2F from pRb, however, the IC50 values were very high, and not pursued further. The interaction between E7 and another cellular target, p300, was characterized by various biochemical and biophysical techniques. The interaction seemed very weak, different from the adenovirus E1A interaction with p300. This suggested that the E1A/p300 interaction would be easier to characterize.

Degree Type

Dissertation

Degree Name

Doctor of Philosophy (PhD)

Graduate Group

Chemistry

First Advisor

Ronen Marmorstein

Keywords

E6, E7, Human Papillomavirus, Inhibitors, Retinoblastoma

Subject Categories

Biochemistry | Chemistry

IDENTIFICATION AND CHARACTERIZATION OF SMALL MOLECULE ANTAGONISTS OF
THE HUMAN PAPILLOMAVIRUS ONCOPROTEINS

Daniela Fera

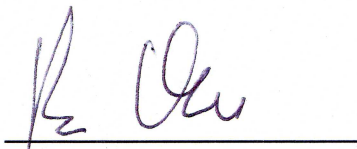
A DISSERTATION

in

Chemistry

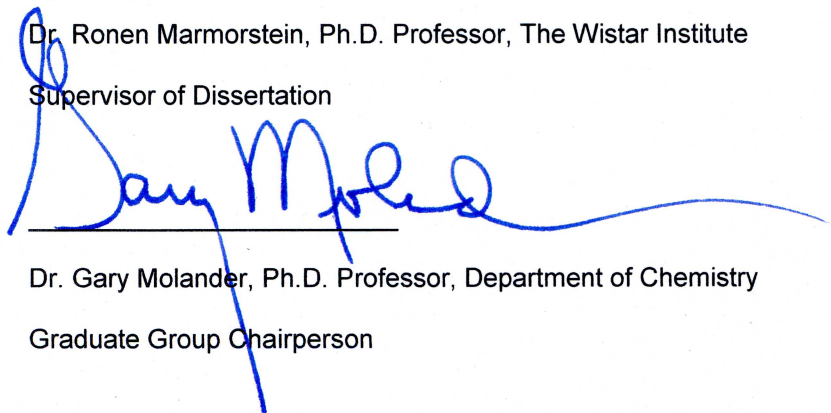
Presented to the Faculties of the University of Pennsylvania in Partial
Fulfillment of the Requirements for the Degree of Doctor of Philosophy

2012



Dr. Ronen Marmorstein, Ph.D. Professor, The Wistar Institute

Supervisor of Dissertation



Dr. Gary Molander, Ph.D. Professor, Department of Chemistry

Graduate Group Chairperson

Dissertation Committee

Dr. David W. Christianson, Ph.D. Professor, Department of Chemistry, Committee Chair

Dr. Scott L. Diamond, Ph.D. Professor, Department of Chemical and Biomolecular Engineering

Dr. Jeffrey G. Saven, Ph.D. Associate Professor, Department of Chemistry

I dedicate this thesis to
my parents Fircu and Viorel,
my parents-in-law Patricia and Randy and their parents Jim and Joan,
my brothers Peter and Valentin,
and my husband Andrew.

ACKNOWLEDGMENTS

Firstly, I would like to express my deepest and utmost gratitude to my thesis advisor and mentor, Dr. Ronen Marmorstein. I could not have accomplished all this work without his patient guidance, support, and enthusiasm. I was very fortunate to work with and learn from him; having him as a mentor has made a significant impact on my scientific and personal development. I will, in many ways, take what I have learned and apply it to my future scientific endeavors.

I would also like to thank members of my thesis committee: Dr. David W. Christianson, Dr. Scott L. Diamond and Dr. Jeffrey G. Saven. They provided very helpful guidance and discussions during my committee meetings.

I benefited greatly from a number of close collaborations throughout the years. I owe many thanks to Dr. David C. Schultz, the director of the Wistar Institute's Molecular Screening Facility who provided me with guidance and discussions throughout the years. I would also like to express my gratitude to Dr. Melvin Reichman and Dr. Preston Scott Donover from the Lankenau Chemical Genomics Center for providing small molecule libraries for screening, as well as for their assistance with several small molecules that I was studying. I would also like to thank Dr. Santosh Hodawadekar, Dr. Donna M. Hury, and Jason Melvin, for various aspects of the small molecule work. I am also grateful for help and discussions from Dr. Chunling Yi and Scott Troutman from the Kissil Laboratory at the Wistar Institute, as well as the discussions with Dr. Joseph L. Kissil. I am also thankful for the help of Jeffrey S. Faust and David E. Ambrose from the Wistar Flow Cytometry Facility. I am very grateful for the contribution that Dr. Kimberly A. Malecka made towards the E6 project, as well as all of the discussions we had regarding high throughput screening, as well as working with the E6 protein.

I would like to thank all the members of the Marmorstein laboratory, past and present, for their help and support over the years. I am incredibly grateful to Dr. Xin Liu, who trained and guided me when I first joined the laboratory. He taught me how to perform various experiments, which was key to my development since it was my first time doing any type of benchwork. I am

also very thankful for the help I received from Dr. Cheng Luo when performing virtual screens. I thank Dr. Adam Olia for his helpful discussions on working with the difficult E6 protein. I am also grateful to all of the other members of our laboratory, for their support and entertainment throughout the years. In particular, I thank Dr. Ruchi Anand, Dr. Jasna Maksimoska, Dr. Michael Brent, Dr. Kimberly Malecka, and Katie Meeth, not only for their scientific contribution, but also for their friendship.

I am thankful to the Department of Chemistry at the University of Pennsylvania and the Wistar Institute for providing a friendly and collaborative work environment. I am also thankful for the funding I received through the Structural Biology and the NIH Chemistry and Biology Interface Training Grants.

Lastly, I would like to express my appreciation towards my friends and family. I am thankful for the friendships that I made at Penn, and for their making my time here more fun. I will miss them dearly and wish them all the best on their future endeavors. I thank my family members for their endless support, and also for being so interested in the science that I do and the progress that I have been making. I thank my parents, Firuca and Viorel Fera, for their unconditional love and for raising me to be so hardworking. I also thank my brothers, Peter and Val, who always believed in me and encouraged me. I am grateful for my parents-in-law, Patricia and Randy Moore, and their parents, Jim and Joan Foran, for providing such wonderful support and for their interest in my projects. I am especially indebted to my husband, Andy, who was always there for me, to listen and help whenever I needed it. Everyone's kindness and support has helped me more than they can imagine.

ABSTRACT

IDENTIFICATION AND CHARACTERIZATION OF SMALL MOLECULE ANTAGONISTS OF THE HUMAN PAPILLOMAVIRUS ONCOPROTEINS

Daniela Fera

Ronen Marmorstein

Human papillomavirus (HPV) is the most common sexually transmitted pathogen, and is associated with almost all cervical cancers, about 20 percent of head and neck cancers and an array of other cancers. Current HPV vaccines offer preventative care, however, long-term benefits are unknown and the vaccines are not effective for therapy. High risk forms of HPV mediate cell transformation via two viral oncoproteins, E6 and E7, which lead to cell cycle disruption and cancer. E7 deregulates the cell cycle and abrogates other pathways mediated by the retinoblastoma protein, pRb. pRb is essential for regulating many cellular activities through its binding and inhibition of E2F transcription activators, and pRb inactivation leads to many cancers. pRb activity can be perturbed by viral oncoproteins, including HPV, that contain an LxCxE motif. E6 mediates cell transformation, in part, by forming a complex with the cellular E3 ligase E6-Association Protein (E6AP) to target p53 for degradation.

To tackle these problems, we performed two high throughput solution screens of ~88,000 compounds to search for (1) compounds that inhibit the ability of HPV-E7 to disrupt pRb/E2F complexes and (2) small molecule inhibitors of the E6/E6AP interaction. The HPV-E7 screen led to the identification of thiadiazolidinedione compounds that bind to pRb with mid-high nanomolar affinity, are competitive with the binding of viral oncoproteins containing an LxCxE motif and are selectively cytotoxic in HPV positive cells alone and in mice. The HPV-E6 screen resulted in 30

inhibitors with in vitro IC_{50} values in the low-micromolar to mid-nanomolar range. Six of these compounds were shown to associate with HPV-E6, block p53 degradation and promote apoptosis in high risk HPV positive cells. These E6 and E7 inhibitors provide promising scaffolds for the development of therapies to treat HPV-mediated pathologies.

An *in silico* screen was also done to identify small molecules that bind directly to E7 and prevent its interaction with E2F. This resulted in two compounds that prevented E7-mediated displacement of E2F from pRb, however, the IC_{50} values were very high, and not pursued further. The interaction between E7 and another cellular target, p300, was characterized by various biochemical and biophysical techniques. The interaction seemed very weak, different from the adenovirus E1A interaction with p300. This suggested that the E1A/p300 interaction would be easier to characterize.

TABLE OF CONTENTS

DEDICATION	ii
ACKNOWLEDGEMENTS	iii
ABSTRACT	v
TABLE OF CONTENTS	vii
LIST OF TABLES	xii
LIST OF FIGURES	xiii
CHAPTER 1: Introduction	1
1.1 Overview of the Human Papillomaviruses.....	2
1.1.1 <i>History of HPV and its Discovery in Causing Cancer</i>	2
1.1.2 <i>The HPV Genome and its Encoded Proteins</i>	4
1.1.3 <i>HPV Infection</i>	7
1.1.4 <i>The Clinical Manifestations of HPV</i>	10
1.2 Targeting HPV Infection.....	12
1.2.1 <i>HPV Vaccines</i>	12
1.2.2 <i>HPV Treatments</i>	13
1.2.3 <i>HPV Inhibitors</i>	13
1.3 Normal Cells and Their Regulation.....	16
1.3.1 <i>Cell Cycle</i>	16
1.3.2 <i>The Functions of the Retinoblastoma Protein, pRb, in Normal Cells</i>	18
1.3.3 <i>The Functions of p53 in Normal Cells</i>	23
1.3.4 <i>Apoptosis</i>	27
1.4 Cellular Transformation and Cancer.....	30
1.4.1 <i>The Links Between pRb and Cancer</i>	30

1.4.2	<i>The Links Between p53 and Cancer.</i>	31
1.4.3	<i>Cellular Transformation Induced by Human Papillomaviruses.</i>	31
1.4.4	<i>Inactivation of pRb and p53 by Viral Oncoproteins.</i>	34
1.5	Overview of Remaining Chapters.	37

CHAPTER 2: Identification and Characterization of Small Molecule Antagonists

	of pRb Inactivation by Viral Oncoproteins.	38
2.1	Introduction.	39
2.2	High-Throughput Screening Results.	46
2.2.1	<i>Identification of HPV-E7 Inhibitors using a High-Throughput Solution Screen.</i>	46
2.2.2	<i>A Family of Thiadiazolidinedione Compounds are Selective for HPV 16-Transformed Cells.</i>	58
2.2.3	<i>The HPV-E7 Inhibitors Function to Disrupt the HPV-E7 Interaction with pRb.</i>	66
2.2.4	<i>The HPV-E7 Inhibitors Function by Binding to pRb Through the LxCxE Binding Motif of Viral Oncoproteins.</i>	69
2.2.5	<i>HPV-E7 Inhibitors Selectively Cause Apoptosis in HPV-Transformed Cells.</i>	77
2.2.6	<i>A Representative Compound can Reduce Tumor Size In Vivo.</i>	82
2.3	High-Throughput Screening Discussion.	84
2.4	Crystallization Results.	87
2.4.1	<i>Crystallization of Unliganded pRb_{AB}.</i>	87
2.4.2	<i>Identification of New Conditions for pRb_{AB} Crystallization.</i>	89
2.5	Crystallization Discussion.	94
2.6	Future Work.	95
2.7	Materials and Methods.	96
2.7.1	<i>Expression and Purification of Proteins.</i>	96
2.7.2	<i>Pull-Down Assay.</i>	98
2.7.3	<i>Compound Libraries.</i>	98
2.7.4	<i>High Throughput Solution Screening and Data Processing.</i>	99

2.7.5	<i>ELISA Assays.</i>	100
2.7.6	<i>Pull-Down Assays with Inhibitors.</i>	101
2.7.7	<i>LC-MS Analysis of Thiadiazolidinedione Compounds.</i>	102
2.7.8	<i>Conformation of Structure by NMR.</i>	102
2.7.9	<i>Isothermal Titration Calorimetry.</i>	102
2.7.10	<i>Cell Culture.</i>	103
2.7.11	<i>MTS Cell Proliferation Assay.</i>	103
2.7.12	<i>Flow Cytometry.</i>	103
2.7.13	<i>Mouse Studies.</i>	104

CHAPTER 3: Identification and Characterization of Small Molecule Human

	Papillomavirus E6 Inhibitors.	105
3.1	Introduction.	106
3.2	High-Throughput Screening Results.	114
3.2.1	<i>Development of a High Throughput Screen and Inhibitor Identification.</i>	114
3.2.2	<i>Identification of Compounds that Prevent E6-E6AP Interaction in vitro.</i>	124
3.2.3	<i>Effects of Compounds on E6 Stability.</i>	129
3.2.4	<i>Identification of Compounds that Prevent HPV16 E6-Mediated p53 Degradation In Vitro.</i>	131
3.2.5	<i>Identification of Compounds that Prevent HPV E6-Mediated p53 Degradation in Cells.</i>	133
3.2.6	<i>E6 Inhibitors Protect Against p53 Degradation by HPV16 E6 and HPV18 E6.</i>	138
3.2.7	<i>The E6-Inhibitor-Mediated Increase in p53 Levels is Correlated with Increased Apoptotic Activity in Cells.</i>	142
3.3	High-Throughput Screening Discussion.	146
3.4	Future Work.	148
3.5	Materials and Methods.	149
3.5.1	<i>Expression and Purification of Recombinant Proteins.</i>	149

3.5.2	<i>ELISA Assay</i>	150
3.5.3	<i>High Throughput screening and Data Processing</i>	150
3.5.4	<i>Thermal Stability Assay</i>	151
3.5.5	<i>In Vitro Pull-Down Assays</i>	152
3.5.6	<i>In vitro p53 Degradation Assay</i>	153
3.5.7	<i>Cell Maintenance</i>	154
3.5.8	<i>MTS Assay</i>	154
3.5.9	<i>p53 Level Assay and Western Blots</i>	154
3.5.10	<i>APO-One Assay</i>	154
3.5.11	<i>Propidium Iodide Staining / Flow Cytometry</i>	155
CHAPTER 4: A Future Outlook on Inhibiting HPV infection		156
4.1	Overview	157
4.2	Effects of Knocking Down E6 and/or E7	158
4.3	pRb, p53, and Other Cellular Proteins as Drug Targets	160
4.4	Development of Vaccines	163
4.5	Conclusions	164
APPENDIX A: Structure-Based Identification of Human Papillomavirus E7 Inhibitors		
	Using an <i>In Silico</i> Approach	165
A.1	Introduction	166
A.2	Results	170
	<i>A.2.1 Identification of Initial Hits by In Silico Screening</i>	170
	<i>A.2.2 E2F Displacement Solution Assay</i>	180
	<i>A.2.3 Inhibitory Activity of Analogs</i>	183
A.3	Discussion	186
A.4	Future Work	188
A.5	Materials and Methods	190

<i>A.5.1 Preparation of Small Molecule Database.</i>	190
<i>A.5.2 High Throughput Virtual Screening.</i>	190
<i>A.5.3 Additional Scoring Functions for Analyzing Hits.</i>	191
<i>2.5.4 Compounds.</i>	191

**APPENDIX B: The Protein Complex Formed Between Human Papillomavirus E7 and
the Transcriptional Co-activator p300.**

the Transcriptional Co-activator p300.	192
B.1 Introduction.	193
B.2 Results.	197
<i>B.2.1 E1A Binds More Strongly to the CH1 Domain of p300 than HPV 16 E7, which Binds More Strongly than HPV 1A E7.</i>	197
<i>B.2.2 Pull Downs Indicated that the CR1-2 Domains of E7 are Necessary for the Interaction with p300.</i>	200
<i>B.2.3 Gel Filtration Showed that Some E7/p300 Complexes can Co-elute.</i>	202
<i>B.2.4 ITC and AUC Suggest that E7 and p300_{CH1} Bind 1:1.</i>	204
<i>B.2.5 Crystallization Efforts of E7/p300 Complexes</i>	209
B.3 Discussion.	211
B.4 Future Work.	213
B.5 Materials and Methods.	214
<i>B.5.1 Expression and Purification of Proteins.</i>	214
<i>B.5.2 Pull Downs.</i>	216
<i>B.5.3 Isothermal Titration Calorimetry.</i>	216
<i>B.5.4 Equilibrium Sedimentation.</i>	216

BIBLIOGRAPHY.	217
----------------------	-----

LIST OF TABLES

Table 1.1. Proteins that interact with pRb, p107, and p130.	21
Table 1.2. Viral proteins that target pRb and p53.	35
Table 2.1. Chemical libraries employed and hits obtained for HPV-E7 inhibitor solution screen.	47
Table 2.2. Parameters for small-molecule screening data.	54
Table 2.3. Compound structures, IC ₅₀ values, and dissociation constants.	60
Table 2.4. Structures and IC ₅₀ values of HPV-E7 inhibitors not pursued further in this study. . .	62
Table 2.5. Purity of the Seven Thiadiazolidinedione Inhibitors.	64
Table 2.6. Inactive Analogs.	65
Table 3.1. Screening Summary.	118
Table 3.2. Secondary assay results summary for inhibitor compounds.	119
Table 3.3. Secondary assay results summary for a representative six inhibitor compounds. . .	140
Table 3.4. Cell cycle analysis results for each cell type.	144
Table 4.1: Small molecule modulators of p53 and their status in drug trials.	162
Table A.1. 28 compounds selected from scaffolds.	172
Table A.2. Compound analogs purchased for additional testing using the ELISA-based assay.	184
Table B.1. Summary of results from ITC and AUC studies on E7/p300 complexes.	208

LIST OF FIGURES

Figure 1.1. Genome of the human papillomavirus type 16.	6
Figure 1.2. Infection of epithelia by HPVs.	9
Figure 1.3. The mammalian cell cycle.	17
Figure 1.4. Regulation of E2F activity by pRb.	20
Figure 1.5. Transcriptional pathways of E2F/pocket protein complexes	22
Figure 1.6. Negative feedback loop between p53 and MDM-2.	25
Figure 1.7. p53 pathways.	26
Figure 1.8. p53 mediated apoptosis.	28
Figure 1.9. Cellular pathways modulated by the HPV E6 and E7 oncoproteins.	33
Figure 1.10. Effect of the HPV E6 and E7 oncoproteins on its two main cellular targets.	36
Figure 2.1. Domain architectures of pRb, E2F, and E7.	40
Figure 2.2. Structures of complexes formed between pRb, E2F and E7.	41
Figure 2.3. Alignment of viral proteins.	44
Figure 2.4. Ribbon and stick figure of the pRb-E7 complex.	45
Figure 2.5. Wild-type and mutant recombinant proteins used in biochemical experiments.	48
Figure 2.6. Pull downs of recombinant proteins used in biochemical experiments.	49
Figure 2.7. Method of high-throughput screening for HPV E7 inhibitors.	50
Figure 2.8. Z' Factor graph.	52
Figure 2.9. Method of high-throughput screening for HPV E7 inhibitors.	53
Figure 2.10. IC ₅₀ curves for disruption of pRb/E2F complexes by E7 in the presence of a family of thiazolidinedione compounds.	61
Figure 2.11. IC ₅₀ curves for inhibitor disruption of HPV-E7/pRb complexes.	67
Figure 2.12. Effect of inhibitors on HPV-E7/pRb pull-downs.	68
Figure 2.13. Ability of inhibitors to prevent LxCxE containing viral oncoproteins from disrupting E2F/pRb complexes.	71

Figure 2.14. Ability of inhibitors to disrupt complexes between pRb and LxCxE containing viral oncoproteins.	72
Figure 2.15. Direct binding of inhibitors to pRb as measured by isothermal titration calorimetry.	73
Figure 2.16. Analysis of reversible inhibitor binding to pRb as measured by isothermal titration calorimetry.	74
Figure 2.17. Analysis of inhibitor binding to E7 as measured by isothermal titration calorimetry.	75
Figure 2.18. Competition assay.	76
Figure 2.19. Cellular toxicity of thiazolidinedione compounds.	78
Figure 2.20. Effects on the cell cycle and apoptosis by the thiazolidinediones 478166 and 478168, an inactive analog, and staurosporine.	81
Figure 2.21. The anti tumor effect of thiazolidinedione compound 478166 <i>in vivo</i>	83
Figure 2.22. Purification of pRB _{AB}	88
Figure 2.23. Crystallization of pRB _{AB}	91
Figure 2.24. pRB _{AB} crystals used as seeds.	92
Figure 2.25. Best pRB _{AB} crystals to date.	93
Figure 3.1. Schematic representation of full length HPV16 E6 protein and NMR structures of the individual domains.	108
Figure 3.2. NMR structure of E6N.	109
Figure 3.3. Model for p53 ubiquitination by E6/E6AP complexes.	110
Figure 3.4. Schematic representation of full length p53 and full length E6AP6.	112
Figure 3.5: Scheme for the high throughput screening assay.	115
Figure 3.6: Pull down assay between E6M and MBP-E6AP.	116
Figure 3.7. IC ₅₀ curves for disruption of E6-E6AP complexes by compounds.	125
Figure 3.8: Pull down assay between MBP-E6AP and E6-GST in the presence of the six compounds studied.	126

Figure 3.9: Pull down assay between GST-pRb and E7 in the presence of the six compounds studied.	127
Figure 3.10: E6/E6AP interaction in the presence of a known inhibitor.	128
Figure 3.11. Effect of inhibitors on E6 thermal stability.	130
Figure 3.12. p53 Degradation assay results.	132
Figure 3.13. Effect of E6 inhibitors on p53 degradation in SiHa (HPV16 transformed) and HeLa (HPV18 transformed)	135
Figure 3.14. Effect of E6 inhibitors on p53 degradation HCT116 (HPV negative) cells.	136
Figure 3.15. Effect of E6 inhibitors on cell toxicity.	137
Figure 3.16. p53 degradation assay results.	139
Figure 3.17. The ability of the compound to induce apoptosis.	143
Figure A.1. Structure of the CR3 domain of HPV1A-E7.	169
Figure A.2. Flow chart of virtual and experimental screening strategy for discovering of E7 inhibitors	179
Figure A.3. Docked model of the CR3 domain of E7 with the highest scoring inhibitors from the virtual screen.	181
Figure A.4. Inhibition of E7-mediated E2F displacement from pRb using the ELISA-based assay.	182
Figure A.5. Inhibition of analogs demonstrated using the ELISA-based assay.	185
Figure A.6. Model of compound 28 (pink) bound to E7 protein (green) as determined using DOCK 4.0.	187
Figure B.1. Functional domains of p300/CBP.	194
Figure B.2. Sequence alignments of p300 CH1 and CH3 domains (top) and ribbon structure of the TAZ1 domain of CBP/p300 (bottom)	196
Figure B.3. Binding of HPV 1A E7 and HPV 16 E7 to the CH1 domain of p300.	198
Figure B.4. Binding of E1A and HPV 16 E7 to the CH1 domain of p300	199
Figure B.5. Mapping the interaction between HPV 16 E7 and the CH1 domain of p300.	201
Figure B.6. Gel Filtration between 16E7 and CH1 of p300.	203

Figure B.7. Isothermal titration calorimetry results. 206

Figure B.8. Analytical ultracentrifugation sedimentation equilibrium of the p300_{CH1}/E7₁₋₅₁
complex. 207

Figure B.9. Crystals formed between HPV16-E7 and p300_{CH1}. 210

CHAPTER 1

Introduction

1.1 Overview of the Human Papillomaviruses

Human papillomaviruses (HPVs) are small DNA viruses which are the cause of benign, premalignant, and malignant lesions of mucuous membranes and stratified epithelia. It only became apparent in the 1970s that HPV is associated with cancerous lesions of the cervix. This discovery eventually led to two prophylactic vaccines, however, work still needs to be done to protect against the large variety of HPVs, as well as to treat those who have already been infected with the virus. Today, HPV is suggested to be one of the most common sexually transmitted diseases, affecting both men and women worldwide. Due to its clinical manifestations, it is of interest to identify treatments for those who have contracted the virus, and have progressed to later stages of infection.

1.1.1 History of HPV and its Discovery in Causing Cancer

Prior to the 1970's, it was believed that human papillomaviruses (HPVs), as well as other viruses could not cause cancer in humans. On the other hand, the oncogenic properties of papillomaviruses became evident in animals much earlier. The infectious nature of warts became known around the turn of the twentieth century. The first link of papillomavirus infection to cancer came in the 1930s when Richard Shope showed that soluble extracts of warts from wild cottontail rabbits contained the Shope papillomavirus, also called the cottontail rabbit papillomavirus (CRPV), and that they were capable of transmitting the disease to other cottontail rabbits (Shope and Hurst, 1933). Shortly thereafter, Peyton Rous and Joseph Beard revealed the tumorigenic potential of this wart virus (Rous and Beard, 1934). Namely, they showed that it would form skin carcinomas after an extended period of time. CRPV has a DNA genome packaged into virus particles, and so it represented the first known DNA tumor virus. This virus was sequenced in the 1980s, and shown to resemble the sequence of HPV 1A. In fact, CRPV has been used as a model for the study of viral tumorigenesis of human papillomaviruses. Studies of bovine

papillomavirus (BPV) further progressed research in this area. In 1959, Olson et al. noticed the induction of bladder tumors in cattle by BPV infection (Olson et al., 1959). A few years later, the transforming ability of BPV was further demonstrated in calf and murine cells in tissue culture. This was the first application of tissue culture studies to papillomavirus research and influenced progress in subsequent years. Additionally, BPV type 1 has served as a prototype for studying the molecular biology of papillomaviruses (Zheng and Baker, 2006).

Human papillomavirus was discovered as a virus found inside of skin warts. The structure of the virus was visualized using the electron microscope in 1949 (Strauss et al., 1949). An analysis of the potentially oncogenic papillomaviruses began in the 1970s, with work by Stefania Jablonska, a dermatologist. She discovered the connection between HPV and skin cancer in 1972 (Jablonska et al., 1972). Several years later, HPV-5 was identified as the strain responsible for skin cancer (Jablonska et al., 1978; Jablonska et al., 1979). Around the same time, Harald zur Hausen, a virologist who studied cancers of the cervix, proposed the role of human papillomaviruses (HPVs) in causing cervical cancer (zur Hausen, 1977; zur Hausen et al., 1975; zur Hausen et al., 1974). This proposal came from his identification of human papillomavirus DNA sequences in cervical cancer biopsies. In 1983 he discovered the tumourigenic HPV type 16, pieces of which were integrated into the host DNA. Furthermore, in 1984, he cloned HPV 16 and HPV 18 from patients that had cervical cancer (Boshart et al., 1984; Durst et al., 1983). Others had also been working on isolating and identifying HPV types in genital warts and laryngeal papillomas (de Villiers et al., 1981; Gissmann et al., 1982; Gissmann and zur Hausen, 1980) and from premalignant genital lesions (Ikenberg et al., 1983). This work resulted in an explosion of studies on the role of HPV in cancers and would eventually lead to the development of prophylactic vaccines against HPV, to be discussed later.

1.1.2 The HPV Genome and its Encoded Proteins

HPV is a small, nonenveloped, double stranded DNA virus that has a circular genome of approximately 8 kilobases (Figure 1.1) (Munger et al., 2001). Its genome can be divided into three major regions: early, late, and a long control region (LCR). The early region encodes for six common open reading frames (ORFs): E1, E2, E4, E5, E6, and E7 which translate into individual proteins. The late region of all papillomavirus genomes encode for L1 and L2 ORFs, which translate into the major and minor capsid proteins, respectively. The LCR region, which comprises approximately 10% of the HPV genome, has no protein-coding function. Instead, it contains *cis* elements that are necessary for the replication and transcription of viral DNA, including the origin of replication and enhancer and promoter regions.

L1 and L2 encode for capsid proteins, which are structural proteins important for virion assembly. They form icosahedral capsids around the viral genome during the generation of progeny virions. E1 and E2 are involved in the initiation of viral replication and regulation of viral transcription. More specifically, E1 proteins of papillomaviruses have both adenosine triphosphatase (ATPase) and DNA helicase activities that are essential for both initiation and elongation of viral DNA replication (Munger et al., 2001). E1 interacts with E2, as well as several host factors. Interestingly, E1 alone binds to DNA as a hexamer non-specifically and with a weak affinity. E2 increases the binding affinity of E1 to DNA and inhibits the non-specificity of the interaction. In fact, the E1-E2 interaction is necessary for DNA replication. In addition to its function in replication, E2 also acts as a transcription factor: it binds as a homodimer to the palindromic sequence ACCN₄GGT within the LCR and can regulate viral gene expression (McBride et al., 1991).

E4 is found both in the cytoplasm and nucleus, interacts with the keratin cytoskeleton and intermediate filaments, and is believed to facilitate viral assembly and release (Munger et al., 2001). E5 appears to have weak transforming abilities. It has been found to localize in intracellular membranes and has been implicated in inducing unscheduled cell proliferation in cooperation with HPV E7, and inhibit gap-junction intercellular communication (DiMaio and

Mattoon, 2001). It also possibly activates growth factor receptors, such as EGFR and other protein kinases. Through its activation of EGFR, E5 can interfere with several signal transduction pathways, including the mitogen-activated protein (MAP) kinase pathway. E5 has also been implicated in interacting with vacuolar H⁺-ATPase, thereby inhibiting proper transport of proteins, such as the major histocompatibility complexes (MHC) class I and II (DiMaio and Mattoon, 2001). E5 can also inhibit apoptosis induced by Fas-ligand and tumour necrosis factor-related apoptosis-inducing ligand (TRAIL) and by ultraviolet light.

HPV E6 and E7 are the main arbitrators in the development of HPV-induced carcinomas. The best known property of E6 proteins from high-risk HPVs (those with the propensity to cause cancer), is the ability to bind and degrade the tumour-suppressor protein p53 through the recruitment of the E3-ubiquitin ligase, E6-associated protein (E6AP). This results in the inhibition of the transcriptional activity of p53, and inhibition of p53-induced apoptosis. In addition, E6 binds to numerous other cellular proteins, discussed later. The main cellular target of HPV E7 is the retinoblastoma protein, pRb. This interaction has been implicated in the degradation of pRb, although this has not been well studied (Boyer et al., 1996). E7 has also been found to interact with complexes formed between pRb and the E2F family of transcription factors and break this complex prematurely, in the absence of cell-cycle regulatory mechanisms. This results in deregulated cell cycle progression. E7 has been found to bind to numerous other cellular proteins as well, which are discussed later.

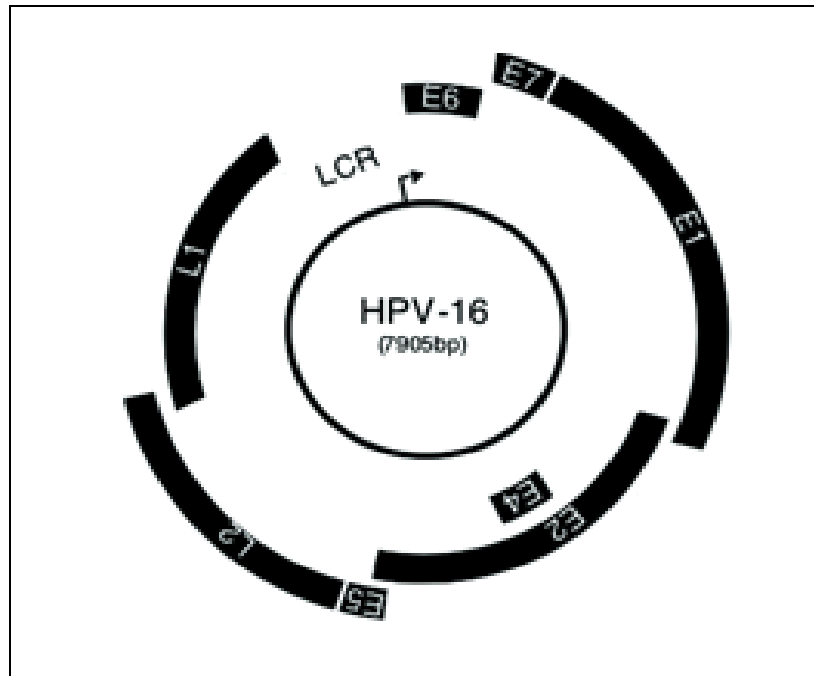


Figure 1.1. Genome of the human papillomavirus type 16. The circular, double stranded DNA genome is denoted schematically. The open reading frame for each early and late gene is shown, along with the LCR. A description of each translated protein is given in the text. This figure is adapted from Munger et al. 2001.

1.1.3 HPV Infection

In a normal stratified squamous epithelium, it is the cells in the bottom layer that divide (Figure 1.2) (Woodman et al., 2007). As they divide, cells are moved upwards and they change shape as they differentiate, becoming flatter as they reach the surface. The cells at the top constantly get detached and replaced by cells from beneath. HPV virions are thought to enter the basal layer cells through microwounds. Attachment of several different HPV types requires heparan sulfate proteoglycans (HSPGs) (Combita et al., 2001; Giroglou et al., 2001a; Giroglou et al., 2001b; Joyce et al., 1999). HPV capsids have also been shown to interact with extracellular matrix components such as laminin-5. Upon conformational changes of the capsid, there is a new interaction with a second receptor, which then triggers the entry of the virus by endocytosis (Horvath et al., 2010).

During initial stages of infection, the viral dsDNA genome is maintained as an episome, an autonomously replicating extrachromosomal element, in the nucleus of the infected cell (Woodman et al., 2007). The virus then takes advantage of the cellular replication machinery to allow for low levels of viral DNA synthesis, resulting in 50-100 episomes per cell (Doorbar and Cubie, 2005; Hebner and Laimins, 2006). This generally occurs in the basal and first supra-basal epidermal layers, and in synchrony with the host cell cycle, only occurring in the S phase (Figure 1.2) (Woodman et al., 2007). Upon differentiation of infected cells, the viral genome is amplified to more than 1000 copies and expression of capsid proteins is induced, resulting in the synthesis of infectious virions that are assembled and released, which can then initiate a new infection (Doorbar and Cubie, 2005; Hebner and Laimins, 2006). This occurs in the midzone and superficial zones (Figure 1.2) (Woodman et al., 2007). The viral proteins override the normal cell cycle exit that occurs in differentiating cells, resulting in a loss in cellular architecture. This leads to squamous intraepithelial lesions (SILs) (Figure 1.2) (Woodman et al., 2007). It is these lesions, or abnormal growths, which are detected in Papanicolaou tests, or Pap smears. At this stage, the SILs can be removed, allowing normal cells to grow in their place. If left untreated, the HPV genome integrates into the host chromosomes by some unknown mechanism. This results in the

loss of E1 and/or E2 expression, and a subsequent upregulation of E6 and E7 oncogene expression. These two oncoproteins then maintain the proliferative state of the infected cells. Both E6 and E7 have functions that stimulate cell cycle progression and both can associate with regulators of the cell cycle. These cells eventually invade nearby tissues, resulting in invasive cancer.

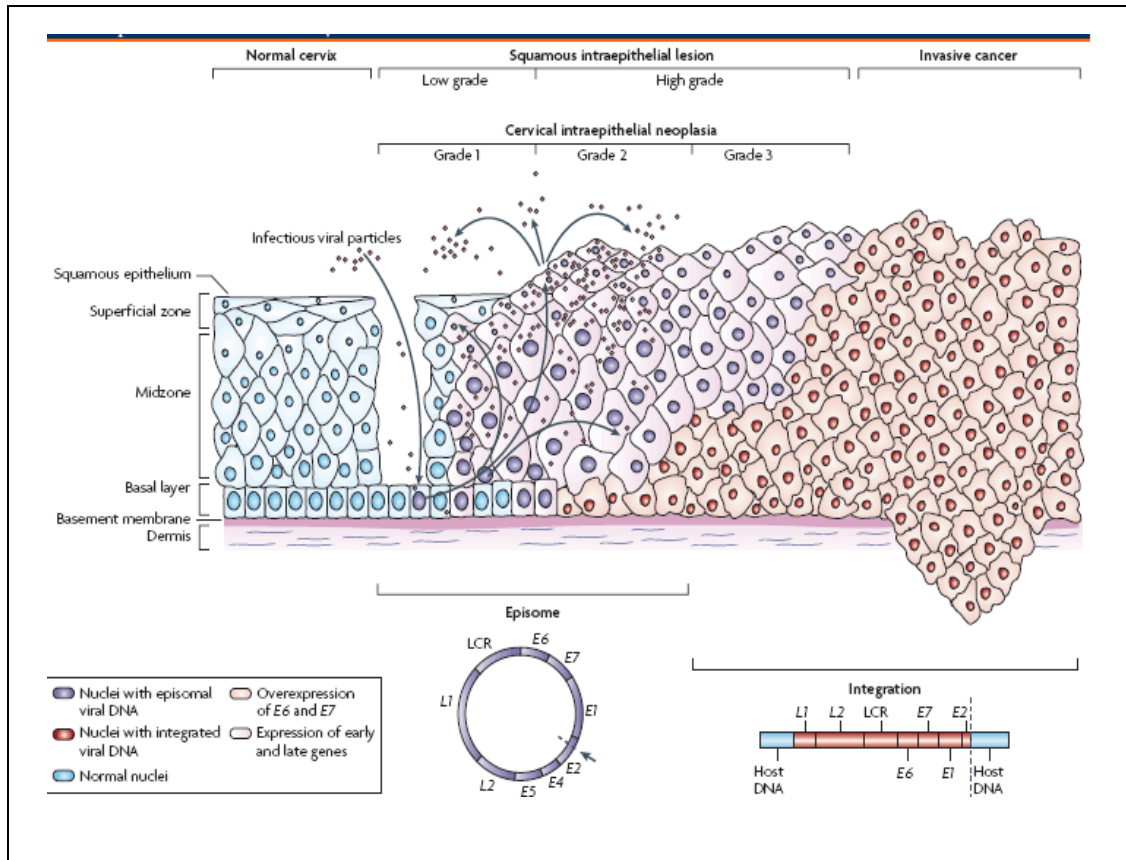


Figure 1.2. Infection of epithelia by HPVs. The epithelium of a cervix is shown, with normal cells on the left hand side and increasing stages of infection towards the right. Normal cells form a stratified epithelium by undergoing differentiation from basal cells (bottom) to keratinocytes (top). Viral particles are thought to infect the basal layer cells through microwounds. At early stages of infection, the HPV genome is maintained as an episome, shown in purple. The viral proteins prevent cell cycle exit associated with cellular differentiation, resulting in squamous intraepithelial lesions (SIL) and a loss in the cellular architecture found in normal cells. Furthermore, the expression of the L1 and L2 capsid proteins occurs in the midzone and superficial zones of the epithelium, resulting in the formation of new virions which can initiate new infections. During malignant transformation, the HPV genome is found integrated in the host DNA, shown in red. At this stage, proliferating cells infected with HPV invade nearby tissues, resulting in invasive cancer. This figure was adapted from Woodman et al. 2007.

1.1.4 *The Clinical Manifestations of HPV*

HPV is the world's most common sexually transmitted infection (Trottier and Franco, 2006) and it is estimated that 291 million women in the world are infected (Burchell et al., 2006). In the United States, it is estimated that 6 million people get newly infected each year. It is also suggested that at any point in time, 42.5% of women have genital HPV infections (Hariri et al., 2011). In fact, it is so common that at least one out of two people get it at some point in their lives. Most HPV infections are cleared with time due to the cellular immune response, however a small proportion of infections become chronic due to the integration of the high risk viral genome into the host's chromosome. Epidemiologic studies predict that approximately 100 million women worldwide will be infected with the oncogenic types HPV 16 or HPV 18 at least once in their lifetime.

HPV has received considerable attention due to its role in human cancer. In particular, HPV is known to be the causative agent of a number of epithelial cancers, most notably cervical cancer, a leading cause of death for women worldwide (McLaughlin-Drubin and Munger, 2009). Importantly, HPV is seen in 99.7% of all cervical cancers in the world (Bosch et al., 1995). HPV infection has also been implicated to have a causative role in about 20% of head and neck cancers as well as several other cancers (Dufour et al., 2011; Sudhoff et al., 2011). HPV infection is also thought to be responsible for the majority of anal and vaginal cancers (De Vuyst et al., 2009) and about 50% and 35% of vulvar and penile cancers, respectively (Chaturvedi, 2010). Most recently, HPV infections have been found to cause cancer of the oropharynx, which is the middle part of the throat including the soft palate, the base of the tongue, and the tonsils. In the United States, more than half of the cancers diagnosed in the oropharynx are linked to HPV-16 (Jayaprakash et al., 2011).

There are over 200 HPV genotypes that have been recognized, and they fall under two general forms based on the pathology of the lesions that they cause, low-risk and high-risk, which cause benign tumors and which have the propensity to cause cancer, respectively (Burd, 2003). At least 40 types of HPVs are known to infect the genital tract and can be easily spread through

direct skin-to-skin contact. Out of the 40, 15 HPV types put women at high risk for cervical cancer. The discovery of the link between HPV and cervical cancer was an important one due to the fact that cervical cancer is one of the leading causes of cancer-related deaths for women worldwide.

1.2 Targeting HPV Infection

1.2.1 HPV Vaccines

Initial attempts to develop vaccines against papillomaviruses began in animal models using bovine papillomaviruses (Campo et al., 1993), canine oral papillomavirus (Suzich et al., 1995) or cotton-tail rabbit papillomavirus (Breitburd et al., 1995). These vaccines were successful and were based on the observation that the virus structural proteins can self-assemble into virus-like particles (VLPs) (Salunke et al., 1986). Eventually, clinical trials with VLPs from HPV types 6, 11, 16, and 18 ensued. These HPV types were used because the VLPs were well tolerated and could induce high titers of neutralizing antibodies and T-cell responses (Emeny et al., 2002; Evans et al., 2001; Harro et al., 2001).

Two vaccines have been developed to date: Gardasil (Siddiqui and Perry, 2006), manufactured by Merck and approved by the FDA in 2006, and Cervarix (Le Tallec et al., 2009), manufactured by Glaxo-Smith-Kline and approved in 2009. Both of these vaccines target HPV 16 and 18, high risk forms that are known to cause 75% of cervical cancers. Gardasil, in addition to these two genotypes, also targets HPV 6 and 11, low risk forms which cause 90% of genital warts. The FDA has approved Gardasil for use in females and males ages 9 to 26 and Cervarix for use in females ages 9 to 25. In males, the vaccines can protect against genital warts, anal cancer, and some potentially precancerous lesions caused by some HPV types.

The HPV vaccines work like other immunizations that protect against viral infections. More specifically, the HPV vaccines are comprised of L1 epitopes. Since the HPV major capsid protein, L1, can spontaneously assemble into VLPs, introducing such epitopes can trigger an antibody response that protects recipients of the vaccine from being infected with the HPV types used in the vaccine (Stanley et al., 2006). These VLPs are non-infectious on their own because they do not contain DNA.

Unfortunately, Gardasil and Cervarix only protect against four types of HPVs and there are currently over 200 genotypes that have been identified. Furthermore, these vaccines are

prophylactic. As a result, they provide no treatment to those who have already been exposed to the virus. Lastly, since these vaccines are fairly new, their clinical benefit will not be known for decades. Consequently, it becomes of interest to search for treatments for people that have been infected with HPV.

1.2.2 HPV Treatments

To date, there are no therapeutic strategies for those who have been exposed to HPV. There are only treatments for the abnormalities caused by the virus. Namely, if HPV infection has caused abnormal cell changes, the solution is generally to remove those areas, or to freeze the abnormal cells by a method called cryotherapy (Hatch, 1995). Or, as is the case for other cancers, radiation therapy and chemotherapy are other treatment options. Unfortunately, these methods have side effects and are not always effective. While the overall 5 year cure rate for cervical cancer is approximately 90%, it is considerably worse (down to 15% according to the American Cancer Society) for cases where the cancer has spread to other organs. Therefore, identifying small molecule inhibitors that target the viral proteins, might be one path for more specifically treating viral infections and the cancers they cause.

1.2.3 HPV Inhibitors

There have been a number of efforts to identify inhibitors against the HPV viral proteins. For example, Carraguard, a sulfated polysaccharide extracted from red algae, has been suggested to work effectively against HPV genital infections (Buck et al., 2006; Roberts et al., 2007). This inhibitor works by preventing HPV from attaching to cells, since it resembles heparan sulfate, which the HPV capsid recognizes. However, like the vaccines, this would only prevent transmission of the virus, and would not help those who are already infected.

Other efforts have sought to identify inhibitors that prevent viral replication. A high-throughput screen of a small molecule compound collection identified biphenyl sulfonacetic

acid, which binds reversibly to E1 and reduces its affinity for ATP to reduce its helicase activity by an allosteric mechanism (White et al., 2005). The specificity of this compound was demonstrated by the fact that it did not inhibit the ATPase activity of other related enzymes. Unfortunately, this inhibitor did not demonstrate the ability to prevent HPV DNA replication in cell-based assays (Faucher et al., 2004). It was suggested that this might be due to the inability of the charged group of the inhibitor to permeate the cell membrane. It was also possible that the cells contained a higher effective concentration of ATP than what was used in the in vitro assay, which rendered the small molecules ineffective.

In general, it is more challenging to target protein-protein interactions by small molecules, due to the relative flatness and larger size of the interfaces, the flexibility of the proteins upon binding, and the stoichiometry of binding (Arkin and Wells, 2004). However, certain protein-protein interfaces seem to be amenable to small molecules, particularly those with "hot spots". In fact, a class of small molecules, called inandiones, have been identified through high throughput screening that can disrupt the HPV E1-E2 interaction, and prevent viral replication (Wang et al., 2004; White et al., 2011; Yoakim et al., 2003). These molecules were optimized to obtain compounds with low nanomolar IC₅₀ values (Goudreau et al., 2007; Wang et al., 2004). These compounds were subsequently shown to bind to a low-risk form of HPV E2, however did not work against high-risk forms of E2.

Since HPV containing tumors have low levels of wild type p53 that is unable to function due to elevated degradation, several therapeutic strategies have focused on p53 stabilization through the blocking of E6 function, either with RNAi or antisense oligodeoxynucleotides (Marquez-Gutierrez et al., 2007; Niu et al., 2006). Such studies have resulted in increased p53 levels and inhibition of tumor growth in both tissue culture and animal models. Spurred by this success, the development of inhibitors to the E6/E6AP interaction, a prerequisite to p53 degradation (Cooper et al., 2003b; Li and Coffino, 1996b), presented an opportunity to stabilize p53 levels and bring about cell cycle arrest or apoptosis in infected cells. Several inhibitors that target the HPV-E6 interaction with E6AP that is required for p53 degradation have been

developed including the Pitx2a protein inhibitor (Wei, 2005), intrabodies (Griffin et al., 2006) and alpha helical peptides (Butz et al., 2000; Liu et al., 2004), however all show modest activity. Another concern with such inhibitors is their ability to permeate the cell membrane, and their stability once in cells. Ten small molecules inhibitors were also identified by Baleja et al. after pharmacophore development and limited *in silico* screening (Baleja et al., 2006b), however only one compound proved to be active in cells and only at high concentrations. Although these studies have not progressed to clinical trials, it demonstrates that it is possible to target HPV-mediated protein-protein interactions effectively with small molecules. No inhibitors against the other HPV oncoprotein, E7, have been reported.

While inhibition of E1 and/or E2 function may be useful in preventing HPV replication, such inhibition would only represent a valuable strategy for the treatment of HPV-associated benign lesions such as warts, in which the viral genome is maintained as an episome, and E1 and E2 are expressed. Expression of these two viral proteins is often lost during the process of malignant transformation (Woodman et al., 2007). Integration of the viral DNA into the host genome often results in increased expression of the E6 and E7 oncogenes. Since both E6 and E7 are essential for the proliferation and survival of cervical carcinoma cells, they are in principle the targets of choice for the treatment of HPV-induced cancers. HPV E6 and E7 are also particularly attractive protein targets since they have no human orthologs.

One reason for the difficulty in targeting HPV infection lies in the fact that most papillomavirus proteins exert their effect by binding to cellular proteins rather than as a result of their intrinsic enzymatic activity. The E6 and E7 proteins inactivate two tumor suppressor proteins, p53 (inactivated by E6) and pRb (inactivated by E7) and as a result, deregulate the cell cycle.

1.3 Normal Cells and Their Regulation

1.3.1 Cell Cycle

The cell cycle consists of a highly regulated series of events that ensures the correct duplication and division of a cell. This process results in the replication of DNA and separation of chromosomes that are then distributed to the resulting daughter cells.

The cell cycle is broken down into four phases: G1, S, G2, and M (Figure 1.3) (Suryadinata et al., 2010). The DNA of the cell gets replicated during S (synthesis) phase and copies are distributed to opposite ends of the cell during M (mitosis) phase. The cell increases in size during the two gap phases, G1 and G2, which occur before S and M phase, respectively. During the gap phases, the cell prepares for either DNA synthesis or mitosis by transcribing and synthesizing components of the replication or mitotic machinery (Lodish H, 2004). There is an additional gap phase, G0, in which the cells have left the cell cycle, quiesced, and are no longer dividing.

Many of the key events of the cell cycle are initiated by the cyclin-dependent kinases (CDKs), which are activated by forming heterodimeric complexes with the cyclin family of proteins (Vousden, 1997). The levels of the different CDKs remain fairly constant throughout the cell cycle. Since they must bind to a cyclin to become active, their activity is regulated by the change in concentrations of cyclins throughout the cell cycle. Cyclin genes are transcribed in a cell-cycle dependent manner and the cyclins are also degraded at specific points of the cell cycle. The cyclin-CDK complexes found during the different parts of the cell cycle are shown in Figure 1.3 (Suryadinata et al., 2010). The resultant complexes, in turn, control the phosphorylation signals that the cell cycle recognizes to transition from one phase to another (Lodish H, 2004). These cyclin-CDK complexes are further regulated by other protein kinases or phosphatases, and by binding certain inhibitor proteins (Vousden, 1997). This allows the cell cycle to respond to various external and internal signals.

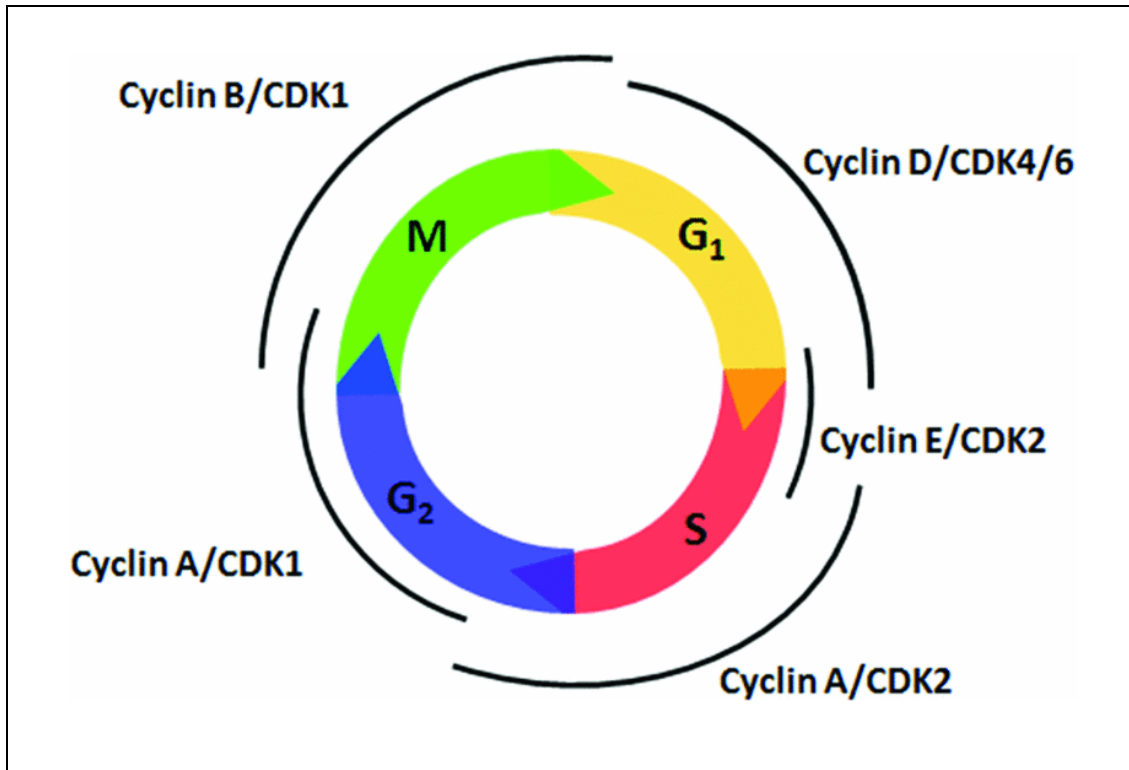


Figure 1.3. The mammalian cell cycle. The cell cycle consists of four major phases: G₁, S, G₂, and M. Activities in each phase of the cell cycle are regulated by complexes formed by different cyclins and cyclin-dependent kinases (CDKs). The CDKs bear the catalytic function of the complex and the cyclins are responsible for activating a given CDK. This figure was adapted from Suryadinata et al., 2010.

The progression into each phase of the cell cycle is further regulated at the various checkpoints. The cell cannot proceed to the next phase until the checkpoint requirements have been met. Several checkpoints ensure that damaged or incomplete DNA is not passed on to the daughter cells. DNA damage is able to arrest cells before S phase and before M phase, during the G₁/S and G₂/M checkpoints, respectively (Vousden, 1997). In fact, p53 plays an important role in triggering control mechanisms at both of these checkpoints. The retinoblastoma protein, pRb, regulates the transition from the G₁ to the S phase of the cell cycle.

1.3.2 The Functions of the Retinoblastoma Protein, pRb, in Normal Cells

The retinoblastoma protein, pRb, is a 105 kilodalton (kDa) protein believed to be constitutively expressed in mammalian cells (Bernards et al., 1989). The phosphorylation level of pRb is regulated throughout the cell cycle: it is hypophosphorylated early in the cell cycle and is increasingly phosphorylated as the cell cycle progresses into S phase. It contains 16 potential sites for phosphorylation by at least three different cyclin-CDK complexes during the cell cycle: by cyclin D-CDK4/6 complexes early in G₁, cyclin E-CDK2 complexes in mid-late G₁, and possibly by cyclin A-CDK2 during S phase (Grana et al., 1998; Sherr, 1996). The activity of the cyclin-CDK complexes is further modulated by other proteins, called cell cycle inhibitors, that fall into two families: the cip/kip family (CDK interacting protein/Kinase inhibitory protein) and the INK4a/ARF family (Inhibitor of Kinase 4/Alternative Reading Frame). These cell cycle inhibitors prevent progression of the cell cycle and act as tumor suppressors.

The hypophosphorylated form of pRb is active in negative growth control. The growth suppressive activity of pRb is mediated through its association with the E2F family of transcription factors, which regulate the expression of a number of genes required for cell cycle progression (Hiebert et al., 1992; Johnson and Schneider-Broussard, 1998). Two other proteins, called p107 and p130, are homologous to pRb in the "pocket domain". They are regulated in a similar fashion to pRb, except that they are phosphorylated at different points of the cell cycle, and their

concentrations vary throughout the cell cycle (Grana et al., 1998; Sidle et al., 1996). They, too, target E2F transcription factors, although not the same ones that are targeted by pRb. The E2F family of transcription factors consists of six members (E2F-1 to E2F-6) and form DNA-binding heterodimers with members of the related DP family of co-activators (Figure 1.4) (Frisch and Mymryk, 2002).

The activity of E2F transcription factors is inhibited by the formation of complexes with pRb or the other pocket proteins. When phosphorylated, pRb releases E2F to transcribe genes necessary for progression into the S phase of the cell cycle as well as for DNA replication (Harbour and Dean, 2000; Harbour et al., 1999; Stevaux and Dyson, 2002). A schematic of this process is shown in Figure 1.4. In addition to regulating the G1 to S phase transition of the cell cycle, the normal function of pRb has also been implicated in apoptosis and differentiation through its direct binding to and inhibition of E2F transcription factors (Harbour and Dean, 2000; Stevaux and Dyson, 2002).

Although E2F is probably the major physiological target through which pRb and the related pocket proteins exert their effects, pRb has also been implicated in the regulation of other transcription factors and other proteins with important regulatory roles, some of which are listed in Table 1.1 (Grana et al., 1998). It has been suggested that pRb interacts with at least 150 other cellular proteins, and more are uncovered as the years go by (Chinnam and Goodrich, 2011). pRb and the related pocket proteins have also been implicated to be involved in numerous cellular pathways, as shown in Figure 1.5 (Stevaux and Dyson, 2002). There is still much that needs to be learned about the *in vivo* roles of pRb and E2F.

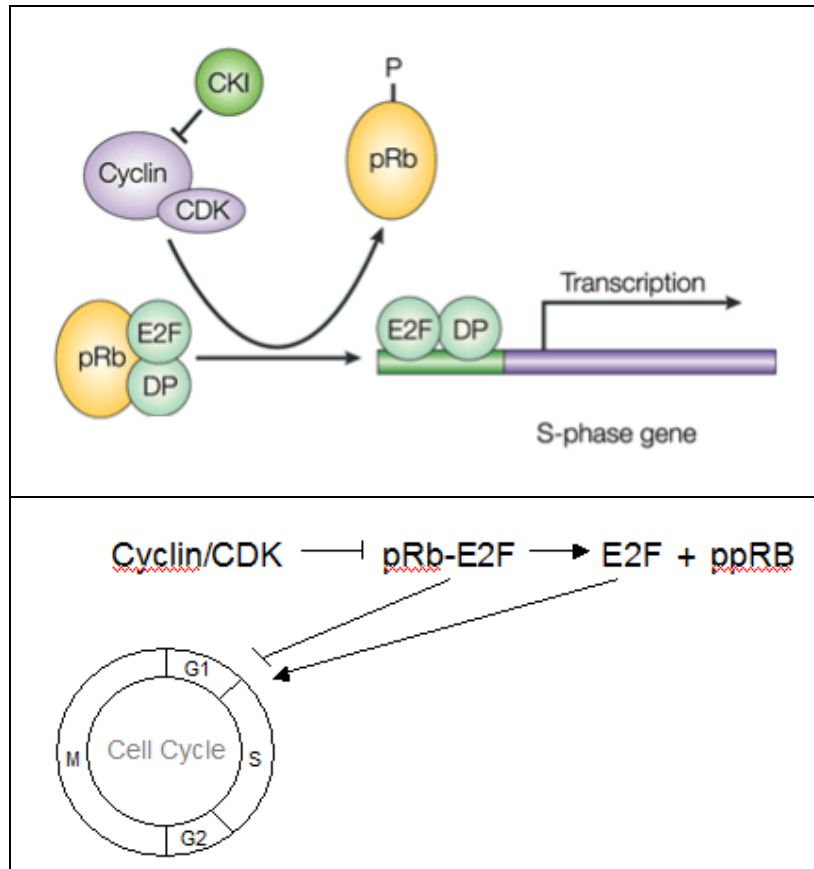


Figure 1.4. Regulation of E2F activity by pRb. (top) pRb binds to E2F/DP heterodimers at promoters to inhibit their transcriptional activity. Phosphorylation of pRb results in a release of pRb from E2F/DP, which can then transcribe genes. This figure is adapted from Frisch and Mymryk, 2002. (bottom) pRb regulates the transition from the G1 to the S phase of the cell cycle. It does this by binding to and inhibiting the transcriptional activity of the E2F family of transcription factors. At certain points in G1, complexes of cyclins and CDKs phosphorylate pRb, which then releases E2F. Upon release, E2F can then transcribe genes necessary for the progression into the S phase of the cell cycle. This figure is adapted from Munger et al. 2001.

<i>Associated protein</i>	<i>Biochemical function</i>	<i>Pocket protein</i>
Cyclin D	CDK subunit	pRB
Cyclins A and E	CDK subunits	p107, p130
RbK	Protein kinase	pRB
E2F family	Transcription factors	pRB, p107, p130
c-Jun	Transcription factor	pRB
ATF-2	Transcription factor	pRB
c-Myc, N-Myc	Transcription factors	pRB, p107
Spl	Transcription factor	pRB, p107
Abl	Nuclear tyrosine kinase	pRB
MDM2	Nuclear protein	pRB
MCM7	DNA replication licensing	pRB, p107, p130
HNuc	Nuclear protein	pRB
RBAp48	Transcription factor-corepressor	pRB
AhR	Transcription factor	pRB
TAFII250/TFIID	Transcription factor	pRB
TFIIIB	RNA pol III-Transcription factor	pRB
UBF	RNA pol I-Transcription factor	pRB
HDAC1	Histone deacetylase	pRB, p107, p130
MyoD	Transcription factor	pRB, p107
HBP1	Transcription factor	pRB, p130
p202	Transcription factor	pRB
C/EBP, NF-IL6	Transcription factor	pRB
NRP/B	Nuclear matrix	pRB
PLH proteins	Transcription factor	pRB, p107, p130
BRG1	Transcription factor	pRB
hBRM	Transcription factor-coactivator	pRB
Id-2	Transcription factor-corepressor	pRB
AP-2	Transcription factor	pRB
Trip230	THR-coactivator	pRB

Table 1.1. Proteins that interact with pRb, p107, and p130. pRb and the pocket proteins are implicated in binding other transcription factors in addition to E2F, as well as kinases, transcription factor co-activators and co-repressors, histone deacetylases, and more. The interactions are not all well understood; more work still needs to be done the functions of pRb in the cell. This table was adapted from Grana et al. 1998.

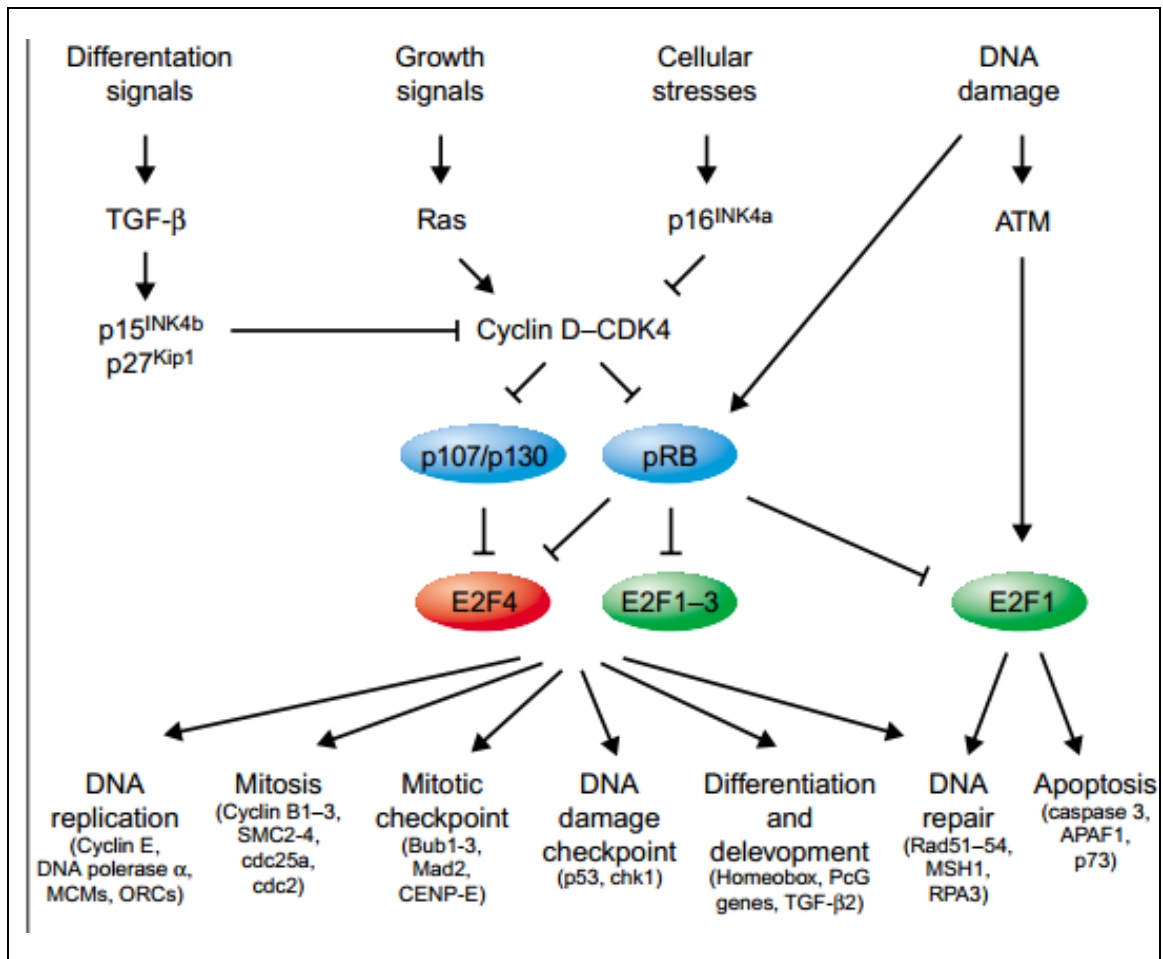


Figure 1.5. Transcriptional pathways of E2F/pocket protein complexes. A number of signaling events activate downstream pathways that involve transcription of genes important for many different activities, such as DNA replication, mitosis, differentiation, DNA repair, apoptosis, etc. pRb and the other pocket proteins, p107 and p130, regulate the activity of the different E2F proteins which can, in turn, regulate the expression of genes necessary for these different events. The activity of pRb and the pocket proteins is further regulated by complexes formed by cyclins and cyclin-dependent kinases, whose activity is modulated by other proteins, such as cell cycle inhibitors such as p16, p27 and p15, GTPases such as Ras, and others. This figure is adapted from Stevaux et al. 2002.

1.3.3 *The Functions of p53 in Normal Cells*

Like pRb, p53 serves many important roles in the cell. In times of stress, a number of signals will activate pathways that will modulate the activity of p53, which in turn will modulate the activities of other proteins so that the cells can repair any problems that may have incurred, or remove the cells entirely to prevent the proliferation of defective cells.

In general, the half-life of p53 is very short (less than 30 minutes) (Reich et al., 1983). p53 is part of an autoregulatory loop where p53 results in the synthesis of MDM-2, which in turn degrades p53 (Figure 1.6) (Lehrbach et al., 2003). MDM-2 acts as an E3 ubiquitin ligase that adds ubiquitin to p53, which results in its degradation (Honda et al., 1997). MDM-2 can also bind to p53 and prevent its ability to interact with the transcriptional machinery to transactivate downstream genes. The p14 ARF (Alternating Reading Frame) protein modulates this process by binding to and inhibiting the activity of MDM-2 (Kamijo et al., 1998). Interestingly, the transcription of this gene is regulated by several transcription factors, including E2F (Bates et al., 1998). p14 ARF, in turn, can regulate the levels of E2F (Martelli et al., 2001).

While normally expressed at low levels in healthy cells, p53 rapidly accumulates in cells that are undergoing stress. A variety of cellular stress signals, such as DNA damage, hypoxia, ribonucleoside triphosphate pool depletion, mitotic spindle damage, nitric oxide signaling and oncogene activation, activate p53 (Brown et al., 2009; Levine et al., 2006; Levine et al., 2007; Vogelstein et al., 2000). In such cases, the interaction between p53 and MDM-2 is disrupted, allowing p53 to perform its biological functions. One of the major functions of p53 is to act as a transcriptional regulator, in which it upregulates or downregulates the expression of a large number of genes (Kim et al., 2003; Vousden, 2009). p53 can also regulate proteins by interacting with them and modulating their functions (Green and Kroemer, 2009). p53 itself is also post-translationally modified during times of stress, being phosphorylated and acetylated by a number of different enzymes (Prives and Hall, 1999; Sakaguchi et al., 1998; Shikama et al., 1999; Sionov and Haupt, 1999)

In general, p53 transactivates genes for temporary cell cycle arrest, permanent cell cycle arrest (senescence), programmed cell death (apoptosis), DNA repair, or other activities (Brown et al., 2009; Horn and Vousden, 2007; Xue et al., 2007). Several of the pathways and proteins involved are shown in [Figure 1.7](#). If the problem is minor and can be fixed, then the cell cycle is stopped long enough for repair, after which it re-enters the cell cycle (Campisi and d'Adda di Fagagna, 2007). Common points for cell cycle arrest occur during G1 and G2 phases, in which repair of DNA sequences or of chromosomes is required, respectively. If the problem is more severe, then the cells senesce or undergo apoptosis (Zuckerman et al., 2009). Because of its role in protecting cells, the p53 protein is often regarded as the "guardian of the genome" or a tumor suppressor.

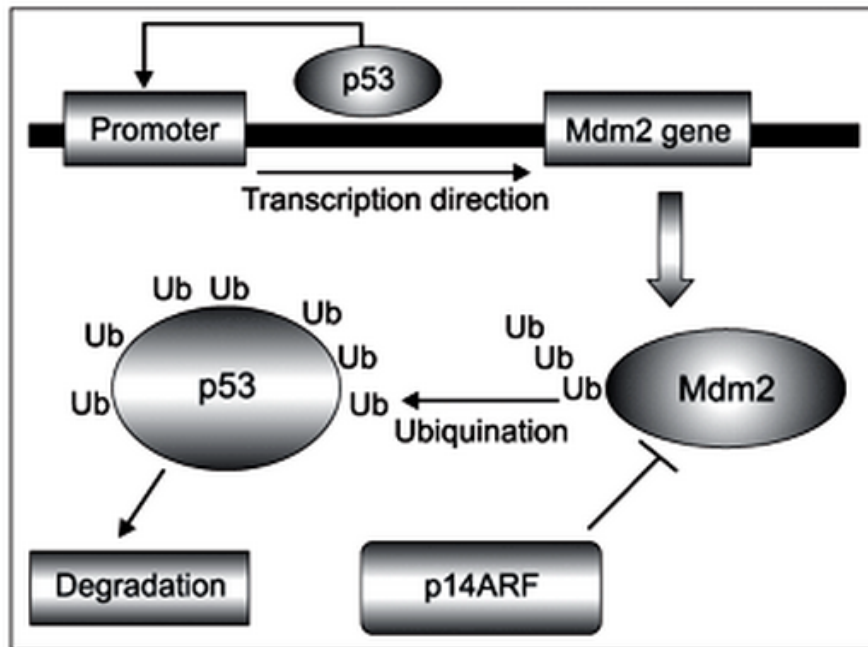


Figure 1.6. Negative feedback loop between p53 and MDM-2. p53 transactivates genes for the expression of MDM-2 protein. MDM-2 inhibits the activity of p53 by forming complexes with it or by acting as an E3 ubiquitin ligase, ubiquitinating p53 and targeting it for degradation. The activity of MDM-2 is also inhibited by p14 ARF, which is also regulated by E2F in addition to other transcription factors. This figure has been adapted from Lehrbach et al. 2003

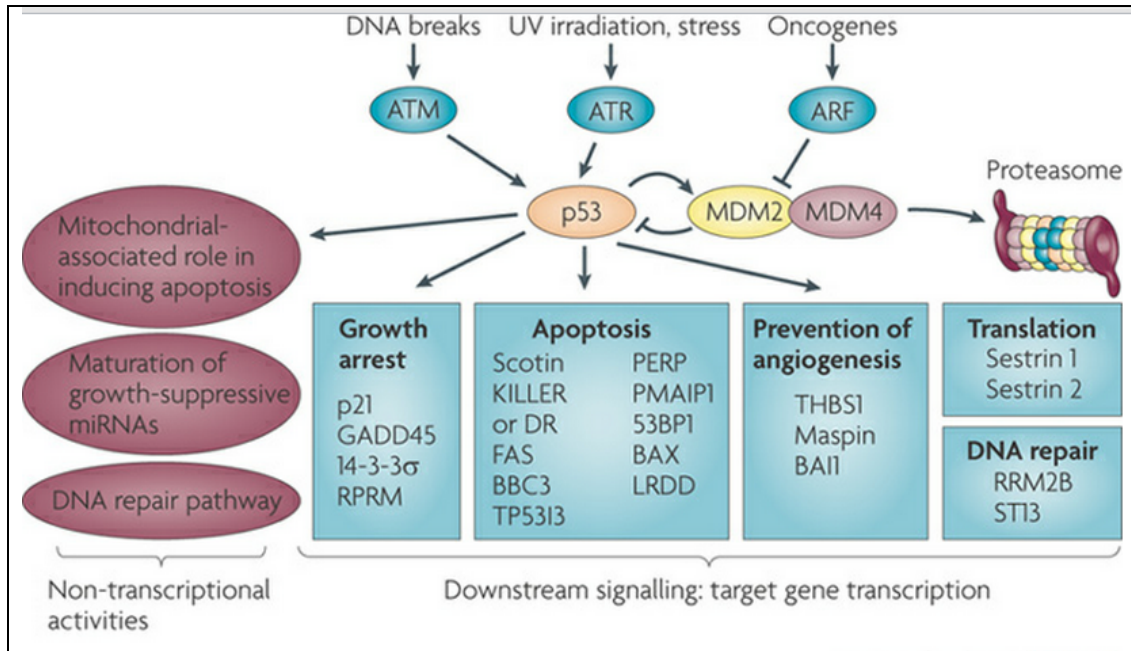


Figure 1.7. p53 pathways. A number of cellular stresses activate pathways that activate p53. Some examples include DNA damage, UV irradiation, and oncogene activation. These, in turn, activate proteins that result in the dissociation of p53-MDM2 complexes, thereby resulting in an activation of p53. p53 then transactivates genes for a variety of cellular responses, including but not limited to, growth arrest, apoptosis, and DNA repair. p53 also has non-transcriptional activities, as indicated. This figure has been adapted from Brown et al., 2009.

1.3.4 Apoptosis

The largest category of genes regulated by p53 are those that induce cell death. Apoptosis, or "programmed cell death", can occur via two linked pathways: the extrinsic pathway, in which signals begin outside of the cell, and the intrinsic pathway, in which signals originate within the cell (Figure 1.8) (Haupt et al., 2003). The extrinsic pathway involves the tumor necrosis factor receptor (TNF-R) family of receptors which form death-inducing signaling complexes (DISC) which results in the activation of caspases, including caspase-8 and caspase-3, which then induce apoptosis (MacFarlane and Williams, 2004). DNA damage triggers the intrinsic pathway and is associated with a depolarization of the mitochondria and a subsequent release of cytochrome c into the cytoplasm. This is governed by the Bcl-2 family of proteins, including Bax, as well as OKL 38 (MacFarlane and Williams, 2004; Vaseva and Moll, 2009; Yao et al., 2008). Cytochrome c, together with apoptosis protease-activating factor 1 (APAF-1) and procaspase-9, form the apoptosome in which caspase-9 is activated and promotes the activation of caspase-3, caspase-6, and caspase-7 (Nicholson and Thornberry, 2003).

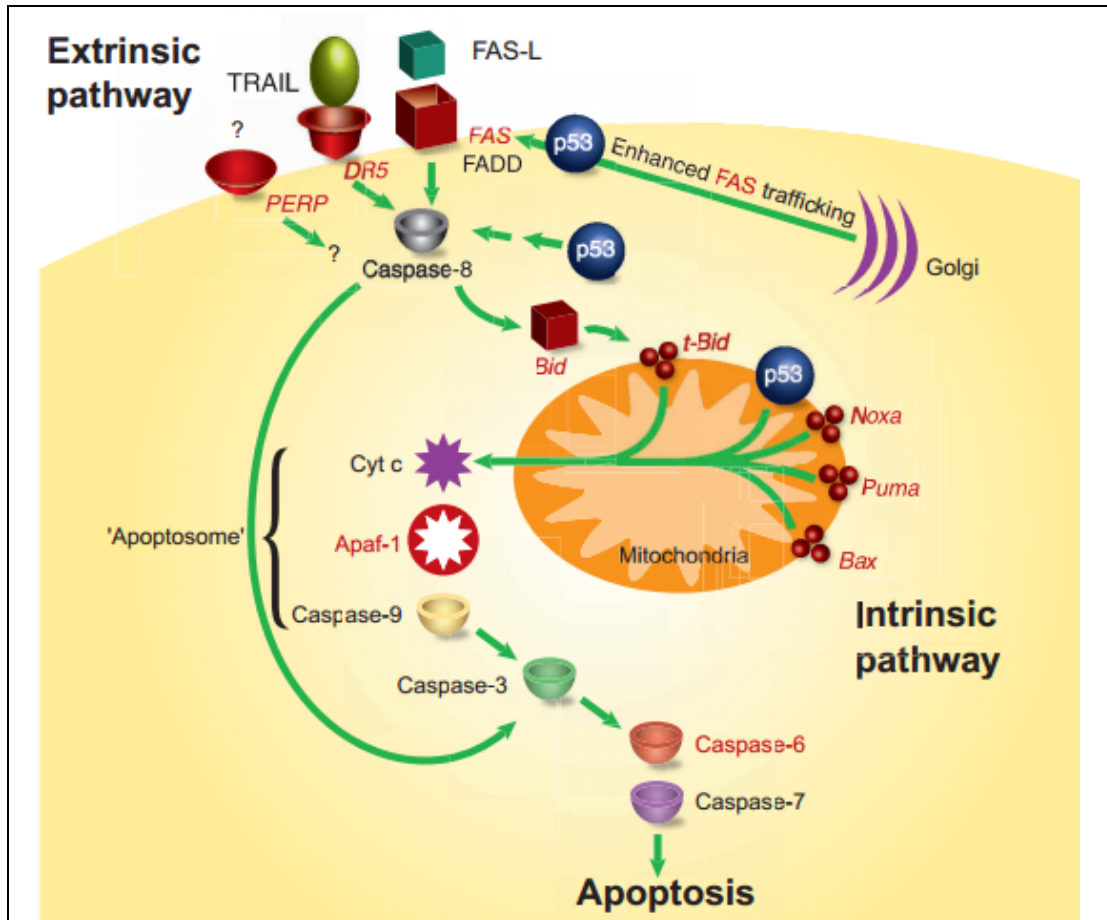


Figure 1.8. p53 mediated apoptosis. In response to extracellular signals, p53 can activate the extrinsic apoptotic pathway by inducing expression for Fas, DR5 and PERP which are activated by various ligands, including FasL and TRAIL. This eventually leads to the activation of caspase-8 and caspase-3 which induce apoptosis. The intrinsic pathway results from intracellular signals. This pathway is dominated by the Bcl-2 family of proteins, including Bax, and others, which aid in the release of cytochrome c from mitochondria. Cytochrome c, along with APAF-1 and Caspase-9, form the apoptosome. Caspase-9 is then activated and promotes the activation of caspase-3, caspase-6, and caspase-7, resulting in apoptosis. This figure has been adapted from Haupt et al. 2003.

There are different mechanisms through which apoptosis can occur. For instance, p53 has been implicated in inducing expression of many of the proteins involved in the apoptotic pathways, and repressing expression of anti-apoptotic proteins, resulting in additional layers controlling the process of apoptosis (Haupt et al., 2003; Kuribayashi and El-Deiry, 2008; Maecker et al., 2000; Vaseva and Moll, 2009). p53 has also been implicated in mediating caspase-independent apoptosis (Cregan et al., 2002; Godefroy et al., 2004). Lastly, p53 has also been implicated in activating apoptosis in a transcription-independent manner, by localizing to the mitochondria and resulting in cytochrome c release (Marchenko et al., 2000).

Intriguingly, E2F appears to be a link between the pRb and p53 pathways. There have been several studies done in mice where inactivation of pRb resulted in tumors with high apoptotic rates, and subsequent deletion of E2F1 led to a reduction in p53 dependent apoptosis (Pan et al., 1998; Tsai et al., 1998). Consequently, free E2F resulting from a loss of pRb function appears to trigger p53-dependent apoptosis. Free E2F is thought to target the ARF protein, which inhibits the inhibitory activity of MDM2 proteins on p53 (Figure 1.7) (Pomerantz et al., 1998; Zhang et al., 1998). Loss of pRb can also trigger p53-independent apoptosis, by the downregulation of antiapoptotic proteins, such as TRAF2 by E2F (Pan and Griep, 1995). This mechanism is not fully understood.

1.4 Cellular Transformation and Cancer

Cancer is characterized by the uncontrolled growth and spread of abnormal cells, as described by the American Cancer Society. It is generally caused by a variety of factors: external factors including chemicals, radiation, infectious organisms, and tobacco, and internal factors including inherited mutations, mutations occurring from metabolism, hormones, and immune conditions. Essentially, the result is a malfunction of the cell cycle control mechanisms. It is estimated that one out of every two men and women will be diagnosed with some form of cancer at some point in their lifetime, according to the American Cancer Society. In the United States alone, it is estimated that approximately thirteen million men and women alive have a history of cancer. Furthermore, the five-year survival rate is estimated at around 65%. There is much research in this field to try to treat cancer by a variety of methods and by targeting many different pathways.

1.4.1 The Links Between pRb and Cancer

Interestingly, the retinoblastoma protein (pRb) was the first protein identified whose mutational inactivation was associated with cancer, a childhood cancer of the eye (Schubert et al., 1994). pRb is now known to have altered activity in many other cancers including osteosarcomas, lung carcinomas and bladder carcinomas (Cordon-Cardo et al., 1997; Hensel et al., 1990; Kitchin and Ellsworth, 1974). It has been shown that the pRb pathway is impaired or inactivated in most human tumors. It is directly inactivated by mutations or deletions or the binding of viral proteins. Most such defects are found in the "pocket domain" of pRb. pRb is also deregulated in other ways, such as by deregulated phosphorylation by upstream kinases, including the cyclin-CDKs complexes, and cell cycle inhibitors. In fact, a loss of pRb-mediated cell cycle control is frequently observed in cancer (Malumbres and Barbacid, 2001; Weinberg, 1995).

1.4.2 The Links Between p53 and Cancer

p53, which also plays many critical roles in the cell, can cause cancer when it is not functioning properly. In fact, the gene encoding for p53 is commonly found mutated in human cancer. In general, p53 must retain its ability to oligomerize and bind specific DNA sequences to fulfill its function (Pietenpol et al., 1994). Not surprisingly, residues within the DNA binding domain of p53 are correlated with known cancerous mutations (Cho et al., 1994a; Ho et al., 2006; Kitayner et al., 2006). Only 5% of p53 mutations occur in the N-terminal and C-terminal domains, whereas 95% fall into the specific DNA-binding domain. p53 is also found deregulated by other means, including defects of other proteins in the p53 pathways (Brown et al., 2009). Like pRb, p53 can also be inactivated by the viral proteins.

1.4.3 Cellular Transformation Induced by Human Papillomaviruses

Upon initial infection by HPVs, the E6 and E7 oncoproteins, which are expressed at low levels, target a number of host proteins that are important in the immune response (Figure 1.9) (Yugawa and Kiyono, 2009a). In most cases, the immune system can fight off the infection, but in cases where it does not, can result in malignant transformation. Upon integration of the HPV genome into the host DNA, the E6 and E7 oncoproteins are overexpressed, resulting in the modulation of many pathways in the cell. Most notably, the greatest effects are on the pRb and p53 tumor suppressors, as discussed later. However, the E7 and E6 oncoproteins do in fact have a number of other cellular targets (Ganguly and Parihar, 2009b; Narisawa-Saito and Kiyono, 2007; Yugawa and Kiyono, 2009b).

The C terminal PDZ binding motif of HPV E6 targets the cytoplasmic membrane proteins hDLG (human homologue of the *Drosophila melanogaster* tumor suppressor protein discs large), Scribble (also a tumour suppressor), MUPP1 (multi-PDZ domain protein), and MAGI-3 (membrane-associated guanylate kinase) for degradation (Gardioli et al., 1999; Grm and Banks, 2004; Nakagawa and Huibregtse, 2000; Thomas et al., 2002). E6 oncoproteins have also been

implicating in modulating the Notch signaling pathway, a pathway important for proliferation and differentiation (Tan et al., 2012). E6 can also bind four-way DNA Holliday junctions and can inhibit p300/CBP acetylation to disrupt p53-dependent gene activation (Ristriani et al., 2000; Ristriani et al., 2001; Thomas and Chiang, 2005). High risk HPV E6 has also been shown to immortalize the host cell by activating telomerase to prevent telomere shortening (Meyerson et al., 1997; Nakamura et al., 1997). E6 can also bind to the pro-apoptotic protein Bak and inhibit its activity (Jackson et al., 2000; Thomas and Banks, 1999). E6 has a number of other cellular targets as well.

Like HPV E6, HPV E7 has also been implicated to bind a plethora of cellular proteins. E7 has been found to interact with the acetyltransferases p300 and P/CAF (Avvakumov et al., 2003; Bernat et al., 2003). In particular, E7 has been found to bind to the region of p300 that is important for binding many transcription factors (Bernat et al., 2003), and to P/CAF to reduce its acetyltransferase activity (Avvakumov et al., 2003). Another group of cellular proteins that bind to high-risk HPV E7 are the histone deacetylases (HDACs), and through this interaction, E7 can silence the interferon regulatory factor 1 (IRF-1) gene that is important for interferon signaling and immune surveillance of persistent HPV infections (Park et al., 2000). E7 can also bind to a pRb related protein, called p600, which may contribute to anchorage-independent growth and transformation (Huh et al., 2005; Nakatani et al., 2005).

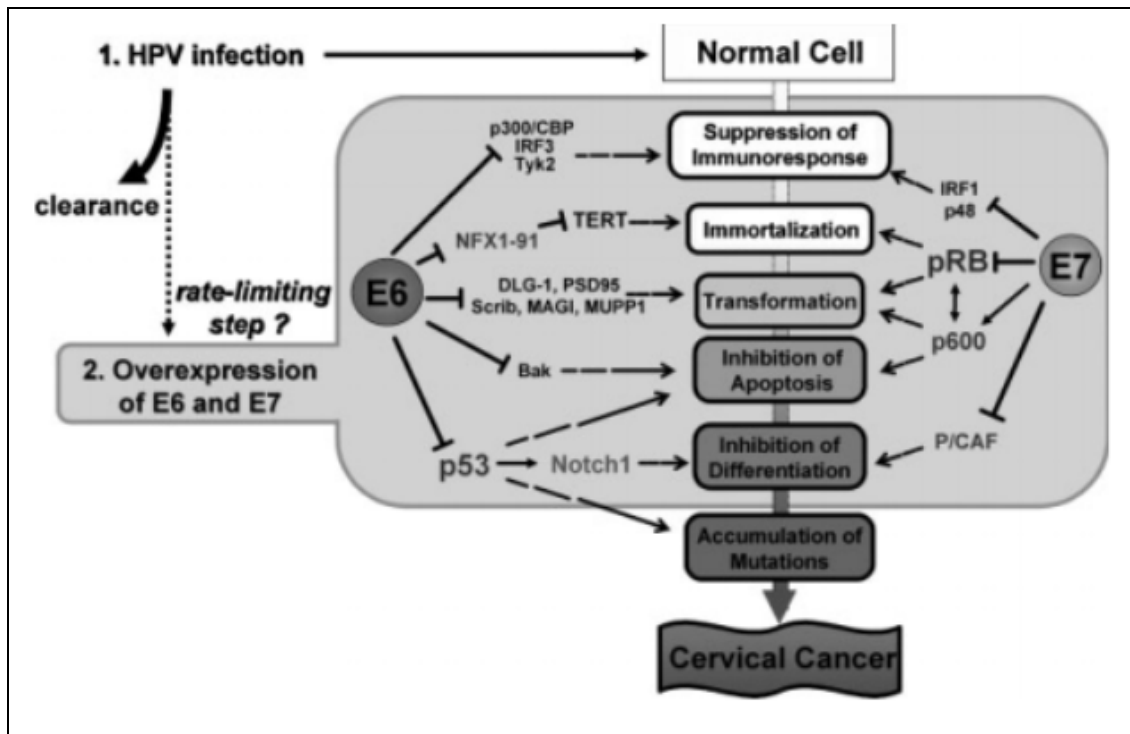


Figure 1.9. Cellular pathways modulated by the HPV E6 and E7 oncoproteins. Upon infection with HPV, the E6 and E7 oncoproteins are expressed to a low level and target proteins important for initiating an immune response. After persistent infection, the HPV genome eventually integrates into the host DNA and there is a concomitant overexpression of E6 and E7. E6 and E7 modulate many pathways for immortalizing the infected cells, inducing their transformation, and apoptosis. Such infections generally result in cancer. The main targets of these oncoproteins are p53 and pRb, as discussed in the text. This figure has been adapted from Yugawa et al. 2009.

1.4.4 Inactivation of pRb and p53 by Viral Oncoproteins

pRb and p53 are the main cellular targets of the human papillomavirus oncoproteins, E7 and E6, respectively. pRb and p53 are found to be deregulated by a number of other DNA tumor viruses as well, which have developed mechanisms to ensure viral replication in a host cellular environment. pRb is a target for inactivation by the viral oncoproteins E1a, E7 and T-antigen from adenovirus, human papillomavirus (HPV), and simian virus 40, respectively, listed in [Table 1.2](#). (Felsani et al., 2006). p53, on the other hand, is a target for inactivation by the E1b, E6 and T-antigen from the same respective viruses ([Table 1.2](#)).

As discussed earlier, one of the main functions of pRb is to regulate the cell cycle, apoptosis and differentiation through its direct binding to and inhibition of the E2F family of transcription factors (Harbour and Dean, 2000; Stevaux and Dyson, 2002). When phosphorylated, pRb releases E2F proteins to transcribe genes necessary for the progression into the S-phase of the cell cycle, as well as for DNA replication (Harbour and Dean, 2000; Harbour et al., 1999; Stevaux and Dyson, 2002). The viral oncoproteins act by binding to hypophosphorylated pRb, disrupting pRb/E2F complexes and thereby leading to dysregulated entry into S-phase of the cell cycle and neoplasia (Ganguly and Parihar, 2009b; Munger et al., 2001). HPV-E7 has also been implicated in the degradation of pRb (Boyer et al., 1996; Giarre et al., 2001; Gonzalez et al., 2001).

In response to deregulated entrance into the S phase of the cell cycle, p53 is normally activated, causing cells to undergo cell cycle arrest or apoptosis (Amundson et al., 1998). However, in high-risk HPV positive cells, HPV E6 forms a complex with the cellular E3 ubiquitin ligase, called E6AP (E6-Associating Protein) and targets p53 for degradation via the ubiquitin-proteasome pathway (Scheffner, 1998; Scheffner et al., 1993). Consequently, the result is a deregulation of DNA damage repair, and a growth of deregulated cells, which leads to cancer. A schematic of this process is shown in [Figure 1.10](#). The cooperation between the two viral oncoproteins, E6 and E7, promotes a cellular environment that supports viral DNA replication by stimulating the constant re-entry into S-phase and preventing p53-dependent cell cycle arrest and apoptosis.

DNA Tumor Virus	Viral Protein	Cellular Target
Human Papillomavirus	E7	pRb
	E6	p53
Adenovirus	E1A	pRb
	E1B	p53
Simian Virus 40	Large T antigen	pRb & p53

Table 1.2. Viral proteins that target pRb and p53. A summary of the different viral oncoproteins from human papillomavirus, adenovirus, and simian virus 40 are shown, along with the main cellular target (p53 or pRb).

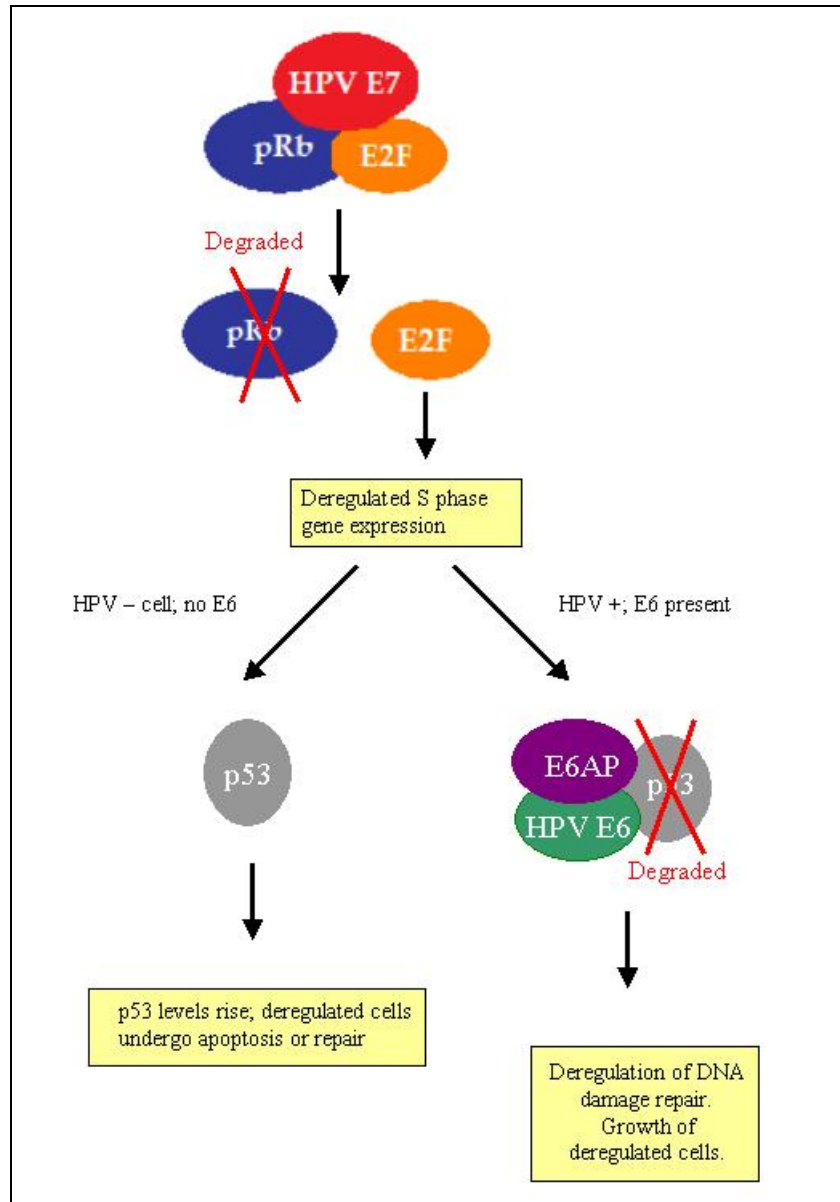


Figure 1.10. Effect of the HPV E6 and E7 oncoproteins on its two main cellular targets.

HPV E7 binds to complexes formed by pRb and E2F and breaks the complex, even in the absence of pRb phosphorylation. This results in premature displacement of E2F from pRb, and a deregulated transition into the S phase of the cell cycle. In response to problems in the cell, p53 levels rise which results in repair mechanisms, cell cycle arrest, or apoptosis. HPV E6, on the other hand, prevents p53 from performing its usual tasks by targeting it for degradation by the proteasome by way of the E3 ubiquitin ligase, E6AP.

1.5 Overview of Remaining Chapters

The remaining chapters mainly focus on our attempts to target and inhibit the main transforming activity of the E6 and E7 oncoproteins from human papillomavirus. These particular oncoproteins are our focus because they are found to be overexpressed in cancer cells where the human papillomavirus genome has been integrated into the host DNA. Additional attempts at targeting E7 and characterizing another putative target are discussed in the appendices.

More specifically, Chapter 2 focuses on a high throughput solution screen that was done to identify small molecule inhibitors that prevent the E7-mediated dissociation of pRb/E2F complexes that generally results in deregulated S-phase progression. The class of small molecule inhibitors are further characterized, and a discussion on current and future co-crystallization efforts is provided.

The use of a similar high-throughput screen will be discussed in Chapter 3, which focuses on several small molecules that were identified that prevent E6-mediated p53 degradation. These small molecules are characterized and future work is discussed.

Future prospects of HPV therapeutic design are discussed in Chapter 4. Our work on identifying E6 and E7 inhibitors, as well as on the work of others of knocking down E6 and E7 expression, help explain the consequences of our small molecule inhibitors. Chapter 4 will also discuss alternate possible therapeutic targets that might complement HPV vaccines to help eradicate the cancers caused by this virus.

Appendix A focuses on an *in silico* approach that was used to identify small molecule inhibitors that bind to the E2F binding pocket of E7. Appendix B focuses on a characterization of the E7-p300 complex.

CHAPTER 2

Identification and Characterization of Small Molecule Antagonists of pRb Inactivation by Viral Oncoproteins

2.1 Introduction

pRb is known to regulate the cell cycle, apoptosis and differentiation and it does so by regulating the E2F family of transcription factors. In particular, pRb binds to and inhibits the transcriptional activity of E2F proteins (Harbour and Dean, 2000; Stevaux and Dyson, 2002). Upon phosphorylation by cyclins/cyclin dependent kinases, pRb releases E2F which results in the transcription of genes necessary for the progression into the S-phase of the cell cycle, as well as for DNA replication (Harbour and Dean, 2000; Harbour et al., 1999; Stevaux and Dyson, 2002). E7, as well as other viral oncoproteins, act by binding to hypophosphorylated pRb, disrupting the pRb/E2F complex and thereby leading to premature entry into S-phase and neoplasia (Ganguly and Parihar, 2009a; Munger et al., 2001). Consequently, a target for treatments against HPV-induced carcinomas would be to identify compounds that inhibit the ability of HPV-E7 to disrupt pRb/E2F complexes.

While the exact mechanism by which E7 displaces E2F from pRb is not fully understood, there are a number of crystal structures of complexes formed between these proteins that give some insight into the mechanism. pRb consists of the cyclin fold domains A and B, which form the pocket of this protein, as well as a C-terminal domain that is subject to cell-cycle dependent posttranslational modifications, such as phosphorylation and acetylation, as well as the recruitment of cyclins/cyclin-dependent kinases (Figure 2.1) (Adams et al., 1999). While the pocket domain of pRb is critical for the biological activity of pRb, the C terminal domain of pRb is also needed for forming a physiological complex with E2F. Domains A and B of pRb form a groove that makes high affinity contacts with the transactivation domain of E2F; the C terminal domain of pRb binds to the marked box region of E2F with a lower affinity (Figure 2.1, Figure 2.2) (Rubin et al., 2005; Xiao et al., 2003). The transactivation domain of E2F is responsible for aiding in the transcriptional activation of genes and the marked box region is the specificity factor of E2F.

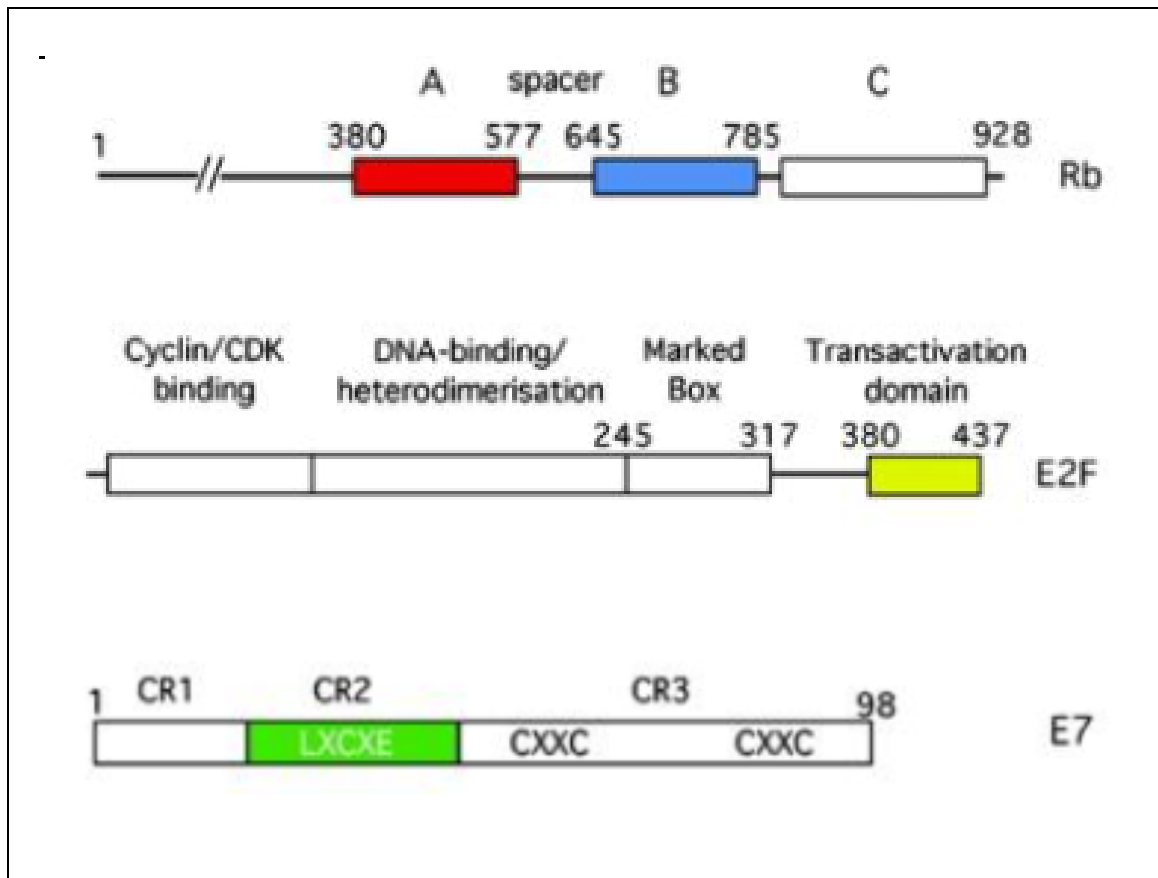


Figure 2.1. Domain architectures of pRb, E2F, and E7. pRb contains three domains: A and B, which form the pocket of this protein and the C terminal domain that is subject to posttranslational modifications. E2F contains a cyclin/CDK binding domain, a DNA binding domain, a marked box domain, and a transactivation domain. E7 contains three conserved regions: CR1, CR2, and CR3. The CR2 domain harbors the highly conserved LxCxE motif. The CR3 domain contains two CXXC motifs that are necessary for binding zinc. This figure was adapted from (Xiao et al., 2003).

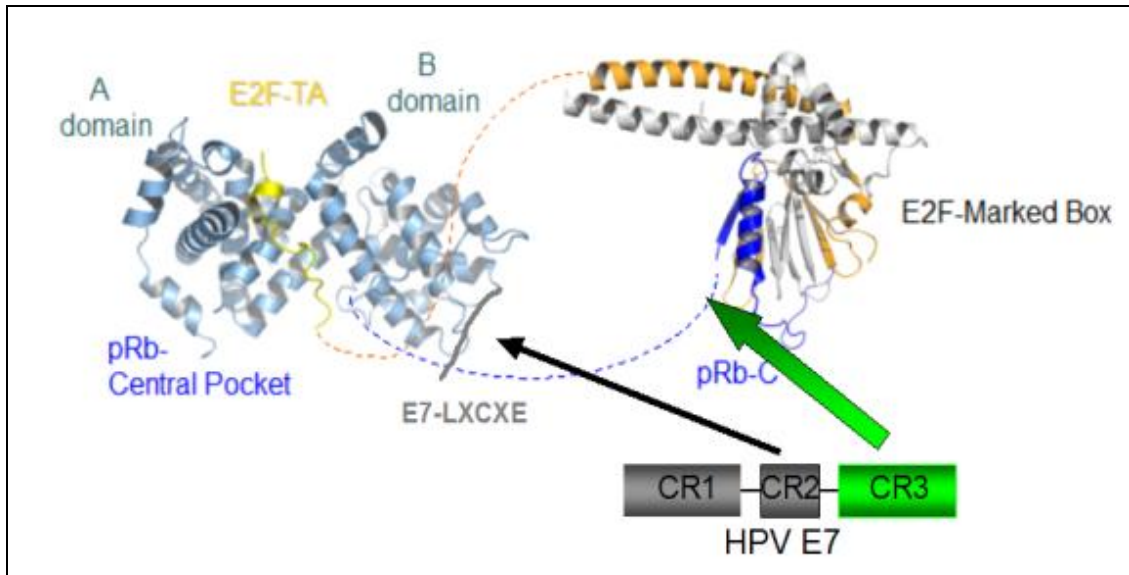


Figure 2.2. Structures of complexes formed between pRb, E2F and E7. A co-crystal structure was solved between the pRb A and B domains and the E2F transactivation domain. The transactivation domain of E2F was shown to make high affinity contacts within the groove formed by the A and B domains of pRb. The C terminal domain of pRb was solved in a separate complex with the marked box region of E2F. While the crystal structure of the CR3 domain of E7 has not been solved in complex with pRb or E2F, biochemical data suggests that it makes contacts with both proteins. The LxCxE motif has been solved in complex with pRb and shown to bind to the B domain, at an opposing face from the transactivation domain of E2F. This figure was adapted from (Xiao et al., 2003) and (Rubin et al., 2005).

The viral oncoproteins make a number of contacts with pRb. The E7 oncoprotein from HPV contains three conserved regions: CR1, CR2, and CR3 (Figure 2.1). The CR1 and CR2 domains are unstructured and functionally homologous to the corresponding domains of Adenovirus E1A and Polyomavirus large T antigen (Felsani et al., 2006). Notably, these viral oncoproteins share a highly conserved LxCxE motif, found in the CR2 domain of E7 (Figure 2.3) (Felsani et al., 2006). The LxCxE motif from viral oncoproteins contribute to disruption of the pRb/E2F complexes by binding to the pRb B domain (Lee et al., 1998). The C-terminal domain of pRb, which is important for the formation of pRb-E2F complexes, is the target of other regions of the viral oncoproteins (Felsani et al., 2006). The CR3 domain of E7 is the zinc-finger domain that makes contacts with pRb and E2F, although the affinities of these interactions are much lower. Interestingly, this zinc-finger domain is not found in the other viral proteins, suggestive that the viral oncoproteins displace E2F from pRb by different mechanisms.

The structure of the pRb pocket domain has been solved in complex with a nine-residue peptide from HPV E7 containing the highly conserved LxCxE motif (Lee et al., 1998). The peptide binds in an extended conformation on the B pocket. The Leu, Cys, and Glu residues point towards the inner part of the groove, making contacts with pRb residues (Figure 2.4) (Lee et al., 1998). The reported dissociation constant of this interaction is approximately 110nM. While the structure of the LxCxE motif of CR2 domain of E1A has not been solved in complex with pRb, it is suggested to bind to the same region.

Interestingly, the CR1 domain of E1A has been shown to compete with E2F for pRb binding: it binds to the same groove between the A and B domains of pRb that the transactivation domain of E2F binds (Liu and Marmorstein, 2007). The mechanism of E1A mediated E2F displacement has been suggested to be a two-step process: first, the CR2 domain of E1A, containing the highly conserved LxCxE motif, drives the initial reaction of ternary complex formation (E1A-pRb-E2F), and second, the increased local concentration of the CR1 domain of E1A proximal to pRb causes the CR1 domain to compete with E2F for binding, thereby causing a dissociation of the complex (Fattaey et al., 1993; Ikeda and Nevins, 1993). Briefly, this suggests

that the LxCxE motif containing domain of E1A acts to recruit the other region necessary for E2F displacement. Although a structure of the CR3 domain of E7 in complex with pRb and E2F has not yet been determined, it is possible that E7 acts in a similar way in that its LxCxE motif containing domain acts to recruit the CR3 domain of E7 to pRb-E2F complexes, to then aid in the dissociation of the complex.

High risk HPV-E7 is a particularly attractive protein target for treatments against HPV-induced carcinomas since it is one of the cancer-causing oncoproteins from this virus and it has no human ortholog. To date, there are no treatments for existing HPV infection leading to nearly all cervical cancers and 20% of head and neck cancers. Furthermore, there are no known small molecule inhibitors that target HPV-E7. Consequently, we sought to identify compounds that inhibit the ability of HPV-E7 to disrupt pRb/E2F complexes.

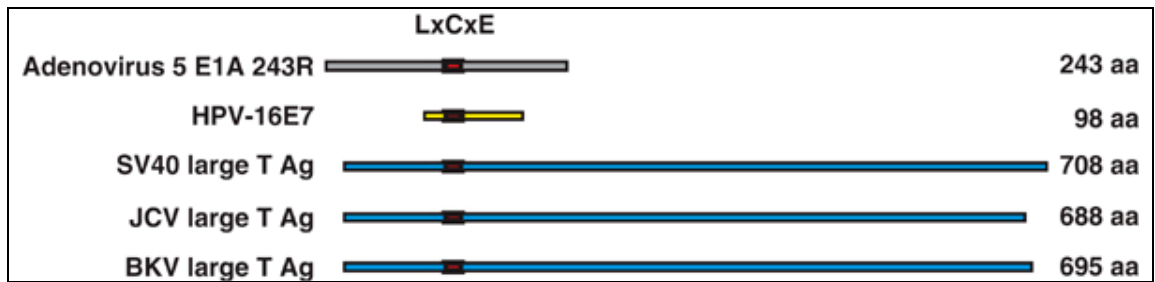


Figure 2.3. Alignment of viral proteins. Viral proteins from adenovirus, human papillomavirus (HPV), simian virus 40 (SV40), JC virus (JCV), and BK virus (BKV) are aligned by the highly conserved LxCxE motif. This figure was adapted from (Felsani et al., 2006)

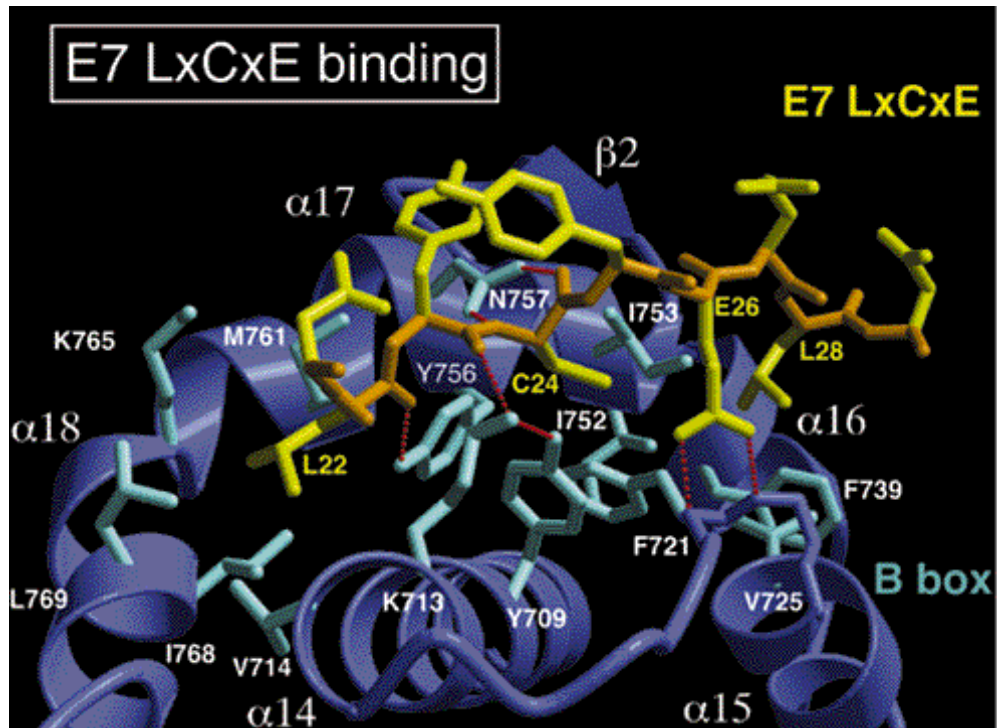


Figure 2.4. Ribbon and stick figure of the pRb-E7 complex. A nine residue peptide from HPV 16 E7, containing the highly conserved LxCxE motif, was solved in complex with the pRb A and B domains. The peptide was shown to bind to the B domain. The Leu, Cys, Glu residues point into the groove and make contacts with residues from pRb. This figure was adapted from (Lee et al., 1998).

2.2 High-Throughput Screening Results

2.2.1 Identification of HPV-E7 Inhibitors Using a High-Throughput Solution Screen

Approximately 88,000 compounds from several diverse small molecule libraries (Table 2.1) were screened to search for inhibitors that prevent E7-mediated displacement of E2F from pRb. The protein constructs that were employed include: 6xHis-HPV16-E7_{CR2-3} (residues 17-98) harboring conserved regions 2 and 3 and the LxCxE motif of HPV-E7 (Figure 2.5), GST-pRb_{ABC} (residues 376-928) harboring the A/B pocket domain and C-terminal region of pRb and untagged E2F_{MB-TA} (residues 243-437) containing the marked-box and transactivation domains of E2F that make pRb contact. 6xHis-HPV16-E7_{CR2-3} was modified to improve its solubility and reduce its tendency to aggregate by substituting two nonconserved cysteine residues in its CR3 domain to the corresponding residues found in low-risk HPV1A-E7 (Figure 2.5). This mutated form of E7 was confirmed to be properly folded according to its elution profile on gel filtration (data not shown), and it exhibited the ability to bind specifically to pRb and dissociate pRb/E2F complexes, as expected (Figure 2.6). Furthermore, it is expected that this mutant binds with the same affinity as the wild-type E7 because the mutations are in the CR3 domain, which binds more weakly to pRb than the LxCxE motif.

The assay used for screening employed an enzyme-linked immunosorbance assay (ELISA) as illustrated in Figure 2.7. A GST-pRb_{ABC}/E2F_{MB-TA} complex was bound to a glutathione-coated 384-well microtiter plate and incubated with 6xHis-HPV16-E7_{CR2-3} in the presence of 1% DMSO (negative control) or 10 μ M of compound dissolved in DMSO. Compounds that inhibit HPV-E7-mediated disruption of pRb/E2F complexes maintain E2F bound to the plate through pRb. Therefore, following plate washing, the amount of E2F remaining bound to the plate, as quantified by a bioassay, is correlated to the potency of the compound in inhibiting HPV-E7-mediated disruption of pRb/E2F complexes.

Library	# Compounds	# Cherry Picks	Hit Percentage	ELISA IC₅₀ < 15.6µM
Spectrum	2,000	11	0.55%	3
Maybridge HitFinder	14,400	32	0.22%	13
OPS, set 9	7,952	50	0.63%	16
OPS, sets 3-6, 10, 12-14	63,587	271	0.43%	88
Total	87,939	364	0.41%	120

Table 2.1. Chemical libraries employed and hits obtained for HPV-E7 inhibitor solution screen. Names of the libraries screened, their size, and the number of hits from each screen are listed. Cherry picks: Number of potential inhibitor compounds from initial screening. Hit percentage: ratio of the number of compounds cherry picked to the total number of compounds in that given library. The right-most column lists the number of compounds with IC₅₀s less than 15.6 µM.

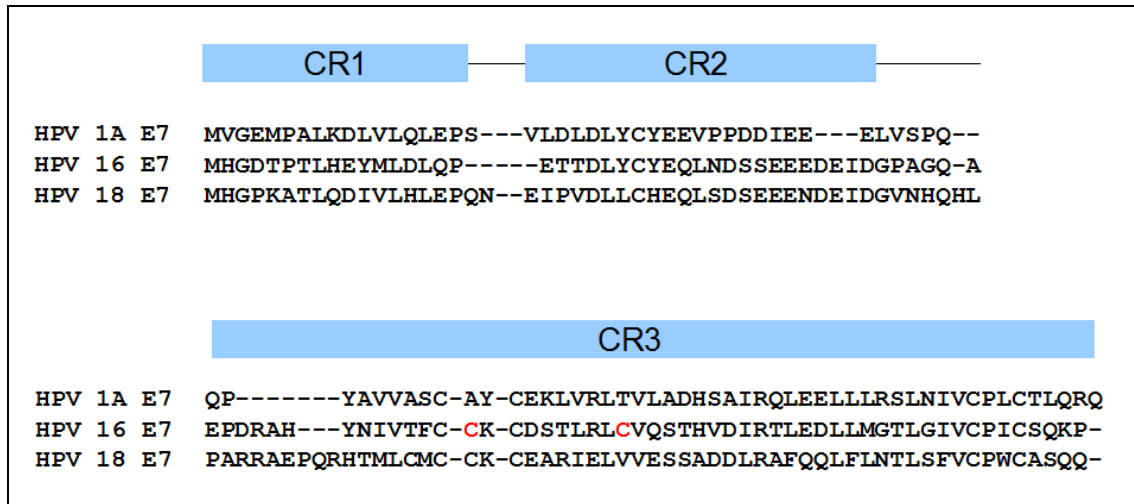


Figure 2.5. Wild-type and mutant recombinant proteins used in biochemical experiments.

Sequence alignment of E7 from HPV 1A, HPV 16, and HPV 18 used in the experiments. The two residues in red in HPV 16 E7 were mutated to the corresponding residues in HPV 1A E7 for use in the biochemical experiments. The first cysteine of HPV 16 E7 was mutated to an alanine; the second cysteine was mutated to a threonine.

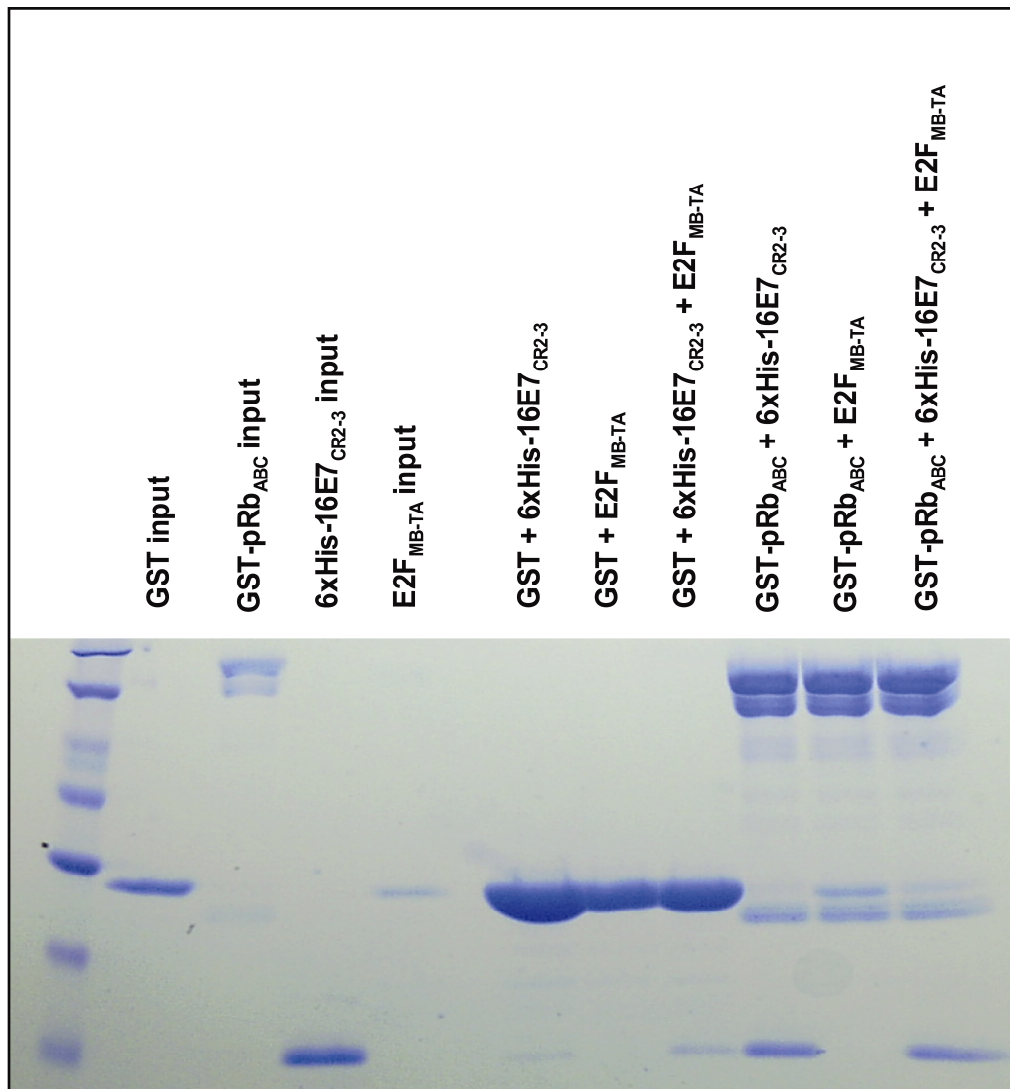


Figure 2.6. Pull downs of recombinant proteins used in biochemical experiments.

GST-pull downs were done between 6xHis-HPV16-E7_{CR2-3} (residues 17-98) containing the two mutations and GST-pRb_{ABC} (residues 376-928) or GST in the presence or absence of E2F_{MB-TA} (residues 243-437). 6xHis-HPV16-E7_{CR2-3} (residues 17-98) containing the two mutations was observed to be functional: it maintained specific binding to GST-pRb_{ABC} and the ability to displace E2F_{MB-TA} from GST-pRb_{ABC}.

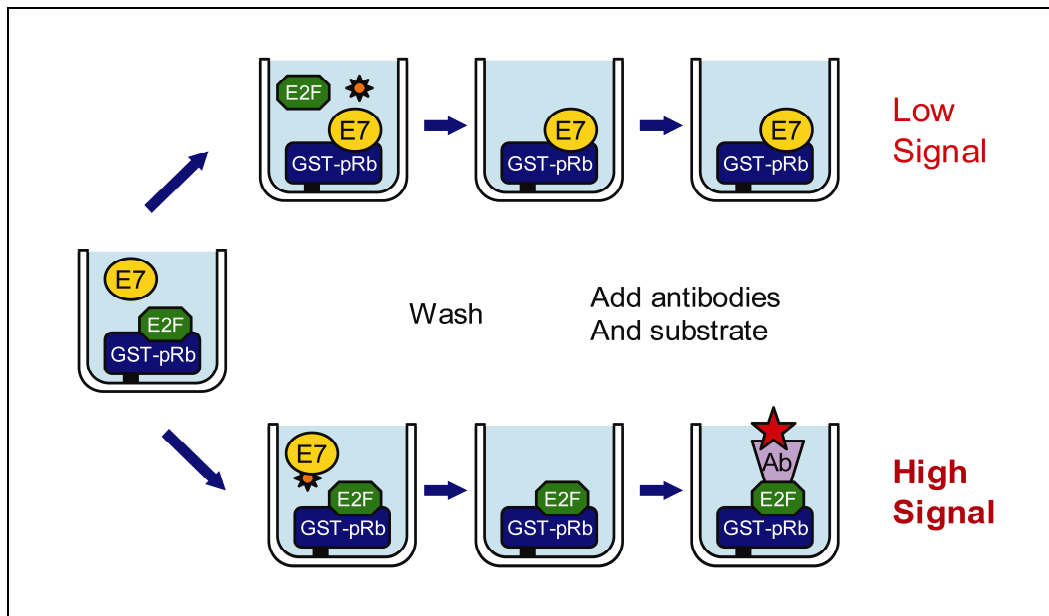


Figure 2.7. Method of high-throughput screening for HPV E7 inhibitors. Illustration of the ELISA-based-assay used for high-throughput screening. The assay is described in detail in the text.

The linear range of the assay was first determined by titration experiments measuring the amount of E2F remaining bound after incubation of the GST-pRb_{ABC}/E2F_{MB-TA} complex with serial dilutions of 6xHis-HPV16-E7_{CR2-3}. Based on these studies, we used 500nM 6xHis-HPV16-E7_{CR2-3} in the drug screening assays to ensure that compounds that blocked HPV-E7 association to pRb would be detected (Figure 2.7). The Z'-factor parameter was used to assess the robustness of the assay during automation in a 384-well format (details are provided in the Methods section). A three day replicate plate experiment consistently yielded Z'-factors between 0.62 and 0.71 indicating that the assay was sufficiently robust for valid drug screening (Zhang et al., 1999). Data from one plate is given in Figure 2.8.

The initial screen resulted in the identification of 364 small molecule HPV-E7 inhibitors. Using liquid stock from the libraries used for screening, we re-tested the activity and potency of all 364 candidate inhibitors in the primary screening assay. These re-test experiments confirmed the activity for 120 of the 364 with IC₅₀ values of 15.6 μM or lower. The remaining 244 compounds either did not show reproducible inhibition, or were not sufficiently potent and were discarded from further analyses (Table 2.1). The 120 confirmed actives were then tested in secondary assays as described below to identify those with selective pharmacological activity in cells. A summary of the process for the identification of confirmed screening hits is shown in Figure 2.9. Key information for interpreting and repeating this screen are given in Table 2.2.

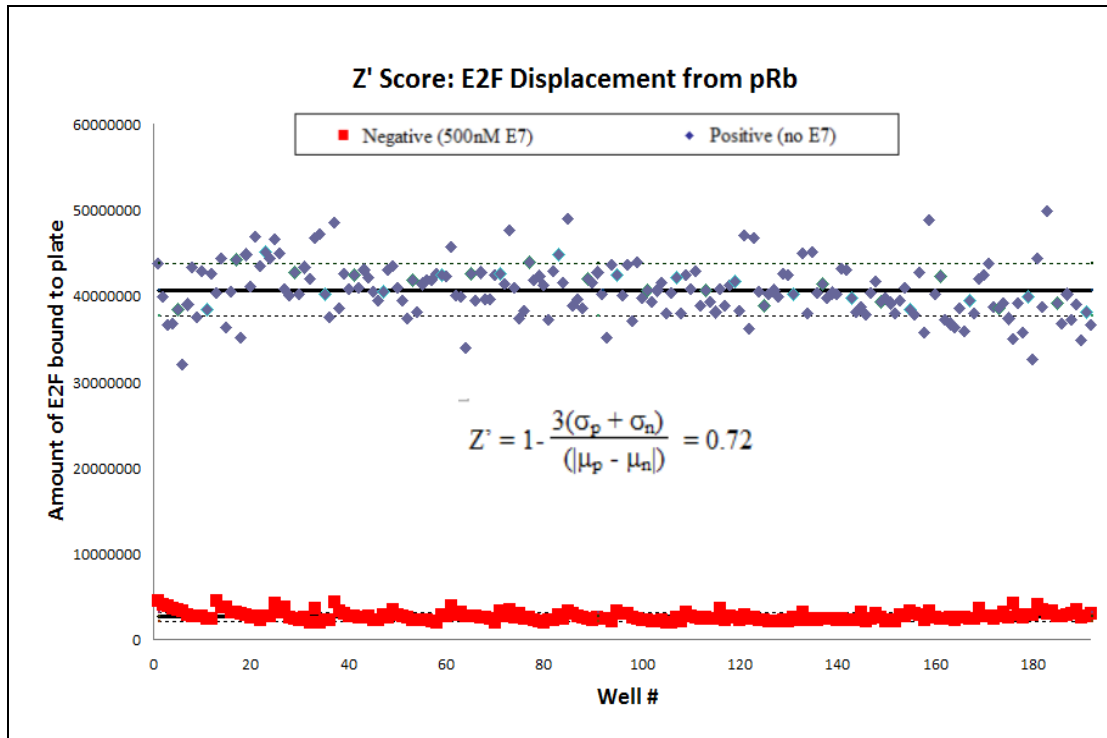


Figure 2.8. Z' Score graph. A representative Z' factor graph is shown for a 384 well plate: 192 positive control (GST-pRb_{ABC} + E2F_{MB-TA}) wells, 192 negative control (GST-pRb_{ABC} + E2F_{MB-TA} + His-HPV16-E7_{CR2-3}) wells. The Z' factor was calculated according to Zhang et al, 1999.

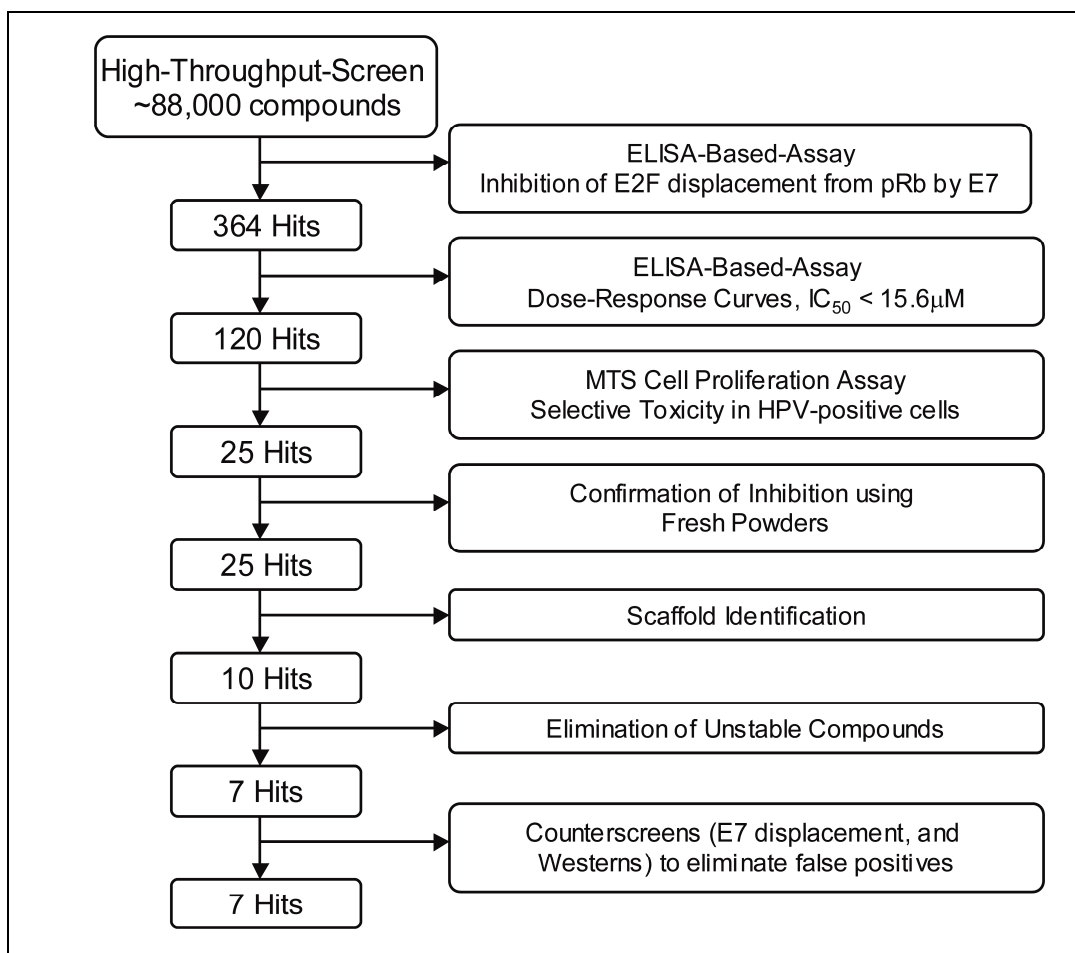


Figure 2.9. Method of high-throughput screening for HPV E7 inhibitors. Flowchart of the steps of inhibitor identification and validation.

Category	Parameters	Details
Assay	<p>Nature of assay</p> <p>Assay strategy</p> <p>Assay protocol</p>	<p>ELISA-based <i>in vitro</i> assay</p> <p>Detection of E2F remaining bound to GST-pRb on a glutathione coated plate after addition of E7 and compound; E2F specific antibodies were used to quantify E2F</p> <p>Key steps are outlined in supplemental procedures</p>
Libraries screened	<p>Nature of the libraries</p> <p>Name, size, and source of libraries</p> <p>Details</p>	<p>All libraries tested were rule of 5-compliant</p> <p>Spectrum Collection from MicroSource Discovery Systems, Inc (Gaylordsville, CT) - 2000 compounds (1 compound per well); Maybridge HitFinder (Cambridge, UK) - 14,400 compounds (5 compounds per well); Orthogonally Pooled Screening (OPS) libraries, (Lankenau Chemical Genomics Center (LCGC), Wynnewood, PA) - 71,539 compounds (10 compounds per well)</p> <p>Details on libraries can be found at each company's website: (Spectrum: http://www.msdiscovery.com/spectrum.html, Maybridge: http://www.maybridge.com/portal/alias__Rainbow/lang__en/tabID__229/DesktopDefault.aspx, and</p>

	<p>Quality control</p> <p>Concentration tested</p>	<p>LCGC: http://www.lcgcinc.com/technology</p> <p>Spectrum, Hitfinder, and OPS compounds assured by vendors as >95% pure, >90% pure, and > 85% pure, respectively. Random LC/MS analysis of screening hits from these libraries confirmed identity >90%.</p> <p>Spectrum compounds tested at 8.3µM; Maybridge compounds tested at 12.5µM; OPS compounds tested at 6.25µM to 12.5µM</p>
HTS process	<p>Format</p> <p>Plate controls</p> <p>Plate number/duration</p> <p>Dispensing systems</p>	<p>384-well white glutathione-coated plates (Fisher Scientific)</p> <p>Positive controls: GST-pRb_{ABC}/E2F_{MB-TA} + DMSO in columns 1 and 23 and negative controls: GST-pRb_{ABC}/E2F_{MB-TA} + 16E7_{CR2-3}/DMSO in columns 2 and 24 in each plate. Uniformity plates (192 positive controls, and 192 negative controls) were distributed throughout the screening plates to ensure both assay and result reliability.</p> <p>Up to 30 plates were screened per day. Entire screen completed in 4 days</p> <p>Compounds delivered using Janus MDT (Perkin Elmer) liquid pipetting station, other reagents</p>

	<p>Output, detector, analysis software</p> <p>Normalization</p> <p>Performance</p>	<p>delivered using Biotek Microfill, washes done with Biotek automated washer</p> <p>Chemiluminescence read using an Envision multilabel plate-reader (Perkin Elmer). Software applications developed by CeuticalSoft (OpenHTS) were used to deconvolute the data</p> <p>The signal from each well was normalized to the negative controls on each plate using $Z = (\chi - \mu) / \sigma$, where χ is the chemiluminescence signal of a given well, μ is the mean of the negative control population, and σ is the standard deviation of the negative control population.</p> <p>Z and Z' plotted per plate. Compounds giving a chemiluminescence signal higher than 3 standard deviations above the mean were considered hits.</p>
Post-HTS analysis	<p>Selection of actives</p> <p>Retesting of initial actives</p> <p>Purity confirmation</p>	<p>Actives were selected from the primary screen using a threshold based on statistical criteria</p> <p>Original samples rearrayed and retested using screening assay in dose-response mode</p> <p>Purity verified by LC/MS after purchase of powders NMR was done to verify structure of representative inhibitor</p>

	Compound purchase/resynthesis	Validated compounds were repurchased from original suppliers
Screen results	Screening positives	List of positives were ranked by % inhibition of E2F displacement and by a defined cutoff threshold
	Validated compounds	Rank order of compounds, based on IC ₅₀ values determined upon retesting of actives
	Comments on active compounds selection	Potency, selective cellular toxicity in human papillomavirus containing cells, compound purity, and other pharmacological parameters such as stability used to rank actives

Table 2.2. Parameters for small-molecule screening data. Information on the format of the high-throughput screening assay, the libraries screened and instrumentation used, the high-throughput screening process, how the screening data was analyzed, and how the final hits were determined is given.

2.2.2 A Family of Thiadiazolidinedione Compounds are Selective for HPV 16-Transformed Cells

To reduce the number of compounds from the primary screen for further characterization, the 120 confirmed hits with IC_{50} values $< 16\mu M$ from the primary screen were assessed for their ability to be cytotoxic or to inhibit proliferation of cervical cancer cells either transformed with HPV16 (SiHa) or not (C-33A) (Yee et al., 1985). The metabolic viability of cells was measured using an MTS assay (3-(4,5-dimethylthiazol-2-yl)-5-(3-carboxymethoxyphenyl)-2-(4-sulfophenyl)-2H-tetrazolium). Compounds were tested at a concentration range of $25\mu M$ to $100nM$. Staurosporine, a non-specific kinase inhibitor, was used as a positive control because it was expected to be toxic in all cells (Ruegg and Burgess, 1989). The 120 confirmed hits were incubated with cells for 48 hours prior to the addition of MTS reagent. The absorbance at 490nm was determined within 3 hours of incubation with MTS reagent. Out of the 120 compounds tested, 25 were either selectively cytotoxic or selectively prevented proliferation of SiHa cells (HPV 16 positive) and not C-33A (HPV negative) cells at concentrations at or below $6\mu M$ (data not shown).

Of the 25 compounds that were selectively cytotoxic or prevented proliferation of SiHa cells, seven shared a similar thiadiazolidinedione ring scaffold attached to a phenyl ring with various substitution patterns attached (Table 2.3) and had IC_{50} values in the ELISA assay that ranged between $0.34 - 7.6\mu M$ (Figure 2.10 and Table 2.3). The remaining compounds were eliminated from further studies due to a variety of reasons including poor reproducibility in activity, significant impurities, and/or structural features suggestive of reactivity, aggregation or other non-specific mechanisms (Table 2.4). Consequently, our studies focused on characterizing the mechanism of inhibition for the seven thiadiazolidinedione compounds listed in Table 2.3. The purity and integrity of these seven compounds, ordered as powders, was confirmed by LC/MS studies and 1H NMR of a representative compound (Table 2.5).

Some structure-activity relationship (SAR) information can be extracted for the seven thiadiazolidinedione compounds. In most of the compounds, there is a phenyl group with various substituents attached at the G2 position (Table 2.3). Interestingly, compound 478419 has a

phenyl group at the G1 position instead of G2. Given that the compounds are pseudo symmetric, it is possible that the phenyl group at the G1 position of compound 478419 may compensate for the phenyl group at the G2 position of the other compounds. This suggests that there may be at least two orientations for the thiadiazolidinedione compounds that allow the phenyl ring to occupy the same binding pocket of its protein target and inhibit HPV-E7. A number of other structural analogs were also tested for inhibition in the ELISA assay ([Table 2.6](#)). These analogs had the sulfur in the heterocycle ring changed to either a carbon, or oxygen, and showed no activity ([Table 2.6](#)). This data suggests that the S heterocycle is necessary for activity, possibly because the larger sulfur atom distorts the ring in such a way to facilitate hydrogen bonding by the oxygens to its protein target or that the S heterocycle has some reactivity that supports activity that the C or O analogs do not.

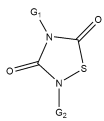
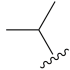
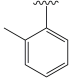
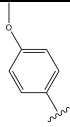
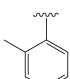
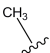
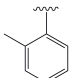
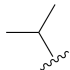
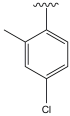
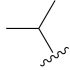
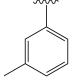
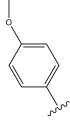

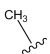
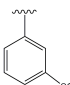
	16E7 (500nM) (μM)	1AE7 (500nM) (μM)	E1A (100nM) (μM)	K_D (μM) (to pRb)	G_1	G_2	LCGC ID
pRb/E2F	7.6 ± 1.2	10.6 ± 1.3	2.8 ± 2.2				478081
pRb	11.2 ± 1.3	7.9 ± 2.1	5.0 ± 1.8	0.165 ± 0.052			
pRb/E2F	2.2 ± 1.6	3.5 ± 1.6	0.64 ± 2.3				478165
pRb	0.57 ± 1.2	3.0 ± 2.3	2.6 ± 1.3	0.104 ± 0.025			
pRb/E2F	1.9 ± 1.3	4.5 ± 1.7	0.24 ± 2.0				478166
pRb	0.50 ± 1.5	3.4 ± 2.0	1.0 ± 2.1	0.106 ± 0.034			
pRb/E2F	3.2 ± 1.3	5.5 ± 1.7	1.3 ± 2.2				478168
pRb	4.5 ± 1.5	4.7 ± 2.1	3.8 ± 1.5	0.187 ± 0.022			
pRb/E2F	4.6 ± 1.3	5.5 ± 1.5	1.1 ± 2.5				478337
pRb	3.2 ± 1.3	5.5 ± 2.7	3.5 ± 1.7	0.210 ± 0.051			
pRb/E2F	2.3 ± 1.6	3.3 ± 1.6	1.7 ± 2.7				478419
pRb	0.40 ± 1.4	1.3 ± 1.3	7.7 ± 1.7	0.381 ± 0.031			
pRb/E2F	0.34 ± 1.9	3.5 ± 1.7	3.2 ± 2.7				478726
pRb	0.29 ± 1.7	4.0 ± 2.5	2.8 ± 2.1	0.815 ± 0.070			

Table 2.3. Compound structures, IC_{50} values, and dissociation constants. ELISA IC_{50} 's for compounds to inhibit viral-mediated disruption of pRb/E2F complexes and for disrupting pRb/viral oncoprotein complexes is given as is their dissociation constants in binding pRb, from ITC.

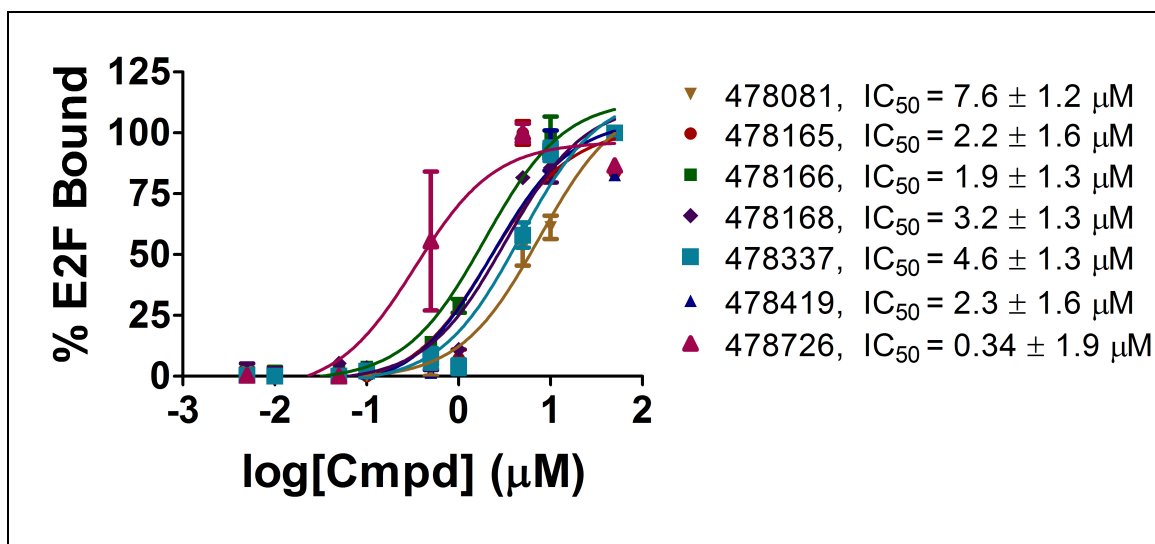
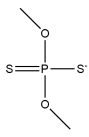
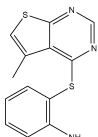
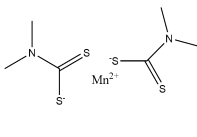
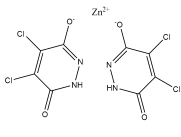
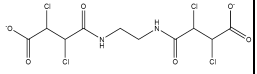
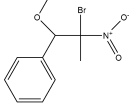
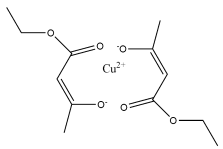
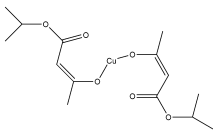
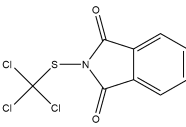
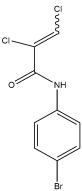
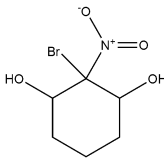
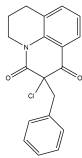
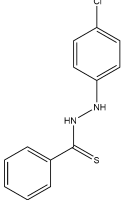
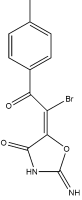
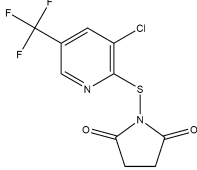


Figure 2.10. IC₅₀ curves for disruption of pRb/E2F complexes by E7 in the presence of a family of thiadiazolidinedione compounds. IC₅₀ curves were generated using the ELISA-based assay described in the Methods. Ten-fold dilutions of inhibitor, starting at 100μM were added to a mixture containing GST-pRb_{ABC}/E2F_{MB-TA} and 6xHis-HPV16-E7_{CR2-3}. The amount of E2F_{MB-TA} remaining was determined by adding a primary antibody specific for E2F1.

ID	819	1359	2396	2401
Structure				
IC ₅₀ (μM)	2.2 ± 3.5	8.5 ± 1.4	< .02	1.6 ± 5.6
ID	2562	5951	6113	6197
Structure				
IC ₅₀ (μM)	4.6 ± 1.2	0.67 ± 5.2	7.2 ± 1.4	12.3 ± 1.3
ID	22724	26009	35307	108618
Structure				
IC ₅₀ (μM)	0.070 ± 6.3	1.0 ± 4.5	15.6 ± 13.5	6.5 ± 3.0
ID	140349	290579	279583	
Structure				
IC ₅₀ (μM)	4.2 ± 10.9	15.6 ± 5.4	< .02	

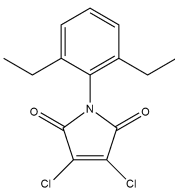
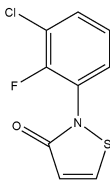
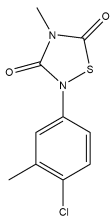
ID	2322	12482	478960	
Structure				
IC ₅₀ (μM)	10.7 ± 1.4	1.3 ± 1.4	2.5 ± 2.0	

Table 2.4. Structures and IC₅₀ values of HPV-E7 inhibitors not pursued further in this study. Several of these compounds were shown to lose activity in the ELISA assay after repeated experiments. The remaining compounds had significant impurities, and/or structural features suggestive of reactivity, aggregation or ability to inhibit by non-specific mechanisms.

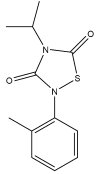
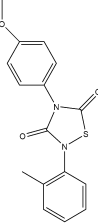
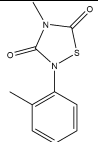
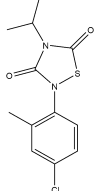
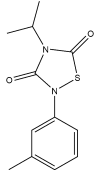
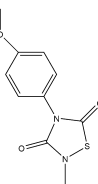
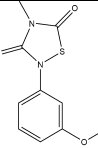
ID	Structure	Purity	Retention Time (min)
LCGC12 478081		92.7%	4.27
LCGC12 478165		89.8%	4.17
LCGC12 478166		80.5%	3.58
LCGC12 478168		94.7%	4.67
LCGC12 478337		96.8%	4.50
LCGC12 478419		91.2%	3.15 ¹ H NMR (500 MHz, CDCl ₃) δ 3.27 (s, 3H), 3.83 (s, 3H), 7.00 (d, 2H, J = 9.1 Hz), 7.27 (d, 2H, J = 9.1 Hz)
LCGC10 478726		97.8%	3.18

Table 2.5. Purity of the Seven Thiadiazolidinedione Inhibitors. Purity was determined by LC/MS. The identify of one representative compound was confirmed by NMR.

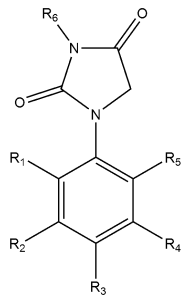
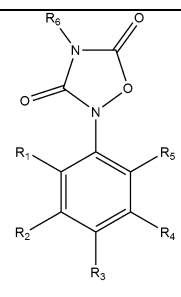
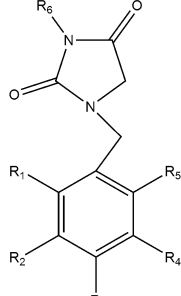
Modifications to Compound			Compound ID/Company
	$R_3 = \text{CH}_3$	$R_6 = \text{H}$	5483026 (Chembridge)
	$R_2 = \text{CH}_3$	$R_6 = \text{H}$	5485426 (Chembridge)
	$R_3 = \text{OCH}_3$	$R_6 = \text{H}$	5485607 (Chembridge)
	$R_3 = \text{Cl}$	$R_6 = \text{H}$	5491463 (Chembridge)
	$R_1 = \text{CH}_3$	$R_6 = \text{H}$	5671776 (Chembridge)
	$R_3 = \text{CH}_3$	$R_6 = \text{CH}_2\text{COOH}$	9032081 (Chembridge)
		$R_6 = \text{Ph-H}$	BTB11141 (Maybridge)
	$R_2, R_3 = \text{Cl}$	$R_6 = \text{CH}_3$	44234 (LCGC)
	$R_2 = \text{CF}_3$	$R_6 = \text{CH}_3$	77333 (LCGC)
	$R_1 = \text{Cl}$	$R_6 = \text{CH}_3$	55683 (LCGC)

Table 2.6. Inactive Analogs. The structures of the thiazolidinedione analogues that showed no detectable activity as HPV-E7 inhibitors are shown, along with the company they were purchased from.

2.2.3 The HPV-E7 Inhibitors Function to Disrupt HPV-E7 Interaction With pRb

Since HPV-E7 interacts with both pRb and E2F for disruption of the pRb/E2F complex, we sought to confirm that the seven active compounds inhibited HPV-E7 activity by directly disrupting HPV-E7 interactions with pRb (Liu et al., 2006b; Munger et al., 2001). For these experiments, we modified the ELISA assay to measure the amount of 6xHis-HPV16-E7_{CR2-3} remaining bound to pRb. We found that an increase in compound concentration led to a displacement of 6xHis-HPV16-E7_{CR2-3} from GST-pRb_{ABC}, suggesting that the compounds prevent the interaction between these two proteins (Figure 2.11). To eliminate potential artifacts from this assay format, we tested the ability of the HPV-E7 inhibitors to disrupt HPV-E7/pRb interaction by performing pull-downs on Ni-NTA beads using His-pRb_{ABC} and GST-tagged full length 16E7 (GST-16E7_{FL}) (Figure 2.12). Consistent with the ELISA assay, the pull-down assay shows that an increase in compound concentration leads to a displacement of GST-E7_{FL} from His-pRb_{ABC}. The IC₅₀ values for the amount of respective compound required for 6xHis-HPV16-E7_{CR2-3} displacement from GST-pRb_{ABC}, as determined by the ELISA assay, were within ten-fold of the corresponding IC₅₀ values of E2F displacement from GST-pRb_{ABC} in the presence of 6xHis-HPV16-E7_{CR2-3} (Table 2.3). These data are consistent with the observation that preventing HPV-E7 binding to pRb inhibits its ability to displace E2F from pRb (Liu et al., 2006b; Munger et al., 2001).

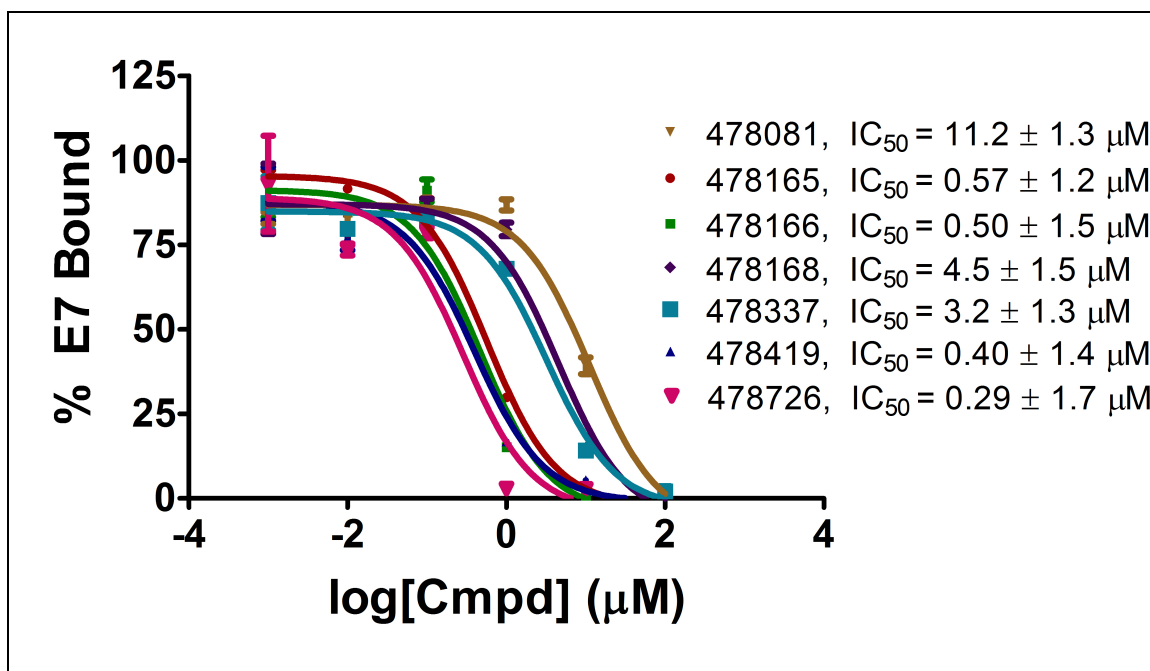


Figure 2.11. IC₅₀ curves for inhibitor disruption of HPV-E7/pRb complexes. IC₅₀ curves were generated using the ELISA assay with ten-fold dilutions of inhibitor, starting at 100μM, which were added to a mixture containing GST-pRb_{ABC} and 6xHis-HPV16E7_{CR2-3}. The amount of E7 remaining was determined by adding a primary anti-His antibody.

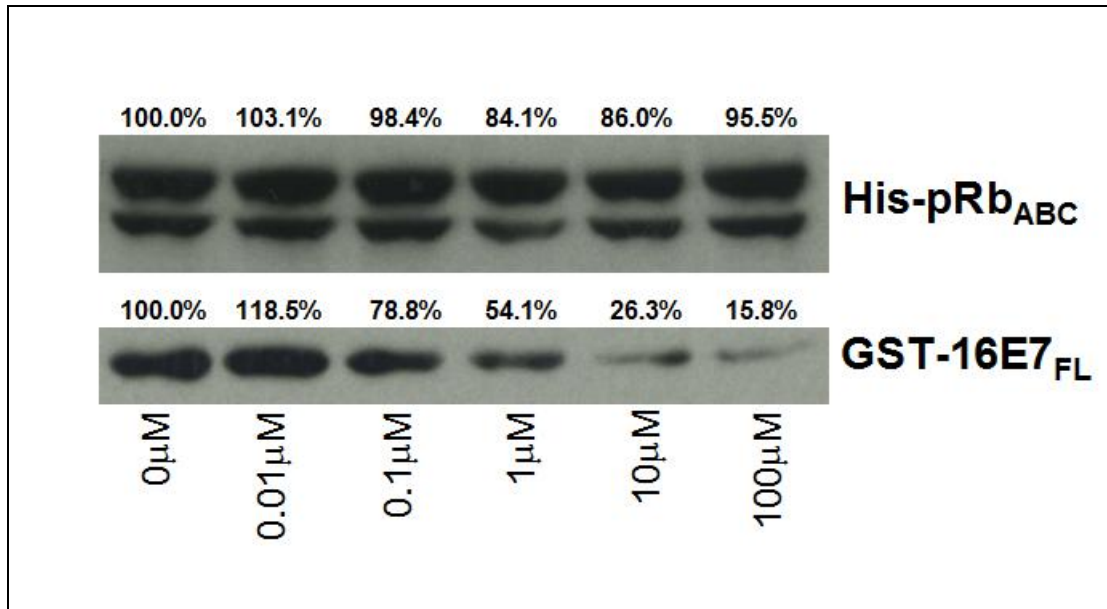


Figure 2.12. Effect of inhibitors on HPV-E7/pRb pull-downs. Different concentrations of inhibitor (compound 478166 is shown) were added and the amount of GST-E7_{FL} remaining bound to pRb was probed by using an anti-GST antibody (bottom panel). The top panel shows the loading control of His-pRb_{ABC} in each lane.

2.2.4 *The HPV-E7 Inhibitors Function by Binding to pRb Through the LxCxE Binding Motif of Viral Oncoproteins*

Since HPV-E7 mediates high affinity pRb binding through the association of its LxCxE motif in its CR2 domain to the B domain of pRb, we hypothesized that the HPV-E7 inhibitors might bind to either the LxCxE motif of HPV-E7 or the B-domain of pRb. To distinguish between these possibilities, we assayed the ability of the thiadiazolidinedione compounds to inhibit the ability of other LxCxE containing viral oncoproteins from disrupting E2F/pRb complexes: HPV-E7 from a low risk HPV form (type 1A) and Adenovirus E1A proteins. E1A was used as a control because it does not dimerize in solution, unlike E7, and has also been shown to displace E2F via a different mechanism (Felsani et al., 2006). For these studies, we modified our ELISA assay to measure disruption of E2F/pRb complexes by substituting 6xHis-HPV1AE7_{CR2-3}, and 6xHis-Ad5E1A_{CR1-3}. As illustrated in [Figure 2.13](#) and [Table 2.3](#), the thiadiazolidinedione compounds show similar levels of inhibition as they did in the presence of 6xHis-HPV16E7_{CR2-3}. The ability of the compounds to prevent an interaction between either 6xHis-HPV1AE7_{CR2-3} or 6xHis-Ad5E1A_{CR1-3} with GST-pRb_{ABC} was also demonstrated ([Figure 2.14](#)). The IC₅₀ values from these experiments ranged from 0.2-11.2 μ M, comparable to the IC₅₀ values for compound inhibition of HPV-16E7 mediated inhibition of E2F/pRb complexes ([Table 2.3](#)). These data suggest that the thiadiazolidinedione inhibitors disrupt the interaction between the pRb B domain and the LxCxE motif of the viral oncoproteins.

Because the LxCxE motif from the viral oncoproteins is likely to be extended and flexible when not in complex with partner proteins, we postulated that the small molecule thiadiazolidinedione inhibitors interact with the structured pRb B domain (Lee et al., 1998). To test this hypothesis, we assayed the ability of the HPV-E7 inhibitors to bind directly to a truncated pRb protein construct containing the A and B domains of the pRb pocket (pRb_{AB}) using isothermal titration calorimetry (ITC). The resulting integrated heat-flow spikes confirmed direct binding of inhibitors to pRb with 1:1 stoichiometry and affinities in the sub-micromolar range ([Figure 2.15](#)). The dissociation constants obtained range from 100 - 800 nM and are provided in

Table 2.3. The reported K_D for the LxCxE E7 peptide binding to pRb is approximately 110nM (Lee et al., 1998) and is comparable to the K_D values obtained for pRb binding to the inhibitors. To confirm that inhibitor binding is reversible, one of the pRb/inhibitor complexes (pRb with compound 478166) was dialyzed overnight and ITC was repeated. As before, a binding curve was obtained yielding a similar dissociation constant and stoichiometry, indicating that the inhibitor was still able to interact with pRb in a reversible fashion (Figure 2.16). To eliminate the possibility of non-specific binding of the thiadiazolidinediones, ITC was carried out with compound 478166 and 6xHis-HPV16-E7_{CR2-3} (Figure 2.17). The observed heats reveals negligible binding, further demonstrating that the compounds are not binding to pRb non-specifically.

To determine if the inhibitors are competitive with HPV-E7 for pRb binding or work through an allosteric mechanism, we employed the ELISA assay to measure the ability of HPV-E7 to displace the compound from pRb as a function of inhibitor concentration. As shown in Figure 2.18, the binding curves of 6xHis-HPV16-E7_{CR2-3} to GST-pRb_{ABC} in the presence of varying concentrations of inhibitor, above and below the dissociation constant of pRb for inhibitor, shows a dependence on the concentration of inhibitor used, where increasing inhibitor concentration is correlated with a rightward shift (higher apparent value) in the K_d values for HPV-E7 binding to pRb. This data suggests that inhibitor and HPV16-E7 bind competitively to pRb. Taking this result together with the observation that these inhibitors are also able to disrupt pRb complexes with HPV1A-E7 and Ad5-E1a (Figure 2.14) suggests that these thiadiazolidinedione inhibitors also bind pRb competitively with other LxCxE containing oncoproteins.

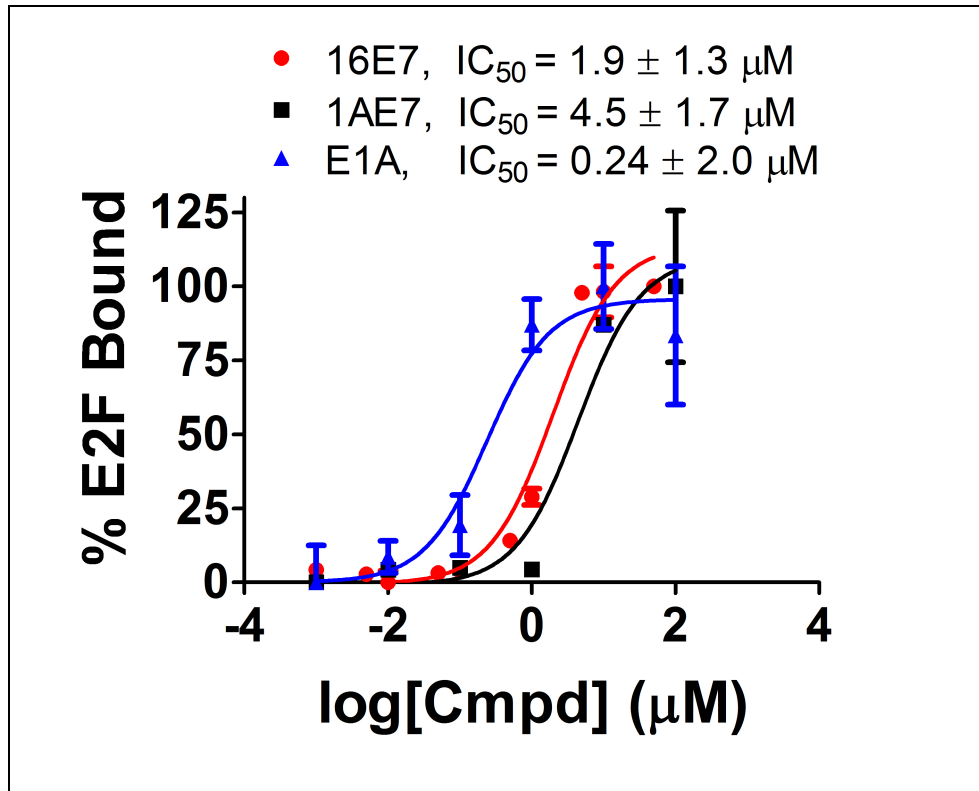


Figure 2.13. Ability of inhibitors to prevent LxCxE containing viral oncoproteins from disrupting E2F/pRb complexes. IC_{50} curves were generated using the ELISA assay. Ten-fold dilutions of inhibitor starting at $100\mu\text{M}$ (compound 478166 is shown) were added to GST-pRb_{ABC}/6xHis-HPV1AE7_{CR2-3} or GST-pRb_{ABC}/6xHis-Ad5E1A_{CR2-3}. The amount of E2F remaining was determined by adding a primary antibody specific for E2F1.

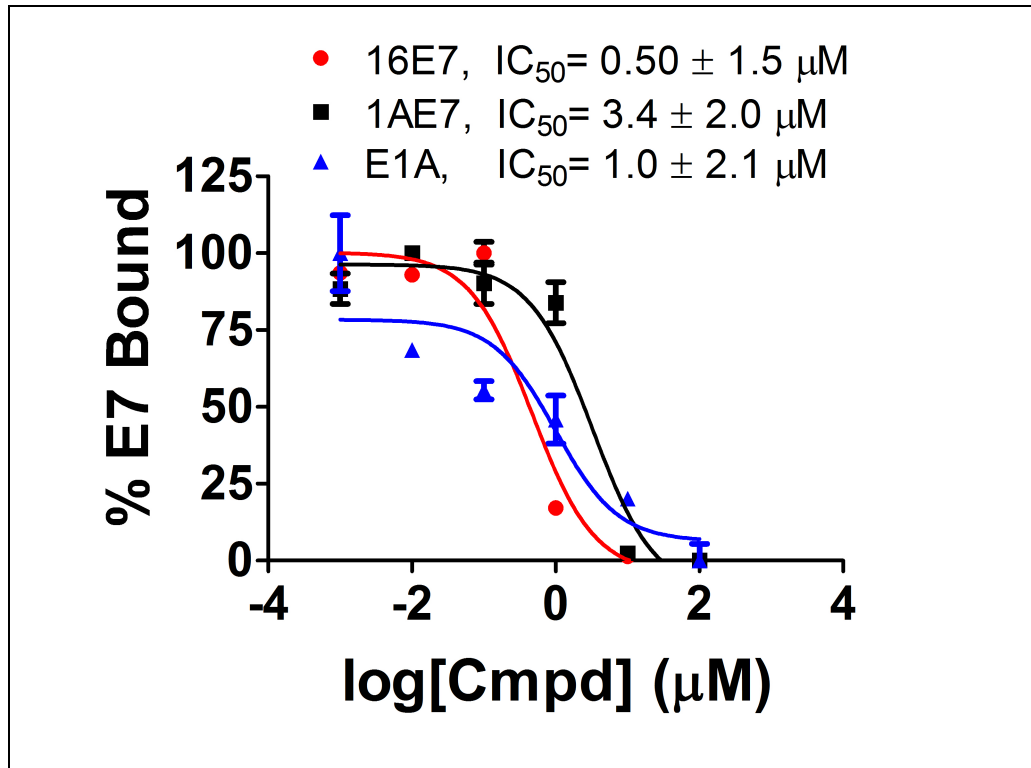


Figure 2.14. Ability of inhibitors to disrupt complexes between pRb and LxCxE containing viral oncoproteins. Compound 478166 was used for the experiment shown. IC_{50} curves for inhibition of viral oncoprotein binding to pRb were generated using the ELISA assay. Ten-fold dilutions of inhibitor starting at $100\mu\text{M}$ were added to GST-pRb_{ABC}/6xHis-HPV-E7_{CR2-3} or GST-pRb_{ABC}/6xHis-Ad5E1A_{CR2-3}. The amount of E7 or E1A remaining was determined by adding a primary anti-His antibody or anti-E1A antibody, respectively.

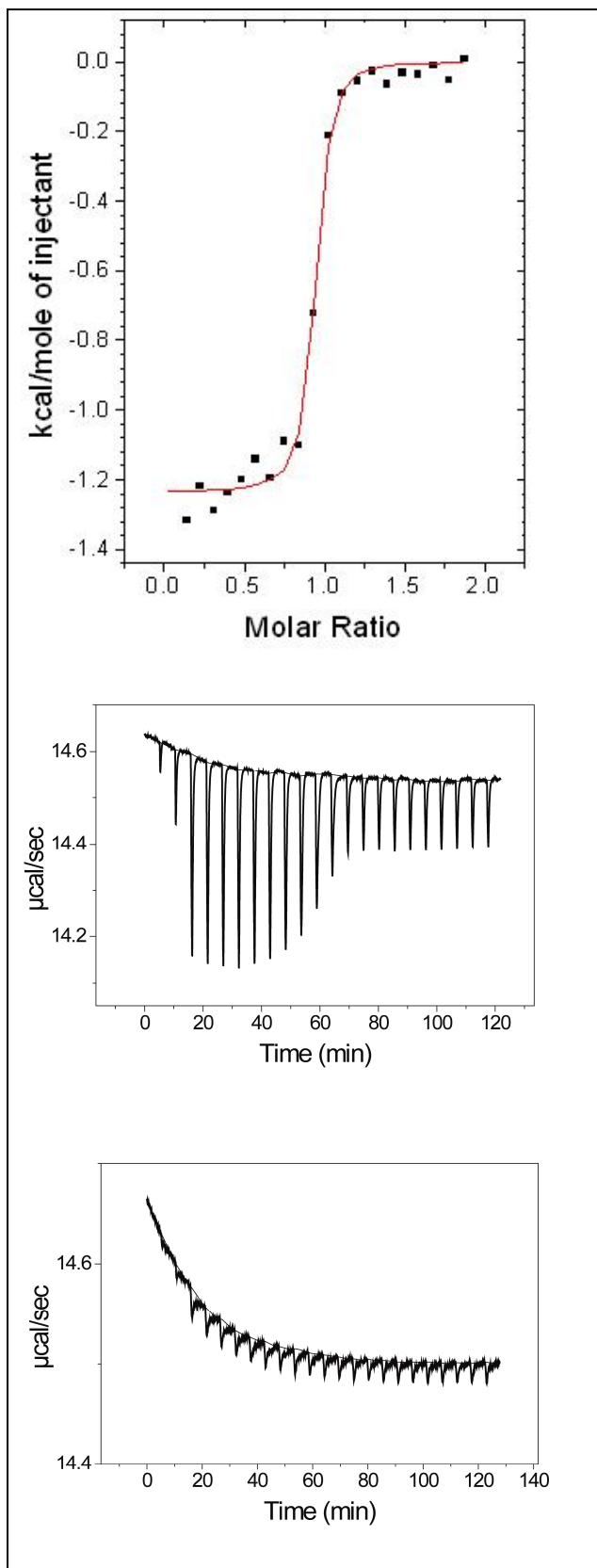


Figure 2.15. Direct binding of inhibitors to pRb as measured by isothermal titration calorimetry.

(top) The curve fit for pRb binding to compound 478081 reveals 1:1

binding with a K_D of 165nM, and dH of -1237 cal/mol. (middle)

Incremental heat effect upon 10µL titrations of 750µM compound 478081 into 0.075µM pRb.

(bottom) Heat effect upon titration of compound 478081 into buffer.

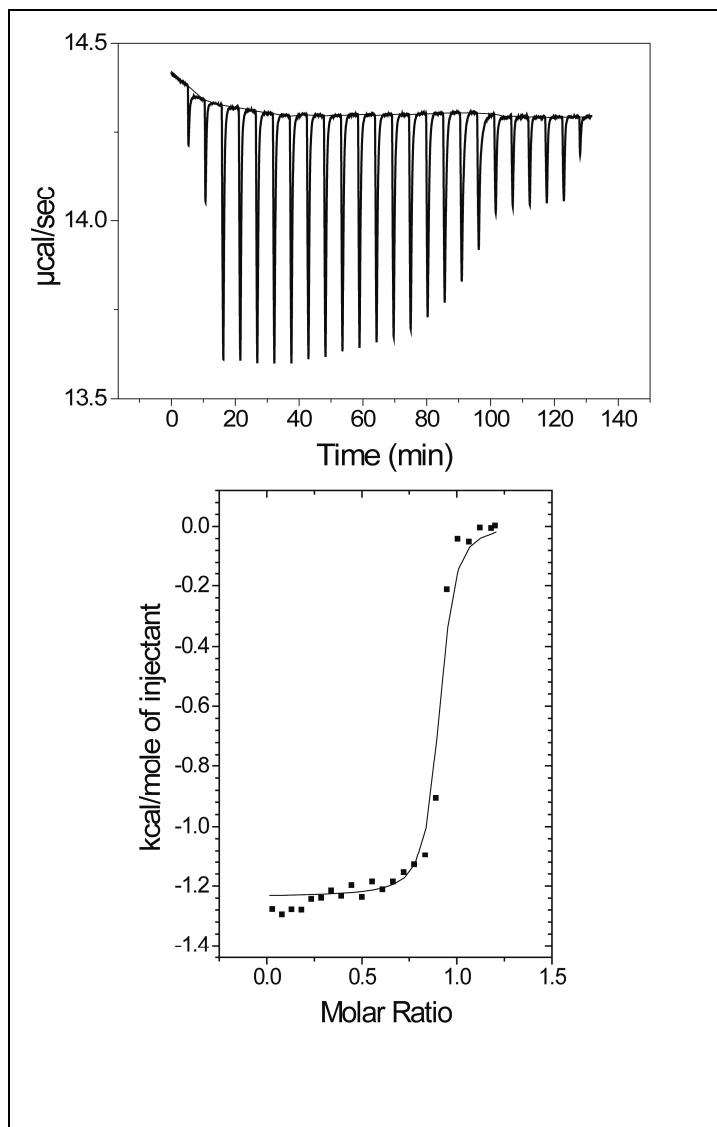


Figure 2.16. Analysis of reversible inhibitor binding to pRb as measured by isothermal titration calorimetry. (top) pRb/compound 478166 inhibitor binding following dialysis to remove bound inhibitor. Incremental heat effect upon 8 μ L titrations of compound 478166 into pRb after the pRb/478166 complex was dialyzed overnight to remove the inhibitor. (bottom) Integrated heat effects showing that the binding is reversible.

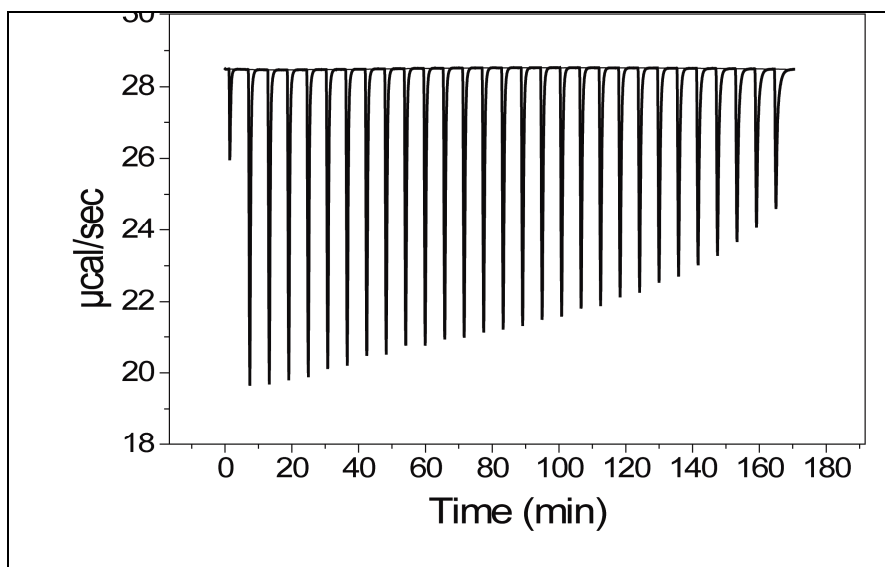


Figure 2.17. Analysis of inhibitor binding to E7 as measured by isothermal titration calorimetry. Heat effect upon titration of 750µM compound 478166 into 75 µM E7 showing there is negligible binding.

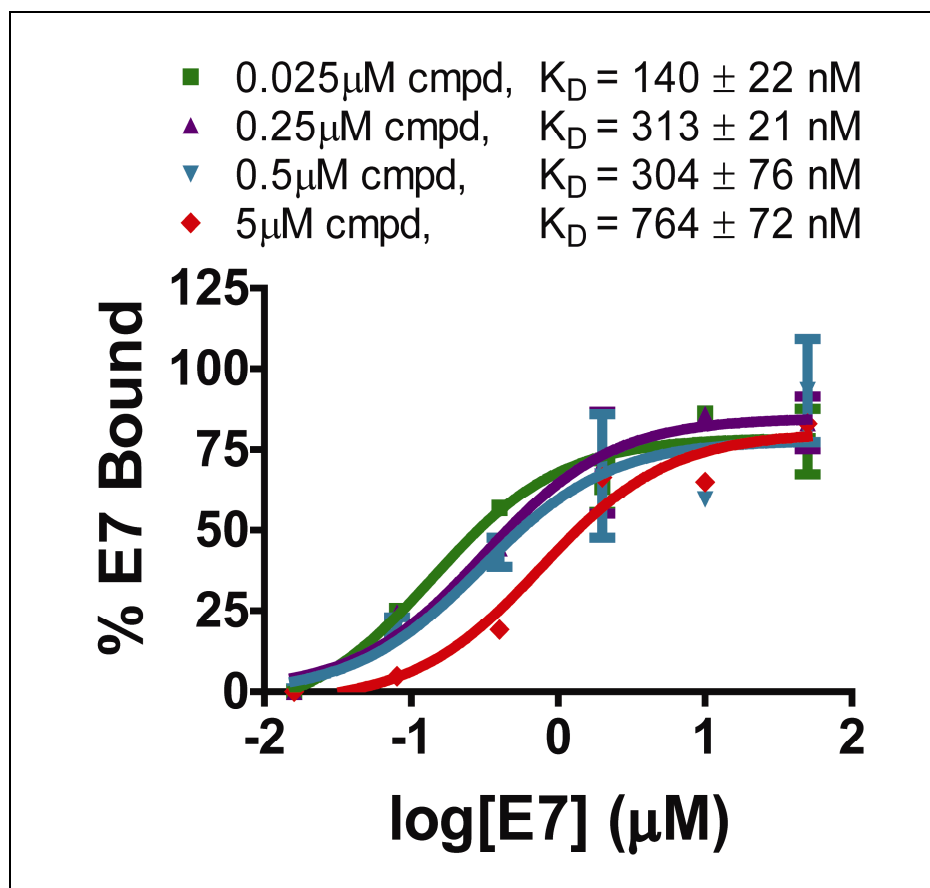


Figure 2.18. Competition assay. The ELISA-based assay was used to determine the mechanism of binding of the small molecules to pRb. Five-fold dilutions of inhibitor were added to pRb and the amount of E7 that was able to bind to pRb was determined. The calculated apparent K_D values for pRB-E7 in the presence of 0.025, 0.25, 0.5 and 5.0 μM of inhibitor 478165 (K_D for pRb of 104 nM) were 140 ± 22 , 313 ± 21 , 304 ± 76 and 764 ± 72 nM, respectively.

2.2.5 HPV-E7 Inhibitors Selectively Cause Apoptosis in HPV-Transformed Cells

Since the seven thiazolidinediones listed in [Table 2.3](#) were cytotoxic or prevented proliferation of SiHa cells due to their role in inactivating pRb, which is mutated in C-33A cells, they were tested in additional cell lines: TC-1, a mouse epithelial line co-transformed with HPV 16 E6/E7 and c-Ha-Ras, HeLa, a human cell line transformed with HPV 18 and HCT116, a human HPV negative colorectal carcinoma cell line containing an intact retinoblastoma gene (DeFilippis et al., 2003; Scheffner et al., 1991; Yee et al., 1985). The levels of cell viability after incubation with compound were determined using the MTS assay as previously described. This time, a concentration range of 100 μM to 3 μM of compound was tested so that the cellular IC_{50} values could be extracted for these seven compounds, and for the ten inactive analogs. As shown in [Figure 2.19](#), the thiazolidinedione compounds had the greatest effect on SiHa cells, followed by TC-1 cells, and to a smaller extent, HeLa cells. The smallest effect was seen in HCT 116 and C-33A cells. While the inhibitors were cytotoxic in all cell lines at 100 μM , they were selectively cytotoxic in HPV-positive cells at the lower compound concentrations. In general, the IC_{50} values of the thiazolidinedione compounds in SiHa cells varied from between 6.25 μM and 12.5 μM to between 25 μM and 50 μM . The IC_{50} values in TC-1 and HeLa cells were slightly higher and varied from between 12.5 μM and 25 μM to between 50 μM and 100 μM . The IC_{50} values in HCT 116 and C-33A cells were all greater than 25 μM . Importantly, the inactive analogs did not demonstrate any effect in any of the cell lines tested (a representative example is shown in [Figure 2.19](#)). Taken together, this data suggests that the seven thiazolidinedione HPV-E7 inhibitors identified in the primary HTS are either selectively cytotoxic or selectively prevent proliferation of HPV transformed cervical cancer cell lines, with a greater effect in cell lines transformed with HPV 16.

◆ SiHa, HPV 16+ ■ TC-1, HPV 16+ ▲ HeLa, HPV 18+
 ◆ HCT-116, HPV - ◆ C-33A, HPV -, pRb mutant

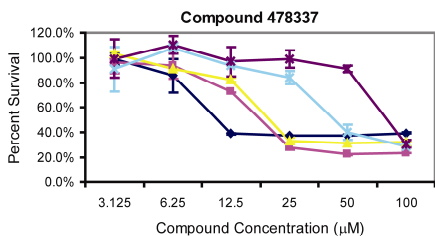
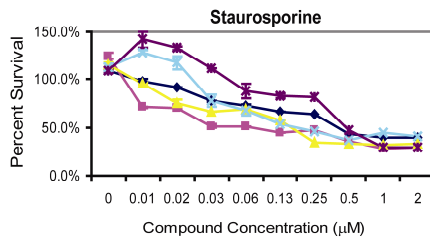
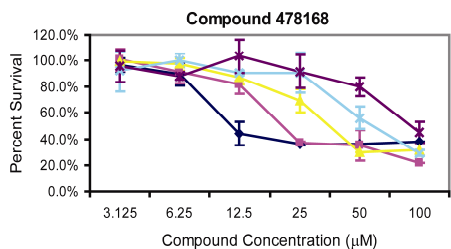
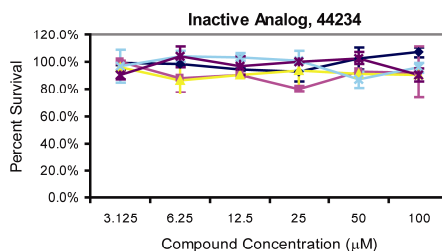
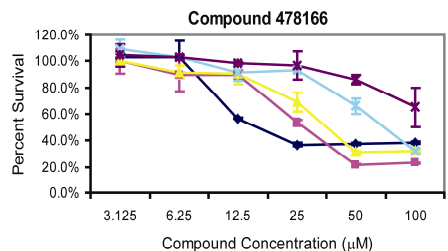
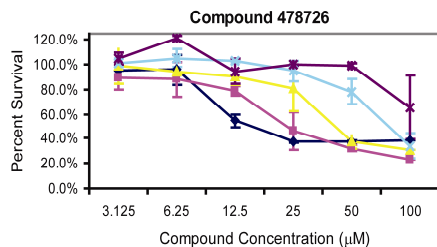
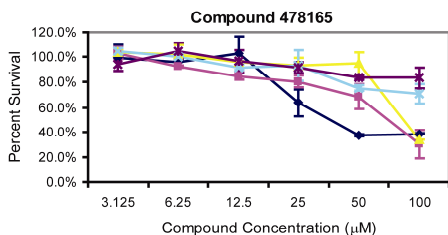
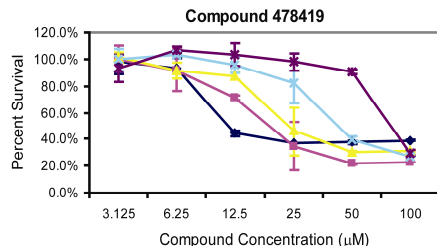
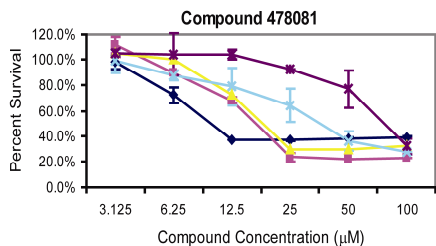


Figure 2.19. Cellular toxicity of thiazolidinedione compounds. Four different cervical cancer cells lines: SiHa, TC-1, HeLa and C-33A and one non-cervical cancer cell line, HCT116, were employed for these studies. 2-fold compound dilutions starting at 100 μ M down to 3.125 μ M for the thiazolidinediones and starting at 2 μ M to 4 nM for staurosporine were incubated for 48 hours with cells before the addition of MTS reagent. After 1-2 hours of incubation with reagent, the absorbance at 490 nm was determined. The percent growth was determined by dividing by the growth in the presence of DMSO control.

Given that the thiadiazolidinedione inhibitors bind to pRb, a critical regulator of the cell cycle, we asked whether they perturb the cell cycle to prevent proliferation or whether they induce apoptosis in cells transformed with HPV. To carry out these studies, we employed SiHa cells (transformed with HPV 16) since the inhibitors were most effective in this cell line. Cells were treated with either DMSO or 10 μ M of two representative thiadiazolidinediones: compounds 478166 and 478168, an inactive analog (compound 44234), or 2 μ M of staurosporine, for 48 hours. DNA content was determined by propidium iodine staining and analyzed by flow cytometry. In agreement with our biochemical results and the MTS cell viability assay, compounds 478166, 478168, and staurosporine most drastically affected SiHa cells whereas the inactive analog had no effect (Figure 2.20). The thiadiazolidinedione inhibitors caused an increase of apoptotic SiHa cells (6.5% and 15.2% of cells were apoptotic when treated with the thiadiazolidinediones 478166 and 478168, respectively, compared to ~1% apoptotic cells that were treated with DMSO or the inactive analog) as did the non-specific kinase inhibitor staurosporine (34.3% of cells were apoptotic) (Figure 2.20). These results are consistent with the MTS data and *in vitro* data, together supporting the interpretation that the thiadiazolidinedione inhibitors antagonize the ability of HPV-E7 to maintain the viability of the HPV transformed cells. These results are also consistent with work by others that E7 knockdown can lead to apoptosis in HPV-positive cells (Jiang and Milner, 2002; Sima et al., 2008).

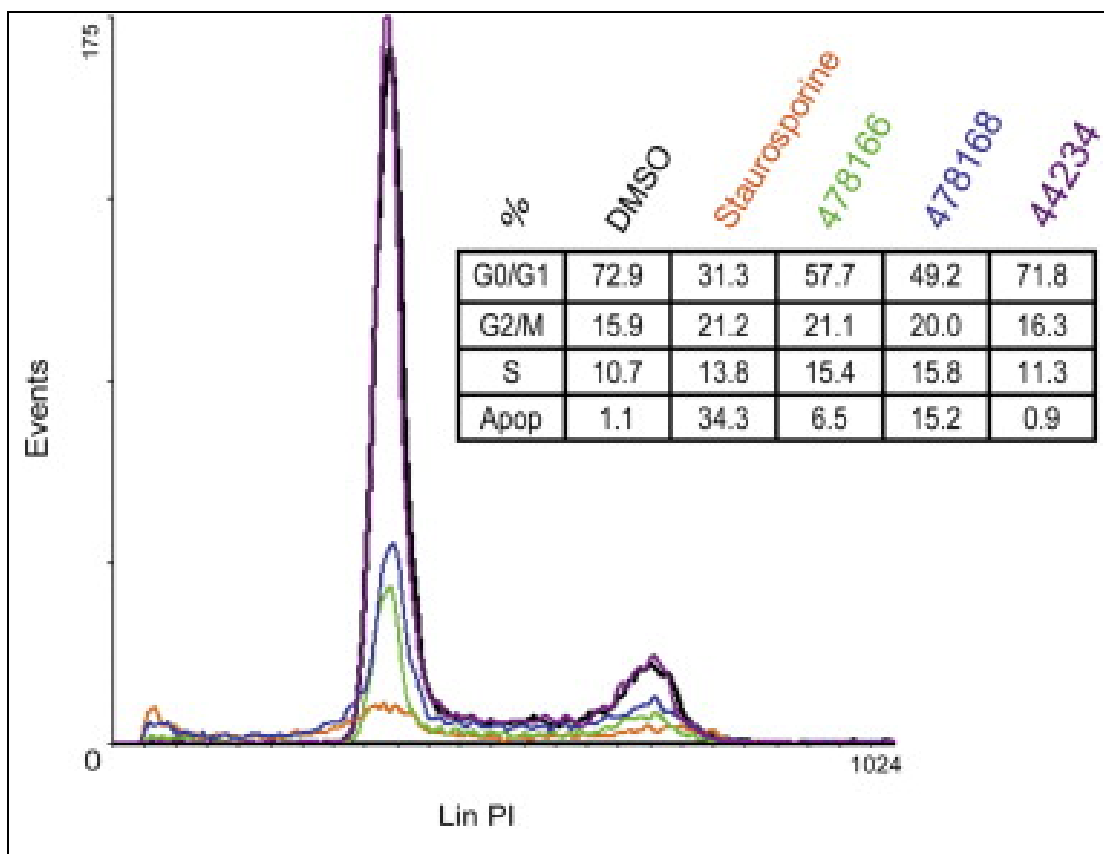


Figure 2.20. Effects on the cell cycle and apoptosis by the thiadiazolidinediones 478166 and 478168, an inactive analog, and staurosporine. To determine any effect on cell cycle or apoptosis, SiHa cells were treated with DMSO or 10 μ M of compounds 478166, 478168, 44234, or 2 μ M staurosporine for 48 hours. After 48 hours, cells were harvested, stained with propidium iodide, and DNA content was analyzed by flow cytometry. The percent of cells in G0/G1, G2/M, S, or apoptotic were determined by the areas under certain sections of the curves.

2.2.6 A Representative Compound Can Reduce Tumor Size *In Vivo*

Since the thiazolidinedione inhibitors exhibited apoptotic activity in cells, we wanted to determine whether or not they would demonstrate anti-tumor activity *in vivo*. A transplantable tumor model was employed in which TC-1 cells were injected subcutaneously into NOD-SCID mice. After five days, treatment was initiated with compound 478166 (n=6) or vehicle only (DMSO) (n=6) by intraperitoneal injection and repeated daily for a total of 14 days. The tumors were measured once every two days. At the conclusion of treatment, a significant reduction in tumor volumes was observed for mice treated with compound compared to vehicle only (Figure 2.21). After 14 days, the average tumor volume of mice treated with DMSO was 3950mm³, whereas the average tumor volume of mice treated with drug was 2270mm³ (p < 0.02). Taken together with our results from the cell-based experiments, it appears that the thiazolidinedione inhibitor can reduce tumor volume *in vivo*, with no deleterious effects observed otherwise on animal health.

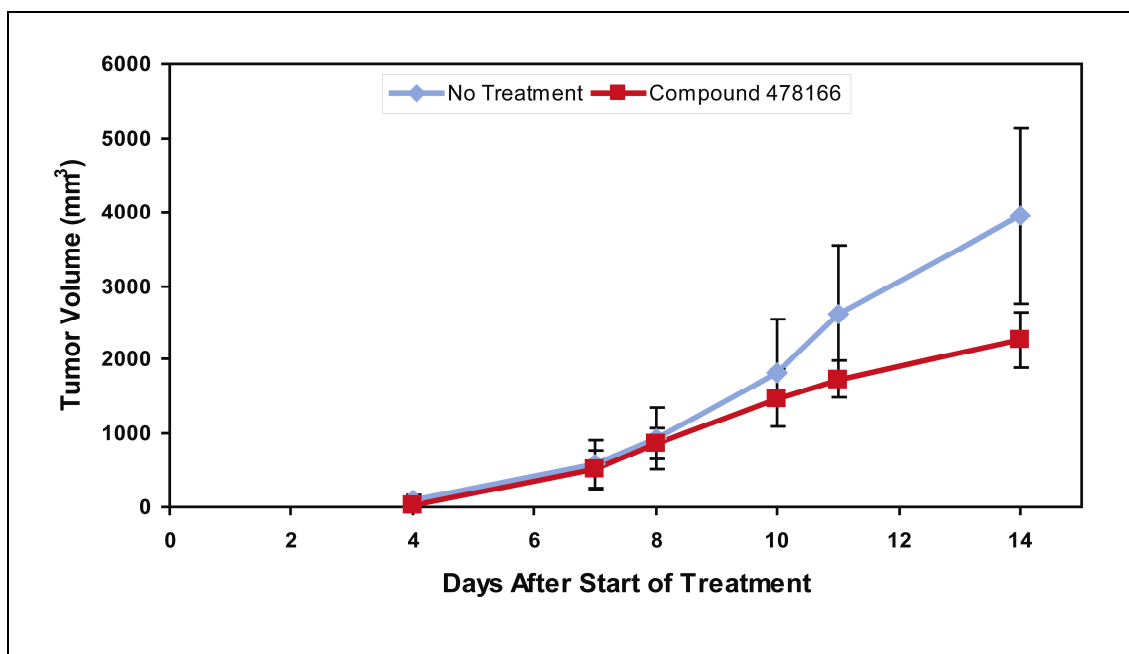


Figure 2.21. The anti tumor effect of thiazolidinedione compound 478166 *in vivo*.

A tumor model was constructed by inoculating 2.0×10^5 TC-1 cells into the right flank of 12 NOD SCID female mice. Treatment was started 5 days post-injection; the mice were treated once a day for 14 days, with IP injections of DMSO or compound 478166 at doses of 10mg/kg. Tumor sizes were measured every two days.

2.3 High-Throughput Screening Discussion

We have described the identification and characterization of structurally similar thiadiazolidinedione compounds that inhibit the interaction between the LxCxE motif of viral oncoproteins and pRb in a competitive manner with sub-micromolar dissociation constants. The identification of these inhibitors is an important finding given that there are no known inhibitors that specifically block the interaction of pRb with viral oncoproteins. Interestingly, other small molecule compounds that show structural similarity to these thiadiazolidinediones have been implicated in possible treatments against neurodegenerative disorders by targeting glycogen synthase kinase-3 (GSK-3) or the peroxisome proliferator-activated receptor γ (PPAR γ) (Luna-Medina et al., 2005; Luna-Medina et al., 2007; Martinex, 2006; Martinez et al., 2005; Martinez et al., 2002; Rosa et al., 2008). The fact that these inhibitors appear to prevent oncoproteins from binding to the LxCxE binding site on pRb suggests that these types of inhibitors provide another route for therapeutics not only against cervical cancer, but also for other diseases caused by viral oncoproteins containing the LxCxE motif.

The B domain of the pRb pocket domain harboring the LxCxE binding site is also the site of interaction with cellular proteins, such as histone deacetylases, cyclin D1, chromatin remodeling enzyme BRG1, and other proteins (Dahiya et al., 2000; Rosa et al., 2008; Singh et al., 2005). However, our studies in cells and in mice show that these inhibitors are not overtly cytotoxic in HPV-negative cells, suggesting that the HPV-E7 inhibitors do not perturb these endogenous interactions, at least to the same extent. The tumors formed by TC-1 cells in mice showed a significant reduction in volume when treated with thiadiazolidinedione 478166, without any noticeable effects on their normal cells, as indicated by a lack of change in animal behavior, implying a potential therapeutic for HPV16-related neoplasms. Furthermore, the cell-based studies reveal that the HPV-E7 inhibitors are more toxic in SiHa cells than HeLa cells. Taken together with our *in vitro* data showing that the compounds bind competitively with E7 to pRb, this suggests that the compounds are either more effective at disrupting the interaction between pRb

and HPV16 E7 than pRb and HPV18 E7 or that the levels of E7 and or pRb are different enough in these cell lines to result in different toxicities. It is also possible that HeLa cell viability is not completely dependent on the HPV-E7 oncoprotein due to additional genetic and epigenetic changes in the tumor genome. Others have shown that the levels of pRb do in fact differ across cervical cancer cell lines, and that there is a difference in the level of pRb phosphorylation, with a greater level of hypophosphorylated pRb in SiHa cells (Scheffner et al., 1991). This observation is consistent with the level of toxicity that we observe in the MTS assay and by cell-cycle analysis, which suggests that the thiadiazolidinedione inhibitors may bind more avidly to hypophosphorylated pRb to prevent the interaction with E7. Furthermore, the increase in apoptosis in SiHa cells upon treatment with the thiadiazolidinedione inhibitors suggests that the inhibitors are antagonizing the ability of E7 to maintain the viability of the HPV-positive cell lines.

While there are reports that E7 has the ability to degrade pRb (Boyer et al., 1996; Giarre et al., 2001; Gonzalez et al., 2001), there are other reports that siRNA or shRNA against E7 results in a de-phosphorylation of pRb, and not an increase in overall pRb levels (Jiang and Milner, 2002; Sima et al., 2008). The de-phosphorylation of pRb by E7 was demonstrated in SiHa and CaSki cells, both of which are transformed with HPV 16. It is possible that the effect on pRb is cell-line dependent, as the former studies (Boyer et al., 1996; Giarre et al., 2001; Gonzalez et al., 2001) were done using different cell lines. We probed for pRb in SiHa, HeLa, TC-1, and HCT 116 cells that were incubated for 48 hours with concentrations of compound 478166 as high as 25 μ M and did not see any change in the levels of pRb or in its phosphorylation state (data not shown). pRb was also probed in the mouse tumors that were treated with compound versus those that were not, and again no change in pRb levels or in its phosphorylation state could be observed (data not shown). It is possible that these compounds work differently from the siRNA and shRNA experiments in that they do not cause a detectable change in the levels of pRb or its phosphorylation state in these cell lines.

The inhibitors identified provide new tools to probe mechanisms involved in HPV transformed cells and may provide a promising chemical scaffold to develop novel therapies to

treat HPV-mediated pathologies. Since HPV mediates cell transformation through the action of two viral oncoproteins, E6 and E7, where E6 targets the p53 tumor suppressor for degradation, it might be particularly advantageous to combine these thiazolidinedione inhibitors with inhibitors that prevent E6-mediated p53 degradation to develop a particularly effective therapeutic strategy to treat HPV-mediated pathologies.

2.4 Crystallization Results

2.4.1 Crystallization of Unliganded pRb_{AB}

Our results from ITC confirm that the thiadiazolidinedione inhibitors bind directly to pRb with submicromolar affinity providing a route for structure-based-drug design of more potent and selective HPV inhibitors. Co-crystallization studies of these small molecules with pRb_{AB} may provide further insight to their mode of interaction and guide further optimization. Since the crystal structure of the pocket domain of the unliganded pRb_{AB} has been determined (Balog et al., 2011), we utilized this protein construct in an attempt to obtain a co-crystal structure of a pRb_{AB}-inhibitor complex.

The protein construct of pRb_{AB} that was used for crystallization contained residues 380–787. Furthermore, residues 578 to 642 from the linker region between the A and B domains were removed and replaced with a thrombin cleavage site (Balog et al., 2011). The short linker was kept intact. The protein was expressed as a GST-fusion and purified to high enough purity for crystallization. The elution profile from size exclusion chromatography is shown in [Figure 2.22](#), along with an SDS-PAGE gel of the eluted fractions. The protein was concentrated to 20 mg/ml for crystallization using sitting drop vapor diffusion. Unfortunately, crystals could not be obtained in the reported condition of 100mM CAPS, 10.6, 10% PEG 3350 at 4 °C (Balog et al., 2011). Consequently, a grid screen around this condition was performed with the hopes of crystallizing the protein in a similar condition. To do this, the percentage of PEG 3350 was varied from 5% to 15% in 2.5% increments. Additionally, the pH of the buffer was varied from pH 10.0 to 11.2. Again, no crystals formed. The protein appeared to precipitate in most of the conditions.

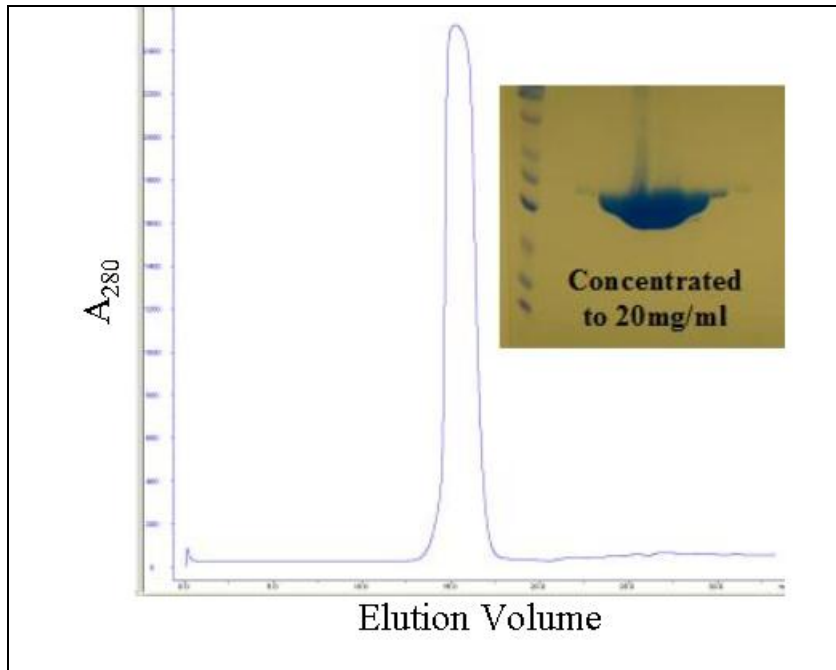


Figure 2.22. Purification of pRB_{AB}. Representative superdex 200 analytical gel filtration chromatogram for pRB_{AB} purification is shown alongside the SDS-PAGE gel of the four major fractions of the peak. The protein is >95% pure and amenable for crystallization.

2.4.2 Identification of New Conditions for pRb_{AB} Crystallization

Since pRb_{AB} would not crystallize in the published condition, all of the available screens were tested, again at 4 °C. This time, crystallization trials were performed with pRb_{AB} alone, as well as in complex with compound 478166, with a 5:1 molar ratio of compound to protein. Briefly, a 100 mM stock of compound 478166 was added to a 20mg/ml solution of pRb. The final DMSO of the mixture was 2.5%. The compound was incubated with pRb for one to two hours before setting up trays. Crystals in a number of conditions were obtained (Figure 2.23, left hand side). Notably, all crystals in conditions containing 2-propanol formed within two days. In addition to these, crystals in a condition containing 1% Tryptone, 50mM Hepes Na, 7.0, and 12% PEG 3350 also formed within two days. Some crystals formed both in the presence and absence of compound, some formed only in the presence of compound, others only in the absence of compound. In some cases, the presence of compound altered the shape of the crystals formed.

Unfortunately, most of the crystals in conditions containing 2-propanol could not be used for structure determination because they formed overlapping rods that could not be separated. Additional optimization would be needed for these conditions. Interestingly, the crystals in the condition containing 10% isopropanol, 100mM Hepes, 7.0, and 10% PEG 4000, formed well separated needle showers. These, however, were too small to freeze for data collection. Therefore, the crystals from 1% Tryptone, 50mM Hepes Na, 7.0, 12% PEG 3350 were pursued. Several cryoprotectants were tested: the best one appeared to be 0.75% Tryptone, 37.5mM Hepes Na, 7.0, 15% PEG 3350, and 25% glycerol. Unfortunately, the crystals only diffracted to about five angstrom resolution (Figure 2.24). Further optimization with this condition was difficult because future crystals that formed were much smaller, and too small to freeze.

Fortunately, after six weeks, new crystals appeared in different conditions. These new crystals were larger, and generally better separated than before (Figure 2.23, right hand side). Since the crystals took a long time to form, we suspected that the linker region between the A and B domains of pRb was cut. A silver stain of a few crystals showed this was not the case (data not shown). Since there were not enough crystals in each drop to test multiple cryoprotectants, the

procedure was repeated in a larger number of wells and at a larger scale (from 96-well format to 24-well format). A grid was created for the four conditions producing slow growing crystals; for this, the PEG concentration was varied. Considering that crystallization took a long time in these conditions, a matrix seeding approach was taken to expedite the nucleation process. Briefly, several crystals from the condition containing 1% Tryptone, 50mM Hepes Na, 7.0, and 12% PEG 3350 were crushed and vortexed using a seed-bead (D'Arcy et al., 2007), and added to each drop. Drops were set up both in the presence and absence of compound.

Several crystals in the condition containing 4% v/v Tacsimate, pH 8.0 and 10-14% PEG 3350 formed within ten days, as opposed to six weeks, this time (Figure 2.25). Only pRb_{AB}-inhibitor drops formed crystals. The crystals in the other three conditions still took a long time to form. Consequently, the crystals from the 4% v/v Tacsimate, pH 8.0 and 10-14% PEG 3350 condition were pursued. Different cryoprotectants were tested and the best one was 4% v/v Tacsimate, pH 8.0, 25% PEG 3350, 10% ethylene glycol, and 12.5% sucrose. Some spots to 2.4 angstrom resolution were seen for the crystals in this condition (Figure 2.25). Complete data could only be collected to 3.4 angstrom resolution, and the structure was determined by molecular replacement using the reported unliganded pRb_{AB} structure as a search model. The crystals formed in the same space group as was previously reported (P2₁2₁2₁). No inhibitor could be found anywhere in the electron density.

The condition containing 4% v/v Tacsimate, pH 8.0 and 10-14% PEG 3350 eventually formed crystals in the absence of inhibitor. The size of these crystals were significantly larger. Since these formed in the absence of inhibitor, compound 478166 was introduced by soaking. To do this, 0.2 μ L of compound at a concentration of 30mM was added to the drop to a final DMSO concentration of approximately 1%. This was done for varying times: from 15 minutes to as long as 24 hours. Cracks in the crystals could be seen after 1 hour. The same cryoprotectant: 4% v/v Tacsimate, pH 8.0 25% PEG 3350, 10% ethylene glycol, and 12.5% sucrose, was used except that the same concentration of compound was added to it. The diffraction qualities of the soaked crystals were significantly worse.

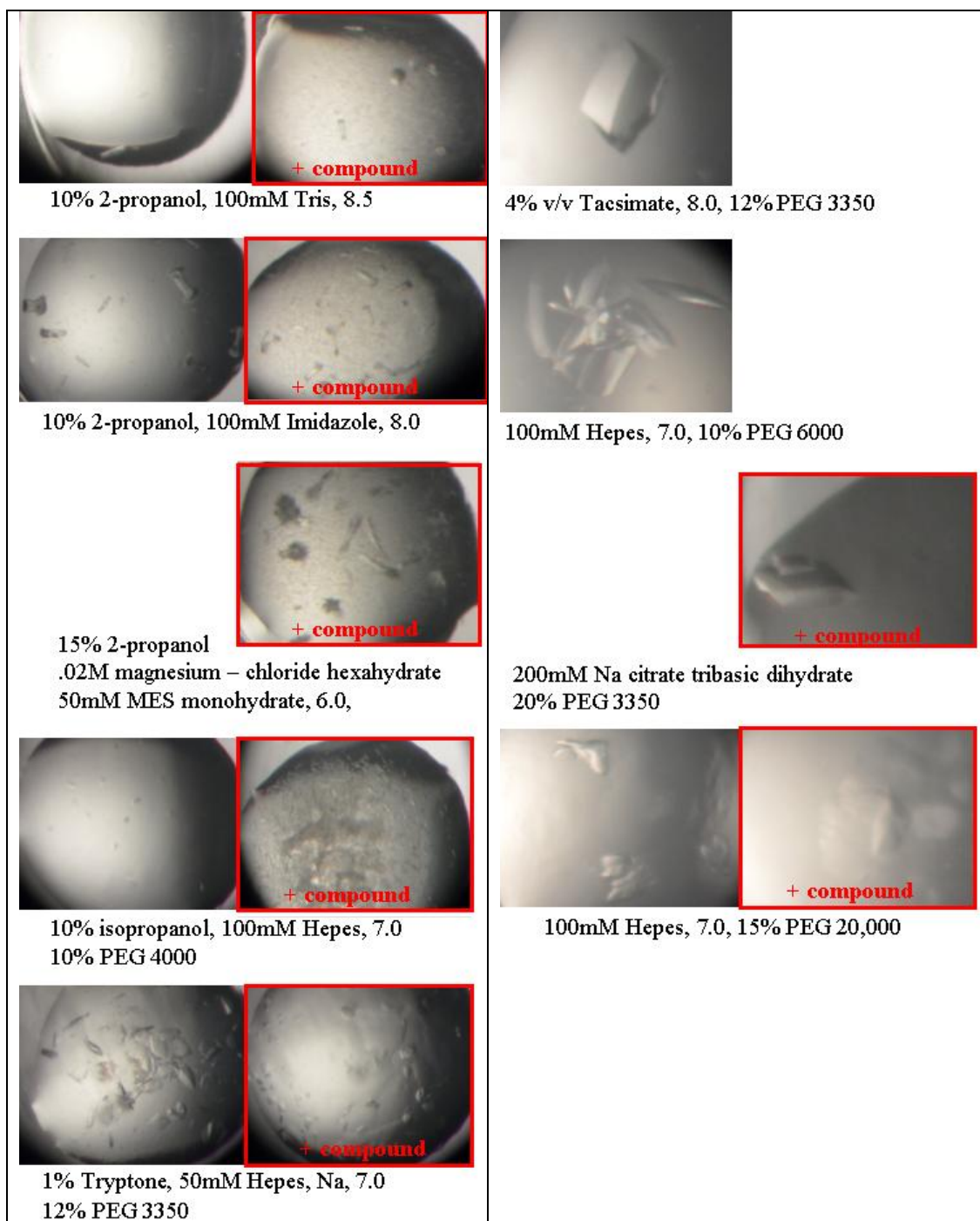


Figure 2.23. Crystallization of pRB_{AB} All crystals obtained of pRB_{AB} in the presence or absence of compound 478166 are shown. Highlighted in red are crystals that formed in the presence of compound. Crystals on the left formed in two days; crystals on the right formed in six weeks.

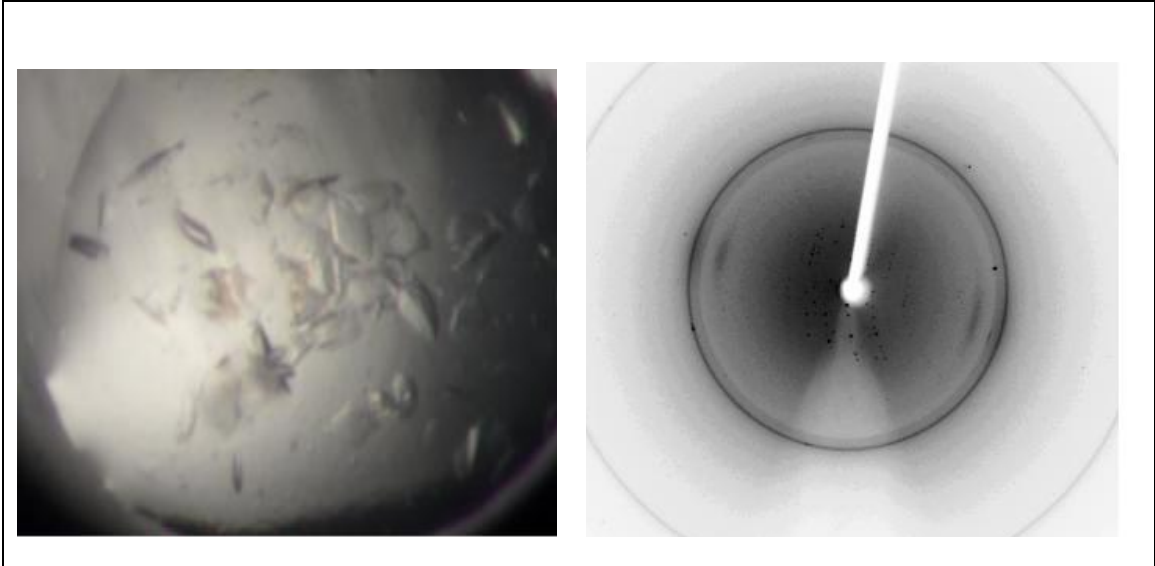


Figure 2.24. pRB_{AB} crystals used as seeds. The above crystals formed using 20mg/mL pRB_{AB} at 4 °C in the condition 1% Tryptone, 50mM Hepes Na, 7.0 and 12% PEG 3350 in the absence of compound. Crystals appeared in 2 days. These crystals only diffract to approximately 5 angstrom resolution.

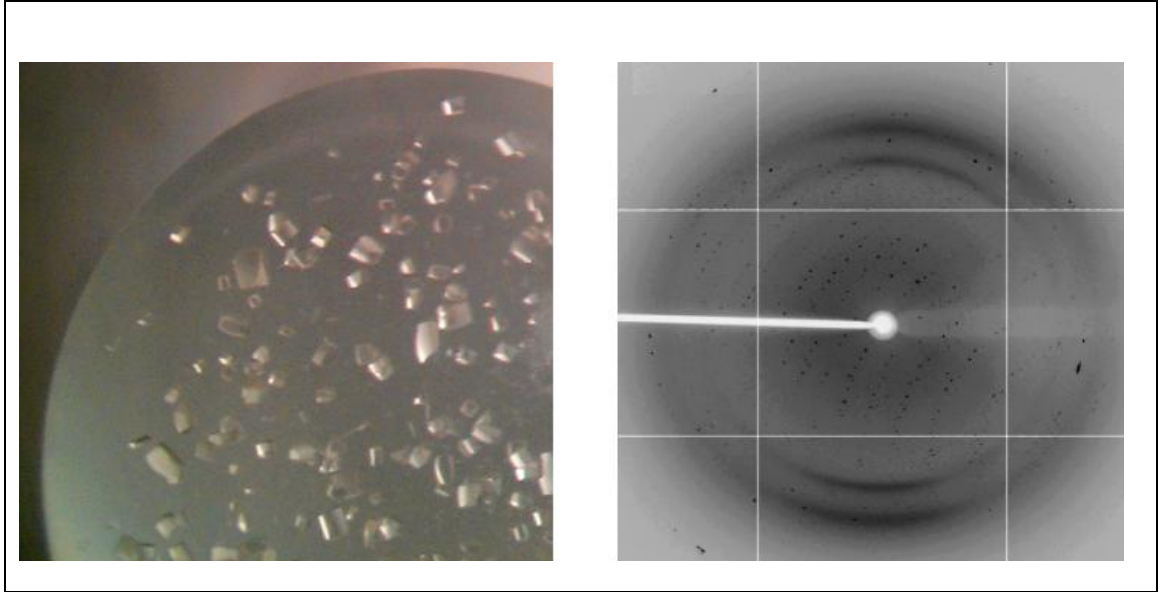


Figure 2.25. Best pR_B_{AB} crystals to date. The above crystals formed using 20mg/mL pR_B_{AB} and compound at 4 °C in the condition 4% v/v Tacsimate pH 8.0 and 12% PEG 3350. Crystals that were crushed from the condition 1% Tryptone, 50mM Hepes Na, 7.0 and 12% PEG 3350 were used as seeds to expedite the formation of crystals. Crystals appeared after 10 days. The structure was solved to 3.4 angstrom resolution.

2.5 Crystallization Discussion

A number of conditions were identified which produce crystals of pRb_{AB} both in the presence of absence of compound 478166. One set of conditions, containing 2-propanol, produced crystals in a matter of days, however, the crystals were of poor quality: they were overlapping and could not be separated surgically. The other set of conditions, containing PEG, produced crystals over a longer period of time that were easier to work with.

The best condition that was pursued (4% v/v Tacsimate, pH 8.0 and 12% PEG 3350) produced crystals that could only be structurally solved to 3.4 Å and the compound could not be found in the resulting electron density map. Performing additive screens might help improve the quality of these crystals. The crystals were very fragile, suggestive of a high solvent content, therefore, other techniques, such as dehydration, might also be useful and may produce better diffracting crystals. It is also possible that the crystal packing of pRb in this condition did not allow for the introduction of inhibitor into the binding site. Therefore, it would be of interest to test crystals from different conditions that might diffract to higher resolution, or in which pRb packs differently.

Our use of matrix seeding appeared mildly successful in the small number of conditions that were tested; it was able to expedite nucleation and reduce the amount of time that was needed for crystallization from six weeks to 10 days for one set of conditions. It is also possible that screening all possible conditions with these crushed crystals as seeds would allow for the production of crystals in additional conditions. This might identify crystals in which the protein packs differently, or those that diffract to a higher resolution. It may also be useful to try this matrix seeding approach with the published crystallization condition (100mM CAPS 10.6, 10% PEG 3350) (Balog et al., 2011).

Lastly, it may also be of interest to go back and optimize the 2-propanol containing conditions. Even though the crystals were overlapping in most of these cases, other additives might help form separated crystals that can be used for structure determination.

2.6 Future Work

The crystallization of the pRb_{AB}-inhibitor complex needs further optimization for structure determination. A structure will give insight into the mechanism of action of these small molecule inhibitors and guide the identification of more potent and specific inhibitors. Since the thiazolidinediones exhibited some toxicity in the HPV negative cell lines at high concentrations, it might still be of interest to reduce their toxicity some more. Other studies that determine the pharmacokinetics of the thiazolidinediones would be of interest as well.

It might also be interesting to study some of the compounds that were eliminated after the primary high-throughput screen and cherry picking process. Since a cell toxicity experiment was used as a secondary assay to eliminate many of the hits from the screen, a number of compounds that were not able to permeate the cell membrane were eliminated. Therefore, it may be of interest to develop a cell-free assay to test the original 120 compounds with IC₅₀s < 15.6 μM. This might help identify other inhibitors that prevent E7-mediated disruption of pRb-E2F complexes. While these compounds may not be able to permeate the cell membrane, future optimization of such compounds might improve their ability to do so.

2.7 Materials and Methods

2.7.1 Expression and Purification of Proteins

His-tagged E7 and E1A. The DNA encoding HPV16-E7_{CR2-3} (residues 17-98), HPV1A-E7_{CR2-3} (residues 16-93) and Ad5-E1A_{CR1-3} (residues 36-189) were cloned into the pRSET vector, containing an N-terminal 6x-histidine tag. HPV-E7 and Ad5-E1A were expressed in *E. coli* BL21(DE3) cells overnight at 25 °C and 18 °C, respectively. Cells were lysed by sonication in a buffer containing 20mM Tris, 7.5, 500mM NaCl, 35mM imidazole, 10 μ M Zn(OAc)₂, 10mM BME and 1x PMSF. The cell lysate was centrifuged at 18,000 RPM and the resulting supernatant was loaded onto a Ni-NTA column pre-equilibrated with 20mM Tris, 7.5, 500mM NaCl, 35mM imidazole, 10 μ M Zn(OAc)₂, and 10mM BME. The column was washed and the bound protein was eluted using an imidazole gradient from 35mM to 250mM. The proteins were further purified using size exclusion chromatography on a superdex 200 analytical column (GE Healthcare Life Sciences) in a buffer containing 20mM Tris, 7.5, 150mM NaCl, and 10mM BME.

GST-tagged pRb_{ABC}. DNA encoding pRb_{ABC} (residues 376-928) was cloned into the pFAST-Bac vector, containing an N-terminal GST tag. Protein was expressed in Sf9 cells for 48 hours before harvesting. Cells were lysed by sonication in a buffer containing 1x PBS, pH 7.4, 100mM NaCl, 10mM BME and 1x PMSF. The cell lysate was centrifuged at 18,000 RPM for 30 minutes and the resulting supernatant was loaded onto GST superflow resin (CLONTECH) pre-equilibrated with 1x PBS, 7.4, 100mM NaCl, and 10mM BME. The column was washed with the same buffer to remove contaminants. The GST-fused protein was then eluted using 1x PBS, 7.4, 100mM NaCl, 10mM GSH, and 10mM BME. The eluent was then concentrated and further purified using a superdex analytical column (GE Healthcare Life Sciences) in a buffer containing 20mM Tris, 7.5, 150mM NaCl, and 10mM BME.

Untagged E2F. The plasmid pGex6P-1-E2F1, encoding the marked-box and transactivation domain of E2F1 (residues 243-437) with an N-terminal GST tag, was provided by Dr. Steven Gambin (MRC, Mill Hill, UK). GST- E2F1_{MB-TA} was expressed in *E. coli* BL21(DE3) CodonPlus RIL cells (Novagen) for 5-6 hours at 30°C and purified as described elsewhere (Liu et al., 2006b). The GST tag was removed using PreScission Protease (GE Healthcare Life Sciences) as described elsewhere to yield an untagged E2F1_{MB-TA} for assay purposes (Liu et al., 2006b).

GST-tagged E7. For pull-down studies, GST-tagged full-length HPV-E7 was cloned into the pGEX-4T-1 vector and expressed in *E. coli* BL21(DE3) cells overnight at 18 °C. Cells were lysed by sonication in a buffer containing 1x PBS, 7.4, 100mM NaCl, 10µM Zn(OAc)₂, 10mM BME and 1x PMSF. The cell lysate was centrifuged at 18,000 RPM for 30 minutes and the resulting supernatant was loaded onto GST superflow resin (CLONTECH) pre-equilibrated with 1x PBS, 7.4, 100mM NaCl, 10µM Zn(OAc)₂, and 10mM BME. The column was washed with the same buffer except that no additional Zn(OAc)₂ was added. The GST-fused protein was then eluted using 1x PBS, 7.4, 100mM NaCl, 10mM GSH, and 10mM BME. The eluent was then concentrated and further purified using a superdex analytical column (GE Healthcare Life Sciences) in a buffer containing 20mM Tris, 7.5, 150mM NaCl, and 10mM BME.

His-tagged pRb_{ABC}. 6xHis-pRb_{ABC} (residues 376-928) was cloned into the pRSET vector, expressed in *E. coli* BL21(DE3) cells overnight at 18 °C and purified as described above for the 6xHis-tagged proteins, except that Zn(OAc)₂ was excluded from the buffers.

Untagged pRb_{AB}. For isothermal titration calorimetry studies, untagged pRb_{AB} (372-787 with the linker from 590-635 removed) was prepared as described elsewhere (Xiao et al., 2003).

Untagged pRb_{AB}. For crystallization, pRb_{AB} (380-787 with a short linker in between the A and B domains) was expressed as and purified as described elsewhere (Balog et al., ; Balog et al., 2011)

GST. In order to make GST protein as a control for pull down experiments, the pGEX-4T-1 vector was transformed into BL21 (DE3) cells and expressed and purified the same way as the GST-fused proteins.

2.7.2 Pull-Down Assay

30µg GST-pRb_{ABC} or GST was incubated with 30µl glutathione-Sepharose 4B beads (Amersham Biosciences) that were pre-equilibrated with a buffer containing 20mM Tris, 7.5, 150mM NaCl, and 0.05% Tween20 for 15 minutes to allow the protein to bind. Then, an equimolar amount of 6xHis-HPV16-E7_{CR2-3} and/or untagged E2F_{MB-TA} was added and allowed to incubate at 4° C for one hour with gentle agitation. After one hour, each set of beads was spun at 500g, unbound proteins were aspirated and the beads were washed with 1mL binding buffer (20mM Tris, 7.5, 150mM NaCl, and 0.05% Tween20). The beads were washed three times with this buffer, and then subjected to SDS-page analysis.

2.7.3 Compound Libraries

2000 compounds comprising the Spectrum Collection from MicroSource Discovery Systems (Gaylordsville, CT), Inc were tested at a final concentration of 8.3µM. A library of 14,400 chemically diverse compounds from Maybridge HitFinder (Cambridge, UK) were tested at a final concentration of 12.5µM. A third set of compounds, comprising 71,539 small molecules, from the orthogonally pooled screening (OPS) libraries, provided by the Lankenau Chemical Genomics Center (Wynnewood, PA) were tested at a final concentration 6.25µM to 12.5µM. The HitFinder

and OPS libraries were orthogonally compressed to contain 5 or 10 compounds per well, respectively.

2.7.4 High Throughput Solution Screening and Data Processing

The screen was performed using laboratory automation in 384-well microtiter plates in screening buffer (20 mM Tris, pH 7.5, 150 mM NaCl and 0.05% Tween20). First, a complex was formed between 100ng/100 μ L GST-pRb_{ABC} and 10ng/100 μ L E2F_{MB-TA} that was incubated for 30-60 minutes. At the same time, 20 μ L of 500nM 6xHis-HPV16-E7_{CR2-3} was added to a 384-well plate (Fisher Scientific) using a Biotek Microfill, containing 0.5 μ L compound dissolved in DMSO (or DMSO control) and allowed to incubate for 30-60 minutes. 40 μ L of GST-pRb_{ABC}/E2F_{MB-TA} complex was then added to each well containing 6xHis-HPV16E7_{CR2-3} and compound, and incubated at room temperature for an additional 30-60 minutes. 50 μ L of the GSTpRb_{ABC}/E2F_{MB-TA}-16E7_{CR2-3} mixture was then transferred to a pre-washed glutathione-coated 384-well plate (Thermo Scientific) using a Janus MDT (Perkin Elmer) liquid pipetting station and allowed to shake for 30 minutes at room temperature. Using an automated plate washer (Biotek), the assay plate was washed with the screening buffer. 50 μ L of primary anti-E2F1 antibody (Millipore) diluted 1:25,000 was added to each well and incubated for 60 minutes on a shaker. Assay plates were washed and 50 μ L of a goat anti-mouse IgG horseradish peroxidase antibody (BioRad) diluted 1:5,000 was added and incubated for 30 minutes with shaking at room temperature. Following a final set of washes, 50 μ L of a 50:50 mixture of ELISA Pico Chemiluminescent Substrate (Pierce) was added to each well and read within 20 minutes using an Envision multilabel plate-reader (Perkin Elmer).

Each plate receiving compounds also contained positive controls: GST-pRb_{ABC}/E2F_{MB-TA} + DMSO in columns 1 and 23 and negative controls GST-pRb_{ABC}/E2F_{MB-TA} + 16E7_{CR2-3}/DMSO in columns 2 and 24. Uniformity plates (192 positive controls, and 192 negative controls) were distributed

throughout the screening plates to ensure both assay and result reliability. All compounds were screened in duplicate. The chemiluminescence signal from each well was normalized to the negative controls on each plate based on the following equation: $Z = (\chi - \mu) / \sigma$, where χ is the chemiluminescence signal of a given well, μ is the mean of the negative control population, and σ is the standard deviation of the negative control population. Compounds giving a chemiluminescence signal higher than 3 standard deviations above the mean were considered hits. Software applications developed by CeuticalSoft (OpenHTS) were used to deconvolute the data from orthogonally pooled screening libraries using methods similar to those described by others (Devlin and Morser, 1996; Ferrand et al., 2005; Motlekar et al., 2008). The data was grouped into four categories: actives (compounds that displayed >50% inhibition of E2F displacement and clearly mapped to a unique well in both the horizontal and vertical directions), ambiguous (compounds that mapped to two or more wells in either dimension), orphan (compounds that displayed inhibition in only one direction) and inactive compounds. 364 compounds (not from the inactive category) were identified as initial hits and requested as cherry picks. The cherry picked compounds were retested with controls to test reproducibility, and their IC_{50} values were determined to find compounds with dose-dependent inhibition.

2.7.5 ELISA Assays

IC_{50} values for inhibition of E2F displacement from pRb by E7 + inhibitors were measured using the same ELISA-based assay as described for the high-throughput screen, except that the assay was performed manually in 96-well format with all volumes doubled. All compounds were solubilized to 50mM in DMSO and diluted for use in the ELISA-based assay at a final DMSO concentration of less than 5%. The concentrations of the compounds in the IC_{50} experiment spanned the range of enzyme activity from no inhibition to complete inhibition. To test E1A-pRb and E7-pRb binding, the assay was modified so that GST-pRb_{ABC} alone was added to HPV-E7_{CR2-3} + compound/DMSO, or Ad5-E1A_{CR1-3} + compound/DMSO. Mouse monoclonal anti-His antibody (Fisher) (1:10,000) and mouse monoclonal Ad5-E1A antibody (Abcam) (1:10,000) were

used to detect how much His-E7_{CR2-3} and E1A_{CR1-3} remained bound to GST-pRb_{ABC} on the plate, respectively. All other steps remained unchanged. To test the mode of inhibition by the inhibitors, each compound was first incubated with pRb for 30-60 min. Different concentrations of HPV- E7_{CR2-3}, ranging from 50 μ M down to 0.05 μ M were added to the GST-pRb_{ABC} + compound mixture and allowed to incubate for 30-60 min. The reaction mixture was then transferred to a glutathione-coated plate, and shaken for 15-20 min. Mouse monoclonal anti-His antibody (Fisher) (1:10,000) was used to detect how much HPV-E7_{CR2-3} remained bound to GST-pRb_{ABC} on the plate. Three independent IC₅₀ measurements were performed for each compound and the average and standard deviation values are reported. All data was imported into the GraphPad Software (Prism) for IC₅₀ or K_D determination. To calculate the IC₅₀ or K_D values, the dose-response curves were fit to one-site (Hill slope = 1) sigmoidal-dose-response curves. The error bars were obtained from the standard errors generated by the GraphPad software.

2.7.6 Pull-Down Assays with Inhibitors

10 μ g His-tagged protein pRb_{ABC} was incubated with 10 μ l Ni-NTA beads (Fisher) in a buffer containing 20mM Tris, 7.5, 150mM NaCl, 35mM Imidazole and 0.05% Tween20 for 15 min. Then, inhibitor and an equimolar amount of GST-HPV16-E7_{FL} to pRb were added and allowed to incubate at 4^o C for 1 hr with gentle agitation. The beads were then washed three times with 1mL buffer (20mM Tris, 7.5, 150mM NaCl, 35mM Imidazole and 0.05% Tween20) and subjected to SDS-page analysis. The samples were transferred to PVDF membrane to be visualized by western blotting. Anti-GST mouse monoclonal antibodies (1:2000) (Calbiochem) and anti-His mouse monoclonal antibodies (1:5000) (Fisher) were used. Bands were visualized by chemiluminescence (Pierce) and exposure to film (Kodak).

2.7.7 LC-MS Analysis of Thiadiazolidinedione Compounds

This experiment was performed by Jason Melvin in the Huryn Laboratory in the Department of Chemistry at the University of Pennsylvania. The compounds determined to be reproducible with dose-dependent inhibition were purchased as powders. The purity of the seven thiadiazolidinediones was verified by LC/MS and the structure of compound 478419 was verified by NMR (described below). Furthermore, the purities of all the compounds were claimed by the company they were purchased from to be >90%. LC-MS analysis was performed using a Waters Micromass ZQ system. The mobile phase contained 0.5% formic acid in H₂O and acetonitrile. The compounds were resolved on a Waters Sunfire C18 4.6x50mm analytical column at a flow rate of 2.0 mL/min with a gradient of 10%-90% acetonitrile over 6 min followed by 1 min at 100% acetonitrile. Percent purity was calculated based on the UV absorption chromatogram.

2.7.8 Conformation of Structure by NMR

This experiment was performed by Jason Melvin in the Huryn Laboratory in the Department of Chemistry at the University of Pennsylvania. ¹H NMR analysis was performed on a Bruker AMX-500 spectrometer. Chemical shifts are reported as δ values relative to internal chloroform (δ 7.27).

2.7.9 Isothermal Titration Calorimetry

ITC was done using a MicroCal VP-ITC isothermal titration calorimeter (MicroCal, Inc). Proteins were dialyzed against a buffer containing 20mM Hepes, 7.5, 150mM sodium chloride and 0.1mM Tris carboxy ethyl phosphene prior to analysis. 8-12 μ L injections of 750-1500 μ M compound (final DMSO concentration of 1.5 %) were titrated into 50-150 μ M pRb_{AB} (containing the same percentage of DMSO) pre-equilibrated to 22 °C. For testing of reversible binding, pRb in complex with compound 478166 was dialyzed overnight in a buffer containing 20mM Hepes, 7.5, 150mM

sodium chloride and 0.1mM Tris carboxy ethyl phosphene. ITC was then repeated by injecting compound 478166 into the dialyzed pRb/478166 complex to see if binding can be reconstituted. For binding of compound to E7, the same protocol was used as for testing the binding to pRb. After subtraction of dilution heats, calorimetric data were analyzed with the MicroCal ORIGIN V5.0 (MicroCal Software, Northampton, MA). Error values obtained from the MicroCal ORIGIN V5.0 software were averaged and reported.

2.7.10 Cell Culture

C-33A and SiHa cell lines were purchased from ATCC and grown in 1x minimal eagle's media (MEM, Cellgro) supplemented with 10% fetal bovine serum (Hyclone), 10 μ g/ml penicillin-streptomycin (Cellgro), 2mM L-glutamine (Cellgro), 1mM sodium pyruvate (Cellgro), and 100 μ M non-essential amino acids (Gibco). HeLa, and HCT116 cell lines were generous gifts from the laboratories of Susan Janicki, and Meenhard Herlyn, respectively, and maintained in the same way.

2.7.11 MTS Cell Proliferation Assay

Cultured cell lines were seeded in 384-well, clear, tissue culture plates (NUNC) at 10,000, 1,000, 1,000, 1000, and 2,000 cells/well for C-33A, SiHa, HeLa, TC-1, or HCT116 cells, respectively in a volume of 20 μ L. The next day, compound dissolved in a final DMSO concentration of 0.5% was added to each well to a final volume of 40 μ L and incubated for 48 hr. Cell viability was then monitored by addition of 8 μ L of MTS reagent (Promega) and measurement at A_{490} using an Envision multilabel plate reader within 3 hr of MTS addition.

2.7.12 Flow cytometry

Cultured cell lines were seeded in 60mm tissue culture dishes (Falcon) at 1×10^5 cells/well. The

next day, 10 μ M compound or DMSO were added and incubated for 48 hr. Cells were then trypsinized, washed with 1.0 mL phosphate-buffered saline (PBS), and fixed in 80% ethanol. Fixed cells were spun at 500g for 5 min, and washed with PBS. Cells were stained with 250 μ L propidium iodide (PI), which was prepared by adding 100 μ L 2mg/ml PI (Sigma) and 10 μ g RNase A (Sigma) into 10mL PBS. Cells were then analyzed at the Wistar Institute Flow Cytometry Core Facility.

2.7.13 Mouse Studies

This experiment was performed by Scott Troutman in the Kissil Laboratory at the Wistar Institute. A tumor model was constructed by inoculating 2.0 x 10⁵ TC-1 cells into the right flank of 12 NOD SCID female mice (Jackson Laboratory, Bar Harbor, ME). Treatment was started 5 days post-injection, as tumors became palpable. The mice were treated once a day for 14 days, with intraperitoneal injections of DMSO (0.1%) or compound 478166 at doses of 10mg/kg. Tumor sizes were measured every two days with calipers and tumor volume, V, (in mm³) was calculated using “ $V = l \times w^2 \times \pi/6$.” At the end of the experiment, all mice were sacrificed and the weights of the detached tumors were measured. The experiments were performed twice with similar results. Statistical analysis was done using the paired Student's *t* test. Errors were obtained by calculating the standard deviations from all the mice in each set. All animal experiments were approved by the Wistar Institutional Animal Care and Use Committee and performed in accordance with relevant institutional and national guidelines.

CHAPTER 3

Identification and Characterization of Small Molecule Human Papillomavirus E6 Inhibitors

3.1 Introduction

The high risk human papillomavirus E6 proteins have the ability to inactivate the tumour suppressor p53 by targeting it for degradation (Werness et al., 1990). To do this, E6 recruits E6AP (E6-Associated Protein), an E3 ubiquitin ligase, by binding to a conserved L-X-X-L-L motif on the ligase and targeting p53 for degradation by the 26S proteasome.

HPV 16 E6 is a 158 amino acid protein comprised of both an N and C terminal domain (E6N and E6C) (Nomine et al., 2005). Each of these domains contain two C-X-X-C motifs, where four cysteines ligate one zinc ion (Figure 3.1). The N terminal domain is connected to the C terminal domain by a central, conserved linker. Each end of the protein consists of a loop region, with the C terminal loop containing a PDZ binding motif. This architecture is seen in the E6 proteins from other human papillomaviruses as well (Nomine et al., 2003).

The full length E6 protein contains six additional cysteines that do not coordinate zinc and these are not conserved. In general, the E6 protein has been difficult to work with *in vitro* due to its propensity to aggregate and precipitate (Lipari et al., 2001; Nomine et al., 2003; Nomine et al., 2006). To try to circumvent this problem, Nominé et al. mutated the nonconserved cysteine residues to serines (Nomine et al., 2003). This construct was shown to behave the same way as wild type E6 in *in vitro* and *in vivo* p53 degradation assays (Nomine et al., 2003; Nomine et al., 2006). Unfortunately, removal of the nonconserved cysteines did not prevent the protein from aggregating and precipitating.

The tendency to aggregate and precipitate was eventually attributed to the E6N domain of HPV 16, which undergoes homodimerization (Lipari et al., 2001). The E6C domain, on the other hand, remains monomeric (Nomine et al., 2005). Work by Nomine et al. showed that the E6N (residues 7-83), even when expressed alone, was poorly behaved whereas E6C (residues 87-158) could easily be concentrated to 1mM (Nomine et al., 2003). Interestingly, the E6C domain also was shown to bind four-way DNA Holliday junctions as well as the full length protein (Nomine et al., 2003).

Just this year, Zanier et al. discovered which residues in E6N were important for dimerization and that mutation of those residues could lead to a highly soluble and well-behaved protein (Zanier et al., 2012). The residues were identified by observing large chemical shifts in several amide groups upon dilution of the protein sample by NMR (Zanier et al., 2012). The NMR structure of full length E6 from HPV 16 was determined, and the N- and C- domains are shown in [Figure 3.1](#) (Zanier et al., 2012). The structures of the E6N and E6C domains are homologous with the exception of the N-terminal regions. The N-terminal region of E6N is a flexible loop, whereas the N-terminal region of E6C folds into a beta strand.

Interestingly, experiments have shown that antibodies that target residue Phe-2 (Giovane et al., 1999), or mutations of this residue (Cooper et al., 2003a; Liu et al., 1999), abolish binding to p53 and therefore p53 degradation. Furthermore, performing point mutations in the dimerization domain of E6N, particularly F47R, drastically improved the solubility of E6. This residue is at the dimer interface, shown in [Figure 3.2](#) (Zanier et al., 2012). This mutant was shown to have similar binding to E6AP as wild-type E6, however, it was unable to degrade p53. This suggested that dimers or higher order oligomers of E6 may be necessary for p53 degradation (Zanier et al., 2012). These results led to a model by which E6 may bind to E6AP and to p53, to lead to p53 ubiquitination ([Figure 3.3](#)) (Zanier et al., 2012). In this model, E6AP binds to one molecule of E6 and makes intermolecular contacts with p53 that is bound to the N-terminus of another molecule of E6. This then results in a trans-ubiquitination event, as depicted in [Figure 3.3](#) (Zanier et al., 2012).

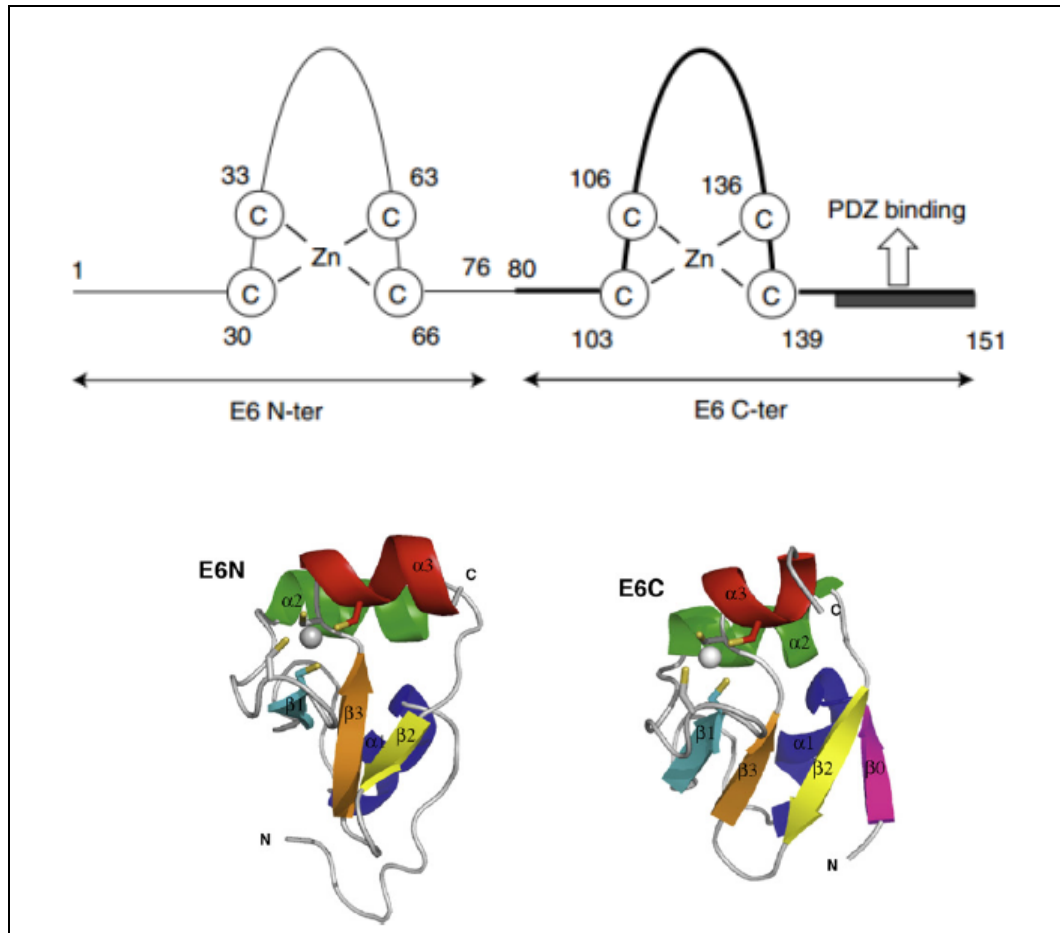


Figure 3.1. Schematic representation of full length HPV16 E6 protein and NMR structures of the individual domains. (Top) Residues numbers are given for each individual domain and the amino acids involved in Zn^{2+} ligation. Full length E6 consists of an N-terminal domain (E6N) and a C-terminal domain (E6C), each of which contains a zinc-binding site. This figure is adapted from Nomine et al, 2005. (Bottom) The NMR structures of each domain reveal two homologous structures consisting of a three-stranded beta sheet and three alpha helix fold. The E6C domain has an additional beta strand. The zinc binding site is peripheral, and ligated by cysteine residues. This figure is adapted from Zanier et al. 2012.

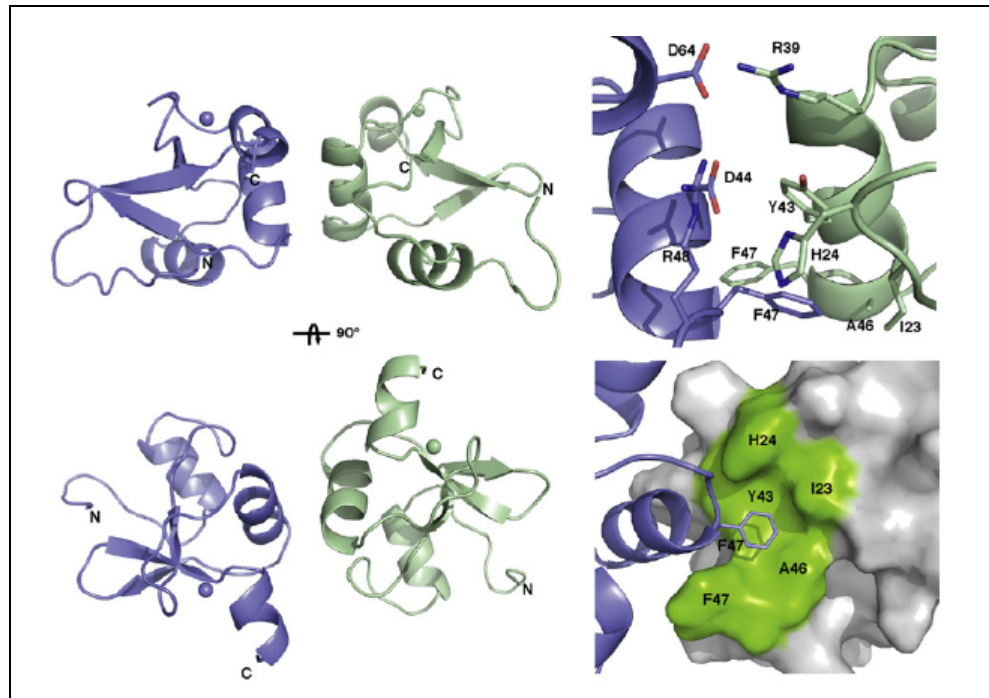


Figure 3.2. NMR structure of E6N. E6N is shown to dimerize. A number of residues at the dimer interface are conserved and their mutation weaken the protein's ability to dimerize and also prevents p53 degradation, even though they retain the ability to bind E6AP. The mutations that do this are H24A, Y43R, Y43E, D44A, D44R, and F47E. F47 mutations have been shown to substantially increase E6 solubility. This figure is adapted from Zanier et al. 2012.

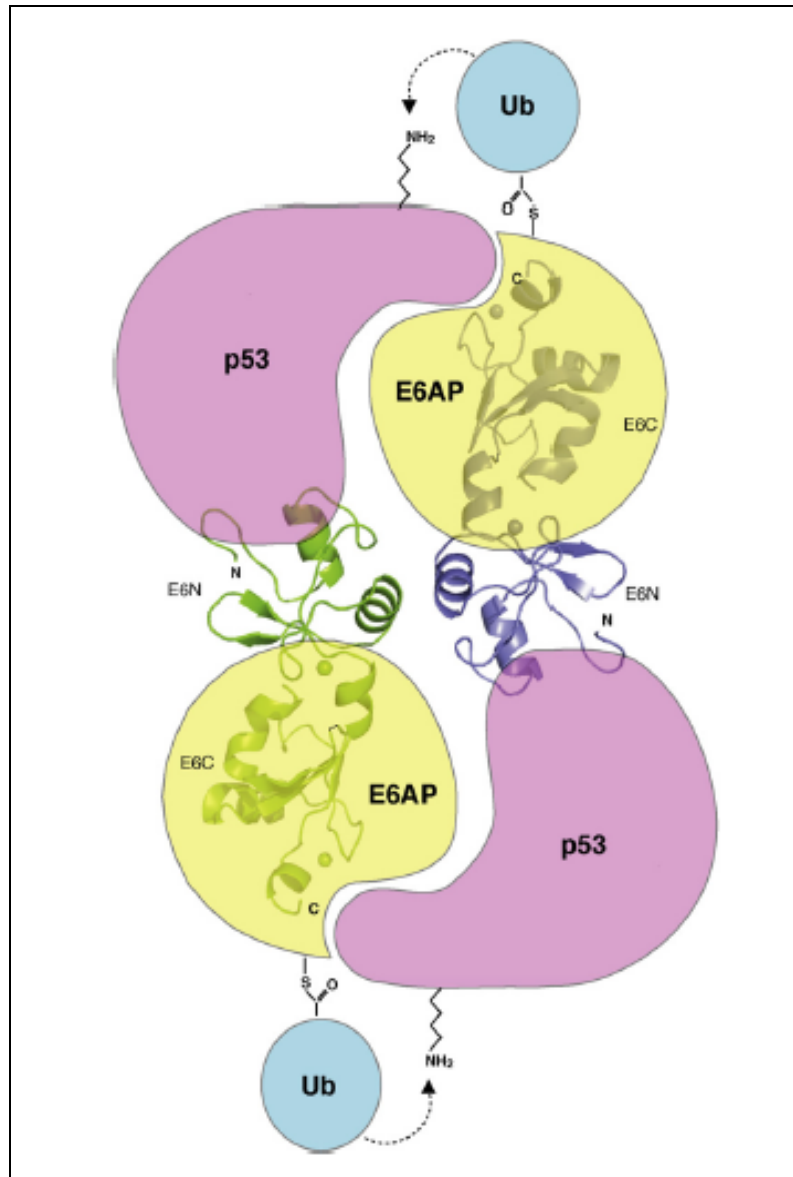


Figure 3.3. Model for p53 ubiquitination by E6/E6AP complexes. The E6 dimer puts E6AP and p53 molecules at opposing ends. It is suggested that the flexible N-terminus of E6 mediates binding to p53. The proximity of E6AP and p53 from different E6 molecules is thought to result in a "trans-ubiquitination event". This figure is adapted from Zanier et al. 2012.

As mentioned earlier, E6AP is an E3 ubiquitin ligase. It contains 875 amino acids, with the final 357 amino acids comprising the C terminus or HECT domain, which catalyzes the transfer of ubiquitin to target proteins (Figure 3.4). When E6 is not present, E6AP has no interaction with or shows any propensity for targeting p53 for degradation (Be et al., 2001; Elston et al., 1998; Huang et al., 1999). A short, α helical peptide N terminal to the HECT domain (residues 403 – 421) is necessary and sufficient for E6 binding. The consensus binding sequence is: L h x ϕ L s h, where L is leucine, h is an amino acid that can accept a hydrogen bond, x is any amino acid, ϕ is a hydrophobic residue, and s is a small amino acid like glycine or alanine (Be et al., 2001). The region of E6 that binds to this consensus sequence is not known, but speculated to be at the periphery of the E6N/E6C interface, since these domains alone cannot bind to peptides from E6AP (Nomine et al., 2006).

When E6 is bound to E6AP, the complex binds p53's core domain for the transfer of ubiquitins (Cooper et al., 2003a; Huijbrege et al., 1993; Li and Coffino, 1996a). Interestingly, it is the DNA binding (DBD), or core domain, of p53 that harbors the vast majority of tumor-derived p53 mutations (Cho et al., 1994b; Viadiu, 2008). The p53 DBD binds the DNA cooperatively, with only tetrameric species present after DNA/domain incubation (Balagurumoorthy et al., 1995). Full length human p53 protein contains 393 amino acids and is comprised of three additional domains: the N terminal transactivation domain, the tetramerization domain, and the C terminal regulatory domain (Figure 3.4). The N terminal transactivation domain interacts with the cellular transcriptional machinery to promote gene transcription (Viadiu, 2008). The crystal structure determined by Jeffrey et al. shows that four tetramerization domains come together as a dimer of dimers (Jeffrey et al., 1995). In fact, the functional quaternary structure of p53 *in vivo* is a tetramer. The regulatory domain is a basic region composed of many lysines and arginines. This is the area where most of the post-translational modifications occur, such as methylation, phosphorylation, acetylation, and ubiquitination (Viadiu, 2008).

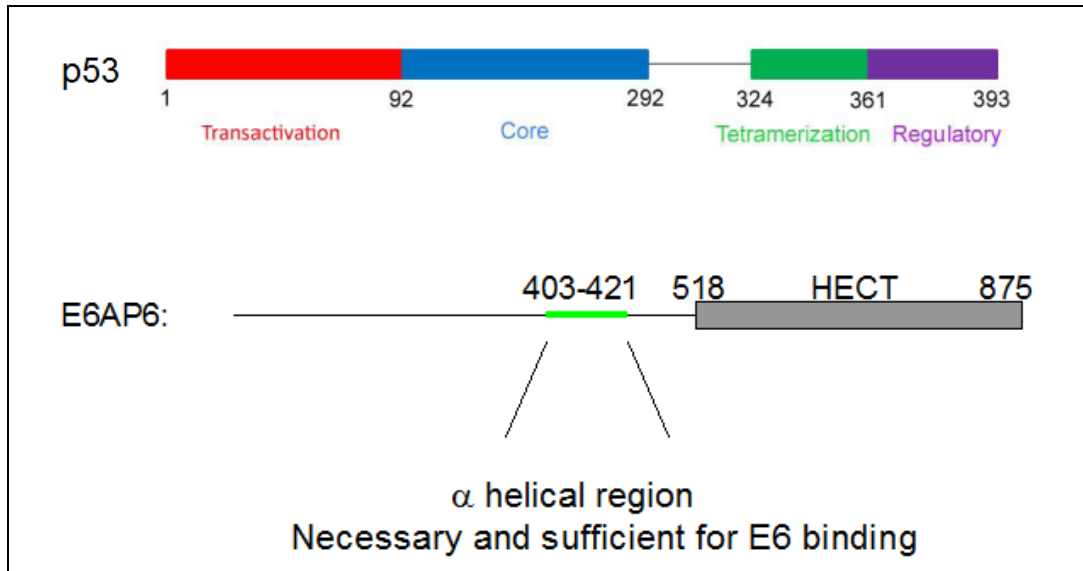


Figure 3.4. Schematic representation of full length p53 and full length E6AP6. p53 contains four domains as indicated. E6AP contains a HECT domain that contains ubiquitin ligase activity. It also harbors a small alpha helical region that is necessary and sufficient for E6 binding. Details are given in the text.

Because the binding of E6 to E6AP is a prerequisite to p53 degradation, our laboratory has focused on identifying small molecules that block E6 binding to E6AP, which would subsequently block p53 degradation and bring about a return of p53 tumor suppressor function. E6 is a small, monomeric protein of 19 kDa (Lipari et al., 2001; Nomine et al., 2003) and since the region of E6AP that is necessary and sufficient for E6 binding is a 20 amino acid α helix (Be et al., 2001; Cooper et al., 2003a; Huibregste et al., 1993), this suggested that it would be feasible to inhibit this interaction with a small molecule compound (Degeterev, 2001; Kutzki, 2002). Towards this end, we developed a high throughput assay to screen for small molecule inhibitors of the E6-E6AP interaction.

3.2 High-Throughput Screening Results

3.2.1 Development of a High Throughput Screen and Inhibitor Identification

A high throughput screen (HTS) for small molecule inhibitors of the E6 / E6AP interaction was designed around a modified sandwich enzyme-linked immunosorbance assay (ELISA) (Figure 3.5). Full length HPV16 E6 was fused C terminally to glutathione-S-transferase (GST). To improve E6 solubility and decrease aggregation, all non-conserved cysteine residues of the HPV16 E6 sequence were substituted (Nomine et al., 2003; Nomine et al., 2006) to the analogous residue found in HPV1A E6 and is referred to as E6M. A very similarly mutated E6 protein has been used by others except that in the other studies all nonconserved cysteines were mutated to serines (Nomine et al., 2003; Nomine et al., 2006). Importantly, Nomine et al showed that mutating the cysteines to serines did not prevent the domain from adopting a stable fold, all mutated positions are on the surface of the calculated structure, and these mutations in the context of the full length E6 protein was shown to display *in vitro* and *in vivo* p53 degradation properties that were comparable to wild-type E6. To ensure that E6M could specifically interact with endogenous E6AP, we performed *in vitro* pulldowns with E6M and E6AP versus other proteins. E6M specifically pulled down E6AP but not other proteins (Figure 3.6).

Residues 363 to 440 of E6AP (isoform II), which contain the LQELLGE motif necessary for E6 binding (Huibregste et al., 1993), were fused N terminally to the maltose binding protein (MBP). Following binding of E6M-GST to glutathione coated wells (NUNC), MBP-E6AP was added to the wells of a 384-well plate at a concentration of 6 μ M in the presence of a small molecule dissolved in DMSO or a DMSO control. This concentration is the reported K_d of the protein-protein interaction (Zanier et al., 2005) and fell at the center of the linear binding range between E6M-GST and MBP-E6AP in our assay parameters. The extent of binding between the two proteins was assessed by incubation with the anti-MBP-HRP antibody (New England BioLabs) and chemiluminescence (Pierce).

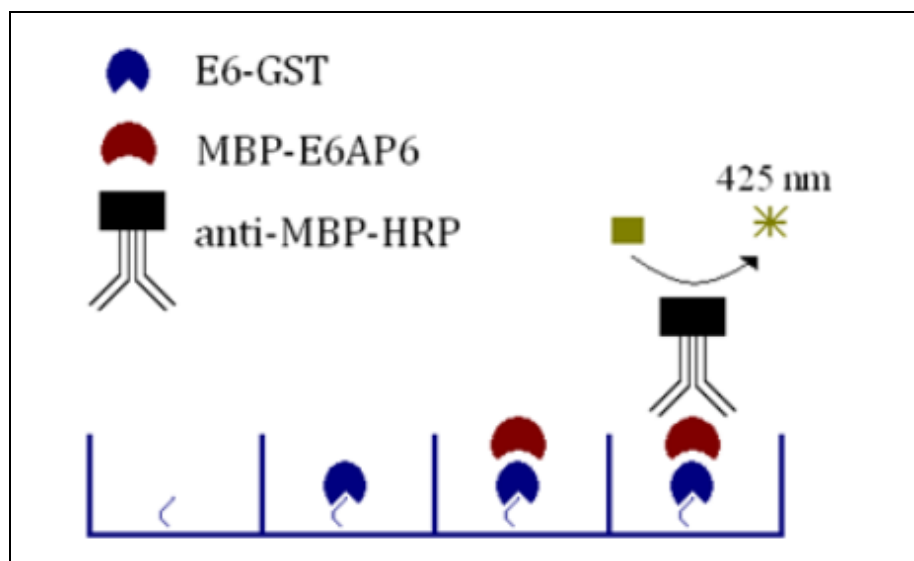


Figure 3.5: Scheme for the high throughput screening assay. The ELISA assay is represented here schematically. DMSO or compound dissolved in DMSO was added with the MBP-E6AP to E6M-GST that was immobilized on a glutathione coated plate. The amount of MBP-E6AP that could bind to E6M-GST was quantitated by using antibodies against MBP.

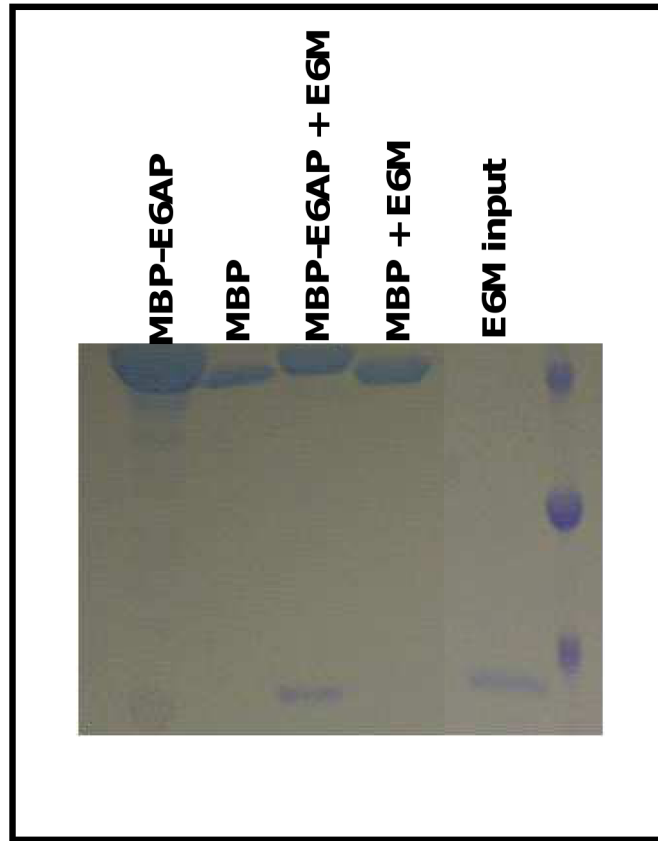


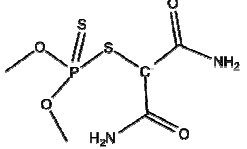
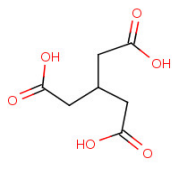
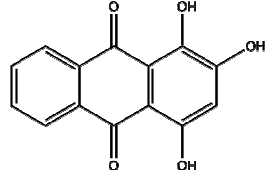
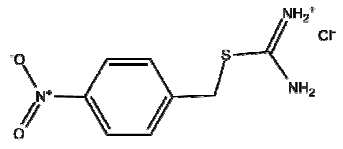
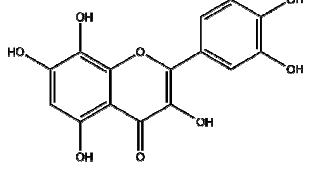
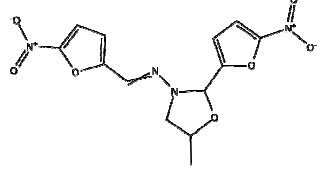
Figure 3.6: Pull down assay between E6M and MBP-E6AP. To show that the mutated E6 behaves properly, we performed pull down assays *in vitro* with E6M + MBP-E6AP versus MBP. The SDS-Page gel shows that E6M specifically pulls down MBP-E6AP, but not MBP alone. This suggests that the E6AP binding properties of E6M are similar to those of wild-type E6.

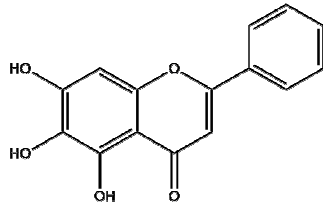
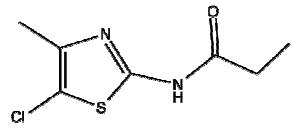
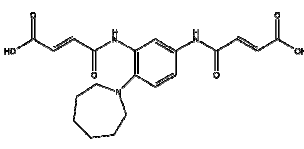
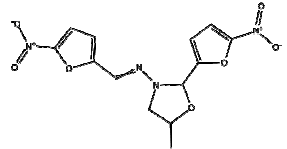
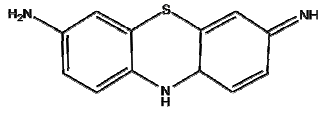
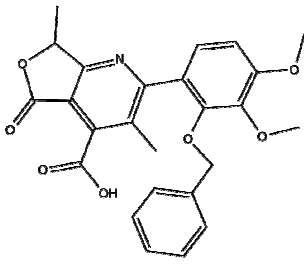
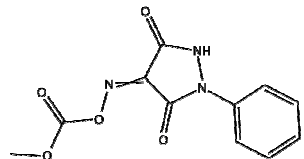
The robustness of the assay was assessed using the Z factor parameter. Using a 96 well format, we optimized conditions to obtain a Z factors of 0.784 (Positive control: E6M-GST + MBP-E6AP, negative control: GST + MBP-E6AP) and 0.624 (Positive control: E6M-GST + MBP-E6AP, Negative control: E6M-GST + MBP). This data indicated that the GST and MBP fusions did not significantly affect the specific interaction between E6M and E6AP. Miniaturization to a 384 well format and automation optimization resulted in Z factors consistently above 0.60.

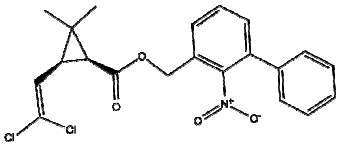
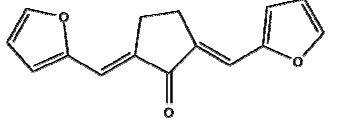
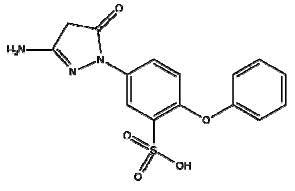
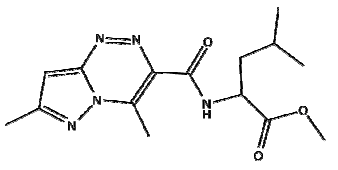
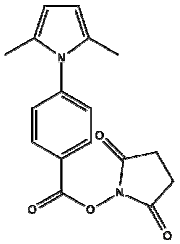
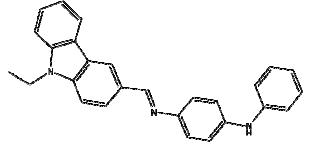
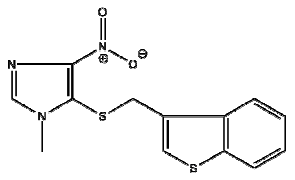
Three different chemically diverse compound libraries were screened: Spectrum (Microsource; 2000 compounds), HitFinder (Maybridge; 14,000 compounds), and the Orthogonally Pooled Screening libraries (OPS, Lankenau Institute for Medical Research; 72,000 compounds), resulting in nearly 90,000 total compounds. The Spectrum library was screened with a single compound per well in duplicate, and the Maybridge and OPS libraries were screened in a compressed format of 5 compounds per well based on the Devlin et al. method for screening and deconvolution of data (Devlin et al., 1996). The initial screening resulted in the selection of 201 potential inhibitors of the E6 - E6AP interaction (a 0.23% primary hit rate) that were further investigated in follow-up studies. All assigned hits were cherry picked and retested at the screening concentration in the ELISA assay. Following retesting, the number of potential inhibitors dropped to 54, producing a hit rate from the entire screen of 0.061% (Table 3.1). After performing secondary assays, the number of compounds was brought down to 30. A summary of the results, which will be discussed throughout the text, is given in Table 3.2.

Library Name	Library Size (# compounds)	Hits	Primary Screen	Secondary Assays
Spectrum	2,000	7	4	4
Maybridge HitFinder	14,400	56*	13	12
OPS	72,000	138*	37	14
TOTALS	88,400	201	54	30

Table 3.1. Screening Summary. Names of the libraries screened, their size, and the number of hits from each screen are shown. Hits: Number of potential inhibitor compounds from the initial screening that achieved the assigned activity cutoff of three standard deviations from the mean. Asterisks show which libraries included ambiguous and orphan hits to the original hit number. Primary Screen: Number of potential inhibitors that again showed inhibition in the ELISA assay at the original screen concentration following cherry picking from their original stock solutions kept frozen. Secondary Assay: Compounds that, following purchase of powders, passed all secondary assays for inhibition.

Name	Screen	ELISA IC ₅₀	<i>In Vitro</i> p53 Degradation ~IC ₅₀	Thermal Stability	Structure
C14	Lankenau	30.6 ± 4.7 nM	25-250 μM	Stabilized	
C17	Lankenau	86.1 ± 37.3 nM	10 – 100 μM	Unchanged	
Purpurin	Spectrum	143 ± 78 nM	250 nM	Stabilized	
E17	Lankenau	148 ± 42 nM	25-250 μM	Stabilized	
Gossypetin	Spectrum	170 ± 21 nM	2.5-25 μM	Stabilized	
B15	Lankenau	178 ± 122 nM	10 – 100 μM	Unchanged	

Baicalein	Spectrum	235 ± 74 nM	250 nM	Stabilized	
A19	Lankenau	295 ± 38 nM	10 – 100 µM	Stabilized	
S05659	Maybridge	311 ± 1.6 nM	250 nM – 2.5 µM	Unchanged	
D5	Lankenau	347 ± 218 nM	10 µM	Stabilized	
C6	Lankenau	363 ± 24 nM	1 – 10 µM	Unchanged	
A14	Lankenau	457 ± 14 nM	100 µM	Unchanged	
A22	Lankenau	477 ± 166 nM	2.5-25 µM	Stabilized	

C9	Lankenau	496 ± 49 nM	10 – 100 μM	Stabilized	
DP00966	Maybridge	573 ± 323 nM	250 μM	Unchanged	
JFD00458	Maybridge	703 ± 54 nM	250 nM	Stabilized	
B11	Lankenau	749 ± 310 nM	2.5 μM	Unchanged	
RH02007	Maybridge	1.41 ± 0.05 μM	25-250 μM	Stabilized	
C22	Lankenau	1.79 ± 0.24 μM	100 μM	Stabilized	
HTS03324	Maybridge	2.27 ± 1.04 μM	2.5 nM	Stabilized	

C16	Lankenau	3.98 ± 3.88 μM	2.5 – 25 μM	Unchanged	
HTS13545	Maybridge	4.11 ± 0.21 μM	2.5 – 25 μM	Stabilized	
HTS10308	Maybridge	5.24 ± 0.03 μM	25 – 60 μM	Unchanged	
DSHS 00884	Maybridge	~ 10 μM	2.5-25 μM	Stabilized	
CD11403	Maybridge	10.9 ± 0.6 μM	25 – 250 μM	Unchanged	
Brazilin	Spectrum	11.2 ± 4.2 μM	25 – 250 nM	Stabilized	
BTB 07267	Maybridge	15.1 ± 1.8 μM	250 nM – 2.5 μM	Stabilized	

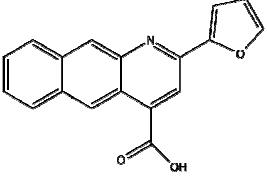
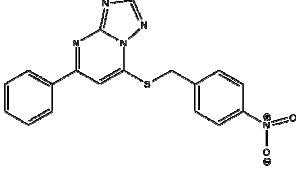
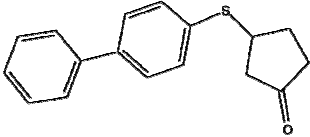
S05896	Maybridge	15.7 ± 1.2 μM	25 – 250 μM	Unchanged	
HTS11967	Maybridge	30.3 ± 10.9 μM	250 nM – 2.5 μM	Stabilized	
D22	Lankenau	36.9 ± 10.3 μM	250 nM	Unchanged	

Table 3.2. Secondary assay results summary for inhibitor compounds. The names, structures and secondary assay results for all thirty identified E6 inhibitor compounds are listed in rank order of their ELISA IC₅₀ values. ELISA IC₅₀ values were determined by performing the assay in duplicate for each compound, followed by normalization of data and subsequent data fitting in GraphPad with log(inhibitor) vs. response (variable slope) non-linear regression fit. The approximate IC₅₀ for p53 degradation (performed *in vitro* with HPV 16 E6 and HPV 18 E6) is reported as a range. The thermal stability result is as described in the text.

3.2.2 Identification of Compounds that Prevent E6-E6AP Interaction *in vitro*

We ranked the potency of the inhibitors by determining the compound concentration that reduced the extent of binding between E6M-GST and MBP-E6AP by 50% (IC₅₀ value). For each of the inhibitors tested, fresh powders were ordered directly from commercial suppliers and 42 of the 54 compounds had IC₅₀ values of 30 μM or less, with more than half of the inhibitors having IC₅₀ values in the low to mid-nanomolar range. The IC₅₀ curves from the ELISA-based assay of six of the compounds, to be discussed in more detail later, are shown along with the structures of the compounds in [Figure 3.7](#). To eliminate any artifacts from the ELISA-based format, these six inhibitors were retested by performing pull downs on amylose beads onto which MBP-E6AP was immobilized. After incubation with inhibitor, the ability of E6M-GST to bind to E6AP was assessed by Western Blot ([Figure 3.8](#)). The inhibitor was able to displace E6M-GST from E6AP in this format, suggesting that the inhibitors can prevent this interaction *in vitro*.

A parallel screen using the same assay format for inhibitors against HPV E7's ability to disrupt the pRb/E2F complex did not identify any of these compounds as hits (data not shown), thereby providing evidence that that these compounds were not non-specifically preventing the interaction between E6M-GST and MBP-E6AP. To further confirm that this was the case, pull-down experiments between pRb and E7, which are known to interact, were done in the presence of increasing concentrations of six of the identified E6 inhibitor compounds with IC₅₀ values in the min nanomolar to low micromolar range ([Figure 3.8](#)). As expected, these compounds did not prevent the interaction between these two proteins up to a compound concentration of 500 μM ([Figure 3.9](#)). To further ensure that the compounds were behaving in a specific manner, five compounds that caused precipitation of E6M were eliminated from the pool of potential inhibitors. Compound 9, which is reported as an E6/E6AP binding inhibitor (Baleja et al., 2006a), showed dose response inhibition of E6-E6AP binding using the ELISA assay developed here ([Figure 3.10](#)). Taking these data together, we are confident that the compounds that we identified in our high-throughput screen specifically disrupt the E6-E6AP interaction.

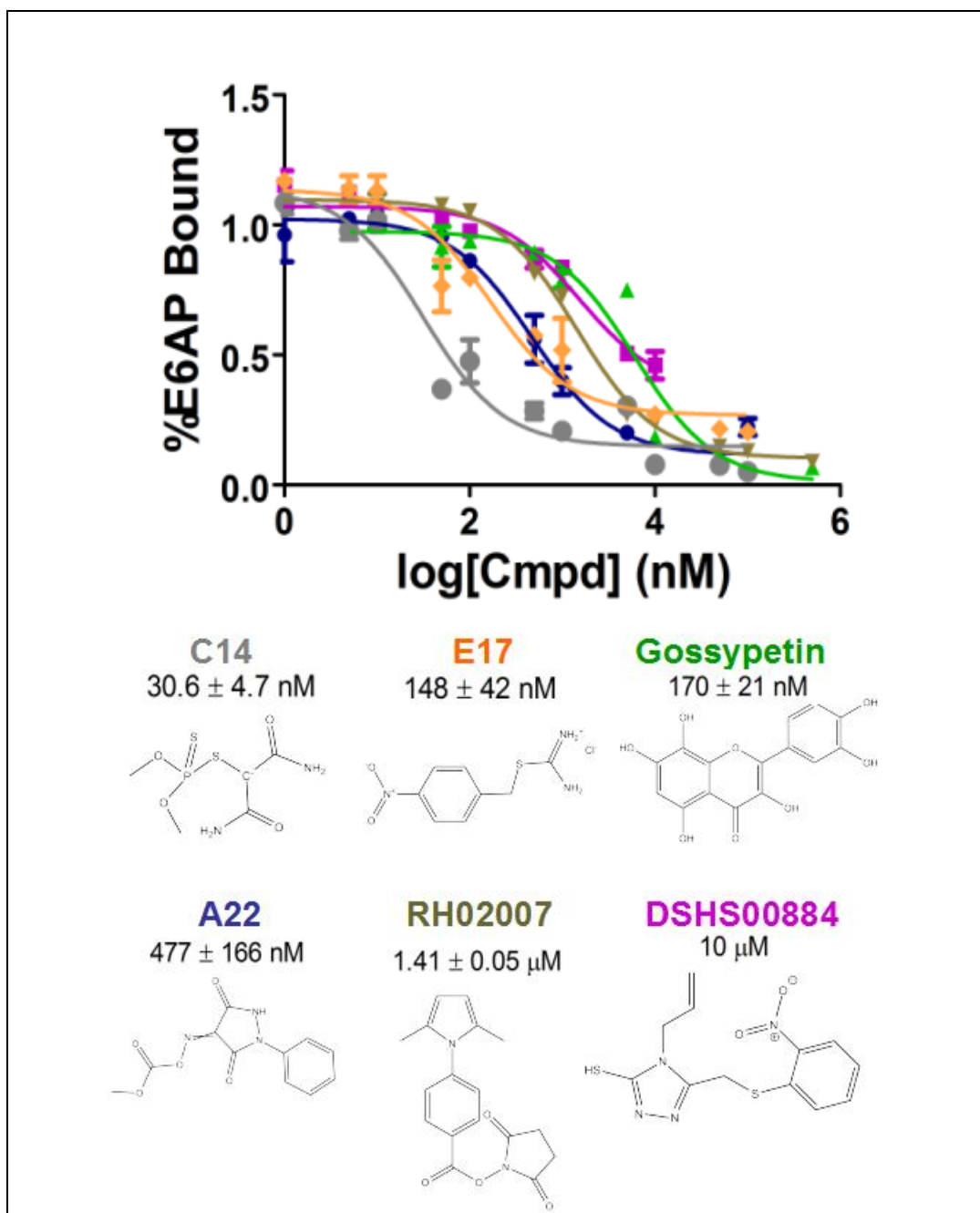


Figure 3.7. IC₅₀ curves for disruption of E6-E6AP complexes by compounds. IC₅₀ curves were generated using the ELISA-based assay described in the Methods. Different dilutions of inhibitor, starting at 500 μM were added to a mixture containing MBP-E6AP and E6-GST. The amount of MBP-E6AP remaining was determined by adding a primary antibody specific for MBP.

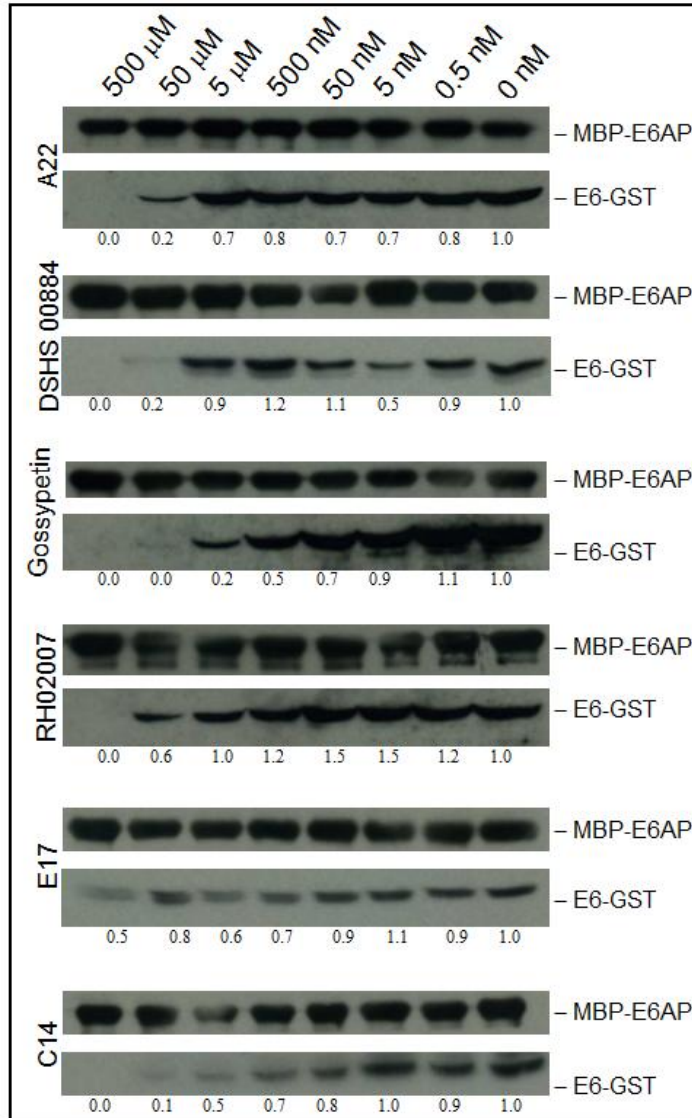


Figure 3.8: Pull down assay between MBP-E6AP and E6-GST in the presence of the six compounds studied. To eliminate any artifacts from the ELISA-based format, the ability of the six compounds to inhibit the E6-E6AP interaction was tested by doing pull-downs on amylose beads. Compounds were testing using ten-fold dilutions, starting at 500 μM. MBP-E6AP was immobilized to the beads and then a complex of E6-GST + inhibitor was added to the mixture. After washing the beads, the amount of E6-GST remaining bound to MBP-E6AP was determined by using anti-GST antibodies. The amount of MBP-E6AP on the amylose beads was determined by using anti-MBP antibodies.

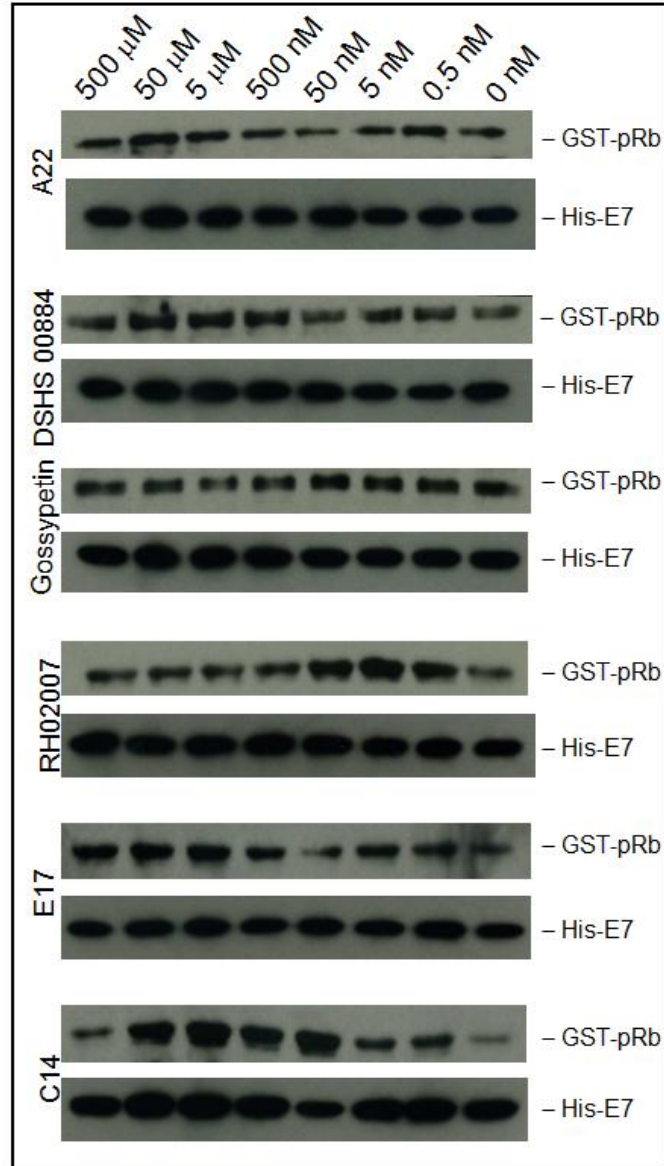


Figure 3.9: Pull down assay between GST-pRb and E7 in the presence of the six compounds studied. These proteins, which are known to interact, have been tested for binding in the presence of increasing concentrations of compound. Compounds were testing using ten-fold dilutions, starting at 500 μ M. To do this, the amount of E7 remaining bound to GST-pRb after incubation with GST-resin and washing was determined using anti-His antibodies. The amount of GST-pRb on the beads was determined by using anti-GST antibodies

Concentration Range: 100 μ M to 1 nM
 $IC_{50} = 1.59 \pm 0.43$ μ M (two data sets)

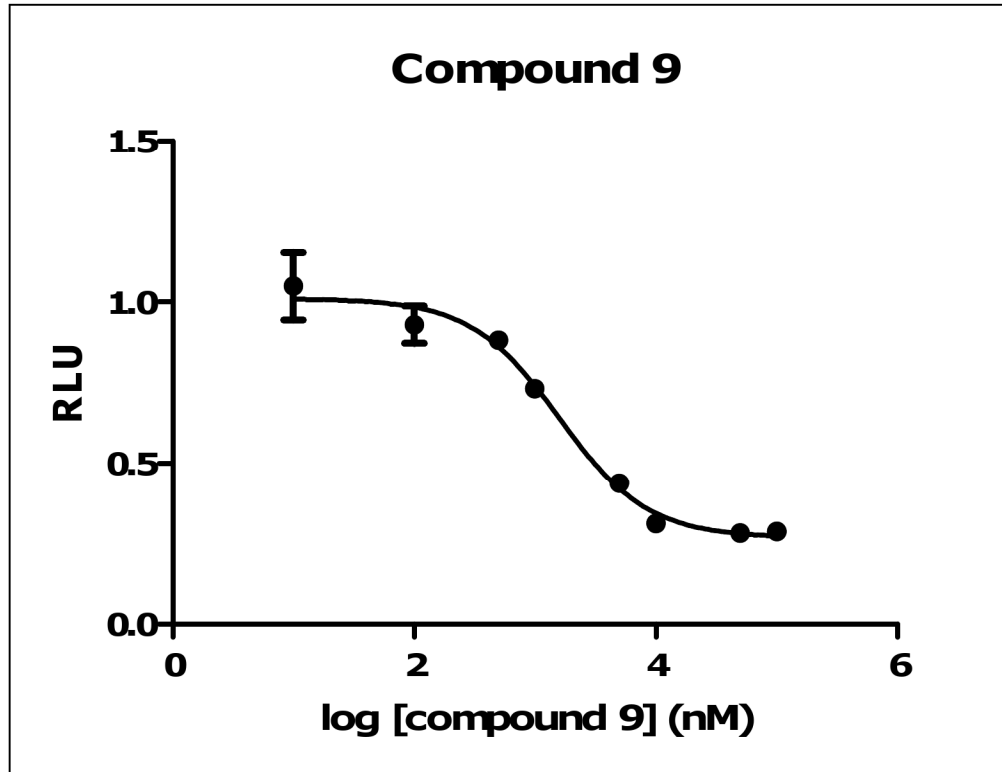


Figure 3.10: E6/E6AP interaction in the presence of a known inhibitor. Compound 9, which is reportedly an E6/E6AP binding inhibitor, (from (Baleja et al., 2006a)) was tested over a range of concentrations and showed a dose response of blocking E6 binding to E6AP in the ELISA assay that we used.

3.2.3 Effects of Compounds on E6 Stability

To determine if the 37 remaining compounds interact with E6, a fluorescent thermal stability assay was employed. This assay monitors protein unfolding in the presence of a given inhibitor where compounds that bind directly to the protein in some manner are generally correlated with a change in the protein melting temperature curve. Full length, untagged E6M was incubated at increasing temperature (20°C - 80°C) with either DMSO control or with compound dissolved in DMSO. The reporter dye, SYPRO orange (Invitrogen), which binds to hydrophobic regions of proteins that are generally exposed upon protein unfolding, was also added.

The control reaction with DMSO showed that E6M was mildly unstable from 20°C to approximately 37°C, after which the protein melted in a standard sigmoidal fashion (Figure 3.11, left panel). Overall, two different types of curves were observed from this assay with added compound. Fourteen compounds resulted in E6M melting curves that were indistinguishable from the protein melting curves without added compound. Unchanged melting curves could indicate that compounds were binding E6M but not significantly stabilizing its structure or that the compound mediated its function in other ways, most likely by binding to E6AP. Eighteen compounds showed significant stabilization of E6M in the region of 20°C to 37°C, which suggested that these compounds were binding to E6M (Figure 3.11, right panel).

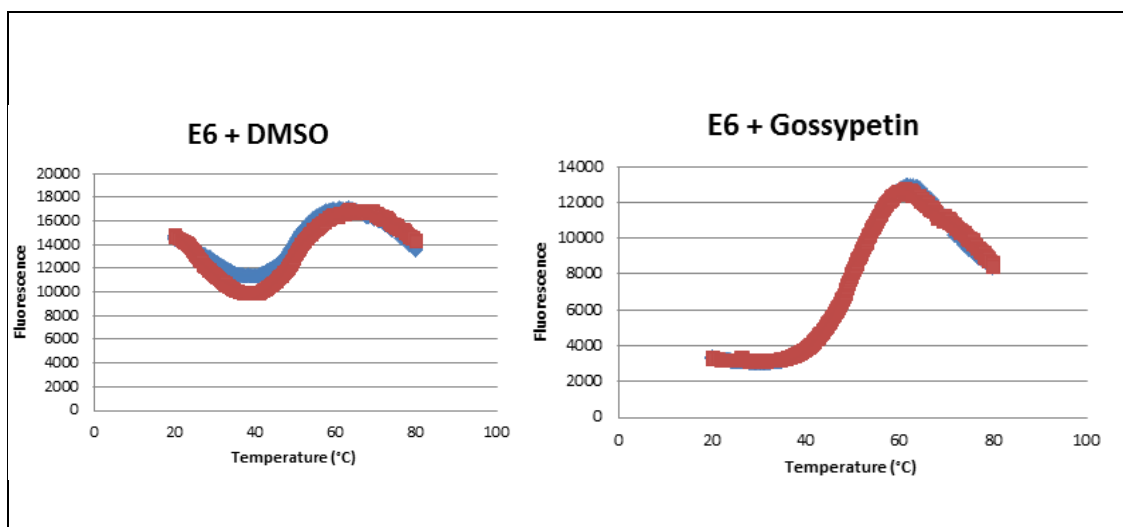


Figure 3.11. Effect of inhibitors on E6 thermal stability. Replicate data (blue and red) for fluorescence at 580 nm vs temperature for each compound are shown as plots. The reporter dye that was used, SYPRO Orange, is known to bind to hydrophobic regions of proteins. Therefore, as samples are heated, an increase in fluorescence is correlated with an increase in protein unfolding. (Left Panel). E6M in 20 mM HEPES, pH 7.5, 500 mM NaCl, and 10 mM BME and 1% DMSO. Inherent protein instability is seen in the region of 20°C to 37°C, as indicated by the higher fluorescence signal. (Right Panel). E6M with gossypetin, representing a compound that stabilizes E6M and results in a curve that no longer has the region of instability from 20°C to 37°C, indicating direct interaction of the compound with E6M.

3.2.4 Identification of Compounds that Prevent HPV16 E6-Mediated p53 Degradation In Vitro

To establish if the E6 inhibitors could function to inhibit the ability of E6 to mediate p53 degradation, we assayed the 37 compounds in a p53 degradation assay. We used a cell free system to factor out the ability of compounds to enter cells. We anticipated that this assay would also help eliminate compounds that were false positives in the ELISA assay, such as those compounds that inhibited GST/glutathione binding or HRP function, and possibilities that could not be easily tested using the fluorescence assay, such as MBP or E6AP precipitation. To carry out these studies, full length, wild type HPV16 E6 and full length, wild type human p53 were translated in separate reactions using the TNT T7 Coupling Reticulocyte System (Promega). Equal amounts of each reaction were mixed together with compound and excess lysate, which contains E6AP and the machinery for ubiquitin-mediated degradation. The amount of p53 present in each sample was determined by a Western blot against the N terminus of human p53 (Santa Cruz Biotechnology).

These studies revealed that 7 compounds showed no effect on p53 degradation in the cell free system. Of the 30 compounds that did modulate p53 degradation, approximate IC_{50} values were observed over a range of concentrations from mid-nanomolar to high micromolar (Table 3.2) with the IC_{50} value representing the concentration of compound needed to reduce p53 degradation levels by 50%. The data for six of the compounds is shown in Figure 3.12. Together, these studies led to the identification of 30 HPV-E6 inhibitors that are able to block the ability of E6 to mediate its oncogenic activity of p53 degradation in a cell free system. The results of these 30 compounds are summarized in Table 3.2.

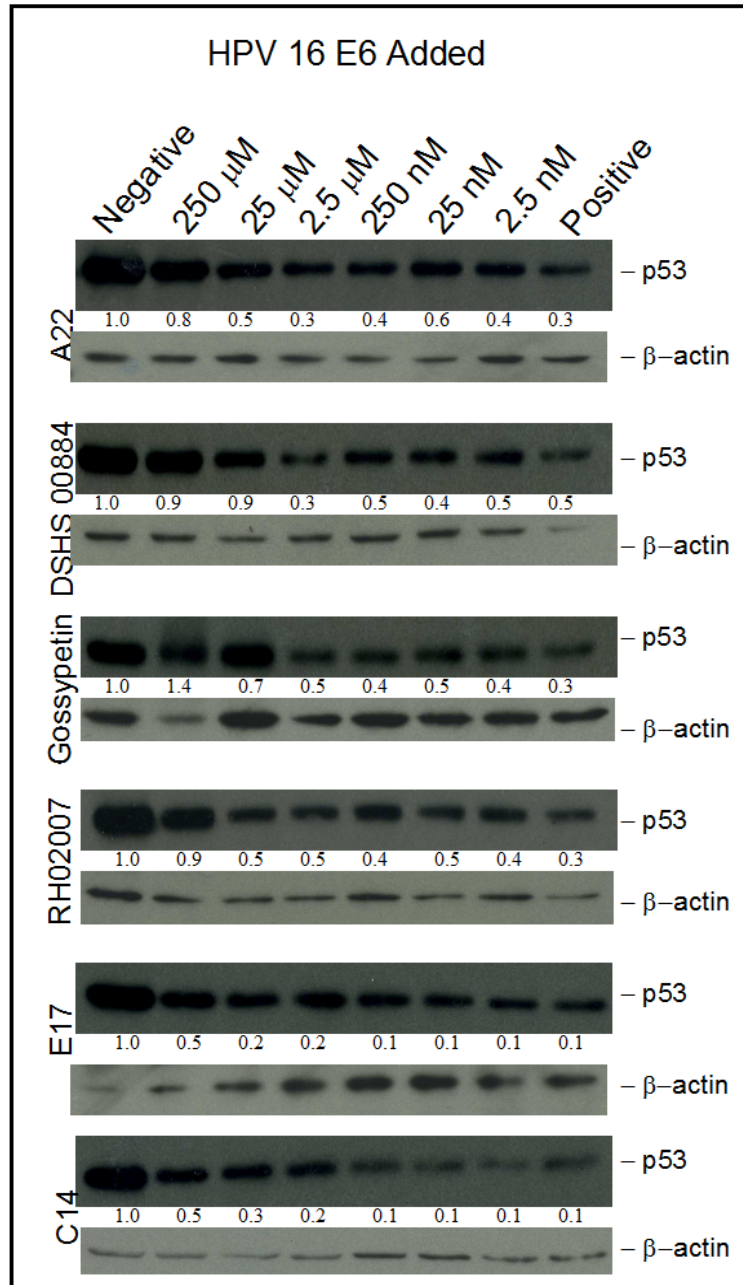


Figure 3.12. p53 Degradation assay results. Representative westerns of p53 degradation reactions treated with increasing concentrations of compound *in vitro* using reticulocyte lysate. Positive controls were E6 + p53 + DMSO while negative controls were p53 + blank reaction + DMSO. Degradation reactions were performed in the presence of HPV 16 E6. Compounds were testing using ten-fold dilutions, starting at 250 μM

3.2.5 Identification of Compounds that Prevent HPV E6-Mediated p53 Degradation in Cells

Through our high throughput screening assay and *in vitro* follow up assays, we identified 30 compounds that inhibited E6-E6AP binding in an isolated system (ELISA) and a complex cell lysate (p53 degradation assay). Each of the 30 compounds was then tested for its functional activity at inhibiting p53 degradation in HPV-positive cells. Two different HPV-positive, tumor derived cell lines were used: SiHa (HPV16 integrated, ATCC) and HeLa (HPV18 integrated, ATCC) (Yee et al., 1985). 48 hours after the addition of compound, cells were lysed and the level of p53 in each sample was assessed by Western blot using an anti-p53 antibody (Santa Cruz Biotechnologies).

Four compounds (DSHS 00884, RH02007, A22 and gossypetin) showed a significant increase in p53 levels in both cell lines over a compound concentration range of 1 to 10 μ M, whereas E17 and C14 protected against p53 degradation by a very small amount in both cell lines. (Figures 3.13). The increases in p53 levels upon increasing compound concentration appear to be more substantial in HeLa cells compared to the SiHa cells and we attribute this to the inherently lower level of p53 protein in HeLa cells (Scheffner et al., 1991). These results suggest that our compounds are effective against not only HPV16 E6, but also against HPV18 E6 as well, in preventing E6-mediated p53 degradation, further suggesting that these compounds can disrupt the 18E6/E6AP interaction.

Concerned that the compounds' effects on p53 were due to nonspecific cell stress, HCT116 cells (colon cancer cells bearing wild type p53) were treated with these six compounds at the same concentrations. Following 48 hours of treatment, cells were lysed and p53 levels were assessed in the same fashion. Ethidium bromide was used as a positive control compound to show that endogenous p53 in these cells could respond appropriately to DNA damage. All compounds failed to increase p53 levels in this cell line except for the ethidium bromide positive control (Figure 3.14). These results suggest that the compounds do not increase p53 by some other mechanism, such as increased p53 expression, but that they specifically prevent E6-mediated degradation in cells infected with HPV.

The remaining six compounds (DSHS00884, A22, RH02007, gossypetin, C14 and E17) were then retested using an MTS cell proliferation assay in HCT116 cells to confirm their lack of cytotoxic effects. Staurosporine, a non-specific kinase inhibitor, was used as a positive control because it was expected to be toxic to the cells (Ruegg and Burgess, 1989). DSHS00884, A22, RH02007, and gossypetin were not toxic at all concentrations tested (1.6 – 25 μ M) and C14 and E17 were not toxic at 12.5 μ M or lower. Furthermore, they did not exhibit significant toxicity to concentrations as high as 25 μ M. (Figure 3.15). We can therefore conclude that these final six compounds (DSHS00884, A22, RH02007, gossypetin, C14 and E17) are specifically stabilizing p53 levels in HPV positive cells by blocking E6-mediated p53 degradation and are not leading to nonspecific cellular death in HPV-negative cells at the given concentrations tested.

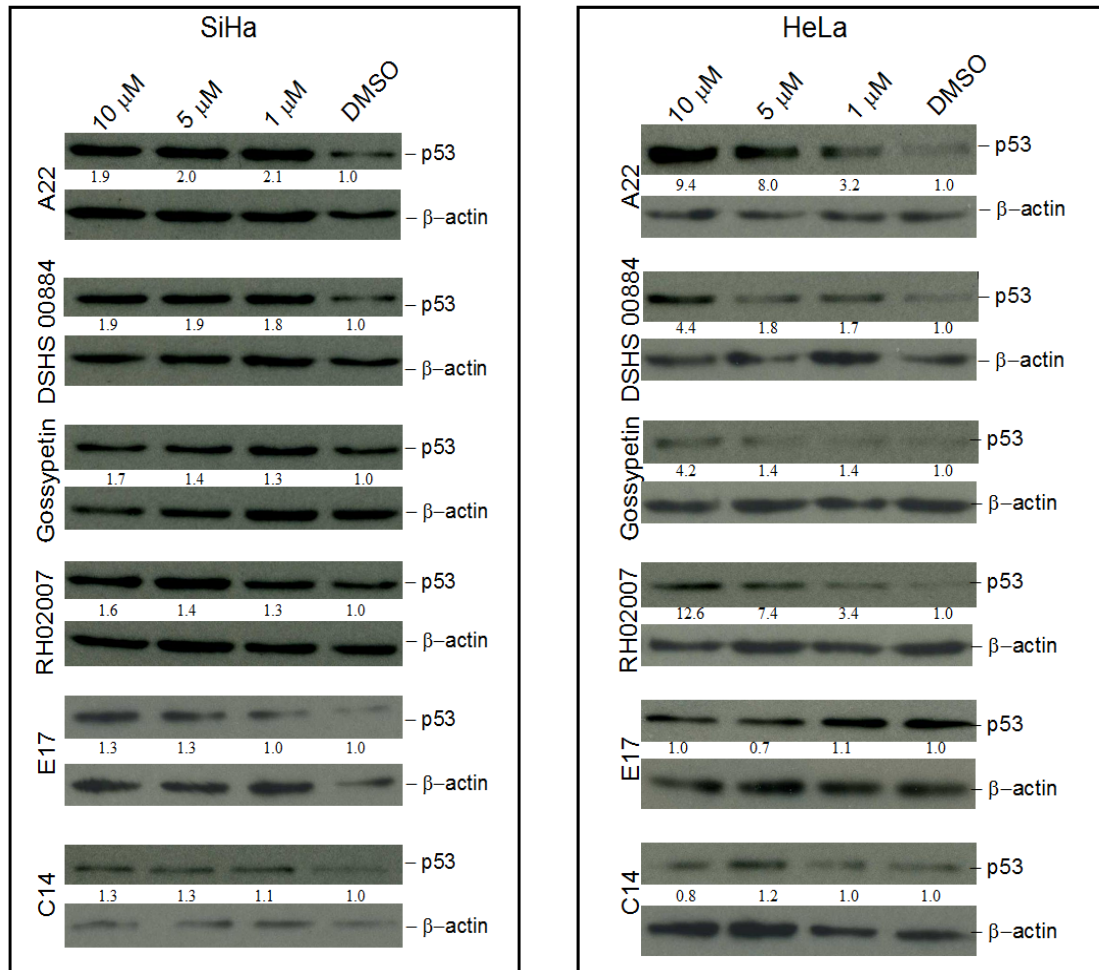


Figure 3.13. Effect of E6 inhibitors on p53 degradation in SiHa (HPV16 transformed) and HeLa (HPV18 transformed). Western blots of SiHa (left) and HeLa (right) cells treated with increasing concentrations of compound (1 μ M, 5 μ M, and 10 μ M). Cells were incubated with compound or DMSO for 48 hours before being harvested and having p53 levels determined by Western Blot using anti-p53 antibodies.

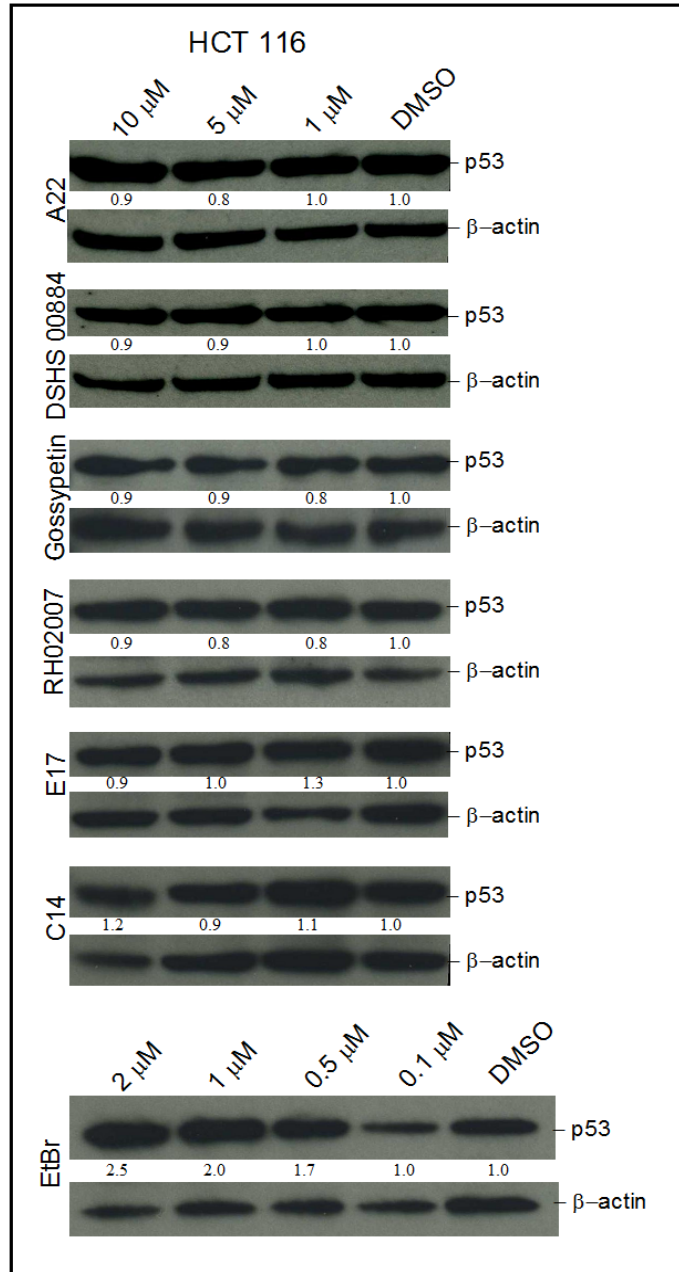


Figure 3.14. Effect of E6 inhibitors on p53 degradation HCT116 (HPV negative) cells.

Western blots HCT116 cells treated with increasing concentrations of compound (1 μM, 5 μM, and 10 μM). Ethidium bromide was tested at lower concentrations (0.1 μM, 0.5 μM, 1 μM, and 2 μM) due to cellular toxicity. Cells were incubated with compound or DMSO for 48 hours before being harvested and having p53 levels determined by Western Blot using anti-p53 antibodies.

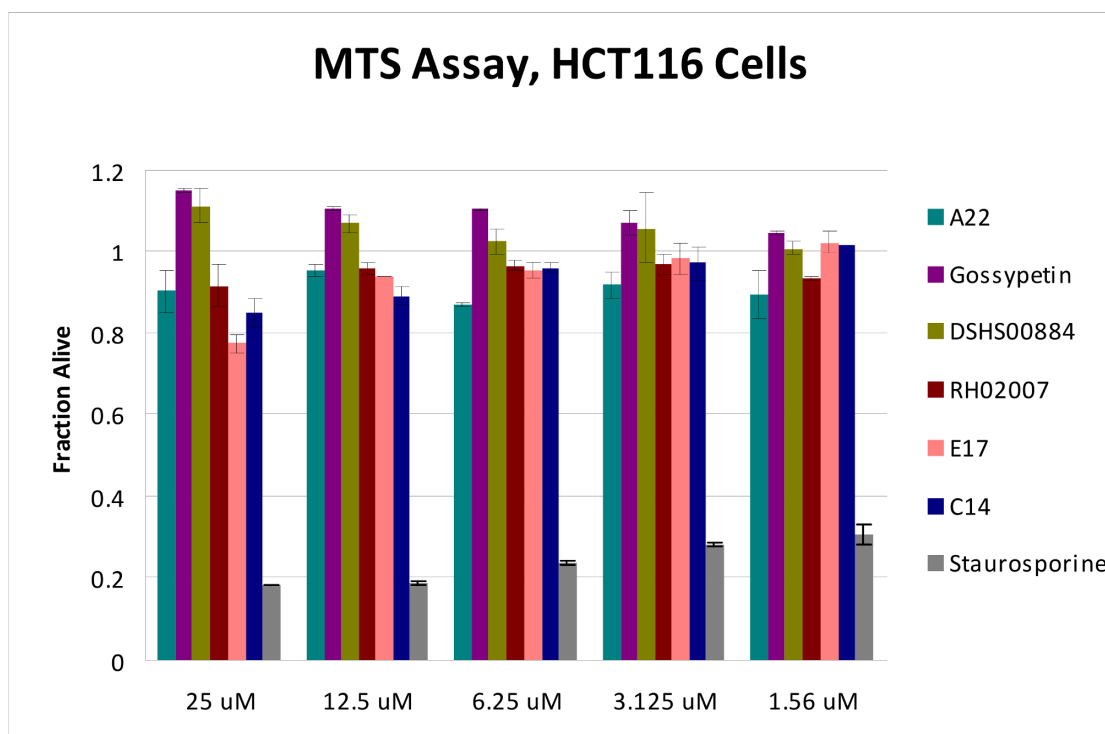


Figure 3.15. Effect of E6 inhibitors on cell toxicity. Representative normalized MTS assay data for the HCT116 control cell lines, a human colorectal cancer cell line bearing wild-type p53 and not containing HPV. All compounds were tested in duplicate and absorbance values were normalized against wells containing the particular cell type and DMSO. Staurosporine, a non specific kinase inhibitor expected to be toxic in all cell lines, was used to ensure that the assay was functional (Ruegg and Burgess, 1989).

3.2.6 E6 Inhibitors Protect Against p53 Degradation by HPV16 E6 and HPV18 E6

Since the six compounds exhibited some inhibitory activity in HeLa cells, which contain HPV18 E6, we tested whether these compounds could prevent p53 degradation in the cell free system in the presence of HPV18 E6. As before, full length, wild-type HPV18 E6 and full length, wild type human p53 were translated using the TNT T7 Coupling Reticulocyte System (Promega). As shown with HPV16 E6, the E6 inhibitors protected against p53 degradation by HPV18 E6 as well ([Figure 3.16, left panels](#)). Furthermore, the level of inhibition is comparable to that against HPV16 E6 ([Figure 3.12](#)). To ensure that the compounds were not resulting in increased p53 levels by some other means, such as an increase of p53 expression, the levels of p53 were determined in the absence of HPV E6. In this case, we found that the compounds alone did not affect p53 levels, leading to the conclusion that the six compounds prevent HPV16 E6, as well as HPV18 E6, from degrading p53 in a dose dependent manner ([Figure 3.16, right panels](#)). Interestingly, the compounds were effective in the cell-free system at higher concentrations than in cells and in the ELISA assay. We attribute this to the fact that the levels of E6 and p53 are higher in our cell free system, thereby requiring more compound to achieve the same result. The results of these six compounds is summarized in [Table 3.3](#).

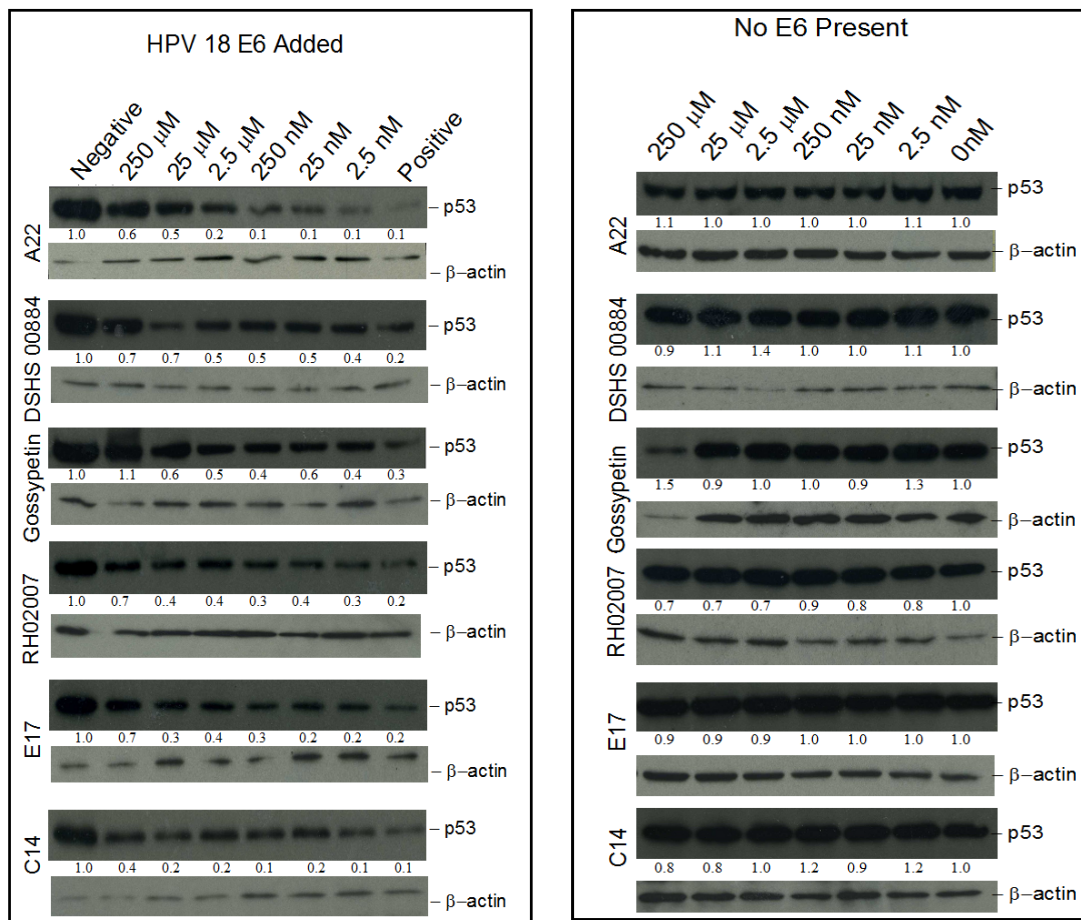


Figure 3.16. p53 degradation assay results. Representative westerns of p53 degradation reactions treated with increasing concentrations of compound *in vitro* using reticulocyte lysate. Positive controls were E6 + p53 + DMSO while negative controls were p53 + blank reaction + DMSO. Degradation reactions were performed in the presence of HPV 18 E6 (left) and in the absence of HPV E6 (right). Ten-fold dilutions of compound were tested, starting at 250 μ M.

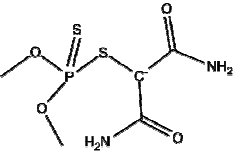
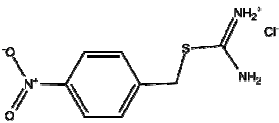
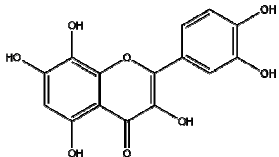
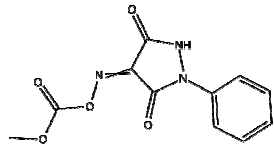
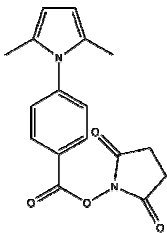
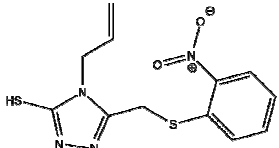
Name	Screen	ELISA IC ₅₀	<i>In Vitro</i> p53 Degradation ~IC ₅₀	Thermal Stability	Structure
C14	Lankenau	30.6 ± 4.7 nM	25-250 μM	Stabilized	
E17	Lankenau	148 ± 42 nM	25-250 μM	Stabilized	
Gossypetin	Spectrum	170 ± 21 nM	2.5-25 μM	Stabilized	
A22	Lankenau	477 ± 166 nM	2.5-25 μM	Stabilized	
RH02007	Maybridge	1.41 ± 0.05 μM	25-250 μM	Stabilized	
DSHS 00884	Maybridge	~ 10 μM	2.5-25 μM	Stabilized	

Table 3.3. Secondary assay results summary for a representative six inhibitor compounds.

The names, structures and secondary assay results for six identified inhibitor compounds are

listed in rank-order of their ELISA IC₅₀ values. The ELISA IC₅₀ values were determined by performing the assay in duplicate for each compound, followed by normalization of data and subsequent data fitting in GraphPad with the aid of log(inhibitor) vs. response (variable slope) plots and non-linear regression fit. The degradation of p53, as determined by the *in vitro* experiments with both HPV 16 and HPV 18 E6, is reported as an approximate IC₅₀ over a concentration range. The thermal stability result is as described in the text.

3.2.7 The E6-Inhibitor-Mediated Increase in p53 Levels is Correlated with Increased Apoptotic Activity in Cells

For the confirmed six compounds, we were curious to determine if an increase in p53 levels could be correlated with apoptosis or cell cycle arrest in the HPV-infected cells. This question was approached with the APO-One assay (Promega) and cell cycle analysis by flow cytometry. Both assays were performed in HCT116, SiHa and HeLa cells. DSHS00884, A22, RH002007, and gossypetin were tested at 20 μ M, while C14 and E17 were tested at 10 μ M. These concentrations were chosen because they showed significant stabilization of p53 in HeLa/SiHa cells and no toxicity in HCT116 cells.

The APO-one assay was carried out very similarly to the MTS assay, except that following incubation of compound for 48 hours and transferring cells to a 384-well plate, a peptide bearing a rhodamine110 fluorescent tag was added to the wells. The peptide is a substrate for caspases 3 and 7 and, upon cleavage, releases the rhodamine110 that when excited at 499 nm results in an increase in fluorescence at 521 nm. Staurosporine, which is known to cause apoptosis in cells, was used as a positive control in this assay. Cell cycle analysis was also performed following fixation and staining with propidium iodide. In this experiment, nocodazole and thymidine, known cell cycle arrest inhibitors, were used as positive controls.

Following compound incubation of 48 hours, A22, gossypetin, RH02007, DSHS00884, E17, and C14 caused both SiHa and HeLa cells to undergo mildly elevated levels of apoptosis than cells treated with DMSO or HCT116 cells treated with compound ([Figure 3.17](#)). There was also a significant increase in apoptosis for 48 hours of treatment of all cell lines with 250 nM staurosporine. Flow cytometry data indicated that none of the compounds displayed any strong cell cycle arrest characteristics as compared with nocodazole or thymidine. ([Table 3.4](#)). Taken together, these data support that 6 compounds can bring about a specific increase in p53 levels, which can be correlated with a mild increase in apoptosis in HPV-positive cells.

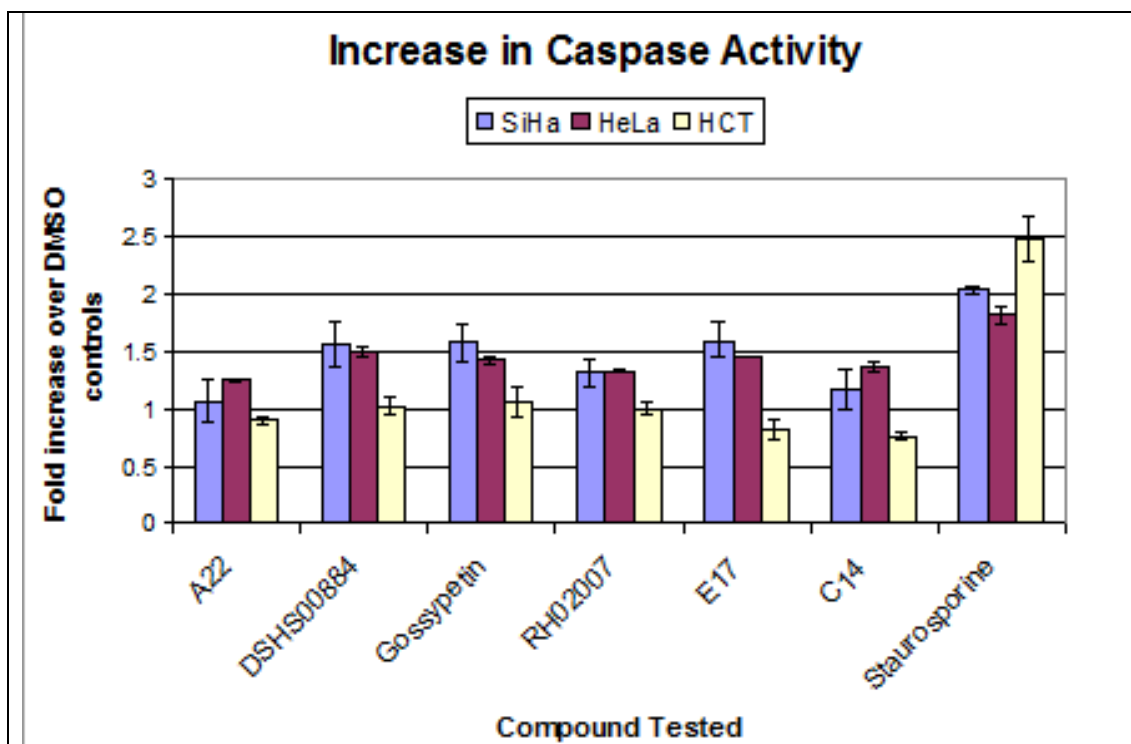


Figure 3.17. The ability of the compound to induce apoptosis. APO-one results for SiHa, HeLa, and HCT116 cells are shown for A22, RH02007, DSHS00884, Gossypetin (tested at 20 μ M for 48 hours), E17 and C14 (tested at 10 μ M for 48 hours) and staurosporine (tested at 250 nM for 48 hours). All compounds were tested in duplicate and fluorescence data was normalized against DMSO treatment in the particular cell type. The signal obtained is proportional to the amount of caspase activity in cells.

Cell Type	Compound	G0/G1 (%)	G2/M (%)	S (%)	Apoptotic (%)
HCT	DMSO	63.7	17.6	16.6	2.65
	Thymidine	32.3	8.66	56.6	3.42
	Nocodazole*	83.8	2.2	2.79	11.2
	A22	64.0	16.2	17.6	2.71
	DSHS 00884	69.2	14.4	15.2	1.53
	Gossypetin	65.4	17.0	15.7	2.28
	RH 02007	62.4	18.8	13.9	5.32
	E17	61.1	20.4	16.7	2.26
	C14	64.3	16.4	17.4	2.45
HeLa	DMSO	67.9	16.4	12.0	4.2
	Thymidine	24.4	19.5	42.5	14.6
	Nocodazole*	6.58	69.9	12.4	12.1
	A22	66.8	16.7	12.2	4.59
	DSHS 00884	68.1	16.1	11.9	4.19
	Gossypetin	67.5	15.4	12.2	5.37
	RH 02007	62.8	19.3	15.2	3.08

	E17	66.2	18.3	12.7	3.29
	C14	69.2	15.9	11.8	3.35
SiHa	DMSO	74.3	15.1	10.1	0.79
	Thymidine	59.2	7.67	27.4	6.12
	Nocodazole*	63.7	3.18	2.03	31.1
	A22	75.1	14.5	9.88	0.79
	DSHS 00884	75.9	14.0	9.51	0.90
	Gossypetin	64.2	20.9	11.9	3.27
	RH 02007	71.2	18.8	9.39	0.86
	E17	75.1	15.8	8.36	0.97
	C14	76.4	13.5	9.52	0.81

Table 3.4. Cell cycle analysis results for each cell type. The percent of cells in each G0/G1, G2/M, S, and apoptotic cells are listed for DMSO, thymidine (cell cycle arrest control), nocodazole (cell cycle arrest control), A22, DSHS 0884, RH 02007, gossypetin, E17 and C14 are listed. All results indicated were obtained after 48 hours of incubation except for nocodazole, which was incubated for 24 hours.

3.3 High-Throughput Screening Discussion

The purpose of this high throughput screen was to identify inhibitors of the E6-E6AP interaction with the downstream effect of protecting against p53 degradation in HPV-infected systems. 30 compounds were identified that are able to inhibit E6 binding to E6AP and subsequently block p53 degradation in a cell-free system by a specific mechanism that does not involve E6 precipitation or degradation. The activity of these compounds in HeLa and SiHa cells relied on their ability to traverse the plasma membrane of both cell types and to not become degraded over the time course of the experiment. Six compounds demonstrated protection against p53 degradation in both SiHa and HeLa cell lines, although two of these (C14 and E17) had only a marginal effect. Furthermore, these six compounds did not increase p53 levels in the absence of E6, as shown in HCT 116 cells and in our cell-free system. This suggests that the compounds specifically block E6-mediated degradation, and do not increase p53 levels by some other mechanism.

The six compounds, A22, gossypetin, RH02007, DSHS 00884, E17, and C14, also mildly induced apoptosis in SiHa and HeLa cells in the experimental 48-hour time period but had no effect on HCT116 cells as compared to cells treated with DMSO in the APO-one assay. While the increases in apoptosis were small, we believe that modification of these lead compounds could identify more potent analogues. Encouragingly, all of the compounds except gossypetin fit the Lipinski rules for drug-likeness and could be further investigated (Lipinski et al., 2001).

Several reasons exist as to why the remaining 24 compounds did not show promising results in cells. It is possible that they were unable to cross the cellular membrane or were degraded over the time course of the experiment. Modifications to these other compounds can be made to overcome these problems and still maintain their E6/E6AP binding inhibitory properties. Similarity searching and testing of their analogs may lead to chemotypes with improved activity.

The results described here also provide useful structure-activity relationship (SAR)

information. For example, gossypetin, brazilin and baicalein share a chromenone scaffold and give similar results in all secondary assays suggesting that this scaffold may be a promising lead for further E6 inhibitor development. Another related pair of compounds is HTS13545 and HTS10308, which differ only in an amino for carbonyl substitution at the 2 position of the pyridine ring. Both compounds have very similar potencies, but HTS13545 stabilized E6M in the thermostability assay while HTS 10308 did not. Perhaps the amine group of HTS13545 donates two hydrogen bonds to E6 thus leading to greater stabilization of the complex.

The intention of this assay was to identify E6 inhibitors that function through direct binding to E6. However, the ELISA assay design could also identify molecules that bind to E6AP. The thermostability assay suggests that at least some of the identified E6 inhibitors are directly binding to E6 due to the visible change in thermostability curves (Figure 3.11). In theory, the small molecules that bind E6 should be competing with the E6AP peptide in a pharmacologically specific manner, which is believed to contact both the E6N and E6C domains (Nomine et al., 2006). Therefore, the small molecules may bind to a region in which both E6N and E6C interact with one another. Those compounds that show no change could be mediating their effects by binding E6 and not significantly stabilizing its structure or binding E6AP instead.

While E6 binds p53, the other oncogenic protein, E7, targets pRB to prematurely release E2F and bring about pRB degradation. Both pathways are purposely inhibited so that HPVs can replicate. Previous studies have shown that continual expression of these two genes is necessary to maintain malignancy while suppression of both genes results in cellular death (Alvarez-Salas and diPaolo, 2007). The studies reported here provide the first potent HPV-E6 inhibitors that might be further developed into therapeutic agents, or as new tools to probe HPV signaling pathways in new ways. The compounds we have discovered and characterized or their congeners could be used as probes together with other agents that block pRB binding to E7 (Fera et al., 2012). Such combination studies could experimentally evaluate their utility as synergistic agents in a therapeutic setting to block HPV transforming effects and bring about apoptosis in HPV-infected cells.

3.4 Future Work

Since the NMR structure of full length E6 is known, it would be of interest to look at chemical shifts upon binding each of the six small molecules discussed. Before doing this, we are working towards confirming the binding of the small molecules to E6 using alternate approaches, such as isothermal titration calorimetry (ITC). Since E6M does not behave well enough to be concentrated high enough for such studies, we are working towards making the construct that Zanier et al. 2012 used for solving the NMR structure. Conceivably, we should be able to concentrate this protein and perform ITC. Afterwards, E6-inhibitor structures would give insight into the mechanism of action of these small molecule inhibitors and guide the identification of more potent and specific inhibitors.

Furthermore, since the studies were performed with cancerous cell lines, which may have many deregulated pathways, it might be of interest to transform normal cells with HPV E6, such as fibroblasts, and then determine the ability of the compounds to prevent p53 degradation and the ability to induce apoptosis. It might be possible to see a stronger effect in such cases, if the compounds are indeed breaking the E6-E6AP complex. Finding a cell line with a more pronounced effect of apoptosis would also make synergy experiments with the E6 and E7 compounds more straightforward. Preliminary experiments hindered quantitation for such analysis because the six E6 inhibitors were not toxic enough to show a significant reduction of SiHa or HeLa cell growth using the MTS assay (data not shown).

Lastly, it might also be interesting to study some of the compounds that were eliminated after testing for inhibition of p53 degradation in cells. It was possible that a number of those compounds were not able to permeate the cell membrane and were discarded as being inactive. If their binding to E6 or E6AP can be characterized, then perhaps modifications to allow easier transport across the cell membrane could make them into effective inhibitors against p53 degradation.

3.5 Materials and Methods

3.5.1 *Expression and Purification of Recombinant Proteins*

E6M: This construct was purified by Kimberly Malecka, Ph.D., a previous graduate student in our laboratory. A modified pET-DUET (Invitrogen) vector was prepared that carried the yeast smt3 gene upstream from multiple cloning site I, where residues 1 – 158 of HPV16 E6 were cloned. The resulting protein, 6xHis-SUMO-E6, was expressed overnight at 18 °C in *Escherichia coli* BL21 (520) cells with 750 µM isopropyl β-D-1-thiogalactopyranoside (IPTG) and 100 µM zinc acetate. Cells were lysed by sonication in 20 mM Hepes, pH 7.5, 500 mM sodium chloride (NaCl), 10 mM β-mercaptoethanol (BME), 10 µM zinc acetate, 5 mM imidazole and 1 mM phenylmethylsulfonyl fluoride (PMSF). Cell debris was pelleted by centrifugation. Protein was immobilized on Ni-NTA resin (Qiagen), washed with buffer containing 30 mM imidazole and eluted with a gradient of 30 – 500 mM imidazole. Fractions were pooled and dialyzed overnight into 20 mM Hepes, 500 mM NaCl, and 10 mM BME at 4°C. SUMO was cleaved from the fusion protein by addition of 6xHis-Ulp1 (SUMO protease) and incubation on ice for one hour. The reaction was passed over pre-equilibrated Ni-NTA resin and free E6M was washed off with 20 mM Hepes, pH 7.5, 500 mM NaCl, 10 mM BME and 30 mM imidazole.

E6M-GST: Residues 1 – 158 of HPV16 E6 were cloned into pGEX-4T-1 (GE Lifesciences). GST-E6M was expressed overnight at 18°C in *Escherichia coli* BL21 (DE3) cells with 750 µM IPTG and 100 µM zinc acetate. Cells were lysed by sonication in 20 mM Hepes, pH 7.5, 500 mM NaCl, 10 mM BME, 10 µM zinc acetate and 1 mM PMSF. Cell debris was pelleted by centrifugation. Protein was immobilized on GST- bind resin (GE Lifesciences) and eluted with 20 mM Hepes, pH 7.5, 500 mM NaCl, 10 mM BME, and 10 mM reduced glutathione.

GST-E6AP and MBP-E6AP: Residues 403 – 421 of human E6AP (isoform 2) were cloned into pGEX-4T-1 and pMAL-c2x (New England BioLabs) respectively. Fusions proteins were

expressed overnight at 18°C in Escherichia coli BL2 1 (DE3) cells with 750 µM IPTG. Cells were lysed by sonication in 20 mM tris, pH 7.5, 50 mM NaCl, 5 mM BME and 1 mM PMSF. Fusion proteins were immobilized on GST-bind resin (GE Lifesciences) or amylose resin (New England BioLabs) and eluted with buffer + 10 mM reduced glutathione or 10 mM maltose respectively.

3.5.2 ELISA Assay

This experiment was performed by Kimberly Malecka Ph.D., a previous graduate student in our laboratory. 50 µL of 30 nM E6M-GST (20 mM Hepes, pH 7.5, 500 mM NaCl, 10 mM BME) was added to each well in a 384-well, black, glutathione coated plate (NUNC). After one hour of incubation with shaking, all wells were washed with 20 mM Hepes, pH 7.5, 500 mM NaCl, 10 mM BME, and 0.1% TWEEN-20. 50 µL of 6 µM MBP-E6AP (1x PBS, 10 mM DTT, 0.1% TWEEN-20, buffer will be used for the rest of the assay) was then added to each well followed by 0.5 µL of DMSO/compound. After one hour of incubation with shaking, all wells were washed with buffer. 50 uL of 1:15,000 anti-MBP-HRP (NEB) was then added to each well and plates were shaken for one hour. Wells were washed one final time with buffer and 50 uL of ELISA Pico chemiluminescence substrate (Pierce) was added and wells were read with an Envision Xcite multilabel plate reader (Perkin Elmer) after thirty minutes. Either 30 nM GST or 6 µM MBP were used for negative controls.

3.5.3 High Throughput screening and Data Processing

This experiment was performed by Kimberly Malecka Ph.D., a previous graduate student in our laboratory. Spectrum and HitFinder compounds were tested at final concentrations of 10 µM and the OPS library was screened at final concentrations of 6 – 10 µM (1.2 - 2 µM for each compound in the pool).

Each 384 well plate receiving compounds during screening contained positive controls (E6-GST

+ MBP-E6AP + DMSO) in columns 2 and 23 and negative controls (GST + MBP-E6AP + DMSO) in columns 1 and 24. Tested compounds were in columns 3 – 22. Uniformity plates (192 positive controls, 192 negative controls) were placed throughout the screening plates as additional quality control measures to ensure both assay and results reliability.

Percent E6-E6AP binding was calculated from raw luminescent values for each test compound (% inhibition = [average positive signal – test compound signal] / [average positive signal – average minimum signal] * 100%). For all screens, compounds that displayed three standard deviation units (~ 50% inhibition) from the average of E6-E6AP binding in the presence of DMSO was assigned as active. Software applications developed by CeuticalSoft (Hudson, NY) in their OpenHTS application toolkit were used to deconvolute the orthogonally compressed data for both HitFinder and OPS. The data was grouped into four categories: actives (compounds that displayed > 50% inhibition of E6-E6AP binding and mapped to a unique well in both the horizontal and vertical direction), ambiguous (compounds that mapped to two or more wells in either dimension), orphan (compound displayed inhibition in one direction but not the other) and inactive compounds. The software was a very convenient tool to 'bin' the data into these active categories as described by others (Devlin 1996)

3.5.4 Thermal Stability Assay

This experiment was performed by Kimberly Malecka Ph.D., a previous graduate student in our laboratory. Individual 20 μ L reactions were set up with 4 μ M E6M, a 1:1000 dilution of SYPRO orange (Invitrogen), 10 μ M compound (final DMSO concentration of 1%) and buffer with a final concentration of 20 mM HEPES, pH 7.5, 500 mM NaCl, and 10 mM BME. Thermal melt curves were obtained by heating the protein from 20°C to 80°C and monitoring fluorescence at 580 nm using a 7900HT Fast Real Time PCR System (Applied Biosystems). Because some compounds were autofluorescent, negative control reactions of each compound alone were also performed to show that their fluorescent properties did not change over the temperature range of the

experiment and ensure that fluorescence was directly representative of E6M melting only (data not shown).

3.5.5 *In Vitro Pull-Down Assays*

This experiment was performed by Kimberly Malecka Ph.D., a previous graduate student in our laboratory. For pulldown of E6M and MBP-E6AP, 50 μ L of resin was pre-equilibrated with 20 mM Hepes, pH 7.5, 500 mM NaCl, 10 mM BME. 30 μ g of matching tagged protein was added with an equimolar amount of the partner protein, excess buffer, and incubated at 4°C for one hour on the nutator. Resin was washed with buffer and then ran out on an SDS-PAGE gel to determine extent of binding between the proteins. Negative controls were performed with tag alone plus the partner protein.

For pulldowns of MBP-E6AP and E6M-GST in the presence of inhibitors, 25 μ g MBP-E6AP was incubated for 30 minutes at 4°C with 25 μ L amylose resin (New England Biolabs) that was prewashed in binding buffer (20 mM Hepes, pH 7.5, 500 mM NaCl, 10 mM BME, and 0.05% TWEEN20). An equal molar amount of E6M-GST was incubated with the indicated concentrations of compound for 1 hour at 20°C. 150 μ L of the E6M-GST/compound mixture was then transferred to tubes containing MBP-E6AP/beads to a final volume of 450 μ L and allowed to incubate at 4°C for 60 minutes with gentle rotation. The beads were then collected by centrifugation at 600g, 4°C for 5 minutes and washed 3 times in 1 ml of binding buffer. The samples were then subjected to SDS-PAGE followed by Western analyses (anti-MBP (1:15000, New England Biolabs), anti-GST (1:5000, Calbiochem)).

For pulldown of GST-pRb and 16 E7, 25 μ g GST-tagged pRb was incubated for 30 minutes at 4°C with 25 μ L GST-bind resin (CLONTECH) that was prewashed in binding buffer (20mM Tris, 7.5, 150mM NaCl, 10mM BME, and 0.05% TWEEN20). An equal molar amount of His-tagged E7

was incubated with the indicated concentrations of compound for 1 hour at 20°C. 150µL of the E7/compound mixture was then transferred to tubes containing pRb/beads to a final volume of 450 µL and allowed to incubate at 4°C for 60 minutes with gentle rotation. The beads were then collected by centrifugation at 600g, 4°C for 5 minutes and washed 3 times in 1 ml of binding buffer. The samples were then subjected to SDS-PAGE followed by Western analyses (anti-GST (1:5000, Calbiochem), anti-His (1:1000, Fisher)).

3.5.6 *In vitro* p53 Degradation Assay

In vitro translation: Full length, wild-type human p53 was cloned into the pRSETa vector (Invitrogen). Full length, wild type human papillomavirus type 16 or 18 E6 was cloned into the pET28a vector (EMD Biosciences). Using the TNT T7 coupled rabbit reticulocyte lysate systems (Promega), each protein was translated in separate reactions.

Degradation: Individual 10 µL degradation reactions were set up with 2 µL p53 translation reaction, 5 µL E6 translation reaction, 0.1 µL compound, and 2.9 µL buffer in a final concentration of 20 mM Tris, pH 7.5, 100 mM NaCl, and 2 mM DTT. Positive control reactions included 0.1 µL DMSO; negative control reactions included 0.1 µL DMSO and 5 µL of a blank translation reaction instead of the E6 translation reaction. All reactions were incubated at 30°C for 2.5 hours. Reaction were then mixed with SDS loading dye and heated at 90°C for five minutes.

Western Blotting: 3 µL of each reaction was run out on a 12% SDS-PAGE gel, transferred to PVDF membrane and then probed with either anti-p53 (1:5000, Bp53-12, Santa Cruz Biotechnology) or anti-beta actin (1:1000, Abcam) followed by anti-mouse conjugated to HRP (1:5000, Bio-RAD). Bands were visualized by chemiluminescence (Pierce) and exposure to film (Kodak).

3.5.7 Cell Maintenance

SiHa, HCT116 and HeLa cells were grown in 1x minimal eagle's media (MEM, Cellgro) supplemented with 10% fetal bovine serum (Hyclone), 10 µg/mL penicillin-streptomycin (Cellgro), 2 mM L-glutamine (cellgro), 1 mM sodium pyruvate (Cellgro), and 100 µM non-essential amino acids (Gibco). All experiments were carried out with cells passaged 30 times or less. The SiHa cell line was ordered from ATCC, while the HeLa cell line was a gift from laboratory of Susan Janicki, Ph.D. and the HCT116 cells were a gift from Meenhard Herlyn, D.V.M, D. Sc.

3.5.8 MTS Assay

20 µL of 50 cells/µL SiHa/HeLa cells or 100 cells/µL HCT116 cells (harvested in media containing 20% FBS) were plated on Day 1 in each well of a 384 well, clear, tissue culture plate (NUNC). On Day 2, 20 µL of DMSO/compound in media containing no FBS was added to each well and cells were incubated for 48 hours. On Day 4, 8 µL of MTS reagent (Promega) was added to each well and the absorbance at 490 nm was read after 3-5 hours.

3.5.9 p53 Level Assay and Western Blots

On Day 1, 120,000 SiHa or 80,000 HeLa cells were plated with 2 mL of media into a 6 well, clear, tissue culture plate (FALCON). On Day 2, 2 µL of DMSO/compound was added to each well. Cells were incubated for 48 hours and on Day 4, cells were washed twice with 2 mL of cold, sterile 1x PBS, then harvested with 300-400 µL of radioimmunoprecipitation (RIPA) buffer (50 mM Tris, 8.0, 150 mM NaCl, 1% NP-40, 0.5% deoxycholic acid, 0.1% SDS) supplemented with complete protease inhibitor cocktail (Roche).

Protein sample concentrations were normalized with the bicinchoninic acid (BCA) protein assay (Pierce). 27 µL of each sample was run on a 12% SDS-page gel and transferred to a PVDF membrane. All membranes were probed with two primary antibodies: p53 (1:500 anti-p53 (Santa

Cruz Biotechnologies)), and beta actin (1:5000 anti-beta actin (Abcam)). All bands were visualized by chemiluminescence (Pierce) and exposure to film (Kodak).

3.5.10 APO-One Assay

On Day 1, 120,000 SiHa cells, 80,000 HeLa cells, or 200,000 HCT cells were plated with 2 mL of media into a 6 well, clear, tissue culture plate. On Day 2, 2 μ L of DMSO/compound was added to each well. Cells were incubated for 48 hours and on Day 4, cells were trypsinized and counted. 10,000 cells in 25 μ L were transferred to a black, 384 well, tissue culture plate (NUNC). 25 μ L of APO-one reagent (Promega) was then added to each well and allowed to incubate at 37°C for 3-4 hours before excitation at 485 nm. The fluorescence at 521 nm was read and the relative fluorescence units (RFU) measured at each time point is proportional to the amount of caspase-3/7 activity. All data points represent the average values \pm SD obtained from two wells assayed independently.

3.5.11 Propidium Iodide Staining / Flow Cytometry

Cells were treated with compound for 1 hour, 24 hours, 48 hours or 72 hours, and then harvested with trypsin. Cell pellets were washed with 1x cold PBS and fixed by addition of ice cold 80% ethanol with constant agitation. After incubating on ice for twenty minutes, cells were pelleted, washed with cold 1x PBS and resuspended in PI buffer (20 μ g/mL propidium iodide (Invitrogen), 6 μ g/mL RNase A (Invitrogen) in 1X PBS). Following incubation in the dark at room temperature, samples were analyzed by flow cytometry.

CHAPTER 4

A Future Outlook on Inhibiting HPV Infection

4.1 Overview

This dissertation has described two high-throughput screens that led to the identification of small molecule inhibitors against the human papillomavirus E6 and E7 oncoproteins. More specifically, six of the E6 inhibitors were found to prevent the E6-E6AP interaction *in vitro* and further prevent p53 degradation both *in vitro* and in cells. The E7 inhibitors were found to work by binding to pRb and preventing its interaction with E7, thereby preventing the premature displacement of E2F from pRb. It was further showed that these compounds induced significant levels of apoptosis when compared to the E6 inhibitors. The E7 inhibitors were also shown to be effective in reducing tumor size in mice. A question now becomes, can the E6 and E7 inhibitors act in a synergistic manner to induce apoptosis in HPV containing cells?

Initial attempts to determine whether or not the inhibitors identified could act synergistically were prevented due to the inability of the E6 inhibitors to induce a significant level of apoptosis in the cell lines studied (SiHa (HPV 16 positive) and HeLa (HPV 18 positive)). Perhaps it would be possible to modify the E6 inhibitors to make them more potent in cells. It might also be possible that targeting E7, as opposed to E6, might be a more effective route in treating HPV-induced cancers. In fact, a number of studies have shown that knocking down E6 expression is less effective at inducing apoptosis in HPV containing cells than knocking down E7 alone or in combination with E6.

4.2 Effects of Knocking Down E6 and/or E7

The effects of abrogating E6 and E7 activity in cells have been determined by other techniques, such as RNA interference, which is increasingly becoming used in functional genomics studies. RNA interference is the post-transcriptional silencing of gene expression by double-stranded RNA molecules (Bayne and Allshire, 2005; Zaratiegui et al., 2007). The introduction of small interfering RNAs (siRNAs) results in the formation of double-stranded RNAs with their target RNA molecule and further targeting them for endonucleolytic cleavage and degradation (Caplen et al., 2001; Elbashir et al., 2001; Fire et al., 1998; Zamore et al., 2000).

In 2002, Jiang and Milner demonstrated the ability to selectively silence exogenous viral genes in mammalian cells using siRNAs (Jiang and Milner, 2002). They focused their studies on CaSKi and SiHa cells, which are both human cervical cancer cell lines containing high risk HPV 16. Furthermore, these cells are deficient in Hdm2, which regulates the levels of p53 in normal cells (Hengstermann et al., 2001). The siRNAs against E6 and E7 that they introduced into the cervical cancer cells degraded E6 and E7 mRNAs, as was expected. A reduction of E6 resulted in an increase in p53 levels, and some reduced cell growth, whereas a reduction of E7 resulted in significant apoptotic cell death. This suggested that HPV E7 is a better target for treatment of HPV-induced carcinomas. Consistent with these results, Steele et al. used synthetic oligonucleotides that were complementary to regions that overlapped with the translation initiation sites of E6 and E7 genes from HPV 18 and showed that antisense E7 oligonucleotides caused the cells from the oral cancer cell line 1483 and from the cervical cancer cell line C41 to die, whereas antisense E6 oligonucleotides did not have this effect (Steele et al., 1993). In all cases described, the nucleotides had no effect on HPV-negative cells.

Unfortunately, the studies using HPV 18 containing cells did not indicate any effects on protein levels upon introduction of the antisense oligonucleotides. Later on, in 2007, Lea et al. determined the effect of using siRNA against E6 and E7 in the HPV 18 bearing cervical cancer cell lines HeLa and C41 (Lea et al., 2007). They found that E6 siRNA caused a complete loss of

E6 alone and that siRNA against E7 caused a loss of both E6 and E7, probably due to the different organization of the HPV 18 genes compared to HPV 16 (Lea et al., 2007). Furthermore, E6 siRNA resulted in an increase of p53 levels and decreased colony formation, whereas E7 siRNA resulted in an increase in p53 and a significant decrease in colony formation when compared to E6 siRNA treated cells. Cell cycle analysis indicated that E7 siRNA induced apoptosis to a much greater extent than E6 siRNA. The conclusion that can be made from this work is that targeting E6 and E7 in combination or E7 alone can be better therapeutically in HPV 18 containing cells. Targeting E6 alone is not very effective at inducing apoptosis or inhibiting proliferation of cancer cells. The ability to induce apoptosis using E6 or E7 siRNA was further demonstrated *in vivo* in mice injected with HeLa cells (Chang et al., 2010). The siRNAs demonstrated highly potent and specific inhibition of HPV-positive tumor growth *in vitro* and *in vivo*. This is contrary to the result in HeLa cells above where E6 siRNA did not produce significant apoptosis. Of course, since the siRNAs were designed differently, it is difficult to say if knocking down E6 alone is sufficient for such a large apoptotic event.

Considering the studies that have been done using siRNA and antisense oligonucleotides against the E6 and E7 oncoproteins from HPV, it is possible that the small molecule E6 inhibitors that we identified through high-throughput screening are not sufficient for inducing significant apoptosis in cells containing HPV. It is possible that targeting E7 with small molecules is necessary. Preventing p53 degradation may not be enough to induce apoptosis since E6 has a number of other cellular targets, as discussed earlier. For example, E6 can also bind to the pro-apoptotic protein Bak, a member of the Bcl-2 family, and inhibit its activity (Jackson et al., 2000; Thomas and Banks, 1999). E6 could have other targets in the p53-mediated apoptosis pathway, and thereby prevent apoptosis from occurring. Perhaps freeing pRb from the E7 oncoprotein allows it to trigger some form of p53-independent apoptosis. Of course, this is all speculative and more needs to be done to determine the effects of these small molecule inhibitors on other cellular pathways.

4.3 pRb, p53, and Other Cellular Proteins as Drug Targets

Interestingly, the E7 thiadiazolidinedione inhibitors that were identified via high-throughput screening, were found to bind directly to pRb, a host cellular protein, and abrogate one of the main functions of the HPV E7 oncoprotein: causing deregulated cell cycle progression to aid in viral replication. The compounds were shown to selectively induce apoptosis in HPV-positive cells. Furthermore, the *in vivo* studies showed that mouse tumors treated with the thiadiazolidinedione inhibitors were reduced without harm to the mice. This demonstrates that pRb could be used as an anti-tumor strategy against HPV-induced carcinomas.

p53 was also demonstrated as a target for anti-tumor treatment. Several groups have focused on trying to re-activate wild-type p53 properties from p53 mutants found in human tumours using small molecules (Levine, 2009). Additional work was done to identify small molecules that activate p53 by blocking protein-protein interactions with its negative regulator, MDM2 (Vassilev, 2004). These molecules are in pre-clinical and Phase 1 drug trials. In another example, cell-based assays were used to identify small molecules or drug combinations that are lethal in cells that have inactive p53 or p53 mutations (Cheok et al., 2007; Issaeva et al., 2004; Lain et al., 2008; Sur et al., 2009). A summary of some of the inhibitors are given in [Table 4.1](#), along with their mechanisms of action and stage in clinical trials (Brown et al., 2009). Given the relative success of targeting p53 in tumor cells, it is conceivable that a similar approach can be used in HPV positive cells in which the E6 oncoprotein targets p53. Perhaps finding inhibitors that bind directly to p53 would be effective.

Considering that pRb and p53 can both be used as drug targets, it is certainly possible that targeting other cellular proteins in HPV positive cells could provide useful therapeutic strategies. For example, inhibitors against histone deacetylases (HDACs) were used effectively to induce p53 independent apoptosis in HPV positive cells (Finzer et al., 2004). These compounds worked by activating the proapoptotic forms of p73, a homologue of p53 and inducing the E2F-p73 pathway. In another example, a compound was used that increased p53 levels as

well as levels of the cyclin-dependent kinase inhibitor p21/WAF-1, a negative regulator of the cell cycle. Other components of the apoptosis machinery or other cellular pathways could be useful targets in treating HPV-induced carcinomas.

Molecule	Mechanism of action	Stage in clinical testing
Reactivate mutant p53		
PRIMA-1	Protein folding ⁴⁹	Phase I (APR-246)
CP-31398	Protein folding ⁴⁶	Preclinical
PhiKan083	Protein thermal stability ⁶⁹	Preclinical
Activate wild-type p53		
Nutlin	MDM2 binding ⁸	Phase I
MI-219	MDM2 binding ⁴⁸	Phase I
Tenovin-6	SIRT1 and SIRT2 inhibition ⁵⁰	Preclinical
RITA	p53 binding ⁵¹	Preclinical
Leptomycin B	CRM1 binding ^{72,135}	Phase I (Elaftocin; withdrawn ¹⁴⁷)
Actinomycin D	RPL11 and RPL5 release ¹¹⁸	Approved (Dactinomycin)
Cyclotherapy (temporal combination of p53 activator and mitotic inhibitor)		
Nutlin*	BI-2536 (PLK1 inhibitor ⁵²) [†]	Phase I/Phase I [§]
Nutlin*	VX680 (Aurora inhibitor [†]) [†]	Phase I/Phase I [§]
Tenovin-6*	Taxol (Tubulin binding ⁵²) [†]	Preclinical/approved [§]
Actinomycin D*	Taxol [†]	Approved/approved [§]
*p53 activator. [†] Mitotic inhibitor. [§] Combinations are not in trial together or have been approved together. D.L.P., unpublished observations. CRM1, exportin 1; PLK1, polo-like kinase 1; RITA, reactivation of p53 and induction of tumour cell apoptosis; RPL, ribosomal protein L; SIRT, sirtuin.		

Table 4.1: Small molecule modulators of p53 and their status in drug trials. Several known small molecules capable of binding to p53 and modulating their activity, as well as their current stage in drug trials are listed. This table is adapted from Brown et al., 2009.

4.4 Development of Vaccines

While small molecule inhibitors might be a useful route for HPV therapeutics, therapeutic vaccines against HPV-infected cells may also be useful. Such vaccines may be able to improve local immune responses and perhaps benefit those who are already infected and are at an early stage of cancer or disease. HPV E6 and E7 are promising targets since they are the only proteins maintained and expressed in HPV-associated carcinomas. Interestingly, some therapeutic vaccines have been tested for their ability to elicit an immune response to premalignant and malignant cells in which E6 and E7 are expressed and shown to have some efficacy against the formation of cancers (Huh and Roden, 2008; Hung et al., 2008; Lin et al., 2007). Work still needs to be done in this area to ensure that such vaccines would be effective in humans.

A combination of therapeutic treatments and prophylactic vaccines might reduce the burden of cancers caused by HPVs. As discussed in Chapter 1, the current prophylactic vaccines, Gardasil and Cervarix, do not offer protection against all cancer-associated HPV types. Furthermore, these vaccines are not effective for people already infected with the HPV types that the vaccines protect against. There have been suggestions of how to improve the vaccine, which may result in protection against many other HPV forms. Namely, since the current two vaccines utilize only the L1 major capsid protein from the virus to form virus-like-particles (VLPs), it might be useful to somehow incorporate the L2 minor capsid protein as well. L2 is not required for the assembly of these VLPs, but it does get integrated into VLPs when coexpressed together with L1. In fact, L2 is important for viral infectivity and plays a role in viral morphogenesis (Unckell et al. 1997, Day et al. 1998). Incorporating L2-epitopes into the current vaccines may result in the antibodies that can cross-neutralize against related HPV-strains and therefore would provide broad spectrum vaccines (Gambhira et al., 2007; Kondo et al., 2008).

4.5 Conclusions

An increase in the understanding of the molecular events affected by the HPV E6 and E7 oncoproteins will provide novel information for identifying new drug targets. Furthermore, solving structures of these oncoproteins with their cellular targets can aid in structure-based drug design efforts. Small molecules can become promising in inhibiting key viral processes in infected cells and become useful therapeutically. A combination of small molecules that target various affected pathways, could lead to a better "cocktail" that would destroy infected cells more effectively. Of course, the hope is that such cocktails do not have side effects.

Our identification of small molecule inhibitors against the HPV E6 and E7 oncoproteins provides a starting point for designing more potent inhibitors that can be useful to treat HPV-mediated pathologies. Of course, work still needs to be done to determine how stable our compounds are in cells, and how well they are distributed. Additional screens against other cellular pathways in HPV positive cells, may also result in a more potent and effective drug combination. Such small molecule drugs, in combination with the vaccines available, may help reduce the burdens of HPV-induced carcinomas.

APPENDIX A

Structure-Based Identification of Human Papillomavirus E7 Inhibitors

Using an *In Silico* Approach

A.1 Introduction

As described in Chapter 2, E7 can disrupt complexes formed between pRb and E2F, even in the absence of cell-cycle regulatory mechanisms, such as pRb phosphorylation. Therefore, in order to prevent uncontrolled cell-cycle progression, it would be useful to find small molecules that bind to and inhibit the function of E7. As described in Chapter 2, a solution high-throughput screen was done that led to the identification of a class of small molecules, called thiadiazolidinediones, that bind to pRb to prevent E7 binding and E2F displacement. We also sought other methods, in parallel, to identify E7 inhibitors, again with an ability to prevent E2F displacement from pRb. More specifically, we decided to perform an *in silico* screen to identify inhibitors that bind directly to E7. Interestingly, Roughley et al. had performed a combination of virtual screening and solution screening against Hsp90, which resulted in potent compounds that reached clinical trials (Roughley et al., 2011). Therefore, combining our results from solution and virtual screening may reveal more potent methods of inhibition against E7.

Virtual screening has been used successfully by a number of other groups to identify small molecule inhibitors against enzymes, such as p300/CBP histone acetyltransferase, BRAF kinase, CK2 kinase, and thymidylate synthase-dihydrofolate reductase (Bowers et al., 2010; Dasgupta et al., 2009; Luo et al., 2008; Martucci et al., 2009; Roughley et al., 2011; Vangrevelinghe et al., 2003; Vinh et al., 2012). In each case, the inhibitors bound the active site and had IC_{50} or K_i values ranging from the low nanomolar to the tens of micromolar range.

Generally, it is more challenging to target protein-protein interactions than to target enzymes with small molecules. A number of virtual screens have been carried out with some success by other groups to inhibit protein-DNA or protein-protein interactions. Still, results indicate that IC_{50} values for disrupting protein-DNA or protein-protein interactions are generally higher than those for disrupting enzymatic activity. Inhibitors that bind to Epstein Barr Virus EBNA1 and prevent it from binding DNA were identified by using the programs DOCK, Xscore, SLIDE, and Autodock (Li et al., 2010). These inhibitors were shown to have inhibition in the 20-

500 μ M concentration range in *in vitro* assays and were able to inhibit activity in cell-based assays. A different virtual screening approach, using the FLAP software, was used to identify inhibitors that disrupt binding of the PB1 and PA subunits of the influenza A virus polymerase (Muratore et al., 2012). In this case, the IC₅₀ values for disrupting the protein-protein interaction were in the range of 25 μ M to 200 μ M. One of the compounds from this screen was found to act as a potent replication inhibitor. The results from these virtual screens indicate that it is possible to disrupt protein-protein interactions with small molecules identified through *in silico* approaches, thereby providing a motivation to identify inhibitors that bind HPV E7 and prevent its interaction with pRb or E2F.

In each virtual screening case, a crystal structure of the enzyme with a substrate, or the protein-protein or protein-DNA complex, had been solved and the structure of the protein was used as a receptor to search for small molecules. In our case, virtual screening was facilitated by the fact that the X-ray crystal structure of the CR3 domain of HPV 1A E7 had been determined (Liu et al., 2006a). This domain is important because it is thought to destabilize the interaction between pRb and E2F and contribute to its disruption. The X-ray crystal structure of the E7 CR3 domain revealed that the CR3 domain forms an obligate zinc homodimer with two conserved surface patches. Mutation of residues within these patches showed that one patch is required for pRb binding and the other is required for E2F binding (Figure A.1) (Liu et al., 2006a).

Since there are no co-crystal structures of the CR3 domain of E7 with either pRb or E2F, the mutational studies that identified the E2F and pRb binding patches were important. These patches on E7 could act as hot spots and could be good targets for small molecules that may prevent protein-protein interactions. Since the pRb binding patch is shallow, it did not seem to be a good target for small molecule inhibitors. The E2F binding patch, on the other hand, forms a pronounced groove which could be a good drug target (Figure A.1). Of note, residues Arg-60 and Leu-61 in the E2F binding region are highly conserved among the E7 proteins. Furthermore, a sequence alignment of E7 proteins showed a high degree of sequence conservation within the CR3 region with greater than 40% identity and 60% homology between proteins, suggesting that

all E7-CR3 regions adopt the same dimeric structure. Consequently, we believed that using the E2F binding pocket in the CR3 domain from HPV 1A E7 would be a good target for small molecule inhibitors against various HPV types.

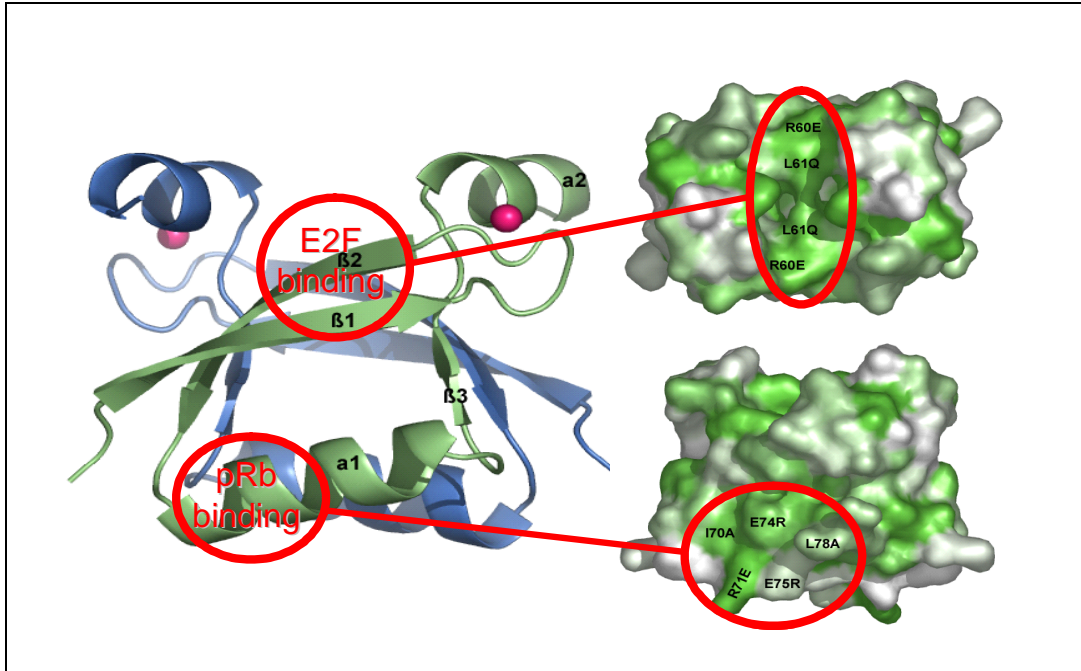


Figure A.1. Structure of the CR3 domain of HPV1A-E7. Highlighted in red are patches shown through mutagenesis to disrupt either E2F or pRb binding. Dark and light green represents highly and partially conserved residues, respectively. Residues that were mutated for analysis are highlighted. This figure has been adapted from (Liu et al., 2006a).

A.2 Results

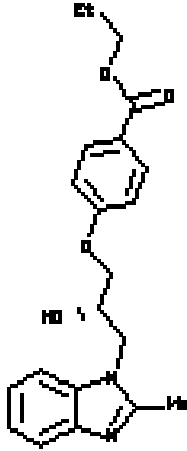
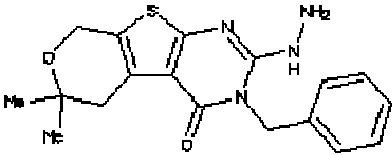
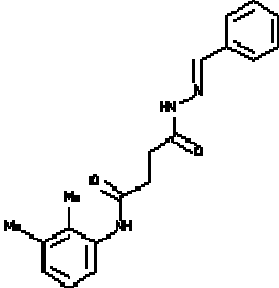
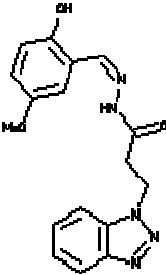
A.2.1 Identification of Initial Hits by In Silico Screening

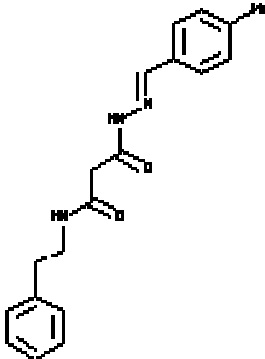
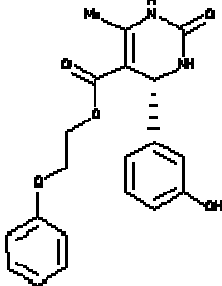
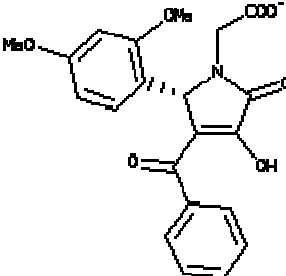
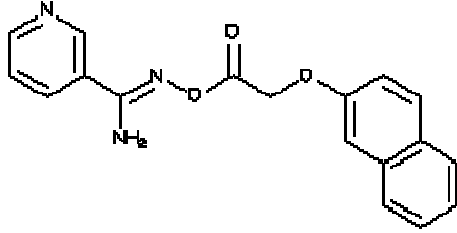
To create a library of compounds for virtual screening, we selected a public database that contained a large number of small molecule compounds that would be available for subsequent solution screening at a nominal cost. To this end, we selected the SPECS database that contained about 200,000 small-molecule compounds. To refine the database further to include compounds that were likely soluble in an aqueous solution and enable eventual testing in solution based assays, we filtered the database for compounds with a log *S* value of greater than -4 by an in-house software called ZLogS, which resulted in a database of approximately 80,000 small-molecule compounds. To screen these compounds efficiently within a reasonable time, we initially used DOCK4.0, a docking program that had already been successfully used as the primary molecular docking program for the identification of inhibitors for HIV-1 protease, influenza hemagglutinin, thymidylate synthase, and parasitic proteases, and more recently against EBNA1 and BRAF kinase (Bodian et al., 1993; DesJarlais and Dixon, 1994; Li et al., 2010; Li et al., 1996; Luo et al., 2008; Shoichet et al., 1993).

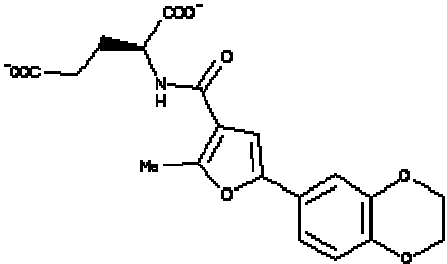
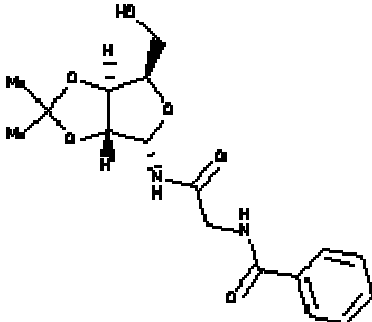
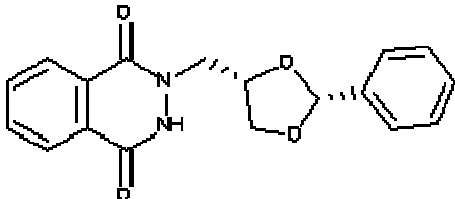
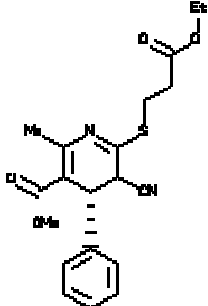
The X-ray crystal structure of the HPV 1A E7 CR3 domain (PDB accession code 2B9D) was used as the target structure in this approach. The goal was to identify small molecules that would inhibit the ability of E7 to displace E2F from pRb. Consequently, the E2F binding site of the CR3 domain of E7 was used as a receptor for compound binding. Residues 60 and 61 of E7 were regarded as critical for E2F binding. Therefore, residues around the center of the pocket, at a radius of 7 Å, were isolated for the construction of a grid for screening. The residues in this radius were determined using PyMol. This radius was large enough to include all residues that were thought to be critical in E2F binding.

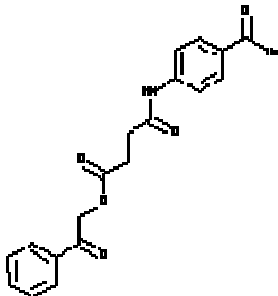
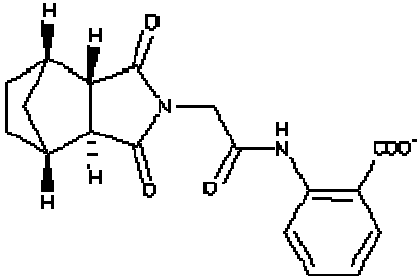
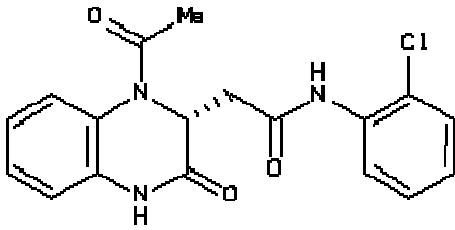
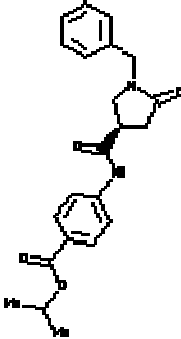
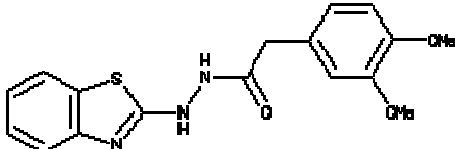
We carried out docking against the 80,000 remaining compounds, and the top 10,000 hits that were generated from the energy scoring function of DOCK4.0 were further analyzed using

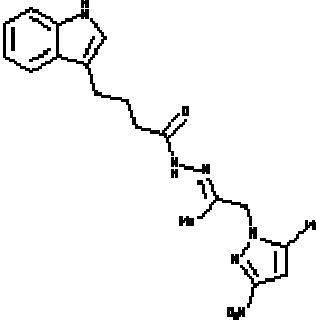
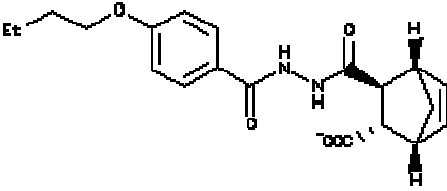
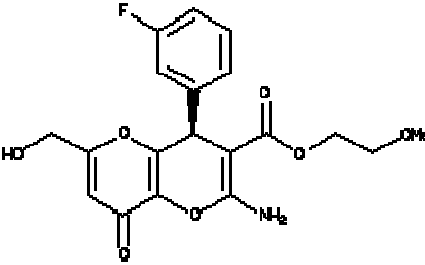
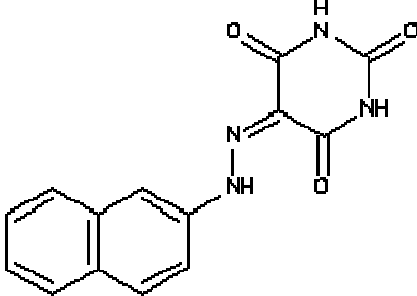
three other docking programs that employed different scoring functions. XScore (version 1.2.1) was used for calculating a binding score for a given protein–ligand complex structure, SLIDE (version 2.3.1) was used for the calculation of hydrogen bonds and the hydrophobic complementarity while considering the flexibility of both protein and ligand, and AutoDock3.0 was used for calculating the free energy of binding using a more extensive energy calculation (Goodsell et al., 1996; Morris et al., 2008; Wang et al., 2002; Zavodszky et al., 2002). The XScore program was first carried out on the top 10,000 candidate compounds that were generated from DOCK 4.0. The top 5,000 compounds from XScore were then selected for reevaluation by the use of the SLIDE scoring function. The top 500 compounds from SLIDE were finally evaluated according to the free energy of binding using the AutoDock 3.0 program. According to their binding modes, free-energy scores, and scaffold diversity, 126 compounds (with binding energies less than -6 kcal/mol) were broken down into 25 manually classified groups. 28 compounds were ordered ([Table A.1](#)) and tested for inhibition of E2F displacement from pRb solution studies by the use of an ELISA-based activity assay system. The procedure of the virtual screening process is given in [Figure A.2](#).

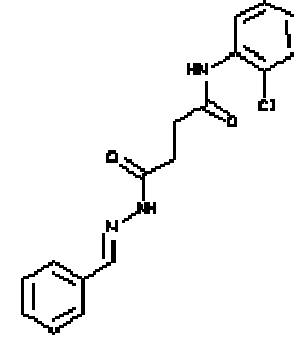
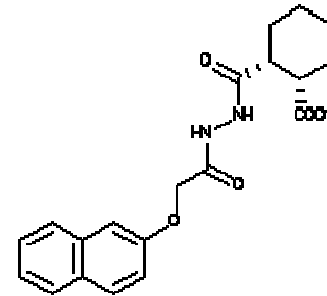
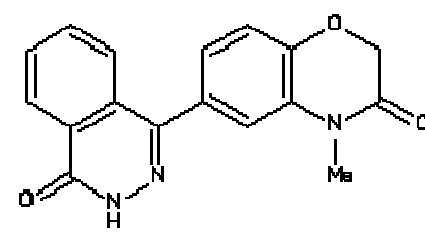
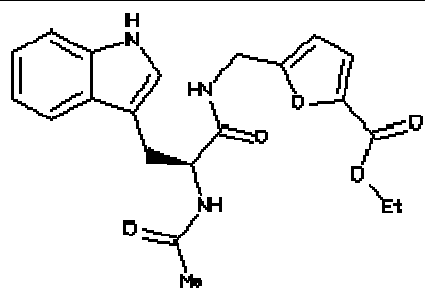
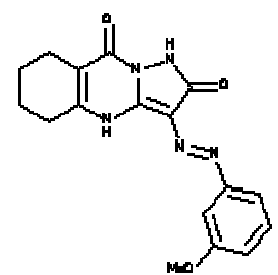
Compound #	Specs ID #	Compound Structure
1	2054351	
2	721641	
3	2147631	
4	4567796	

5	3057615	
6	4113520	
7	721194	
8	4087899	

9	4411369	 <p>Chemical structure of a molecule featuring a carboxylate group (COO⁻) attached to a chiral center, which is also bonded to a methyl group (Me) and a benzodioxole ring system.</p>
10	4419735	 <p>Chemical structure of a complex molecule with multiple stereocenters, a benzamide group, and a benzene ring.</p>
11	331840	 <p>Chemical structure of a benzimidazole derivative with a benzodioxole ring system.</p>
12	4473270	 <p>Chemical structure of a pyridine ring with a chlorine atom (Cl), a methyl group (Me), and an ethyl ester group (Et).</p>

13	2062851	
14	4592843	
15	807232	
16	1072143	
17	483442	

18	4646471	
19	2110216	
20	2219427	
21	4119057	

22	2133815	
23	4657081	
24	366896	
25	643444	
26	4649622	

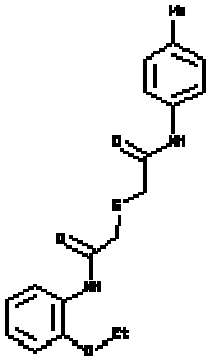
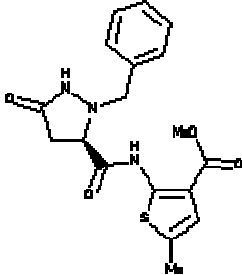
27	646344	
28	646839	

Table A.1. 28 compounds selected from scaffolds. These compounds were purchased from the Specs Company for additional testing using the ELISA-based assay. These compounds were selected from 25 different scaffolds of the 126 hits from the virtual screen. The Specs ID number is shown as well as the structure of each compound.

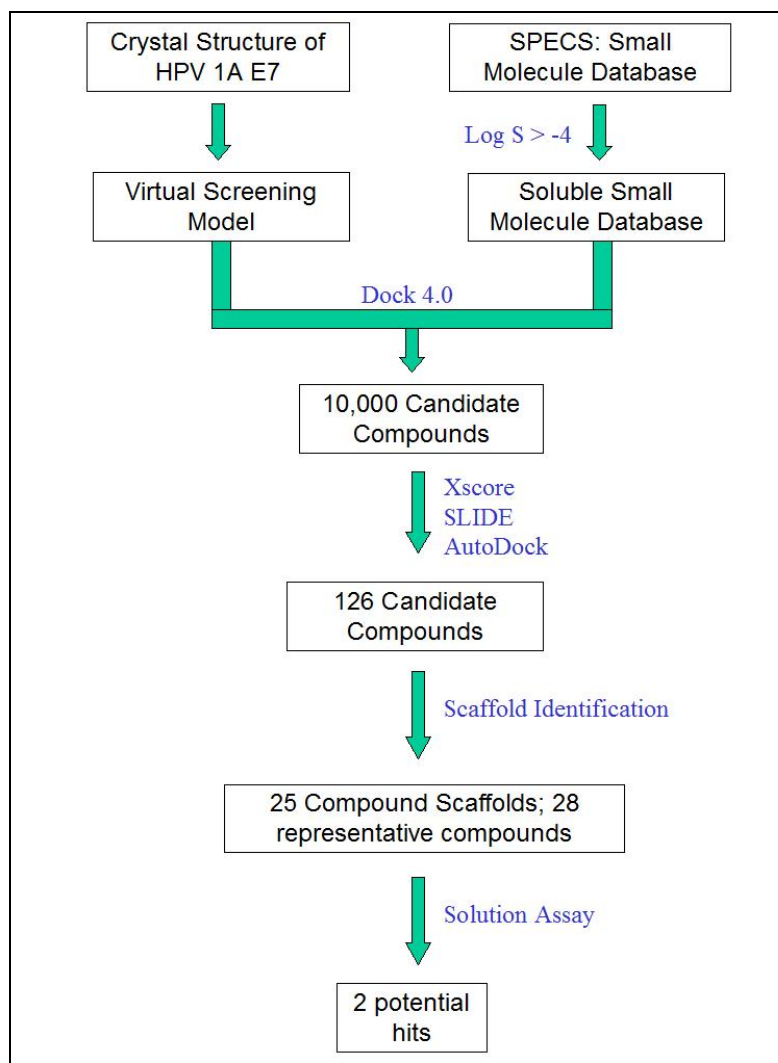


Figure A.2. Flow chart of virtual and experimental screening strategy for discovering of E7 inhibitors. The HPV 1A E7 crystal structure was computationally fitted into a 7 Å grid that contained every residue of the E2F-binding pocket. This was used to dock a library of compounds from the SPECS database. Compounds were pre-selected for solubility in aqueous solution using a log *S* value of greater than −4. A database of ~80,000 small-molecule compounds were then analyzed by one primary docking program (DOCK 4.0). The top 10,000 compound candidates were then evaluated using three scoring functions (Xscore, SLIDE, and AutoDock) to calculate the free energy of binding. The top 126 compounds were then broken down into 25 scaffolds from which a total of 28 compounds were ordered for testing in a solution assay.

A.2.2 E2F Displacement Solution Assay

Twenty-eight compounds obtained through the virtual screen were tested using the ELISA assay that has been described earlier in Chapter 2. Briefly, a complex between GST-pRb and E2F was preformed at the same time that a complex between His-tagged 1AE7 and increasing concentrations of compound was formed. The GSTpRb-E2F complex was applied to 96-well glutathione-coated microtiter plates. E7 with the increasing concentration of compound was then be added and the amount of E2F that remained bound was quantified using an anti-E2F antibody and a secondary antibody to detect a chemi-luminescence signal, as was depicted in [Figure 2.7](#). Compounds to be eliminated were those with a low chemi-luminescence signal, suggesting that E2F was displaced from pRb since E7 function was not inhibited.

Two compounds, compound 12 and 28, showed a dose-dependent inhibition of E7 in that more E2F remained bound to the plate upon increasing compound concentration. The structures of these compounds as well as how they were docked, are shown in [Figure A.3](#) along with the data from the ELISA assay in [Figure A.4](#). The models indicate that the compounds bind with different orientations to E7. Unfortunately, the IC_{50} values of these compounds appeared very high ($>500\mu\text{M}$). It is possible that the compounds inhibit E7 at very high concentrations due to weak binding. False positives were also a concern: the compounds might have been aggregating and causing inhibition of E7. Lastly, the high compound concentrations may have caused some precipitation of E2F or pRb, again resulting in lower amounts of E2F remaining bound to the pRb on the plate.

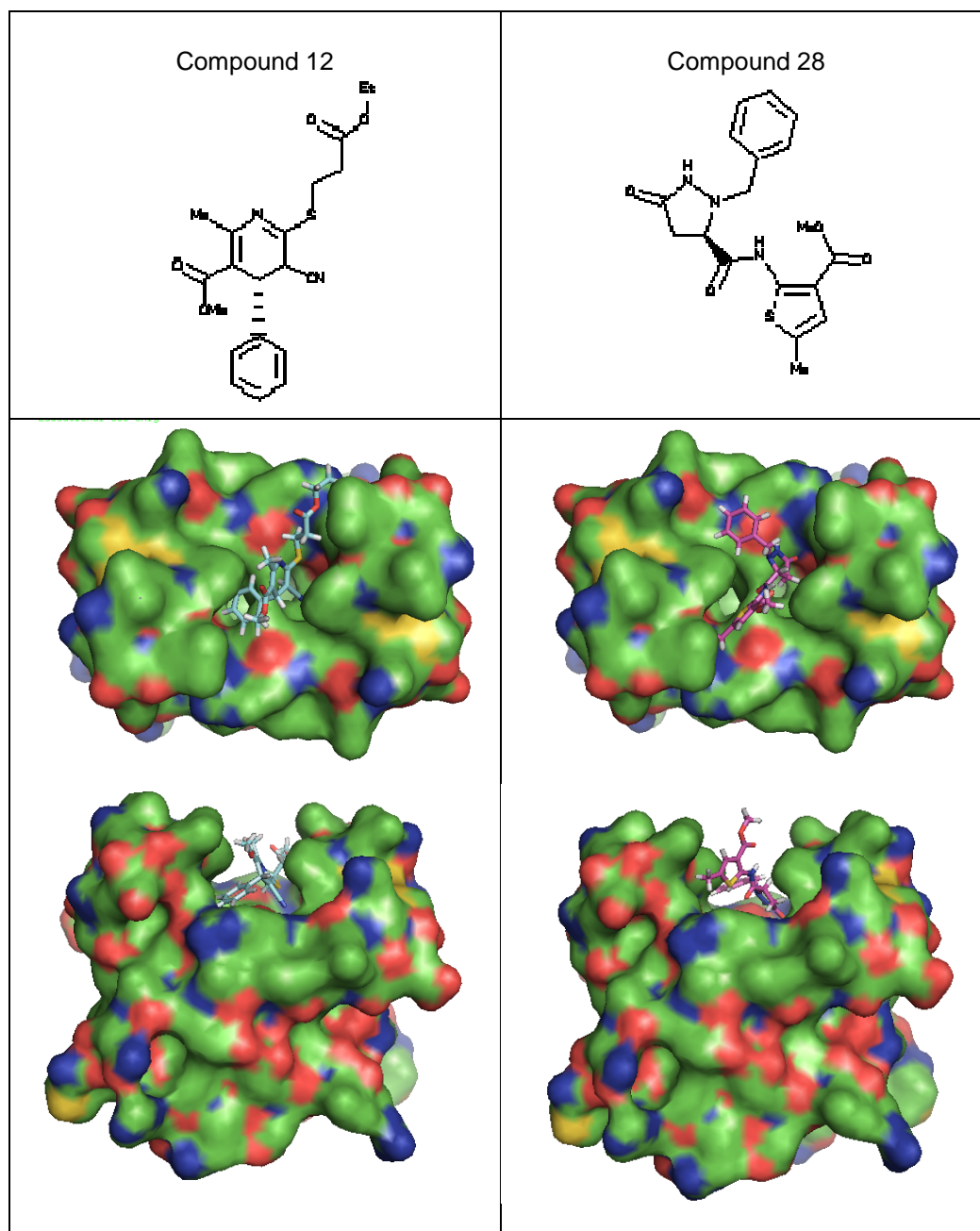


Figure A.3. Docked model of the CR3 domain of E7 with the highest scoring inhibitors from the virtual screen. The compounds were docked into the pocket of E7 that has been shown by mutagenesis to be important for binding to E2F. The two inhibitors have different orientations in the pocket. The structures of the highest scoring compounds, compounds 12 and 28, are shown (left and right, respectively). Their interactions with E7 are shown at two different orientations, 90 degrees from each other.

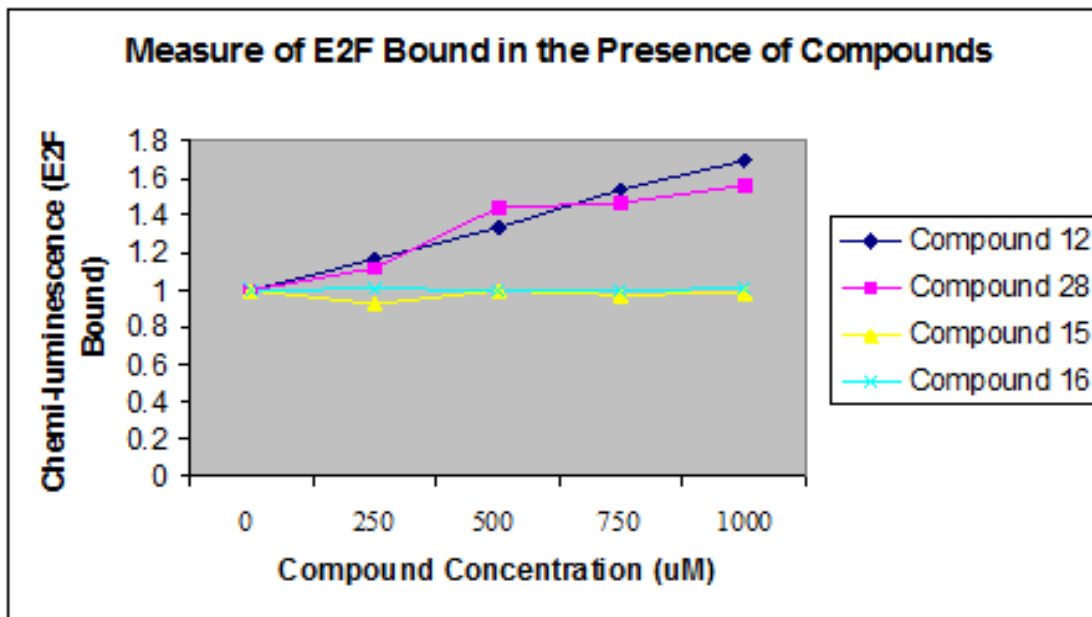


Figure A.4. Inhibition of E7-mediated E2F displacement from pRb using the ELISA-based assay. Different concentrations of compound were added to E7 before addition to the pRb/E2F complex and the amount of E2F remaining bound to pRb was quantitated using anti-E2F antibodies. 4 compounds are shown: 2 compounds (12 and 28) showed a dose-dependent inhibition of E2F displacement from pRb, whereas compounds 15 and 16 were ineffective.

A.2.3 Inhibitory Activity of Analogs

In order to test the validity of these compounds as inhibitors, and with the hope of finding more potent inhibitors, analogs of compounds 12 and 28 were ordered from the Specs Company and Chembridge companies, respectively, and tested using the same assay. Five analogs of each compound were ordered; their structures are shown in [Table A.2](#). For compound 12, analogs that contained the dihydropyridine attached to a benzene group were ordered. For compound 28, analogs that contained a pyrazolidinone attached to a thiophene via an amide bond were ordered ([Table A.2](#)). The ten new compounds were then tested using the ELISA-based assay as before. Unfortunately, none of the new compounds were able to prevent E2F displacement from pRb in the presence of E7 more effectively than the original hits, compounds 12 and 28, that were obtained using DOCK 4.0. The results from the ELISA assay are shown in [Figure A.5](#). As can be seen from the curves, the analogs inhibited less efficiently than the original hits and some did not inhibit at all.

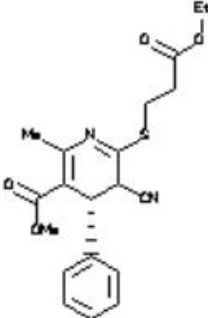
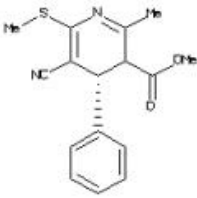
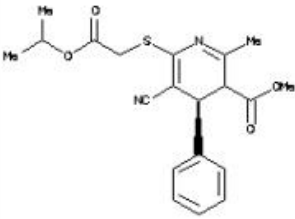
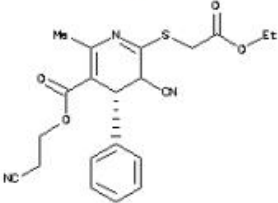
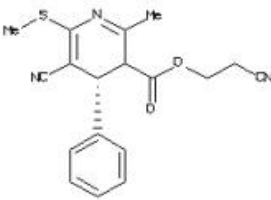
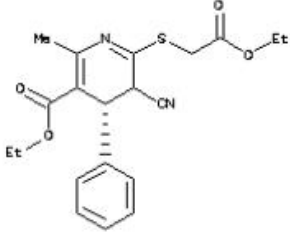
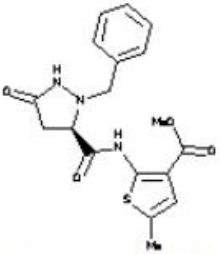
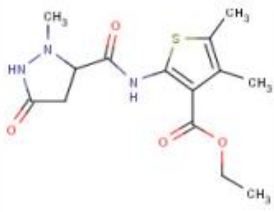
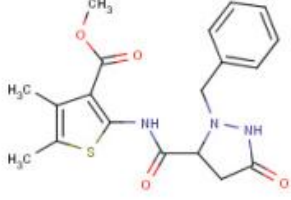
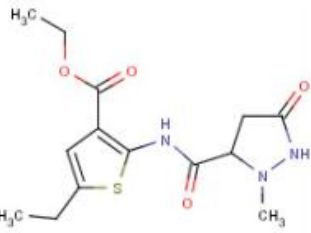
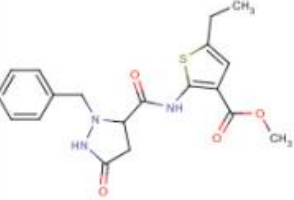
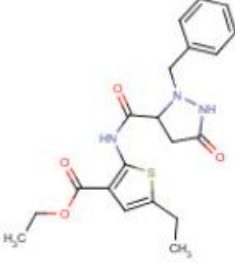
 <p style="text-align: center;">Compound 12</p>		
		
 <p style="text-align: center;">Compound 28</p>		
		

Table A.2. Compound analogs purchased for additional testing using the ELISA-based assay. Five analogs of compounds 12 were purchased; they are shown in the top two rows. Five analogs of compound 28 were ordered; they are shown in the bottom two rows. These analogs were also tested in the ELISA-based assay to try to identify better compounds.

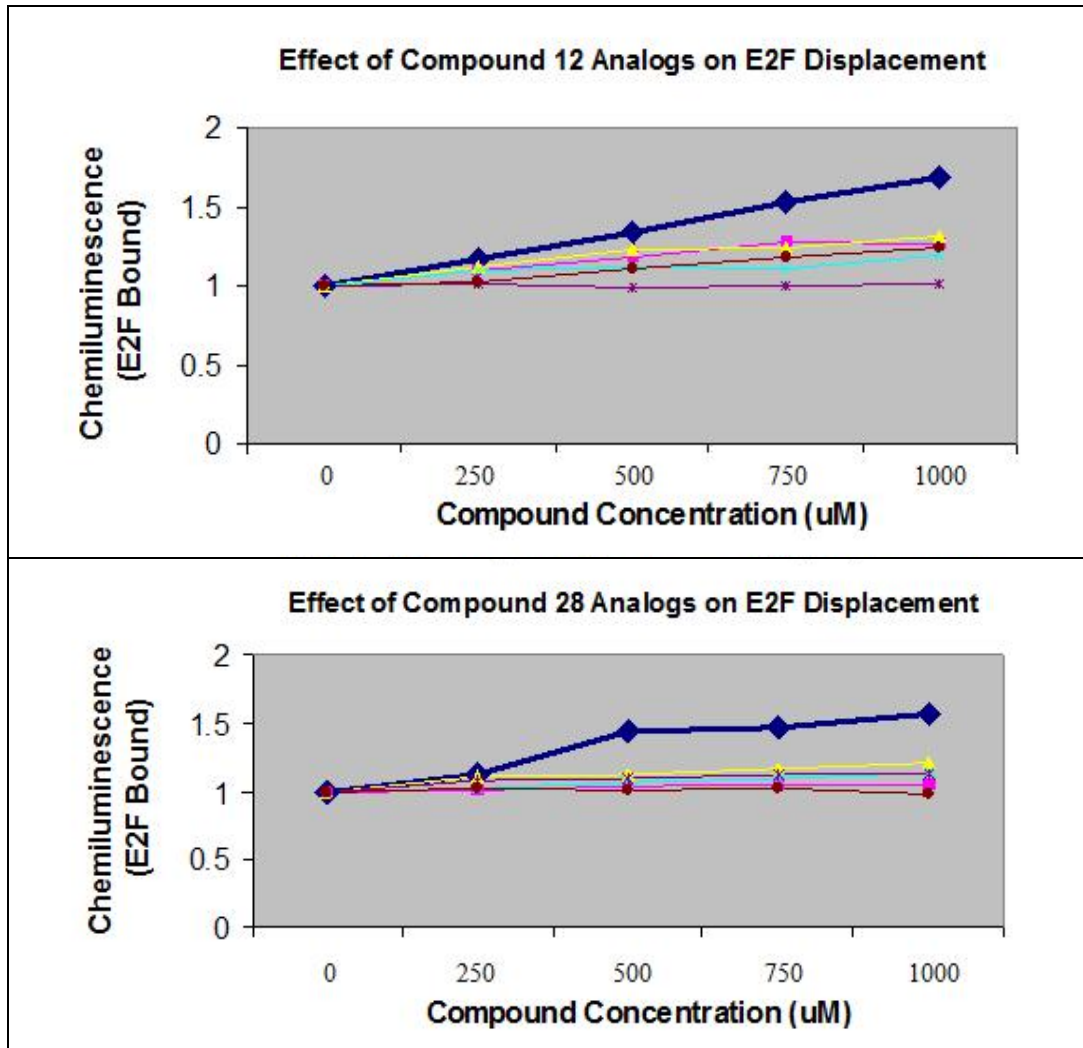


Figure A.5. Inhibition of analogs demonstrated using the ELISA-based assay. Compounds 12 and 28 are shown in bold (blue) in each graph and the analogs are shown as thinner lines of different color. As before, different concentrations of compound were added to E7 prior to addition to the pRb/E2F complex. The amount of E2F was quantified using anti-E2F antibodies.

A.3 Discussion

One major concern with the identified compounds, compound 12 and 28, was that inhibition could only be seen at very high concentrations. Furthermore, some precipitation was seen, making it unclear as to whether or not the compounds were binding to E7 specifically. It is possible that the compounds were aggregating at high concentrations and inhibiting E7. Or, the compounds could have been causing one or more of the proteins to precipitate, again giving a false positive result.

In order to better understand why these compounds did not work so well, the orientations that DOCK 4.0 predicted for the two compounds in the pocket of E7 were analyzed. This revealed only one potential hydrogen bond between compound 28 and E7 and none between compound 12 and E7. For compound 28, the nitrogen from the pyrazolidinone ring appears to hydrogen bond with an oxygen from the peptide backbone of residue Arg-60. The distance between the oxygen and hydrogen atoms is 2.3 angstroms (Figure A.6). There did not seem to be any possible pi-pi stacking interactions between either compound and the protein. Therefore, it seems that the majority of the interactions were due to van der Waal's forces.

Since the activity of the compounds were so weak, modifying the compounds so that additional hydrogen bonds or pi-stacks could be formed, may increase binding to E7 and therefore inhibition. Unfortunately, the compounds bind so weakly that co-crystallization with E7 would not be practical. At this stage, modifying the compounds using information from the docked structure might be useful. However, it is also possible that the compounds are not really binding as the program suggests. For instance, in the case of the virtual screening done against thymidylate synthase-dihydrofolate reductase, the resultant compounds were found to bind in the active site in the crystal structure, whereas the virtual screen was done against a pocket outside of the active site (Dasgupta et al., 2009). Therefore, it might be more instructive to do other *in silico* screens with a modified target or different libraries to find more potent inhibitors against E7 as a starting point before pursuing inhibitor optimization or co-crystallization efforts.

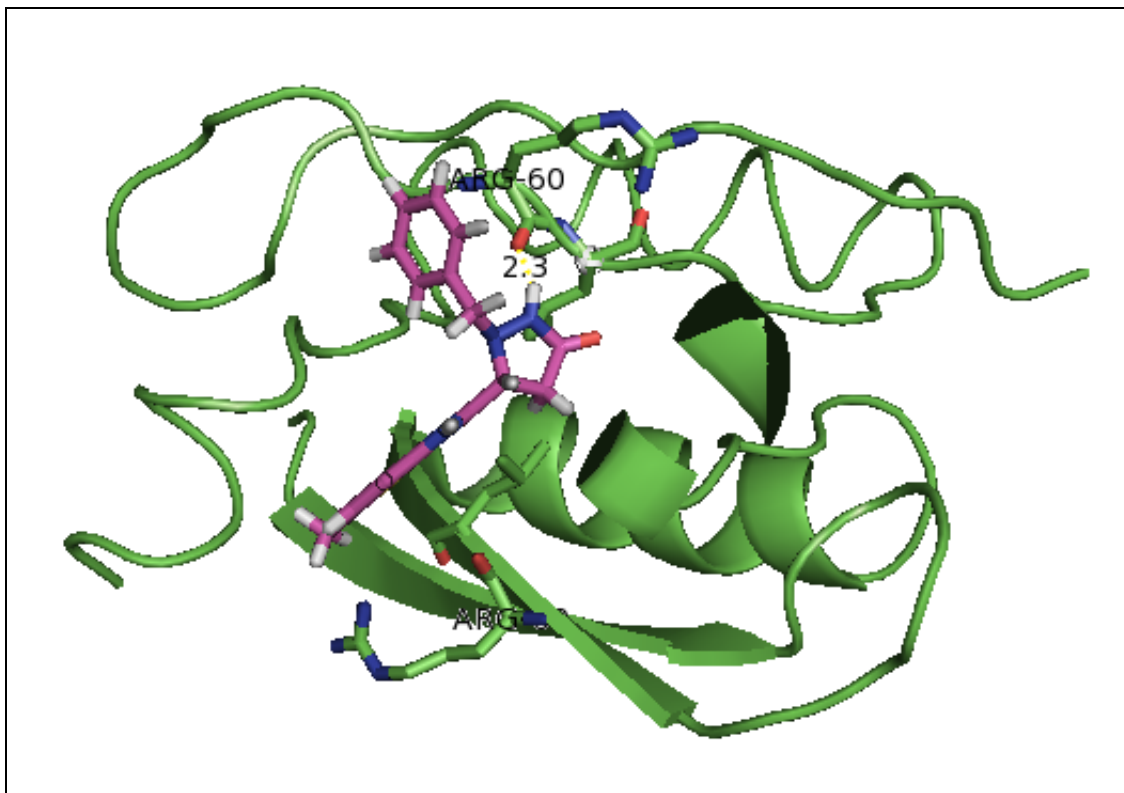


Figure A.6. Model of compound 28 (pink) bound to E7 protein (green) as determined using DOCK 4.0. The nitrogen from the pyrazolidinone ring appears to hydrogen bond with an oxygen from the peptide backbone of residue Arg-60. The distance between the hydrogen atom and oxygen atom are shown.

A.4 Future Work

A number of changes to the current virtual screening approach could potentially lead to improved results. Firstly, doing similarity screens using an additional small molecule library, such as ChemBridge, for analogs of compound 12 and 28 might be useful. The analogs that were tested in this study were not re-docked to determine if there are any clashes with the protein. As a result, re-docking them and docking new analogs might identify new compounds that may work just as well as compounds 12 or 28, or those that work even better. Or, the docked analogs may give insight into why the compounds were ineffective. Secondly, performing chemical screens using DOCK 4.0 to search for compounds that are chemically complementary to the pocket of E7 might also help identify more specific and potent hits. Lastly, the use of other docking and scoring programs might provide better results. It has been suggested the GLIDE and Surflex, as compared to DOCK, are more successful at ranking known inhibitors in an experiment that includes randomly chosen drug-like molecules in addition to known inhibitors of an enzyme (Cross et al., 2009; Kellenberger et al., 2004). These programs were also able to more accurately dock the ligands in a similar pose as seen in x-ray crystal structures. GOLD has also been suggested to outperform DOCK (Zhou et al., 2007).

With regards to the design of the receptor for small molecule screening, it might be helpful to modify the size or shape of the E7 pocket for docking. The NMR structure of HPV 45 revealed an obligate zinc homodimer in which the shape of the E2F binding pocket is slightly different from that of HPV 1A E7 (Ohlenschlager et al., 2006). Furthermore, co-crystallization of the CR3 domain of HPV E7 with E2F would give further insight into how to target the protein-protein interface with small molecules more efficiently. While the inhibitors from the virtual screen targeted the E2F-binding pocket of E7, the compounds appeared to bind near residues Arg 60 and Leu 61, and possibly compete with E2F for binding to E7. Furthermore, it had been shown that mutating each of these residues alone reduces the ability of E7 to bind to E2F, but does not abrogate binding completely (Liu et al., 2006a). Consequently, in order to break the E7-E2F

interaction, there may be other residues that need to be targeted, of which would be identified in a crystal structure of an E7-E2F complex.

A.5 Materials and Methods

A.5.1 Preparation of Small Molecule Database

The modified small molecular database that contains approximately 80,000 molecules for virtual screening was generated as a SPECS subset from the ZINC database (Irwin and Shoichet, 2005) with a predicted solubility filter ($\log S > -4$). ZLogS (unpublished) was a gift from Dr. MY Zheng in the Drug Discovery and Design Center, SIMM, Chinese Academy of Sciences. ZlogS performs solubility prediction based on the generalized atom additive model and stepwise multiple linear regression (SMLR). Eight putative relationships between the atomic solvent assessable surface area, electro-descriptors and atomic contribution of water solubility were investigated.

A.5.2 High Throughput Virtual Screening

The X-ray crystal structure of the HPV 1A E7 CR3 domain (PDB accession code 2B9D) was used as the target structure in this approach (Liu et al., 2006a). A heuristic docking and consensus scoring strategy was used to evaluate the results of the virtual screening. Specifically, DOCK 4.0 was used as the primary screening tool that used the E2F binding site of the CR3 domain of E7 (PDB accession code 2B9D) as a receptor for compound binding (Ewing et al., 2001). During the docking procedure, Kollman all-atom charges were assigned to the protein, and Gasteiger charges were assigned to the small molecules in the SPECS database. In the docking search, the conformational flexibilities of the molecules from the database were considered. We used 30 configurations per ligand-building cycle and 50 maximum anchor orientations in the anchor-first docking algorithm. The compounds were held fairly rigid by the program; only the torsion angles were allowed to vary. All docked configurations were energy minimized by the use of 100 maximum iterations and 1 minimization cycle.

A.5.3 Additional Scoring Functions for Analyzing Hits

We screened the target database, and the top 10,000 molecules were taken as the hit list for further analysis. These molecules were re-ranked by the use of, in succession, XSCORE (version 1.2.1), the docking and scoring module of SLIDE (version 2.3.1), and AutoDock 3.0 (Goodsell et al., 1996; Morris et al., 2008; Wang et al., 2002; Zavodszky et al., 2002). On the basis of the results of these scoring functions, the molecules were ranked, and the top 126 molecules were extracted and were carefully considered for their receptor binding and scaffold diversity. We purchased 28 available candidate compounds from different scaffolds for the *in vitro* assay.

2.5.4 Compounds

All compounds used were ordered from SPECS or Chembridge companies which reported purities of over 90% for all compounds as analyzed by LCMS. Compounds were stored as powder in a dessicator and resuspended to 100 mM in DMSO prior to use.

APPENDIX B

The Protein Complex Formed Between Human Papillomavirus E7
and the Transcriptional Co-activator p300

B.1 Introduction

p300 is a transcriptional co-activator which promotes gene transcription by acting as a protein bridge, or scaffold, that connects different transcription factors to the basic transcriptional apparatus. This allows for the assembly of multi-component transcription coactivator complexes (Chan and La Thangue, 2001). It also has histone acetyltransferase (HAT) activity which allows it to influence chromatin structure by modulating nucleosomal histones (Ogryzko et al., 1996). It has also been shown to acetylate key transcription factors, such as p53 and pRb, thereby regulating protein function (Chan et al., 2001; Grossman, 2001). They are involved in multiple, signal-dependent transcription events. Consequently, it is not surprising that the deregulation of p300 is implicated in many types of diseases (Giles et al., 1998).

Interestingly, p300 was originally identified through its specific interaction with E1A from adenovirus (Eckner et al., 1994). E1A has been shown to hijack the cellular transcription machinery by competing with essential transcription factors for binding to CBP/p300 (Ferrari et al., 2008; Ferreon et al., 2009). Such interactions have also been implicated in epigenetic reprogramming, leading to cellular transformation (Ferrari et al., 2008). The formation of viral oncoprotein complexes with p300 has also been indicated to cause a loss of cell growth control and a block of cellular differentiation, leading to cancers (Turnell and Mymryk, 2006).

p300 contains two homologous transactivation zinc-finger domains, called TAZ1 and TAZ2, that contain two cysteine/histidine-rich regions, called CH1 and CH3, respectively. p300 also has a third cysteine/histidine-rich region, called the CH2 domain. The domain architecture is shown in [Figure B.1](#). The sequences of the CH1 and CH3 domain are structurally homologous, but bind different proteins. In fact, the primary function of these domains is protein recognition. Currently, more than thirty transcription factors have been found to bind to the TAZ domains.

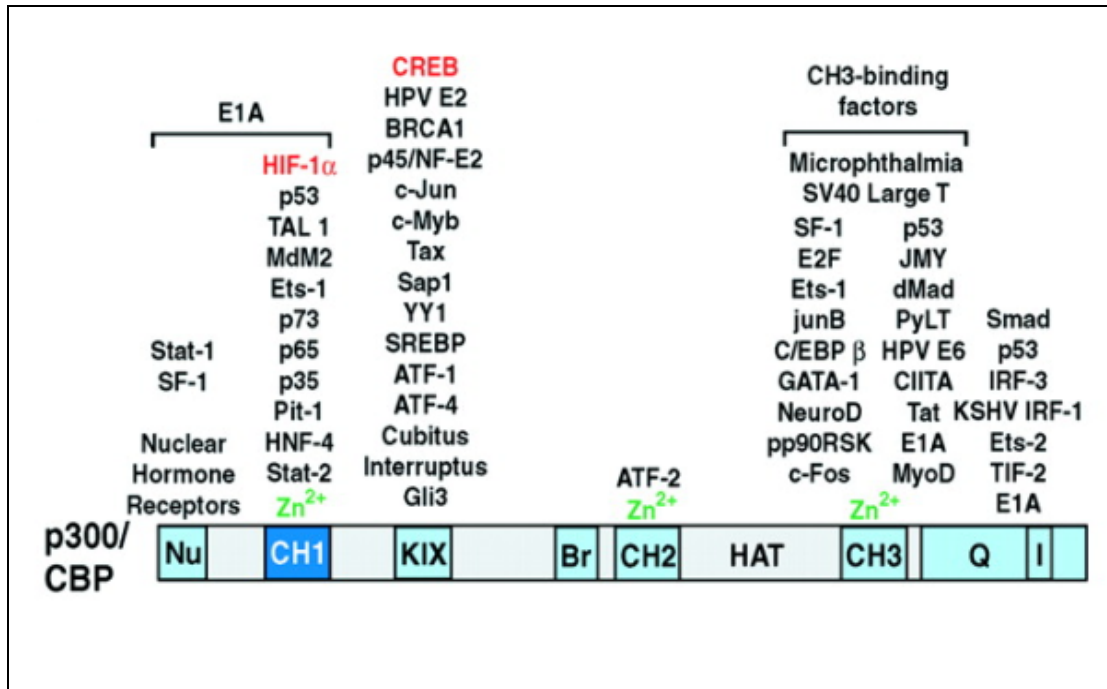


Figure B.1. Functional domains of p300/CBP. Domains are: nuclear hormone receptor-binding domain (Nu), cysteine/histidine-rich domains (CH1, CH2, and CH3), CREB-binding domain (KIX), bromodomain (Br), histone acetyltransferase domain (HAT), glutamine-rich domain (Q), and IRF-3-binding domain (I). The CH1 and CH3 domains are structurally homologous and also have been termed the TAZ1 and TAZ2 domains, respectively. This figure has been adapted from (Freedman et al., 2002).

The sequences of the CH1 and CH3 domains are also fairly conserved and shown in [Figure B.2](#). The structure of the CH1 domain alone (residues 323-424) has been determined using NMR and shown to be composed of four α -helices and three Zn^{2+} -binding sites formed by HCCC sequence motifs ([Figure B.2](#)) (De Guzman et al., 2005). The structure of the CH1 domain is stabilized partly by Zn^{2+} binding as well as by a single hydrophobic core formed by the four helices. A comparison with crystal structures of TAZ1 in complex with the HIF-1 α transcription factor and CITED2 transactivator reveal no change in structure upon binding to these target proteins (Freedman et al., 2003; Freedman et al., 2002).

HPV E7 has been suggested to bind to the CH1, CH2, and CH3 domains of p300, but most prominently to the CH1 domain (Bernat et al., 2003). The downstream effects of these interactions have not been well studied. Since E7 binds to a region of p300 that is known to bind many transcription factors, this interaction can have many other negative downstream effects, leading to problems in the cell. Complexes of regulators with p300 could serve as functional targets of the HPV E7 protein through which it might exert its transforming activity. Lastly, since E1A, which is similar to E7 in sequence, has been shown to abrogate the normal functions of p300 and cause transformation, it is possible that E7 functions in a similar manner thereby providing another motivation to study the E7-p300 complex.

To date, there are no current structures of the E7-p300 complex. Therefore, it becomes of interest to probe the E7-p300 interaction, and then determine ways to disrupt the interaction. Although studies by others have shown that the TAZ1 domain of p300 binds to the CR1, CR2 and small segment of the CR3 region of HPV E7, the techniques used in this study involved techniques that can detect weak interactions (Bernat et al., 2003). Consequently, we sought to repeat the mapping experiments to better understand the nature of the E7-p300 interaction. Furthermore, we sought to determine the strength of this complex with the goal of eventually trying to crystallize it.

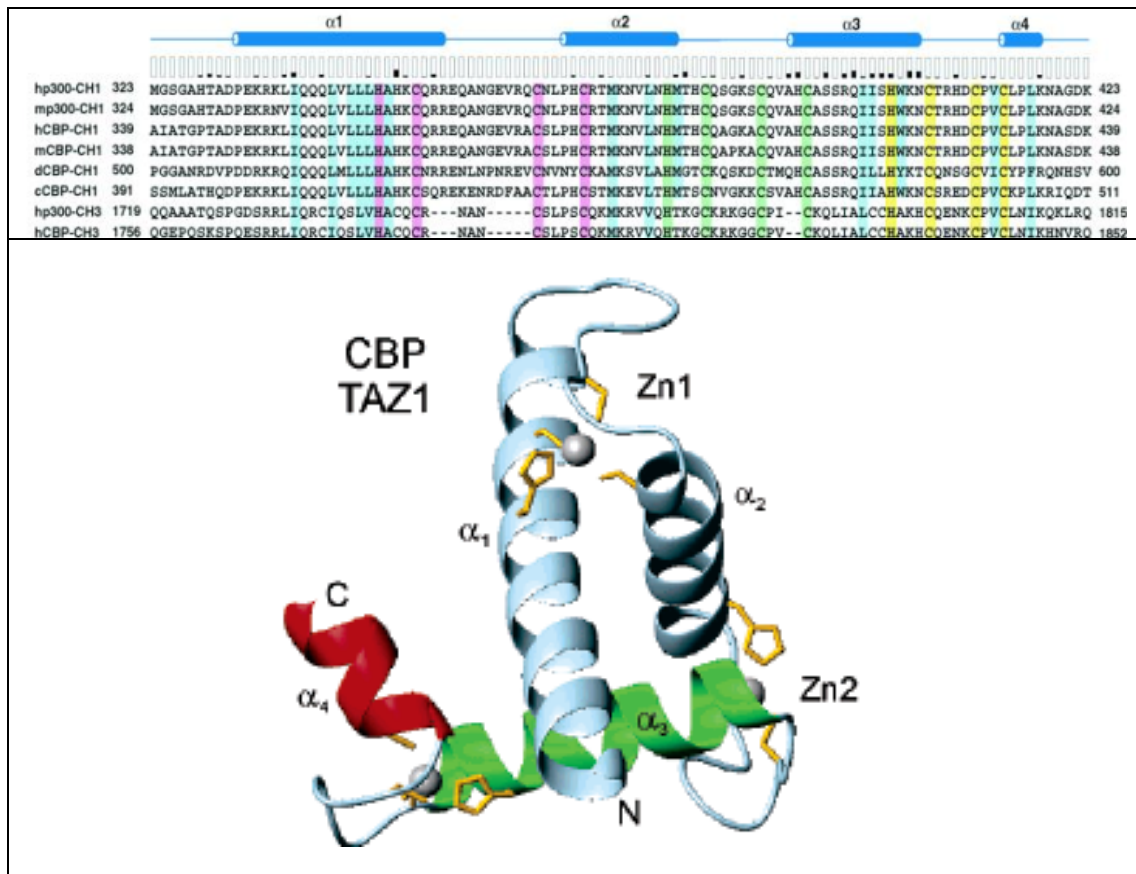


Figure B.2. Sequence alignments of p300 CH1 and CH3 domains (top) and ribbon structure of the TAZ1 domain of CBP/p300 (bottom). (top) The sequence of human p300 CH1 is aligned with homologous regions of p300 and CBP. The histidine and cysteines involved in zinc binding are shaded in violet, green, or yellow. Blue residues are those that form the hydrophobic core of the CH1 structure. Most of these residues are conserved in the CH3 domain as well. The aligned sequences are: h, *Homo sapiens*, b, *Bos taurus*, m, *Mus musculus*, x, *Xenopus Laevis*, d, *Drosophila melanogaster*, c *Caenorhabditis elegans*. This figure has been adapted from (Freedman et al., 2002). (bottom) The NMR structure of the TAZ1 domain of CBP/p300 reveals four helices and three zinc-binding sites. The three longer helices (designated α_1 , α_2 , and α_3) pack across each other to form a triangular structure. The three Zn^{2+} sites lie at the vertices of this triangle. The zinc atoms are shown as pale gray spheres. This figure has been adapted from De Guzman et al., 2005.

B.2 Results

B.2.1 E1A Binds More Strongly to the CH1 Domain of p300 than HPV 16 E7, Which Binds More Strongly than HPV 1A E7

We first wanted to determine whether high risk HPV 16 E7 or low risk HPV 1A E7 binds more strongly to the CH1 domain of p300, or if they both bind with similar affinities. To test this, full length E7 from each form of HPV was expressed with an N-terminal GST tag and purified. Binding was assessed by doing *in vitro* pull down assays on GST beads with the CH1 domain of p300 (untagged). The buffer used for these studies was 20mM Tris, 8.0, 100mM NaCl, 10mM BME, and 0.05% TWEEN20. The samples were analyzed by SDS-PAGE, shown in [Figure B.3](#). A very faint band was seen for HPV 1A E7 and a slightly darker one for HPV 16 E7. Therefore, this indicated that high risk HPV 16 E7 binds more strongly than low risk HPV 1A E7 to the CH1 domain of p300. p300_{CH1} did not bind to GST alone, indicating that the binding to E7 was specific. The stoichiometry of binding could not be assessed from the gel, although it seems that the interaction is weak since only a small fraction of the input was bound to HPV 16 E7.

We next wanted to compare the binding of HPV 16 E7 and Adenovirus 5 E1A to the CH1 domain of p300. For these studies, the CH1 domain of p300 was fused to a GST-tag, and E7 and E1A were expressed with N-terminal 6x-histidine-tags. Again, pull down assays were done on GST beads with the same buffer as before. The gel revealed that the band for E1A was much darker than that for E7 suggesting that E1A binds more tightly to the CH1 domain of p300 than E7 ([Figure B.4](#)). E1A and E7 did not bind to the control sample, GST, indicating that the interactions of p300_{CH1} with E1A or E7 were specific. Because larger proteins tend to stain better than smaller proteins, it is difficult to say what the stoichiometry of binding is. Consequently, binding stoichiometry was evaluated by other means, as is discussed later.

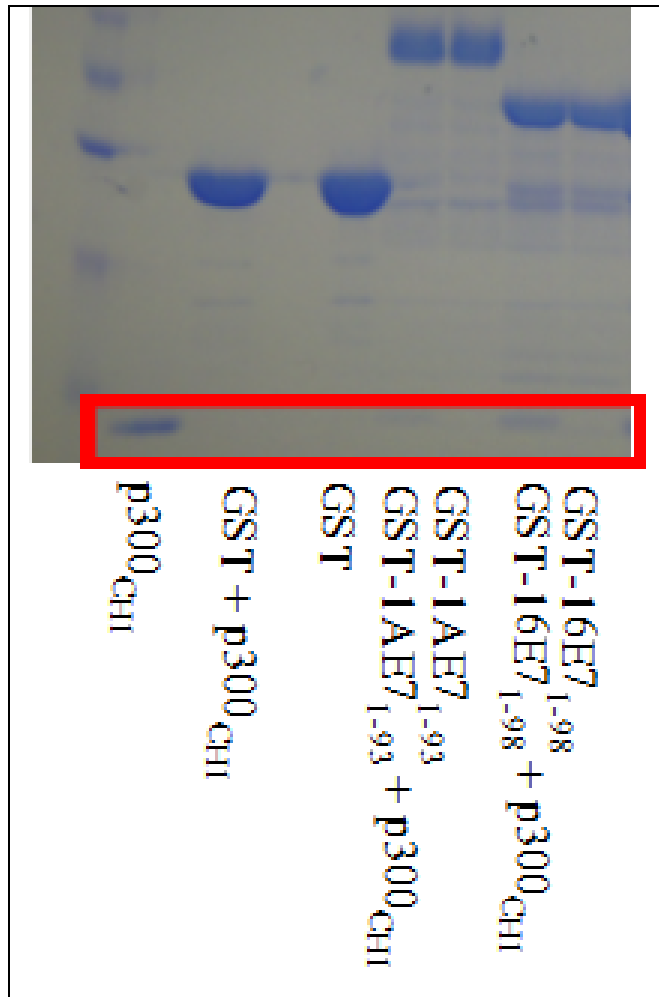


Figure B.3. Binding of HPV 1A E7 and HPV 16 E7 to the CH1 domain of p300. An SDS-PAGE gel is shown for pull downs done between p300_{CH1} and full length E7 proteins. The region where p300_{CH1} runs on the gel is boxed in red. Results are explained in the text.

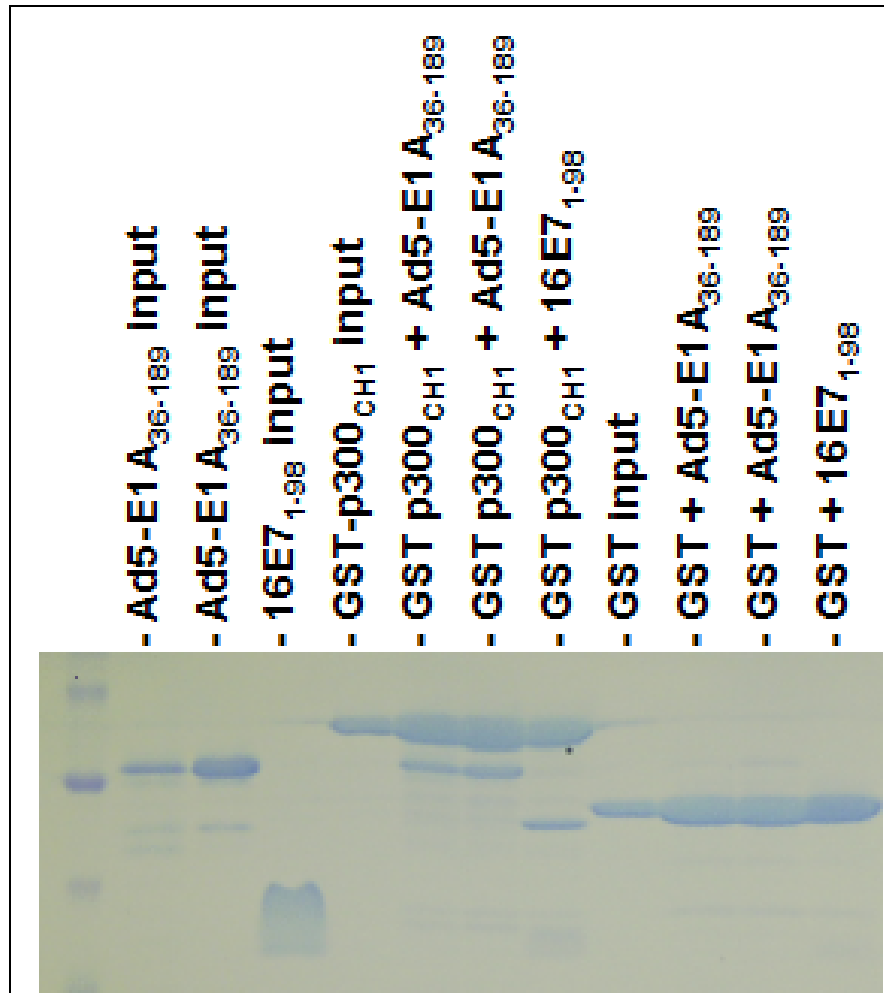


Figure B.4. Binding of E1A and HPV 16 E7 to the CH1 domain of p300. An SDS-PAGE gel is shown for pull downs done between p300_{CH1} and E7 or E1A. Results are explained in the text.

B.2.2 Pull Downs Indicated that the CR1-2 Domains of E7 are Necessary for the Interaction with p300

Since E7 was able to bind to p300_{CH1}, we decided to map the site of interaction on HPV16 E7. To do this, different deletion constructs of HPV16-E7 were made: HPV16-E7₁₋₉₈ (full length), HPV16-E7₁₇₋₉₈, HPV16-E7₄₆₋₉₈, HPV16-E7₁₋₅₁, HPV16-E7₁₋₄₆, HPV16-E7₁₇₋₄₆, HPV16-E7₁₋₁₇, and tested for their ability to bind to the CH1 domain of p300 using pull downs in a buffer of 20mM Tris, 8.0, 50mM NaCl, and 10mM BME. The results are shown in [Figure B.5](#). As can be seen from the gel, all constructs were able to bind to p300_{CH1} except for the CR3 domain of HPV16-E7 (residues 46-98). Of note, HPV16-E7₁₋₉₈, HPV16-E7₁₋₅₁, HPV16-E7₁₋₄₆ bound to p300_{CH1} most strongly, HPV16-E7₁₇₋₉₈ bound more weakly, and HPV16-E7₁₋₁₇ and HPV16-E7₁₇₋₄₆ bound the weakest. These results suggest that the CR2 domain, consisting of residues 17-46, was necessary but not sufficient for the interaction with the CH1 domain of p300. In fact the CR1-2 domains, consisting of residues 1-46, were sufficient for the interaction, suggesting that residues 1-17 increase the binding affinity. The CR3 domain (residues 46-98) did not seem to interact at all with the CH1 domain of p300.

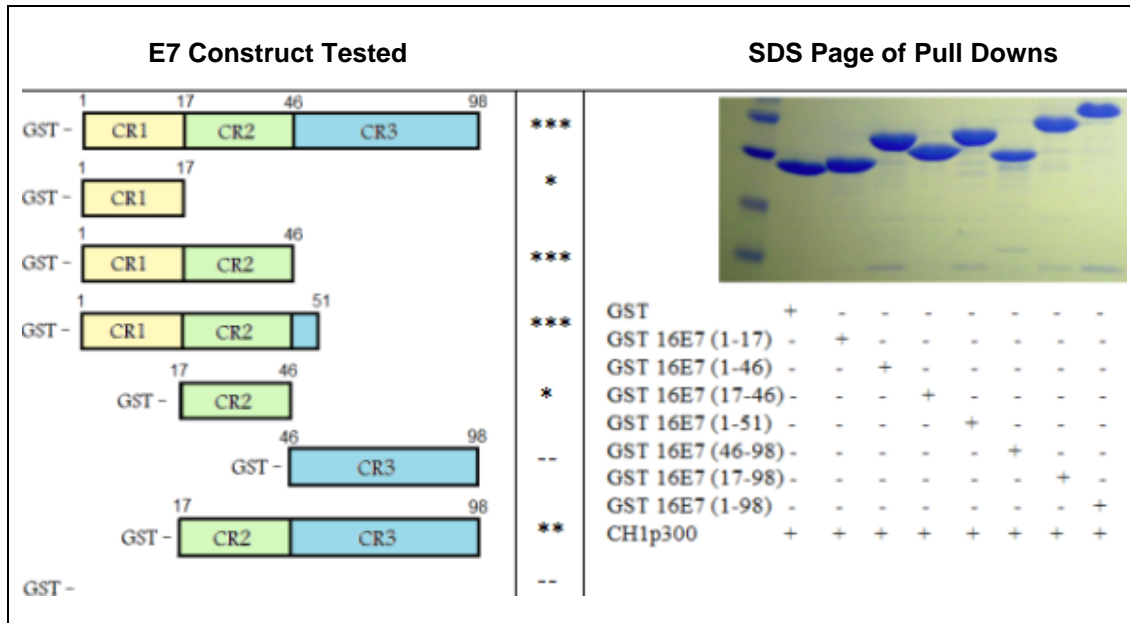


Figure B.5. Mapping the interaction between HPV 16 E7 and the CH1 domain of p300. On the left are the constructs of HPV16-E7 that were tested in pull down experiments. On the right is an SDS gel for each pull down experiment done between the CH1 domain of p300 and different constructs of E7. The asterisks (*) in the middle column indicate the level of binding, with more asterisks suggesting a stronger interaction. Dashes (--) indicate that no interaction was seen.

B.2.3 Gel Filtration Showed that some E7/p300 Complexes can Co-elute

Since an interaction could be seen between HPV16-E7 and p300_{CH1} using pull down experiments, complexes of these two proteins were run on gel filtration to ensure that the binding was strong enough to eventually pursue co-crystallization studies. The proteins could be co-expressed in bacteria, however, this method introduced additional contaminants, such as chaperones that could not be excluded from the complex that was purified (data not shown). Since the complex was more pure when the proteins were purified individually, this method was pursued. Therefore, in order to form the HPV16-E7/p300_{CH1} complexes, the proteins were purified individually and then equal molar amounts of each protein were combined and incubated overnight before running size exclusion chromatography using a superdex 200 preparatory column.

Size exclusion chromatography was done with a buffer of 20mM Tris, 50mM NaCl, and 10mM BME. The buffer was adjusted to pH 8.0 for HPV16-E7₁₋₉₈ and HPV16-E7₁₇₋₉₈ and to pH 7.0 for HPV16-E7₁₋₅₁. Higher salt generally disrupted the complexes (data not shown). Runs were performed with untagged proteins. The constructs of HPV16 E7 tested in complex with the CH1 domain of p300 were: HPV16-E7₁₋₉₈, HPV16-E7₁₇₋₉₈, and HPV16-E7₁₋₅₁. These proteins were also run individually for comparison against any complexes that formed. Consistent with results from the pull down experiments, only HPV16-E7₁₋₉₈ and HPV16-E7₁₋₅₁, were able to co-elute with p300_{CH1}, suggesting that a complex was formed between the two proteins (Figure B.6). HPV16-E7₁₇₋₉₈, whose binding to p300_{CH1} was weaker, did not co-elute with p300_{CH1} (data not shown). As indicated from the SDS-PAGE gels, adding E7 to p300_{CH1} shifted the elution pattern of p300_{CH1} to the left, towards a higher molecular weight, indicative of complex formation (Figure B.6).

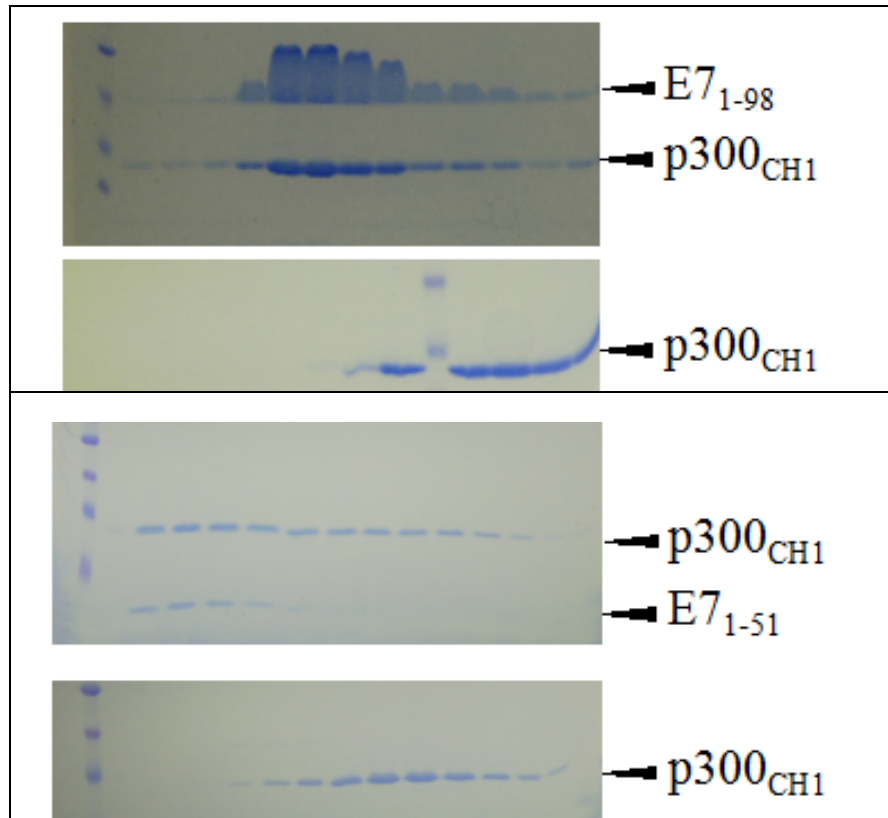


Figure B.6. Gel Filtration between 16E7 and CH1 of p300. The elution profile is shown using SDS-PAGE gels. Full length HPV16-E7 (top panel) in complex with the CH1 domain of p300 is compared to the elution profile of the CH1 domain of p300 alone. Similarly, residues 1-51 of HPV16-E7 (bottom panel) in complex with the CH1 domain of p300 is compared to the elution profile of the CH1 domain of p300 alone.

B.2.4 ITC and AUC Suggest that E7 and p300_{CH1} Bind 1:1

Isothermal titration calorimetry (ITC) and analytical ultracentrifugation (AUC) sedimentation equilibrium experiments were done in order to determine the binding stoichiometry between E7 and p300_{CH1}, as well as the dissociation constants of their complexes. AUC sedimentation equilibrium experiments were also done on the individual proteins to determine their oligomerization states. These experiments were done with untagged HPV16-E7₁₋₉₈, untagged p300_{CH1}, and untagged HPV16-E7₁₋₅₁ in a buffer of 20mM Tris, 50mM NaCl, and 10mM BME. As was done for gel filtration, the buffers for these experiments were adjusted to pH 8.0 for HPV16-E7₁₋₉₈ and to pH 7.0 for HPV16-E7₁₋₅₁.

For ITC, 1.2-1.5mM p300_{CH1} was titrated into 60μM HPV16-E7₁₋₉₈ or 175μM HPV16-E7₁₋₅₁ at a temperature of 15 °C. The resulting heats were integrated and were able to fit both to a one- and two-site model, making the binding stoichiometry of E7:p300 ambiguous according to this technique. The integrated heats are shown in [Figure B.7](#). Therefore, AUC sedimentation equilibrium experiments were pursued using the same protein constructs to help clarify this result. In each case, AUC sedimentation equilibrium experiments were performed using three different protein concentrations and three different speeds onto which to perform a global fit. AUC sedimentation equilibrium experiments were performed at 4 °C with HPV16-E7₁₋₉₈ and HPV16-E7₁₋₅₁, each alone and in complex with p300_{CH1}. p300_{CH1} alone was also run.

The sedimentation equilibrium of HPV16-E7₁₋₅₁ in complex with p300_{CH1} was determined using speeds 20K RPM, 24K RPM, and 35K RPM. The data fit to a single species model with a molecular weight equivalent to a 1:1 protein complex. Consequently, the model $A + B \rightleftharpoons AB$ was attempted, and it fit with an RMSD of less than 0.02. The globally fit data is shown in [Figure B.8](#). To determine the oligomeric state of E7₁₋₅₁ and p300_{CH1} when alone in solution, the experiment was performed using speeds 27K RPM, 32K RPM, and 36K RPM. E7₁₋₅₁ and p300_{CH1} both fit to a single species model corresponding to their molecular weights, indicating that they are monomeric when alone in solution. This data is summarized in [Table B.1](#).

The sedimentation equilibrium of HPV16-E7₁₋₉₈ in complex with p300_{CH1} was determined using speeds 15.5K RPM, 19K RPM, and 25.8K RPM. The data fit to the model $nA \leftrightarrow An$, $An + B \leftrightarrow AnB$, where B is equivalent to two p300_{CH1} molecules, with an RMSD of less than 0.02. 16E7₁₋₉₈ alone was tested at 22K RPM, 25.8 RPM, and 36.5K RPM, and fit to a dimer, consistent with results described elsewhere (Clements et al., 2000). This data is also summarized in [Table B.1](#). The AUC sedimentation equilibrium experiments in combination with the ITC data suggest that the binding is 1:1 in the case of p300_{CH1}:HPV16-E7₁₋₅₁ and 2:2 in the case of p300_{CH1}:HPV16-E7₁₋₉₈ ([Table B.1](#)).

The dissociation constants were also determined for the protein complexes using AUC sedimentation equilibrium and ITC. ITC estimated that the K_D s of the p300_{CH1}:HPV16-E7₁₋₅₁ and p300_{CH1}:HPV16-E7₁₋₉₈ complexes are approximately 0.29 μ M and 2.0 μ M, respectively ([Table B.1](#)). AUC estimated that the K_D s of the p300_{CH1}:HPV16-E7₁₋₅₁ and p300_{CH1}:HPV16-E7₁₋₉₈ complexes are approximately 1.6 μ M and 0.6 μ M ([Table B.1](#)).

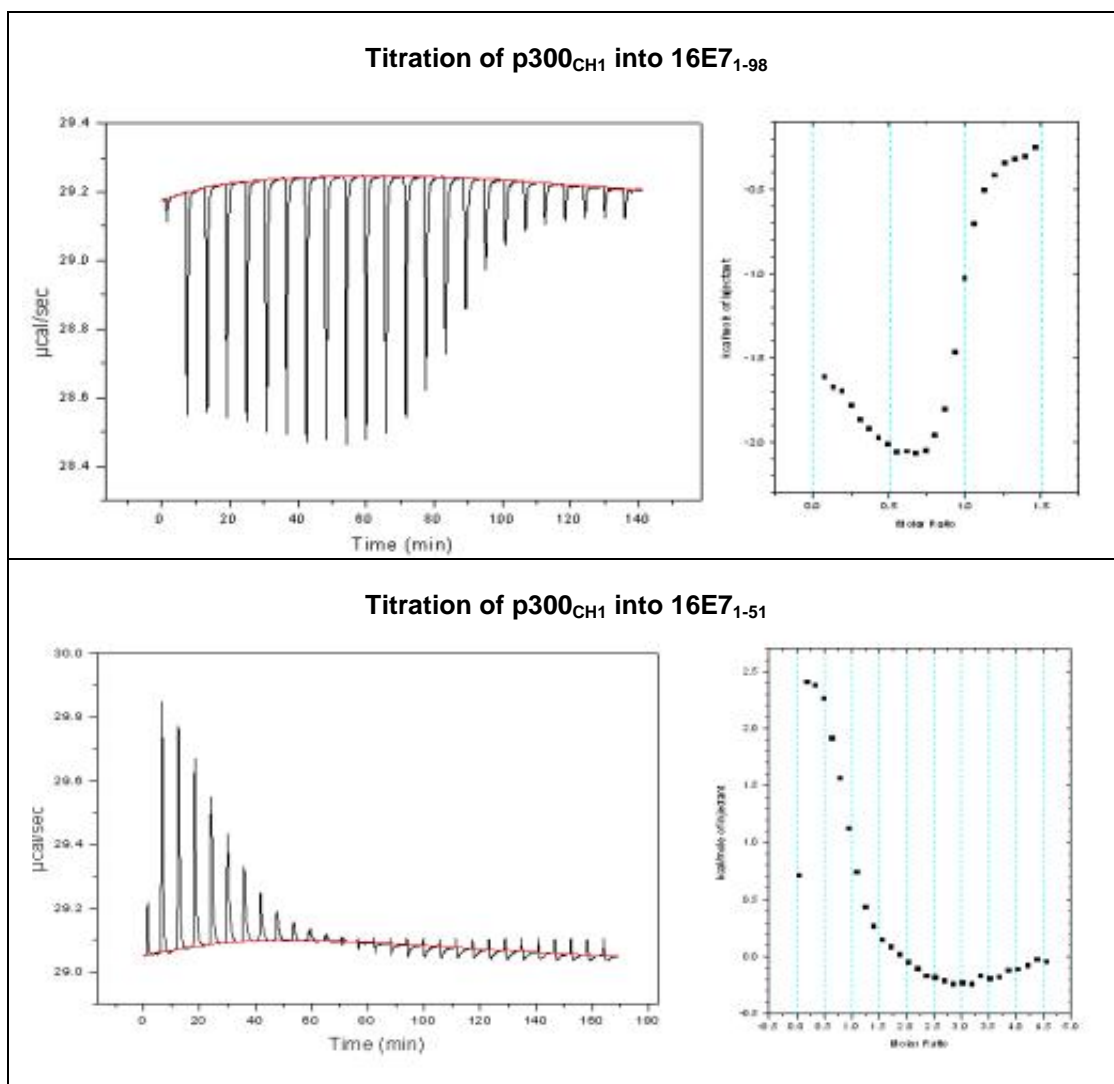


Figure B.7. Isothermal titration calorimetry results. (Top) 1.2 mM p300_{CH1} was titrated into 60 μ M untagged full length HPV16-16E7. (Bottom) 1.2 mM p300_{CH1} was titrated into 175 μ M HPV16-E7₁₋₅₁. The heat spikes are shown (left) as are the integrated heats (right).

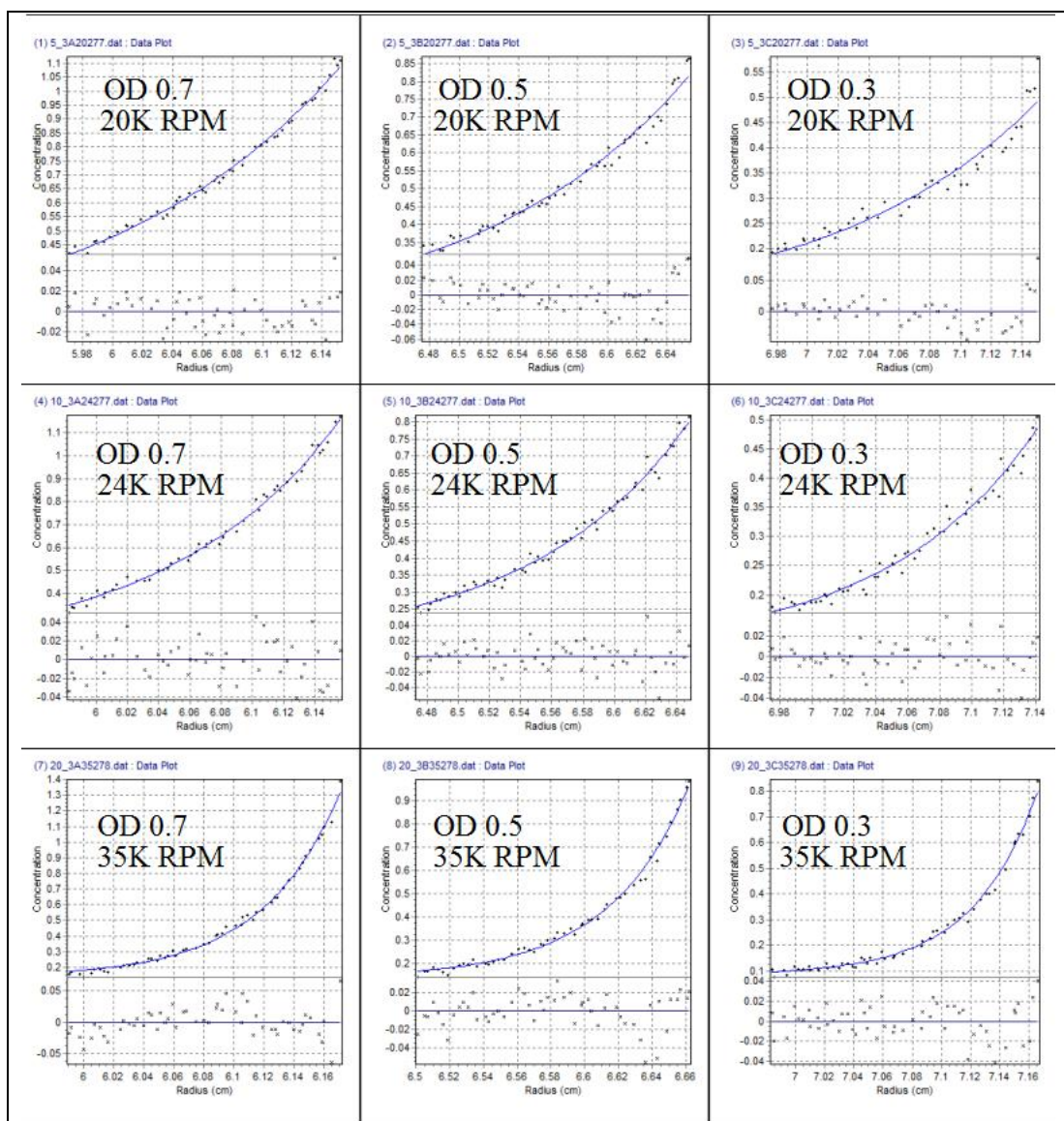


Figure B.8. Analytical ultracentrifugation sedimentation equilibrium of the p300_{CH1}/HPV16-E7₁₋₅₁ complex. The experiment was performed using three protein complex concentrations and three speeds, as indicated. All of the data was fit globally to a single species model, as well as to a 1:1 binding model: $A + B \rightleftharpoons AB$.

	Stoichiometry/Oligomerization State	K_D (AUC) (μM)	K_D (ITC) (μM)
p300_{CH1}	Monomer	NA	NA
16E7₁₋₉₈	Dimer	NA	NA
16E7₁₋₅₁	Monomer	NA	NA
16E7₁₋₉₈/ p300_{CH1}	2:2	0.62	2.0
16E7₁₋₅₁/ p300_{CH1}	1:1	1.6	0.29

Table B.1. Summary of results from ITC and AUC studies on E7/p300_{CH1} complexes. The oligomerization state of the individual proteins is indicated, along with the binding stoichiometry of the complexes and their associated dissociation constants from each method. NA denotes that the information is not applicable.

B.2.5 Crystallization Efforts of E7/p300 Complexes

Experiments involving pull downs and size exclusion chromatography indicated that a protein complex between HPV16-E7₁₋₉₈ and p300_{CH1} does form, making crystallography a possible route for structure determination. Co-crystallization trials of HPV16-E7₁₋₉₈ and HPV16-E7₁₋₅₁ in complex with p300_{CH1} were done at 20 °C and at 4 °C. The only crystals that formed are shown in [Figure B.9](#). These crystals formed using HPV16-E7₁₋₉₈ and p300_{CH1} at 4 °C, were too small to freeze, and could not be reproduced. Additive screening was also done around the most promising conditions, but no crystals resulted. Furthermore, a grid was created to try to crystallize the protein complex in similar conditions. For the grid screens, the percentage of ethanol was varied, as well as the pH for each of the two conditions. Again, crystals did not form. One possible reason for the inability to crystallize the complex is that much of E7 is likely disordered. Therefore, other protein constructs of p300 should be sought, as well as co-crystallization with E1A, which seemed to bind more strongly to p300_{CH1}. Even a co-crystal structure of E1A in complex with p300_{CH1} would shed light onto how E7 binds to p300_{CH1} since E1A and E7 have some similarities in sequence, especially in the highly conserved LxCxE motif that is found in the CR2 domain of E7.

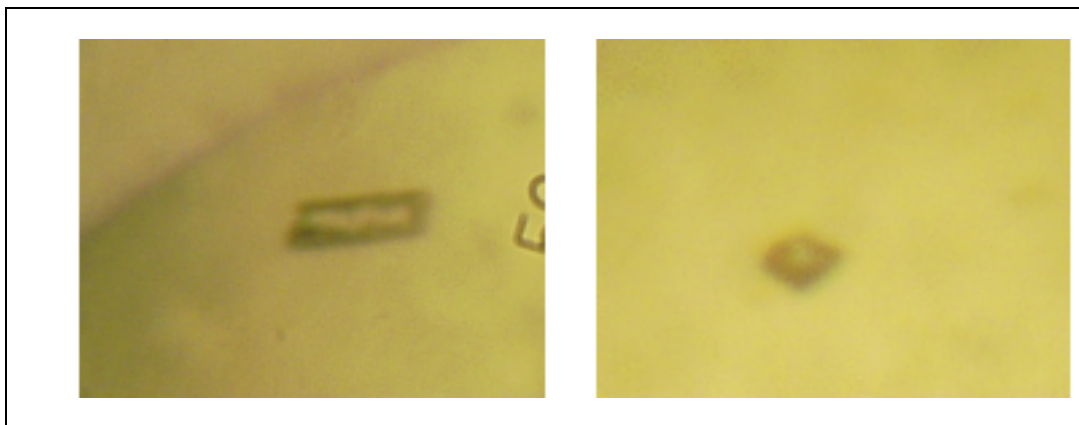


Figure B.9. Crystals formed between HPV16-E7 and p300_{CH1}. The crystal on the left formed in the condition 0.1M Tris, 8.5, 10% v/v ethanol; the crystal on the right formed in the condition 100mM MES, 6.0, 15% v/v ethanol, and 200 μ M Zn(OAc)₂.

B.3 Discussion

To date, there are no structures for an E7-p300 complex. In this study, the region of HPV16-E7 necessary for binding to the CH1 domain of p300 was mapped to the N-terminus of E7. The first 46 residues of E7 were deemed necessary and sufficient for the interaction. ITC and AUC sedimentation equilibrium experiments indicated that E7 binds to p300 with a stoichiometry of 1:1 and 2:2, for the truncated and full length versions of E7, respectively. Unfortunately, due to a lack of structural data, the molecular basis for E7 binding to p300 is still unclear.

The NMR structure of the CH1 domain of p300 has been determined in complex with other proteins such as the transcription factor HIF-1 α and the CITED2 transactivator (Freedman et al., 2003; Freedman et al., 2002). Interestingly, both of these proteins bind p300_{CH1} in different ways. Taken together with the fact that this domain of p300 is known to bind many transcription factors, it can be difficult to predict how E7 binds to p300. This is further made challenging by the fact that there is no significant sequence homology between E7₁₋₄₆ and HIF-1 α or CITED2. Still, because the CH1 domain of p300 has such a large number of binding partners, the binding of HPV E7 to this domain can lead to many deleterious effects in the cell. Therefore, it is still of interest to determine how they bind. Once that is determined, it would be of interest to try to block the E7-p300 interaction, possibly through the use of small molecules.

Most of the experiments done with E7 and p300_{CH1} indicated that the binding is salt-dependent and likely involves more hydrophilic than hydrophobic interactions. The dissociation constants were found to be in the low micromolar range in low salt (50mM) buffers. The salt-dependence of the interaction was seen in the size exclusion chromatography studies, and the dissociation constants were determined using ITC and sedimentation equilibrium studies. As a result, it is possible that the interaction between E7 and p300_{CH1} is mediated by some other protein or protein complex. Since p300 is thought to bind to the CR1-2 domains of E7, the domains that mediate tight binding with pRb, we were curious to see if pRb could form a trimeric

complex with E7 and p300. Pull downs were done and no trimeric complex was seen (data not shown). It is possible that there are other proteins that help mediate binding between E7 and p300, which have yet to be determined. Since HPV E2 has been implicated in binding to p300 (Marcello et al., 2000), it may also be of interest to look at E2-p300 complexes, as well as possible ternary complexes with HPV E7.

B.4 Future Work

Interestingly, our pull downs showed that E1A exhibits stronger binding to p300_{CH1} than does HPV16-E7. Therefore, a next logical step would be to characterize the binding between E1A and p300_{CH1}, and try to co-crystallize the complex formed between these two proteins. A co-crystal structure of the E1A-p300 complex could give insight into how E7 might bind to p300 since E1A and E7 have some similarities in sequence, especially in the highly conserved LxCxE motif that is found in the CR2 domain of E7. It would also be of interest to see if E1A and E7 bind competitively to the CH1 domain of p300.

In addition to trying to co-crystallize the E1A-p300_{CH1} complex, it would also be of interest to test different constructs of p300 for binding to E7 or E1A. Since this study only focused on the CH1 domain of p300, there was no indication of whether other regions of p300 might be important for the interaction. In addition to looking at larger p300 constructs, it might also be interesting to look at p300 from other organisms and compare their binding to HPV16-E7 and E1A. The identification of a stronger protein complex would be more suitable for structural studies by X-ray crystallography.

B.5 Materials and Methods

B.5.1 Expression and Purification of Proteins

GST-tagged E7 proteins. The DNA encoding HPV16-E7₁₋₉₈ (full length), HPV16-E7₁₇₋₉₈, HPV16-E7₄₆₋₉₈, HPV16-E7₁₋₅₁, HPV16-E7₁₋₄₆, HPV16-E7₁₇₋₄₆, HPV16-E7₁₋₁₇, and HPV1A-E7₁₋₉₃ (full length) were cloned into the pGEX-4T-1 vector, containing an N-terminal GST tag. Proteins were expressed in *E. coli* BL21(DE3) cells overnight at 18 °C. Cells were lysed by sonication in a buffer containing 1x PBS, 7.4, 100mM NaCl, 10 μ M Zn(OAc)₂, 10mM BME and 1x PMSF. The cell lysate was centrifuged at 18,000 RPM for 30 minutes and the resulting supernatant was loaded onto GST superflow resin (CLONTECH) pre-equilibrated with 1x PBS, 7.4, 100mM NaCl, 10 μ M Zn(OAc)₂, and 10mM BME. The column was washed with the same buffer except that no additional Zn(OAc)₂ was added. The GST-fused protein was then eluted using 1x PBS, 7.4, 100mM NaCl, 10mM GSH, and 10mM BME. The eluent was then concentrated and further purified using a superdex analytical column (GE Healthcare Life Sciences) in a buffer containing 20mM Tris, 7.5, 150mM NaCl, and 10mM BME.

Untagged E7 proteins. To purify untagged E7 constructs, E7 was expressed and purified as a GST-fusion as described above. After loading on the GST superflow column and washing off the contaminants, the protein was subjected to thrombin (Enzyme Research) cleavage at 20°C for 1 hour. The cleaved protein and protease were washed off the column. Ion exchange was then performed to separate E7 from the thrombin using high-trap Q HP column (Fisher) with a salt gradient (buffer A: 20mM Tris, 7.5, 50mM NaCl, 10mM BME; buffer B: 20mM Tris, 7.5, 750mM NaCl, 10mM BME). Fractions containing E7 were pooled, concentrated and run on gel filtration using a superdex 200 analytical column (GE Healthcare Life Sciences) in a buffer containing 20mM Tris 7.5, 150mM NaCl, and 10mM BME.

His-tagged E7 and E1A proteins. The DNA for HPV16-E7₁₋₉₈ (full length) and Ad5-E1A_{CR1-3} (residues 36-189) were cloned into the pRSET vector, containing an N-terminal 6x-histidine tag.

HPV-E7 and Ad5-E1A were expressed in *E. coli* BL21(DE3) cells overnight at 25 °C and 18 °C, respectively. Cells were lysed by sonication in a buffer containing 20mM Tris, 7.5, 500mM NaCl, 35mM imidazole, 10 μ M Zn(OAc)₂, 10mM BME and 1x PMSF. The cell lysate was centrifuged at 18,000 RPM for 30 minutes and the resulting supernatant was loaded onto a Ni-NTA column (Fisher) pre-equilibrated with 20mM Tris, 7.5, 500mM NaCl, 35mM imidazole, 10 μ M Zn(OAc)₂, and 10mM BME. The column was washed and the bound protein was eluted using an imidazole gradient from 35mM to 250mM. The proteins were further purified using size exclusion chromatography on a superdex 200 analytical column (GE Healthcare Life Sciences) in a buffer containing 20mM Tris, 7.5, 150mM NaCl, and 10mM BME.

Untagged p300. The DNA encoding the CH1 domain of human p300 (residues 323-424) was cloned into the pRSET-A vector, containing no tag. The p300_{CH1} was expressed in *E. coli* Rosetta cells overnight at 18 °C. Cells were lysed by sonication in a buffer containing 20mM Tris, 7.5, 50mM NaCl, 10 μ M Zn(OAc)₂, 2mM DTT, and 1x PMSF. The cell lysate was centrifuged at 19,000 RPM for 30 minutes and the resulting supernatant was loaded onto SP resin (GE Health) pre-equilibrated with 20mM Tris, 7.5, 50mM NaCl, and 2mM DTT. After being loaded, the column was then washed with 20mM Tris, 7.5, 50mM NaCl, and 2mM DTT to remove contaminants. The protein was then eluted with 20mM Tris, 7.5, 100mM NaCl, and 2mM DTT, concentrated, and further purified on a superdex 200 analytical column (GE Healthcare Life Sciences) in a buffer containing 20mM Tris, 7.5, 150mM NaCl, and 10mM BME.

GST-tagged p300. The DNA encoding the CH1 domain of human p300 (residues 323-424) was cloned into the pGEX-4T-1 vector, containing an N-terminal GST tag. The protein was expressed, lysed, and purified, as described above for the GST-tagged E7 proteins.

GST alone. In order to make GST protein as a control for pull down experiments, the pGEX-4T-1 vector was transformed into BL21 (DE3) cells and expressed and purified the same way as the GST-fused proteins.

B.5.2 Pull Downs

30 μg of GST protein was first incubated with 25 μL GST superflow resin (CLONTECH), that was prewashed in binding buffer, for 15 minutes at 4 $^{\circ}$ C. Then, an equal molar amount of p300 was added to the mixture and incubated for 1 hour with gentle rotation at 4 $^{\circ}$ C. The buffer used in each pull down is given in the text. The final reaction volume was approximately 300 μL . The beads were then collected by centrifugation at 600g, at 4 $^{\circ}$ C, for 5 minutes and washed three times using 1mL of binding buffer. Samples were then subjected to SDS-PAGE analysis.

B.5.3 Isothermal Titration Calorimetry

ITC was done using a MicroCal VP-ITC isothermal titration calorimeter (MicroCal, Inc). Proteins were run through size exclusion chromatography columns in matching buffers prior to analysis. 8-12 μL injections of 750-1500 μM of p300 were titrated into 50-150 μM E7 pre-equilibrated to 15 $^{\circ}\text{C}$. After subtraction of dilution heats, calorimetric data were analyzed with the MicroCal ORIGIN V5.0 (MicroCal Software, Northampton, MA).

B.5.4 Equilibrium Sedimentation

Analytical ultracentrifugation of the E7/p300 complex was performed at 4 $^{\circ}\text{C}$ with absorbance optics by using a Beckman Optima XL-I analytical ultracentrifuge, using a 4-hole rotor. The partial specific volume and viscosity were estimated by using Sednterp (Lave TM, 1992). Analysis was performed by using six-channel centerpieces with quartz windows. Protein samples were analyzed at three different protein and protein complex concentrations; the optical densities used were 0.3, 0.5, and 0.7. A global fit of the data was performed for each sample using the program HeteroAnalysis. The quality of the fit was assessed from the RMSD value.

BIBLIOGRAPHY

- Adams, P. D., Li, X. T., Sellers, W. R., Baker, K. B., Leng, X. H., Harper, J. W., Taya, Y., and Kaelin, W. G. (1999). Retinoblastoma protein contains a C-terminal motif that targets it for phosphorylation by cyclin-cdk complexes. *Molecular and Cellular Biology* 19, 1068-1080.
- Alvarez-Salas, L., and diPaolo, J. (2007). Molecular approaches to cervical cancer therapy. *Current drug discovery technologies* 4, 208 - 219.
- Amundson, S. A., Myers, T. G., and Fornace, A. J., Jr. (1998). Roles for p53 in growth arrest and apoptosis: putting on the brakes after genotoxic stress. *Oncogene* 17, 3287-3299.
- Arkin, M. R., and Wells, J. A. (2004). Small-molecule inhibitors of protein-protein interactions: progressing towards the dream. *Nat Rev Drug Discov* 3, 301-317.
- Avvakumov, N., Torchia, J., and Mymryk, J. S. (2003). Interaction of the HPV E7 proteins with the pCAF acetyltransferase. *Oncogene* 22, 3833-3841.
- Balagurumoorthy, P., Sakamoto, H., Lewis, M. S., Zambrano, N., Clore, G. M., Gronenborn, A. M., Appella, E., and Harrington, R. E. (1995). Four p53 DNA-binding domain peptides bind natural p53-response elements and bend the DNA. *Proc Natl Acad Sci U S A* 92, 8591-8595.
- Baleja, J., Cherry, J., Liu, Z., Gao, H., Nicklaus, M., Voigt, J., Chen, J., and Androphy, E. (2006a). Identification of inhibitors to papillomavirus type 16 E6 protein based on three-dimensional structures of interacting proteins. *Antiviral Research* 72, 49 - 59.
- Baleja, J. D., Cherry, J. J., Liu, Z., Gao, H., Nicklaus, M. C., Voigt, J. H., Chen, J. J., and Androphy, E. J. (2006b). Identification of inhibitors to papillomavirus type 16 E6 protein based on three-dimensional structures of interacting proteins. *Antiviral Res* 72, 49-59.
- Balog, E. R., Burke, J. R., Hura, G. L., and Rubin, S. M. (2011). Crystal structure of the unliganded retinoblastoma protein pocket domain. *Proteins* 79, 2010-2014.
- Bates, S., Phillips, A. C., Clark, P. A., Stott, F., Peters, G., Ludwig, R. L., and Vousden, K. H. (1998). p14ARF links the tumour suppressors RB and p53. *Nature* 395, 124-125.
- Bayne, E. H., and Allshire, R. C. (2005). RNA-directed transcriptional gene silencing in mammals. *Trends Genet* 21, 370-373.
- Be, X., Hong, Y., Wei, J., Androphy, E. J., Chen, J. J., and Baleja, J. D. (2001). Solution Structure Determination and Mutational Analysis of the Papillomavirus E6 Interacting Peptide of E6AP. *Biochemistry* 40, 1293 - 1299.
- Bernards, R., Shackleford, G. M., Gerber, M. R., Horowitz, J. M., Friend, S. H., Schartl, M., Bogenmann, E., Rapaport, J. M., McGee, T., Dryja, T. P., and et al. (1989). Structure and expression of the murine retinoblastoma gene and characterization of its encoded protein. *Proc Natl Acad Sci U S A* 86, 6474-6478.
- Bernat, A., Avvakumov, N., Mymryk, J. S., and Banks, L. (2003). Interaction between the HPV E7 oncoprotein and the transcriptional coactivator p300. *Oncogene* 22, 7871-7881.

- Bodian, D. L., Yamasaki, R. B., Buswell, R. L., Stearns, J. F., White, J. M., and Kuntz, I. D. (1993). Inhibition of the fusion-inducing conformational change of influenza hemagglutinin by benzoquinones and hydroquinones. *Biochemistry* 32, 2967-2978.
- Bosch, F. X., Manos, M. M., Munoz, N., Sherman, M., Jansen, A. M., Peto, J., Schiffman, M. H., Moreno, V., Kurman, R., and Shah, K. V. (1995). Prevalence of human papillomavirus in cervical cancer: a worldwide perspective. International biological study on cervical cancer (IBSCC) Study Group. *J Natl Cancer Inst* 87, 796-802.
- Boshart, M., Gissmann, L., Ikenberg, H., Kleinheinz, A., Scheurlen, W., and zur Hausen, H. (1984). A new type of papillomavirus DNA, its presence in genital cancer biopsies and in cell lines derived from cervical cancer. *Embo J* 3, 1151-1157.
- Bowers, E. M., Yan, G., Mukherjee, C., Orry, A., Wang, L., Holbert, M. A., Crump, N. T., Hazzalin, C. A., Liszczak, G., Yuan, H., *et al.* (2010). Virtual ligand screening of the p300/CBP histone acetyltransferase: identification of a selective small molecule inhibitor. *Chem Biol* 17, 471-482.
- Boyer, S. N., Wazer, D. E., and Band, V. (1996). E7 protein of human papilloma virus-16 induces degradation of retinoblastoma protein through the ubiquitin-proteasome pathway. *Cancer Research* 56, 4620-4624.
- Breitburd, F., Kirnbauer, R., Hubbert, N. L., Nonnenmacher, B., Trin-Dinh-Desmarquet, C., Orth, G., Schiller, J. T., and Lowy, D. R. (1995). Immunization with viruslike particles from cottontail rabbit papillomavirus (CRPV) can protect against experimental CRPV infection. *J Virol* 69, 3959-3963.
- Brown, C. J., Lain, S., Verma, C. S., Fersht, A. R., and Lane, D. P. (2009). Awakening guardian angels: drugging the p53 pathway. *Nat Rev Cancer* 9, 862-873.
- Buck, C. B., Thompson, C. D., Roberts, J. N., Muller, M., Lowy, D. R., and Schiller, J. T. (2006). Carrageenan is a potent inhibitor of papillomavirus infection. *PLoS Pathog* 2, e69.
- Burchell, A. N., Winer, R. L., de Sanjose, S., and Franco, E. L. (2006). Chapter 6: Epidemiology and transmission dynamics of genital HPV infection. *Vaccine* 24 *Suppl* 3, S3/52-61.
- Burd, E. M. (2003). Human papillomavirus and cervical cancer. *Clinical Microbiology Reviews* 16, 1-+.
- Butz, K., Denk, C., Ullmann, A., Scheffner, M., and Hoppe-Seyler, F. (2000). Induction of apoptosis in human papillomaviruspositive cancer cells by peptide aptamers targeting the viral E6 oncoprotein. *Proc Natl Acad Sci U S A* 97, 6693-6697.
- Campisi, J., and d'Adda di Fagagna, F. (2007). Cellular senescence: when bad things happen to good cells. *Nat Rev Mol Cell Biol* 8, 729-740.
- Campo, M. S., Grindlay, G. J., O'Neil, B. W., Chandrachud, L. M., McGarvie, G. M., and Jarrett, W. F. (1993). Prophylactic and therapeutic vaccination against a mucosal papillomavirus. *J Gen Virol* 74 (Pt 6), 945-953.
- Caplen, N. J., Parrish, S., Imani, F., Fire, A., and Morgan, R. A. (2001). Specific inhibition of gene expression by small double-stranded RNAs in invertebrate and vertebrate systems. *Proc Natl Acad Sci U S A* 98, 9742-9747.

- Chan, H. M., Krstic-Demonacos, M., Smith, L., Demonacos, C., and La Thangue, N. B. (2001). Acetylation control of the retinoblastoma tumour-suppressor protein. *Nat Cell Biol* 3, 667-674.
- Chan, H. M., and La Thangue, N. B. (2001). p300/CBP proteins: HATs for transcriptional bridges and scaffolds. *J Cell Sci* 114, 2363-2373.
- Chang, J. T., Kuo, T. F., Chen, Y. J., Chiu, C. C., Lu, Y. C., Li, H. F., Shen, C. R., and Cheng, A. J. (2010). Highly potent and specific siRNAs against E6 or E7 genes of HPV16- or HPV18-infected cervical cancers. *Cancer Gene Ther* 17, 827-836.
- Chaturvedi, A. K. (2010). Beyond cervical cancer: burden of other HPV-related cancers among men and women. *J Adolesc Health* 46, S20-26.
- Cheek, C. F., Dey, A., and Lane, D. P. (2007). Cyclin-dependent kinase inhibitors sensitize tumor cells to nutlin-induced apoptosis: a potent drug combination. *Mol Cancer Res* 5, 1133-1145.
- Chinnam, M., and Goodrich, D. W. (2011). RB1, development, and cancer. *Curr Top Dev Biol* 94, 129-169.
- Cho, Y., Gorina, S., Jeffrey, P. D., and Pavletich, N. P. (1994a). Crystal structure of a p53 tumor suppressor-DNA complex: understanding tumorigenic mutations. *Science* 265, 346-355.
- Cho, Y., Gorina, S., Jeffrey, P. D., and Pavletich, N. P. (1994b). Crystal Structure of the p53 Tumor Suppressor-DNA Complex: Understanding Tumorigenic Mutations. *Science* 265, 346 - 355.
- Clements, A., Johnston, K., Mazarrelli, J. M., Ricciardi, R. P., and Marmorstein, R. (2000). Oligomerization properties of the viral oncoproteins adenovirus E1A and human papillomavirus E7 and their complexes with the retinoblastoma protein. *Biochemistry* 39, 16033-16045.
- Combita, A. L., Touze, A., Bousarghin, L., Sizaret, P. Y., Munoz, N., and Coursaget, P. (2001). Gene transfer using human papillomavirus pseudovirions varies according to virus genotype and requires cell surface heparan sulfate. *FEMS Microbiol Lett* 204, 183-188.
- Cooper, B., Schneider, S., Bohl, J., Jiang, Y.-h., Beudet, A., and Pol, S. V. (2003a). Requirement of E6AP and the features of human papillomavirus E6 necessary to support degradation of p53. *Virology* 306, 87 - 99.
- Cooper, B., Schneider, S., Bohl, J., Jiang, Y., Beudet, A., and Vande Pol, S. (2003b). Requirement of E6AP and the features of human papillomavirus E6 necessary to support degradation of p53. *Virology* 306, 87-99.
- Cordon-Cardo, C., Sheinfeld, J., and Dalbagni, G. (1997). Genetic studies and molecular markers of bladder cancer. *Semin Surg Oncol* 13, 319-327.
- Cregan, S. P., Fortin, A., MacLaurin, J. G., Callaghan, S. M., Cecconi, F., Yu, S. W., Dawson, T. M., Dawson, V. L., Park, D. S., Kroemer, G., and Slack, R. S. (2002). Apoptosis-inducing factor is involved in the regulation of caspase-independent neuronal cell death. *J Cell Biol* 158, 507-517.
- Cross, J. B., Thompson, D. C., Rai, B. K., Baber, J. C., Fan, K. Y., Hu, Y., and Humblet, C. (2009). Comparison of several molecular docking programs: pose prediction and virtual screening accuracy. *J Chem Inf Model* 49, 1455-1474.

- D'Arcy, A., Villard, F., and Marsh, M. (2007). An automated microseed matrix-screening method for protein crystallization. *Acta Crystallogr D Biol Crystallogr* 63, 550-554.
- Dahiya, A., Gavin, M. R., Luo, R. X., and Dean, D. C. (2000). Role of the LXCXE binding site in Rb function. *Molecular and Cellular Biology* 20, 6799-6805.
- Dasgupta, T., Chitnumsub, P., Kamchonwongpaisan, S., Maneeruttanarungroj, C., Nichols, S. E., Lyons, T. M., Tirado-Rives, J., Jorgensen, W. L., Yuthavong, Y., and Anderson, K. S. (2009). Exploiting structural analysis, in silico screening, and serendipity to identify novel inhibitors of drug-resistant falciparum malaria. *ACS Chem Biol* 4, 29-40.
- De Guzman, R. N., Wojciak, J. M., Martinez-Yamout, M. A., Dyson, H. J., and Wright, P. E. (2005). CBP/p300 TAZ1 domain forms a structured scaffold for ligand binding. *Biochemistry* 44, 490-497.
- de Villiers, E. M., Gissmann, L., and zur Hausen, H. (1981). Molecular cloning of viral DNA from human genital warts. *J Virol* 40, 932-935.
- De Vuyst, H., Clifford, G. M., Nascimento, M. C., Madeleine, M. M., and Franceschi, S. (2009). Prevalence and type distribution of human papillomavirus in carcinoma and intraepithelial neoplasia of the vulva, vagina and anus: a meta-analysis. *Int J Cancer* 124, 1626-1636.
- DeFilippis, R. A., Goodwin, E. C., Wu, L., and DiMaio, D. (2003). Endogenous human papillomavirus E6 and E7 proteins differentially regulate proliferation, senescence, and apoptosis in HeLa cervical carcinoma cells. *J Virol* 77, 1551-1563.
- Degeterev, A. (2001). Identification of small molecule inhibitors of interaction between the BH3 domain and Bcl-XL. *Nature Cell Biology* 3, 173 - 182.
- DesJarlais, R. L., and Dixon, J. S. (1994). A shape- and chemistry-based docking method and its use in the design of HIV-1 protease inhibitors. *J Comput Aided Mol Des* 8, 231-242.
- Devlin, J. J., Liang, A., Trinh, L., Polokoff, M. A., Senator, D., Zhang, W., Kondracki, J., Kretschmer, P. J., Morser, J., Lipson, S. E., *et al.* (1996). High Capacity Screening of Pooled Compounds: Identification of the Active Compound Without Re-Assay of Pool Members. 37Drug Development Research.
- Devlin, J. J., Liang, A., Trinh, L., Polokoff, M.A., Senator, D., Zheng, W., Kondracki, J., Kretschmer, P.J., and Morser, J., Lipson, S.E., Spann, R., Loughlin, J.A., Dunn, K.V., Morrissey, M.M. (1996). High Capacity Screening of Pooled Compounds: Identification of the Active Compound Without Re-Assay of Pool Members. , Vol 37: Drug Development Research).
- DiMaio, D., and Mattoon, D. (2001). Mechanisms of cell transformation by papillomavirus E5 proteins. *Oncogene* 20, 7866-7873.
- Doorbar, J., and Cubie, H. (2005). Molecular basis for advances in cervical screening. *Mol Diagn* 9, 129-142.
- Dufour, X., Beby-Defaux, A., Agius, G., and Lacau St Guily, J. (2011). HPV and head and neck cancer. *Eur Ann Otorhinolaryngol Head Neck Dis*.

- Durst, M., Gissmann, L., Ikenberg, H., and zur Hausen, H. (1983). A papillomavirus DNA from a cervical carcinoma and its prevalence in cancer biopsy samples from different geographic regions. *Proc Natl Acad Sci U S A* *80*, 3812-3815.
- Eckner, R., Ewen, M. E., Newsome, D., Gerdes, M., DeCaprio, J. A., Lawrence, J. B., and Livingston, D. M. (1994). Molecular cloning and functional analysis of the adenovirus E1A-associated 300-kD protein (p300) reveals a protein with properties of a transcriptional adaptor. *Genes Dev* *8*, 869-884.
- Elbashir, S. M., Lendeckel, W., and Tuschl, T. (2001). RNA interference is mediated by 21- and 22-nucleotide RNAs. *Genes Dev* *15*, 188-200.
- Elston, R., Napthine, S., and Doorbar, J. (1998). *Journal of General Virology* *79*, 371 - 374.
- Emeny, R. T., Wheeler, C. M., Jansen, K. U., Hunt, W. C., Fu, T. M., Smith, J. F., MacMullen, S., Esser, M. T., and Paliard, X. (2002). Priming of human papillomavirus type 11-specific humoral and cellular immune responses in college-aged women with a virus-like particle vaccine. *J Virol* *76*, 7832-7842.
- Evans, T. G., Bonnez, W., Rose, R. C., Koenig, S., Demeter, L., Suzich, J. A., O'Brien, D., Campbell, M., White, W. I., Balsley, J., and Reichman, R. C. (2001). A Phase 1 study of a recombinant viruslike particle vaccine against human papillomavirus type 11 in healthy adult volunteers. *J Infect Dis* *183*, 1485-1493.
- Ewing, T. J., Makino, S., Skillman, A. G., and Kuntz, I. D. (2001). DOCK 4.0: search strategies for automated molecular docking of flexible molecule databases. *J Comput Aided Mol Des* *15*, 411-428.
- Fattaey, A. R., Harlow, E., and Helin, K. (1993). Independent regions of adenovirus E1A are required for binding to and dissociation of E2F-protein complexes. *Mol Cell Biol* *13*, 7267-7277.
- Faucher, A. M., White, P. W., Brochu, C., Grand-Maitre, C., Rancourt, J., and Fazal, G. (2004). Discovery of small-molecule inhibitors of the ATPase activity of human papillomavirus E1 helicase. *J Med Chem* *47*, 18-21.
- Felsani, A., Mileo, A. M., and Paggi, M. G. (2006). Retinoblastoma family proteins as key targets of the small DNA virus oncoproteins. *Oncogene* *25*, 5277-5285.
- Fera, D., Schultz, D. C., Hodawadekar, S., Reichman, M., Donover, P. S., Melvin, J., Troutman, S., Kissil, J. L., Huryn, D. M., and Marmorstein, R. (2012). Identification and characterization of small molecule antagonists of pRb inactivation by viral oncoproteins. *Chem Biol* *19*, 518-528.
- Ferrand, S., Schmid, A., Engeloch, C., and Glickman, J. F. (2005). Statistical evaluation of a self-deconvoluting matrix strategy for high-throughput screening of the CXCR3 receptor. *Assay Drug Dev Technol* *3*, 413-424.
- Ferrari, R., Pellegrini, M., Horwitz, G. A., Xie, W., Berk, A. J., and Kurdistani, S. K. (2008). Epigenetic reprogramming by adenovirus e1a. *Science* *321*, 1086-1088.
- Ferreon, J. C., Martinez-Yamout, M. A., Dyson, H. J., and Wright, P. E. (2009). Structural basis for subversion of cellular control mechanisms by the adenoviral E1A oncoprotein. *Proc Natl Acad Sci U S A* *106*, 13260-13265.

- Finzer, P., Krueger, A., Stohr, M., Brenner, D., Soto, U., Kuntzen, C., Krammer, P. H., and Rosl, F. (2004). HDAC inhibitors trigger apoptosis in HPV-positive cells by inducing the E2F-p73 pathway. *Oncogene* 23, 4807-4817.
- Fire, A., Xu, S., Montgomery, M. K., Kostas, S. A., Driver, S. E., and Mello, C. C. (1998). Potent and specific genetic interference by double-stranded RNA in *Caenorhabditis elegans*. *Nature* 391, 806-811.
- Freedman, S. J., Sun, Z. Y., Kung, A. L., France, D. S., Wagner, G., and Eck, M. J. (2003). Structural basis for negative regulation of hypoxia-inducible factor-1alpha by CITED2. *Nat Struct Biol* 10, 504-512.
- Freedman, S. J., Sun, Z. Y., Poy, F., Kung, A. L., Livingston, D. M., Wagner, G., and Eck, M. J. (2002). Structural basis for recruitment of CBP/p300 by hypoxia-inducible factor-1 alpha. *Proc Natl Acad Sci U S A* 99, 5367-5372.
- Frisch, S. M., and Mymryk, J. S. (2002). Adenovirus-5 E1A: paradox and paradigm. *Nat Rev Mol Cell Biol* 3, 441-452.
- Gambhira, R., Karanam, B., Jagu, S., Roberts, J. N., Buck, C. B., Bossis, I., Alphas, H., Culp, T., Christensen, N. D., and Roden, R. B. (2007). A protective and broadly cross-neutralizing epitope of human papillomavirus L2. *J Virol* 81, 13927-13931.
- Ganguly, N., and Parihar, S. P. (2009a). Human papillomavirus E6 and E7 oncoproteins as risk factors for tumorigenesis. *Journal of Biosciences* 34, 113-123.
- Ganguly, N., and Parihar, S. P. (2009b). Human papillomavirus E6 and E7 oncoproteins as risk factors for tumorigenesis. *J Biosci* 34, 113-123.
- Gardioli, D., Kuhne, C., Glaunsinger, B., Lee, S. S., Javier, R., and Banks, L. (1999). Oncogenic human papillomavirus E6 proteins target the discs large tumour suppressor for proteasome-mediated degradation. *Oncogene* 18, 5487-5496.
- Giarre, M., Caldeira, S., Malanchi, I., Ciccolini, F., Leao, M. J., and Tommasino, M. (2001). Induction of pRb degradation by the human papillomavirus type 16 E7 protein is essential to efficiently overcome p16INK4a-imposed G1 cell cycle Arrest. *J Virol* 75, 4705-4712.
- Giles, R. H., Peters, D. J., and Breuning, M. H. (1998). Conjunction dysfunction: CBP/p300 in human disease. *Trends Genet* 14, 178-183.
- Giovane, C., Trave, G., Briones, A., Lutz, Y., Wasyluk, B., and Weiss, E. (1999). Targetting of the N-terminal domain of the human papillomavirus type 16 E6 oncoprotein with monomeric ScFvs blocks the E6-mediated degradation of cellular p53. *J Mol Recognit* 12, 141-152.
- Giroglou, T., Florin, L., Schafer, F., Streeck, R. E., and Sapp, M. (2001a). Human papillomavirus infection requires cell surface heparan sulfate. *J Virol* 75, 1565-1570.
- Giroglou, T., Sapp, M., Lane, C., Fligge, C., Christensen, N. D., Streeck, R. E., and Rose, R. C. (2001b). Immunological analyses of human papillomavirus capsids. *Vaccine* 19, 1783-1793.
- Gissmann, L., Diehl, V., Schultz-Coulon, H. J., and zur Hausen, H. (1982). Molecular cloning and characterization of human papilloma virus DNA derived from a laryngeal papilloma. *J Virol* 44, 393-400.

- Gissmann, L., and zur Hausen, H. (1980). Partial characterization of viral DNA from human genital warts (*Condylomata acuminata*). *Int J Cancer* 25, 605-609.
- Godefroy, N., Lemaire, C., Renaud, F., Rincheval, V., Perez, S., Parvu-Ferecatu, I., Mignotte, B., and Vayssiere, J. L. (2004). p53 can promote mitochondria- and caspase-independent apoptosis. *Cell Death Differ* 11, 785-787.
- Gonzalez, S. L., Stremlau, M., He, X., Basile, J. R., and Munger, K. (2001). Degradation of the retinoblastoma tumor suppressor by the human papillomavirus type 16 E7 oncoprotein is important for functional inactivation and is separable from proteasomal degradation of E7. *Journal of Virology* 75, 7583-7591.
- Goodsell, D. S., Morris, G. M., and Olson, A. J. (1996). Automated docking of flexible ligands: applications of AutoDock. *J Mol Recognit* 9, 1-5.
- Goudreau, N., Cameron, D. R., Deziel, R., Hache, B., Jakalian, A., Malenfant, E., Naud, J., Ogilvie, W. W., O'Meara, J., White, P. W., and Yoakim, C. (2007). Optimization and determination of the absolute configuration of a series of potent inhibitors of human papillomavirus type-11 E1-E2 protein-protein interaction: a combined medicinal chemistry, NMR and computational chemistry approach. *Bioorg Med Chem* 15, 2690-2700.
- Grana, X., Garriga, J., and Mayol, X. (1998). Role of the retinoblastoma protein family, pRB, p107 and p130 in the negative control of cell growth. *Oncogene* 17, 3365-3383.
- Green, D. R., and Kroemer, G. (2009). Cytoplasmic functions of the tumour suppressor p53. *Nature* 458, 1127-1130.
- Griffin, H., Elston, R., Jackson, D., Ansell, K., Coleman, M., Winter, G., and Doorbar, J. (2006). Inhibition of papillomavirus protein function in cervical cancer cells by intrabody targeting. *J Mol Biol* 355, 360-378.
- Grm, H. S., and Banks, L. (2004). Degradation of hDlg and MAGIs by human papillomavirus E6 is E6-AP-independent. *J Gen Virol* 85, 2815-2819.
- Grossman, S. R. (2001). p300/CBP/p53 interaction and regulation of the p53 response. *Eur J Biochem* 268, 2773-2778.
- Harbour, J. W., and Dean, D. C. (2000). The Rb/E2F pathway: expanding roles and emerging paradigms. *Genes & Development* 14, 2393-2409.
- Harbour, J. W., Luo, R. X., Santi, A. D., Postigo, A. A., and Dean, D. C. (1999). Cdk phosphorylation triggers sequential intramolecular interactions that progressively block Rb functions as cells move through G1. *Cell* 98, 859-869.
- Hariri, S., Unger, E. R., Sternberg, M., Dunne, E. F., Swan, D., Patel, S., and Markowitz, L. E. (2011). Prevalence of genital human papillomavirus among females in the United States, the National Health And Nutrition Examination Survey, 2003-2006. *J Infect Dis* 204, 566-573.
- Harro, C. D., Pang, Y. Y., Roden, R. B., Hildesheim, A., Wang, Z., Reynolds, M. J., Mast, T. C., Robinson, R., Murphy, B. R., Karron, R. A., *et al.* (2001). Safety and immunogenicity trial in adult volunteers of a human papillomavirus 16 L1 virus-like particle vaccine. *J Natl Cancer Inst* 93, 284-292.
- Hatch, K. D. (1995). Cryotherapy. *Baillieres Clin Obstet Gynaecol* 9, 133-143.

- Haupt, S., Berger, M., Goldberg, Z., and Haupt, Y. (2003). Apoptosis - the p53 network. *J Cell Sci* 116, 4077-4085.
- Hebner, C. M., and Laimins, L. A. (2006). Human papillomaviruses: basic mechanisms of pathogenesis and oncogenicity. *Rev Med Virol* 16, 83-97.
- Hengstermann, A., Linares, L. K., Ciechanover, A., Whitaker, N. J., and Scheffner, M. (2001). Complete switch from Mdm2 to human papillomavirus E6-mediated degradation of p53 in cervical cancer cells. *Proc Natl Acad Sci U S A* 98, 1218-1223.
- Hensel, C. H., Hsieh, C. L., Gazdar, A. F., Johnson, B. E., Sakaguchi, A. Y., Naylor, S. L., Lee, W. H., and Lee, E. Y. (1990). Altered structure and expression of the human retinoblastoma susceptibility gene in small cell lung cancer. *Cancer Res* 50, 3067-3072.
- Hiebert, S. W., Chellappan, S. P., Horowitz, J. M., and Nevins, J. R. (1992). The interaction of RB with E2F coincides with an inhibition of the transcriptional activity of E2F. *Genes Dev* 6, 177-185.
- Ho, W. C., Fitzgerald, M. X., and Marmorstein, R. (2006). Structure of the p53 core domain dimer bound to DNA. *J Biol Chem* 281, 20494-20502.
- Honda, R., Tanaka, H., and Yasuda, H. (1997). Oncoprotein MDM2 is a ubiquitin ligase E3 for tumor suppressor p53. *FEBS Lett* 420, 25-27.
- Horn, H. F., and Vousden, K. H. (2007). Coping with stress: multiple ways to activate p53. *Oncogene* 26, 1306-1316.
- Horvath, C. A., Boulet, G. A., Renoux, V. M., Delvenne, P. O., and Bogers, J. P. (2010). Mechanisms of cell entry by human papillomaviruses: an overview. *Virology* 40, 11.
- Huang, L., Kinnucan, E., Wang, G., Beaudenon, S., Howley, P. M., Huibregste, J. M., and Pavletich, N. P. (1999). Structure of an E6AP-UbcH7 Complex: Insights into Ubiquitination by the E2-E3 Enzyme Cascade. *Science* 286, 1321 - 1326.
- Huh, K. W., DeMasi, J., Ogawa, H., Nakatani, Y., Howley, P. M., and Munger, K. (2005). Association of the human papillomavirus type 16 E7 oncoprotein with the 600-kDa retinoblastoma protein-associated factor, p600. *Proc Natl Acad Sci U S A* 102, 11492-11497.
- Huh, W. K., and Roden, R. B. (2008). The future of vaccines for cervical cancer. *Gynecol Oncol* 109, S48-56.
- Huibregste, J. M., Scheffner, M., and Howley, P. M. (1993). Localization of the E6-AP Regions that Direct Human Papillomavirus E6 Binding, Association with p53, and Ubiquitination of Associated Proteins. *Molecular and Cellular Biology* 13, 4918 - 4927.
- Hung, C. F., Ma, B., Monie, A., Tsen, S. W., and Wu, T. C. (2008). Therapeutic human papillomavirus vaccines: current clinical trials and future directions. *Expert Opin Biol Ther* 8, 421-439.
- Ikeda, M. A., and Nevins, J. R. (1993). Identification of distinct roles for separate E1A domains in disruption of E2F complexes. *Mol Cell Biol* 13, 7029-7035.
- Ikenberg, H., Gissmann, L., Gross, G., Grussendorf-Conen, E. I., and zur Hausen, H. (1983). Human papillomavirus type-16-related DNA in genital Bowen's disease and in Bowenoid papulosis. *Int J Cancer* 32, 563-565.

- Irwin, J. J., and Shoichet, B. K. (2005). ZINC--a free database of commercially available compounds for virtual screening. *J Chem Inf Model* **45**, 177-182.
- Issaeva, N., Bozko, P., Enge, M., Protopopova, M., Verhoef, L. G., Masucci, M., Pramanik, A., and Selivanova, G. (2004). Small molecule RITA binds to p53, blocks p53-HDM-2 interaction and activates p53 function in tumors. *Nat Med* **10**, 1321-1328.
- Jablonska, S., Dabrowski, J., and Jakubowicz, K. (1972). Epidermodysplasia verruciformis as a model in studies on the role of papovaviruses in oncogenesis. *Cancer Res* **32**, 583-589.
- Jablonska, S., Orth, G., Jarzabek-Chorzelska, M., Rzesa, G., Obalek, S., Glinski, W., Favre, M., and Croissant, O. (1978). Immunological studies in epidermodysplasia verruciformis. *Bull Cancer* **65**, 183-190.
- Jablonska, S., Orth, G., Jarzabek-Chorzelska, M., Rzesa, G., Obalek, S., Glinski, W., Favre, M., and Croissant, O. (1979). Epidermodysplasia verruciformis versus disseminated verrucae planae: is epidermodysplasia verruciformis a generalized infection with wart virus? *J Invest Dermatol* **72**, 114-119.
- Jackson, S., Harwood, C., Thomas, M., Banks, L., and Storey, A. (2000). Role of Bak in UV-induced apoptosis in skin cancer and abrogation by HPV E6 proteins. *Genes Dev* **14**, 3065-3073.
- Jayaprakash, V., Reid, M., Hatton, E., Merzianu, M., Rigual, N., Marshall, J., Gill, S., Frustino, J., Wilding, G., Loree, T., *et al.* (2011). Human papillomavirus types 16 and 18 in epithelial dysplasia of oral cavity and oropharynx: a meta-analysis, 1985-2010. *Oral Oncol* **47**, 1048-1054.
- Jeffrey, P. D., Gorina, S., and Pavletich, N. P. (1995). Crystal structure of the tetramerization domain of the p53 tumor suppressor at 1.7 angstroms. *Science* **267**, 1498-1502.
- Jiang, M., and Milner, J. (2002). Selective silencing of viral gene expression in HPV-positive human cervical carcinoma cells treated with siRNA, a primer of RNA interference. *Oncogene* **21**, 6041-6048.
- Johnson, D. G., and Schneider-Broussard, R. (1998). Role of E2F in cell cycle control and cancer. *Front Biosci* **3**, d447-448.
- Joyce, J. G., Tung, J. S., Przysiecki, C. T., Cook, J. C., Lehman, E. D., Sands, J. A., Jansen, K. U., and Keller, P. M. (1999). The L1 major capsid protein of human papillomavirus type 11 recombinant virus-like particles interacts with heparin and cell-surface glycosaminoglycans on human keratinocytes. *J Biol Chem* **274**, 5810-5822.
- Kamijo, T., Weber, J. D., Zambetti, G., Zindy, F., Roussel, M. F., and Sherr, C. J. (1998). Functional and physical interactions of the ARF tumor suppressor with p53 and Mdm2. *Proc Natl Acad Sci U S A* **95**, 8292-8297.
- Kellenberger, E., Rodrigo, J., Muller, P., and Rognan, D. (2004). Comparative evaluation of eight docking tools for docking and virtual screening accuracy. *Proteins* **57**, 225-242.
- Kim, H. J., Kim, H. J., Lim, S. C., Kim, S. H., and Kim, T. Y. (2003). Induction of apoptosis and expression of cell cycle regulatory proteins in response to a phytosphingosine derivative in HaCaT human keratinocyte cells. *Mol Cells* **16**, 331-337.
- Kitayner, M., Rozenberg, H., Kessler, N., Rabinovich, D., Shaulov, L., Haran, T. E., and Shakked, Z. (2006). Structural basis of DNA recognition by p53 tetramers. *Mol Cell* **22**, 741-753.

- Kitchin, F. D., and Ellsworth, R. M. (1974). Pleiotropic effects of the gene for retinoblastoma. *J Med Genet* 11, 244-246.
- Kondo, K., Ochi, H., Matsumoto, T., Yoshikawa, H., and Kanda, T. (2008). Modification of human papillomavirus-like particle vaccine by insertion of the cross-reactive L2-epitopes. *J Med Virol* 80, 841-846.
- Kuribayashi, K., and El-Deiry, W. S. (2008). Regulation of programmed cell death by the p53 pathway. *Adv Exp Med Biol* 615, 201-221.
- Kutzki, O. (2002). Development of a potent Bcl-XL antagonist based on alpha helix mimicry. *Journal of American Chemical Society* 124, 11838 - 11839.
- Lain, S., Hollick, J. J., Campbell, J., Staples, O. D., Higgins, M., Aoubala, M., McCarthy, A., Appleyard, V., Murray, K. E., Baker, L., *et al.* (2008). Discovery, in vivo activity, and mechanism of action of a small-molecule p53 activator. *Cancer Cell* 13, 454-463.
- Lave TM, S. B., Ridgeway TM, Pelletier SL (1992). *Analytical Ultracentrifugation in Biochemistry and Polymer Science.* (London, United Kingdom: Royal Society of Chemistry).
- Le Tallec, D., Doucet, D., Elouahabi, A., Harvengt, P., Deschuyteneer, M., and Deschamps, M. (2009). Cervarix, the GSK HPV-16/HPV-18 AS04-adjuvanted cervical cancer vaccine, demonstrates stability upon long-term storage and under simulated cold chain break conditions. *Hum Vaccin* 5, 467-474.
- Lea, J. S., Sunaga, N., Sato, M., Kalahasti, G., Miller, D. S., Minna, J. D., and Muller, C. Y. (2007). Silencing of HPV 18 oncoproteins With RNA interference causes growth inhibition of cervical cancer cells. *Reprod Sci* 14, 20-28.
- Lee, J. O., Russo, A. A., and Pavletich, N. P. (1998). Structure of the retinoblastoma tumour-suppressor pocket domain bound to a peptide from HPV E7. *Nature* 391, 859-865.
- Lehrbach, D. M., Nita, M. E., and Ceconello, I. (2003). Molecular aspects of esophageal squamous cell carcinoma carcinogenesis. *Arq Gastroenterol* 40, 256-261.
- Levine, A. J. (2009). The common mechanisms of transformation by the small DNA tumor viruses: The inactivation of tumor suppressor gene products: p53. *Virology* 384, 285-293.
- Levine, A. J., Feng, Z., Mak, T. W., You, H., and Jin, S. (2006). Coordination and communication between the p53 and IGF-1-AKT-TOR signal transduction pathways. *Genes Dev* 20, 267-275.
- Levine, A. J., Hu, W., Feng, Z., and Gil, G. (2007). Reconstructing signal transduction pathways: challenges and opportunities. *Ann N Y Acad Sci* 1115, 32-50.
- Li, N., Thompson, S., Schultz, D. C., Zhu, W., Jiang, H., Luo, C., and Lieberman, P. M. (2010). Discovery of selective inhibitors against EBNA1 via high throughput in silico virtual screening. *PLoS One* 5, e10126.
- Li, R., Chen, X., Gong, B., Selzer, P. M., Li, Z., Davidson, E., Kurzban, G., Miller, R. E., Nuzum, E. O., McKerrow, J. H., *et al.* (1996). Structure-based design of parasitic protease inhibitors. *Bioorg Med Chem* 4, 1421-1427.
- Li, X., and Coffino, P. (1996a). High-Risk Human Papillomavirus E6 Protein has Two Distinct Binding Sites within -53, of Which Only One Determines Degradation. *Journal of Virology* 70, 4509 - 4516.

- Li, X., and Coffino, P. (1996b). High-risk human papillomavirus E6 protein has two distinct binding sites within p53, of which only one determines degradation. *J Virol* **70**, 4509-4516.
- Lin, Y. Y., Alphs, H., Hung, C. F., Roden, R. B., and Wu, T. C. (2007). Vaccines against human papillomavirus. *Front Biosci* **12**, 246-264.
- Lipari, F., McGibbon, G. A., Wardrop, E., and Cordingley, M. G. (2001). Purification and Biophysical Characterization of a Minimal Functional Domain and of an N-terminal Zn²⁺-Binding Fragment from the Human Papillomavirus Type 16 E6 Protein. *Biochemistry* **40**, 1196 - 1204.
- Lipinski, C. A., Lombardo, F., Dominy, B. W., and Feeney, P. J. (2001). Experimental and computational approaches to estimate solubility and permeability in drug discovery and development settings. *Adv Drug Deliv Rev* **46**, 3-26.
- Liu, X., Clements, A., Zhao, K., and Marmorstein, R. (2006a). Structure of the human Papillomavirus E7 oncoprotein and its mechanism for inactivation of the retinoblastoma tumor suppressor. *J Biol Chem* **281**, 578-586.
- Liu, X., Clements, A., Zhao, K. H., and Marmorstein, R. (2006b). Structure of the human Papillomavirus E7 oncoprotein and its mechanism for inactivation of the retinoblastoma tumor suppressor. *Journal of Biological Chemistry* **281**, 578-586.
- Liu, X., and Marmorstein, R. (2007). Structure of the retinoblastoma protein bound to adenovirus E1A reveals the molecular basis for viral oncoprotein inactivation of a tumor suppressor. *Genes & Development* **21**, 2711-2716.
- Liu, Y., Chen, J. J., Gao, Q., Dalal, S., Hong, Y., Mansur, C. P., Band, V., and Androphy, E. J. (1999). Multiple functions of human papillomavirus type 16 E6 contribute to the immortalization of mammary epithelial cells. *J Virol* **73**, 7297-7307.
- Liu, Y., Liu, Z., Androphy, E., Chen, J., and Baleja, J. D. (2004). Design and characterization of helical peptides that inhibit the E6 protein of papillomavirus. *Biochemistry* **43**, 7421-7431.
- Lodish H, B. A., Matsudaira P, Kaiser CA, Scott MP, Ziprusky SL, Darnell J, (2004). *Molecular Cell Biology*, 5th edn (New York, NY: Freeman and Company.).
- Luna-Medina, R., Cortes-Canteli, M., Alonso, M., Santos, A., Martinez, A., and Perez-Castillo, A. (2005). Regulation of inflammatory response in neural cells in vitro by thiazolidinone derivatives through peroxisome proliferator-activated receptor gamma activation. *Journal of Biological Chemistry* **280**, 21453-21462.
- Luna-Medina, R., Cortes-Canteli, M., Sanchez-Galiano, S., Morales-Garcia, J. A., Martinez, A., Santos, A., and Perez-Castillo, A. (2007). NP031112, a thiazolidinone compound, prevents inflammation and neurodegeneration under excitotoxic conditions: Potential therapeutic role in brain disorders. *Journal of Neuroscience* **27**, 5766-5776.
- Luo, C., Xie, P., and Marmorstein, R. (2008). Identification of BRAF inhibitors through in silico screening. *J Med Chem* **51**, 6121-6127.
- MacFarlane, M., and Williams, A. C. (2004). Apoptosis and disease: a life or death decision. *EMBO Rep* **5**, 674-678.

- Maecker, H. L., Koumenis, C., and Giaccia, A. J. (2000). p53 promotes selection for Fas-mediated apoptotic resistance. *Cancer Res* 60, 4638-4644.
- Malumbres, M., and Barbacid, M. (2001). To cycle or not to cycle: a critical decision in cancer. *Nat Rev Cancer* 1, 222-231.
- Marcello, A., Massimi, P., Banks, L., and Giacca, M. (2000). Adeno-associated virus type 2 rep protein inhibits human papillomavirus type 16 E2 recruitment of the transcriptional coactivator p300. *J Virol* 74, 9090-9098.
- Marchenko, N. D., Zaika, A., and Moll, U. M. (2000). Death signal-induced localization of p53 protein to mitochondria. A potential role in apoptotic signaling. *J Biol Chem* 275, 16202-16212.
- Marquez-Gutierrez, M. A., Benitez-Hess, M. L., DiPaolo, J. A., and Alvarez-Salas, L. M. (2007). Effect of combined antisense oligodeoxynucleotides directed against the human papillomavirus type 16 on cervical carcinoma cells. *Arch Med Res* 38, 730-738.
- Martelli, F., Hamilton, T., Silver, D. P., Sharpless, N. E., Bardeesy, N., Rokas, M., DePinho, R. A., Livingston, D. M., and Grossman, S. R. (2001). p19ARF targets certain E2F species for degradation. *Proc Natl Acad Sci U S A* 98, 4455-4460.
- Martinex, A. (2006). TDZD: Selective GSK-3 inhibitors with great potential for Alzheimer disease. *Neurobiology of Aging* 27, S13-S13.
- Martinez, A., Alonso, M., Castro, A., Dorronsoro, I., Gelpi, J. L., Luque, F. J., Perez, C., and Moreno, F. J. (2005). SAR and 3D-QSAR studies on thiazolidinone derivatives: Exploration of structural requirements for glycogen synthase kinase 3 inhibitors. *Journal of Medicinal Chemistry* 48, 7103-7112.
- Martinez, A., Alonso, M., Castro, A., Perez, C., and Moreno, F. J. (2002). First non-ATP competitive glycogen synthase kinase 3 beta (GSK-3 beta) inhibitors: Thiazolidinones (TDZD) as potential drugs for the treatment of Alzheimer's disease. *Journal of Medicinal Chemistry* 45, 1292-1299.
- Martucci, W. E., Udier-Blagovic, M., Atreya, C., Babatunde, O., Vargo, M. A., Jorgensen, W. L., and Anderson, K. S. (2009). Novel non-active site inhibitor of *Cryptosporidium hominis* TS-DHFR identified by a virtual screen. *Bioorg Med Chem Lett* 19, 418-423.
- McBride, A. A., Romanczuk, H., and Howley, P. M. (1991). The papillomavirus E2 regulatory proteins. *J Biol Chem* 266, 18411-18414.
- McLaughlin-Drubin, M. E., and Munger, K. (2009). Oncogenic activities of human papillomaviruses. *Virus Res* 143, 195-208.
- Meyerson, M., Counter, C. M., Eaton, E. N., Ellisen, L. W., Steiner, P., Caddle, S. D., Ziaugra, L., Beijersbergen, R. L., Davidoff, M. J., Liu, Q., *et al.* (1997). hEST2, the putative human telomerase catalytic subunit gene, is up-regulated in tumor cells and during immortalization. *Cell* 90, 785-795.
- Morris, G. M., Huey, R., and Olson, A. J. (2008). Using AutoDock for ligand-receptor docking. *Curr Protoc Bioinformatics Chapter 8*, Unit 8 14.
- Motlekar, N., Diamond, S. L., and Napper, A. D. (2008). Evaluation of an orthogonal pooling strategy for rapid high-throughput screening of proteases. *Assay Drug Dev Technol* 6, 395-405.

- Munger, K., Basile, J. R., Duensing, S., Eichten, A., Gonzalez, S. L., Grace, M., and Zacny, V. L. (2001). Biological activities and molecular targets of the human papillomavirus E7 oncoprotein. *Oncogene* *20*, 7888-7898.
- Muratore, G., Goracci, L., Mercorelli, B., Foeglein, A., Digard, P., Cruciani, G., Palu, G., and Loregian, A. (2012). Small molecule inhibitors of influenza A and B viruses that act by disrupting subunit interactions of the viral polymerase. *Proc Natl Acad Sci U S A* *109*, 6247-6252.
- Nakagawa, S., and Huibregtse, J. M. (2000). Human scribble (Vartul) is targeted for ubiquitin-mediated degradation by the high-risk papillomavirus E6 proteins and the E6AP ubiquitin-protein ligase. *Mol Cell Biol* *20*, 8244-8253.
- Nakamura, T., Williams-Simons, L., and Westphal, H. (1997). A human papillomavirus type 18 E6/E7 transgene sensitizes mouse lens cells to human wild-type p53-mediated apoptosis. *Oncogene* *14*, 2991-2998.
- Nakatani, Y., Konishi, H., Vassilev, A., Kurooka, H., Ishiguro, K., Sawada, J., Ikura, T., Korsmeyer, S. J., Qin, J., and Herlitz, A. M. (2005). p600, a unique protein required for membrane morphogenesis and cell survival. *Proc Natl Acad Sci U S A* *102*, 15093-15098.
- Narisawa-Saito, M., and Kiyono, T. (2007). Basic mechanisms of high-risk human papillomavirus-induced carcinogenesis: roles of E6 and E7 proteins. *Cancer Sci* *98*, 1505-1511.
- Nicholson, D. W., and Thornberry, N. A. (2003). Apoptosis. Life and death decisions. *Science* *299*, 214-215.
- Niu, X. Y., Peng, Z. L., Duan, W. Q., Wang, H., and Wang, P. (2006). Inhibition of HPV 16 E6 oncoprotein expression by RNA interference in vitro and in vivo. *Int J Gynecol Cancer* *16*, 743-751.
- Nomine, Y., Charbonnier, S., Miguet, L., Potier, N., Dorselaer, A. V., Atkinson, A., Trave, G., and Kieffer, B. (2005). 1H and 15N resonance assignment, secondary structure and dynamic behavior of the C-terminal domain of human papillomavirus oncoprotein E6. *Journal of Biomolecular NMR* *31*, 129 - 141.
- Nomine, Y., Charbonnier, S., Ristriani, T., Stier, G., Masson, M., Cavusglu, N., Dorselaer, A. V., Weiss, E., Kieffer, B., and Trave, G. (2003). Domain Substructure of HPV E6 Oncoprotein: Biophysical Characterization of the E6 C-Terminal DNA-Binding Domain. *Biochemistry* *42*, 4909 - 4917.
- Nomine, Y., Masson, M., Charbonnier, S., Zanier, K., Ristriani, T., Deryckere, F., Sibler, A.-P., Desplancq, D., Atkinson, R. A., Weiss, E., *et al.* (2006). Structural and Functional Analysis of E6 Oncoprotein: Insights in the Molecular Pathways of Human Papillomavirus-Mediated Pathogenesis. *Molecular Cell* *21*, 665 - 678.
- Ogryzko, V. V., Schiltz, R. L., Russanova, V., Howard, B. H., and Nakatani, Y. (1996). The transcriptional coactivators p300 and CBP are histone acetyltransferases. *Cell* *87*, 953-959.
- Ohlenschlager, O., Seiboth, T., Zengerling, H., Briese, L., Marchanka, A., Ramachandran, R., Baum, M., Korbas, M., Meyer-Klaucke, W., Durst, M., and Gorlach, M. (2006). Solution structure of the partially folded high-risk human papilloma virus 45 oncoprotein E7. *Oncogene* *25*, 5953-5959.
- Olson, C., Pamukcu, A. M., Brobst, D. F., Kowalczyk, T., Satter, E. J., and Price, J. M. (1959). A urinary bladder tumor induced by a bovine cutaneous papilloma agent. *Cancer Res* *19*, 779-782.

- Pan, H., and Griep, A. E. (1995). Temporally distinct patterns of p53-dependent and p53-independent apoptosis during mouse lens development. *Genes Dev* 9, 2157-2169.
- Pan, H., Yin, C., Dyson, N. J., Harlow, E., Yamasaki, L., and Van Dyke, T. (1998). Key roles for E2F1 in signaling p53-dependent apoptosis and in cell division within developing tumors. *Mol Cell* 2, 283-292.
- Park, J. S., Kim, E. J., Kwon, H. J., Hwang, E. S., Namkoong, S. E., and Um, S. J. (2000). Inactivation of interferon regulatory factor-1 tumor suppressor protein by HPV E7 oncoprotein. Implication for the E7-mediated immune evasion mechanism in cervical carcinogenesis. *J Biol Chem* 275, 6764-6769.
- Pietenpol, J. A., Tokino, T., Thiagalingam, S., el-Deiry, W. S., Kinzler, K. W., and Vogelstein, B. (1994). Sequence-specific transcriptional activation is essential for growth suppression by p53. *Proc Natl Acad Sci U S A* 91, 1998-2002.
- Pomerantz, J., Schreiber-Agus, N., Liegeois, N. J., Silverman, A., Alland, L., Chin, L., Potes, J., Chen, K., Orlow, I., Lee, H. W., *et al.* (1998). The Ink4a tumor suppressor gene product, p19Arf, interacts with MDM2 and neutralizes MDM2's inhibition of p53. *Cell* 92, 713-723.
- Prives, C., and Hall, P. A. (1999). The p53 pathway. *J Pathol* 187, 112-126.
- Reich, N. C., Oren, M., and Levine, A. J. (1983). Two distinct mechanisms regulate the levels of a cellular tumor antigen, p53. *Mol Cell Biol* 3, 2143-2150.
- Ristriani, T., Masson, M., Nomine, Y., Laurent, C., Lefevre, J. F., Weiss, E., and Trave, G. (2000). HPV oncoprotein E6 is a structure-dependent DNA-binding protein that recognizes four-way junctions. *J Mol Biol* 296, 1189-1203.
- Ristriani, T., Nomine, Y., Masson, M., Weiss, E., and Trave, G. (2001). Specific recognition of four-way DNA junctions by the C-terminal zinc-binding domain of HPV oncoprotein E6. *J Mol Biol* 305, 729-739.
- Roberts, J. N., Buck, C. B., Thompson, C. D., Kines, R., Bernardo, M., Choyke, P. L., Lowy, D. R., and Schiller, J. T. (2007). Genital transmission of HPV in a mouse model is potentiated by nonoxynol-9 and inhibited by carrageenan. *Nat Med* 13, 857-861.
- Rosa, A. O., Kaster, M. P., Binfare, R. W., Morales, S., Martin-Aparicio, E., Navarro-Rico, M. L., Martinez, A., Medina, M., Garcia, A. G., Lopez, M. G., and Rodrigues, A. L. S. (2008). Antidepressant-like effect of the novel thiazolidinone NP031115 in mice. *Progress in Neuro-Psychopharmacology & Biological Psychiatry* 32, 1549-1556.
- Roughley, S., Wright, L., Brough, P., Massey, A., and Hubbard, R. E. (2011). Hsp90 inhibitors and drugs from fragment and virtual screening. *Top Curr Chem* 317, 61-82.
- Rous, P., and Beard, J. W. (1934). A Virus-Induced Mammalian Growth with the Characters of a Tumor (the Shope Rabbit Papilloma) : lii. Further Characters of the Growth: General Discussion. *J Exp Med* 60, 741-766.
- Rubin, S. M., Gall, A. L., Zheng, N., and Pavletich, N. P. (2005). Structure of the RbC-terminal domain bound to E2F1-DP1: A mechanism for phosphorylation-induced E2F release. *Cell* 123, 1093-1106.
- Ruegg, U. T., and Burgess, G. M. (1989). Staurosporine, K-252 and UCN-01: potent but nonspecific inhibitors of protein kinases. *Trends Pharmacol Sci* 10, 218-220.

- Sakaguchi, K., Herrera, J. E., Saito, S., Miki, T., Bustin, M., Vassilev, A., Anderson, C. W., and Appella, E. (1998). DNA damage activates p53 through a phosphorylation-acetylation cascade. *Genes Dev* 12, 2831-2841.
- Salunke, D. M., Caspar, D. L., and Garcea, R. L. (1986). Self-assembly of purified polyomavirus capsid protein VP1. *Cell* 46, 895-904.
- Scheffner, M. (1998). Ubiquitin, E6-AP, and their role in p53 inactivation. *Pharmacol Ther* 78, 129-139.
- Scheffner, M., Huibregtse, J. M., Vierstra, R. D., and Howley, P. M. (1993). The HPV-16 E6 and E6-AP complex functions as a ubiquitin-protein ligase in the ubiquitination of p53. *Cell* 75, 495-505.
- Scheffner, M., Munger, K., Byrne, J. C., and Howley, P. M. (1991). The state of the p53 and retinoblastoma genes in human cervical carcinoma cell lines. *Proc Natl Acad Sci U S A* 88, 5523-5527.
- Schubert, E. L., Hansen, M. F., and Strong, L. C. (1994). The retinoblastoma gene and its significance. *Ann Med* 26, 177-184.
- Sherr, C. J. (1996). Cancer cell cycles. *Science* 274, 1672-1677.
- Shikama, N., Lee, C. W., France, S., Delavaine, L., Lyon, J., Krstic-Demonacos, M., and La Thangue, N. B. (1999). A novel cofactor for p300 that regulates the p53 response. *Mol Cell* 4, 365-376.
- Shoichet, B. K., Stroud, R. M., Santi, D. V., Kuntz, I. D., and Perry, K. M. (1993). Structure-based discovery of inhibitors of thymidylate synthase. *Science* 259, 1445-1450.
- Shope, R. E., and Hurst, E. W. (1933). Infectious Papillomatosis of Rabbits : with a Note on the Histopathology. *J Exp Med* 58, 607-624.
- Siddiqui, M. A., and Perry, C. M. (2006). Human papillomavirus quadrivalent (types 6, 11, 16, 18) recombinant vaccine (Gardasil): profile report. *BioDrugs* 20, 313-316.
- Sidle, A., Palaty, C., Dirks, P., Wiggan, O., Kiess, M., Gill, R. M., Wong, A. K., and Hamel, P. A. (1996). Activity of the retinoblastoma family proteins, pRB, p107, and p130, during cellular proliferation and differentiation. *Crit Rev Biochem Mol Biol* 31, 237-271.
- Sima, N., Wang, W., Kong, D., Deng, D., Xu, Q., Zhou, J., Xu, G., Meng, L., Lu, Y., Wang, S., and Ma, D. (2008). RNA interference against HPV16 E7 oncogene leads to viral E6 and E7 suppression in cervical cancer cells and apoptosis via upregulation of Rb and p53. *Apoptosis* 13, 273-281.
- Singh, M., Krajewski, M., Mikolajka, A., and Holak, T. A. (2005). Molecular determinants for the complex formation between the retinoblastoma protein and LXCXE sequences. *Journal of Biological Chemistry* 280, 37868-37876.
- Sionov, R. V., and Haupt, Y. (1999). The cellular response to p53: the decision between life and death. *Oncogene* 18, 6145-6157.
- Stanley, M., Lowy, D. R., and Frazer, I. (2006). Chapter 12: Prophylactic HPV vaccines: underlying mechanisms. *Vaccine* 24 Suppl 3, S3/106-113.

- Steele, C., Cowser, L. M., and Shillitoe, E. J. (1993). Effects of human papillomavirus type 18-specific antisense oligonucleotides on the transformed phenotype of human carcinoma cell lines. *Cancer Res* 53, 2330-2337.
- Stevaux, O., and Dyson, N. J. (2002). A revised picture of the E2F transcriptional network and RB function. *Current Opinion in Cell Biology* 14, 684-691.
- Strauss, M. J., Shaw, E. W., and et al. (1949). Crystalline virus-like particles from skin papillomas characterized by intranuclear inclusion bodies. *Proc Soc Exp Biol Med* 72, 46-50.
- Sudhoff, H. H., Schwarze, H. P., Winder, D., Steinstraesser, L., Gorner, M., Stanley, M., and Goon, P. K. (2011). Evidence for a causal association for HPV in head and neck cancers. *Eur Arch Otorhinolaryngol* 268, 1541-1547.
- Sur, S., Pagliarini, R., Bunz, F., Rago, C., Diaz, L. A., Jr., Kinzler, K. W., Vogelstein, B., and Papadopoulos, N. (2009). A panel of isogenic human cancer cells suggests a therapeutic approach for cancers with inactivated p53. *Proc Natl Acad Sci U S A* 106, 3964-3969.
- Suryadinata, R., Sadowski, M., and Sarcevic, B. (2010). Control of cell cycle progression by phosphorylation of cyclin-dependent kinase (CDK) substrates. *Biosci Rep* 30, 243-255.
- Suzich, J. A., Ghim, S. J., Palmer-Hill, F. J., White, W. I., Tamura, J. K., Bell, J. A., Newsome, J. A., Jenson, A. B., and Schlegel, R. (1995). Systemic immunization with papillomavirus L1 protein completely prevents the development of viral mucosal papillomas. *Proc Natl Acad Sci U S A* 92, 11553-11557.
- Tan, M. J., White, E. A., Sowa, M. E., Harper, J. W., Aster, J. C., and Howley, P. M. (2012). Cutaneous beta-human papillomavirus E6 proteins bind Mastermind-like coactivators and repress Notch signaling. *Proc Natl Acad Sci U S A*.
- Thomas, M., and Banks, L. (1999). Human papillomavirus (HPV) E6 interactions with Bak are conserved amongst E6 proteins from high and low risk HPV types. *J Gen Virol* 80 (Pt 6), 1513-1517.
- Thomas, M., Laura, R., Hepner, K., Guccione, E., Sawyers, C., Lasky, L., and Banks, L. (2002). Oncogenic human papillomavirus E6 proteins target the MAGI-2 and MAGI-3 proteins for degradation. *Oncogene* 21, 5088-5096.
- Thomas, M. C., and Chiang, C. M. (2005). E6 oncoprotein represses p53-dependent gene activation via inhibition of protein acetylation independently of inducing p53 degradation. *Mol Cell* 17, 251-264.
- Trottier, H., and Franco, E. L. (2006). The epidemiology of genital human papillomavirus infection. *Vaccine* 24 Suppl 1, S1-15.
- Tsai, K. Y., Hu, Y., Macleod, K. F., Crowley, D., Yamasaki, L., and Jacks, T. (1998). Mutation of E2f-1 suppresses apoptosis and inappropriate S phase entry and extends survival of Rb-deficient mouse embryos. *Mol Cell* 2, 293-304.
- Turnell, A. S., and Mymryk, J. S. (2006). Roles for the coactivators CBP and p300 and the APC/C E3 ubiquitin ligase in E1A-dependent cell transformation. *Br J Cancer* 95, 555-560.

- Vangrevelinghe, E., Zimmermann, K., Schoepfer, J., Portmann, R., Fabbro, D., and Furet, P. (2003). Discovery of a potent and selective protein kinase CK2 inhibitor by high-throughput docking. *J Med Chem* *46*, 2656-2662.
- Vaseva, A. V., and Moll, U. M. (2009). The mitochondrial p53 pathway. *Biochim Biophys Acta* *1787*, 414-420.
- Vassilev, L. T. (2004). Small-molecule antagonists of p53-MDM2 binding: research tools and potential therapeutics. *Cell Cycle* *3*, 419-421.
- Viadiu, H. (2008). Molecular architecture of tumor suppressor p53. *Curr Top Med Chem* *8*, 1327-1334.
- Vinh, N. B., Simpson, J. S., Scammells, P. J., and Chalmers, D. K. (2012). Virtual screening using a conformationally flexible target protein: models for ligand binding to p38alpha MAPK. *J Comput Aided Mol Des* *26*, 409-423.
- Vogelstein, B., Lane, D., and Levine, A. J. (2000). Surfing the p53 network. *Nature* *408*, 307-310.
- Vousden, G. P. a. K. H. (1997). *Oncogenes and Tumour Suppressors* (Oxford: Oxford University Press).
- Vousden, K. H. (2009). Functions of p53 in metabolism and invasion. *Biochem Soc Trans* *37*, 511-517.
- Wang, R., Lai, L., and Wang, S. (2002). Further development and validation of empirical scoring functions for structure-based binding affinity prediction. *J Comput Aided Mol Des* *16*, 11-26.
- Wang, Y., Coulombe, R., Cameron, D. R., Thauvette, L., Massariol, M. J., Amon, L. M., Fink, D., Titolo, S., Welchner, E., Yoakim, C., *et al.* (2004). Crystal structure of the E2 transactivation domain of human papillomavirus type 11 bound to a protein interaction inhibitor. *J Biol Chem* *279*, 6976-6985.
- Wei, Q. (2005). Pitx2a binds to human papillomavirus type 18 E6 protein and inhibits E6-mediated P53 degradation in HeLa cells. *J Biol Chem* *280*, 37790-37797.
- Weinberg, R. A. (1995). The retinoblastoma protein and cell cycle control. *Cell* *81*, 323-330.
- Werness, B. A., Levine, A. J., and Howley, P. M. (1990). Association of human papillomavirus types 16 and 18 E6 proteins with p53. *Science* *248*, 76-79.
- White, P. W., Faucher, A. M., and Goudreau, N. (2011). Small molecule inhibitors of the human papillomavirus E1-E2 interaction. *Curr Top Microbiol Immunol* *348*, 61-88.
- White, P. W., Faucher, A. M., Massariol, M. J., Welchner, E., Rancourt, J., Cartier, M., and Archambault, J. (2005). Biphenylsulfonacetic acid inhibitors of the human papillomavirus type 6 E1 helicase inhibit ATP hydrolysis by an allosteric mechanism involving tyrosine 486. *Antimicrob Agents Chemother* *49*, 4834-4842.
- Woodman, C. B., Collins, S. I., and Young, L. S. (2007). The natural history of cervical HPV infection: unresolved issues. *Nat Rev Cancer* *7*, 11-22.

- Xiao, B., Spencer, J., Clements, A., Ali-Khan, N., Mittnacht, S., Broceno, C., Burghammer, M., Perrakis, A., Marmorstein, R., and Gamblin, S. J. (2003). Crystal structure of the retinoblastoma tumor suppressor protein bound to E2F and the molecular basis of its regulation. *Proceedings of the National Academy of Sciences of the United States of America* *100*, 2363-2368.
- Xue, W., Zender, L., Miething, C., Dickins, R. A., Hernando, E., Krizhanovsky, V., Cordon-Cardo, C., and Lowe, S. W. (2007). Senescence and tumour clearance is triggered by p53 restoration in murine liver carcinomas. *Nature* *445*, 656-660.
- Yao, K., Ye, P., Zhang, L., Tan, J., Tang, X., and Zhang, Y. (2008). Epigallocatechin gallate protects against oxidative stress-induced mitochondria-dependent apoptosis in human lens epithelial cells. *Mol Vis* *14*, 217-223.
- Yee, C., Krishnan-Hewlett, I., Baker, C. C., Schlegel, R., and Howley, P. M. (1985). Presence and expression of human papillomavirus sequences in human cervical carcinoma cell lines. *Am J Pathol* *119*, 361-366.
- Yoakim, C., Ogilvie, W. W., Goudreau, N., Naud, J., Hache, B., O'Meara, J. A., Cordingley, M. G., Archambault, J., and White, P. W. (2003). Discovery of the first series of inhibitors of human papillomavirus type 11: inhibition of the assembly of the E1-E2-Origin DNA complex. *Bioorg Med Chem Lett* *13*, 2539-2541.
- Yugawa, T., and Kiyono, T. (2009a). Molecular mechanisms of cervical carcinogenesis by high-risk human papillomaviruses: novel functions of E6 and E7 oncoproteins. *Rev Med Virol* *19*, 97-113.
- Yugawa, T., and Kiyono, T. (2009b). Molecular mechanisms of cervical carcinogenesis by high-risk human papillomaviruses: novel functions of E6 and E7 oncoproteins. *Reviews in Medical Virology* *19*, 97-113.
- Zamore, P. D., Tuschl, T., Sharp, P. A., and Bartel, D. P. (2000). RNAi: double-stranded RNA directs the ATP-dependent cleavage of mRNA at 21 to 23 nucleotide intervals. *Cell* *101*, 25-33.
- Zanier, K., Charbonnier, S., Mireille Baltzinger, Nomine, Y., Altschuh, D., and Trave, G. (2005). Kinetic Analysis of the Interactions of Human Papillomavirus E6 Oncoproteins with the Ubiquitin Ligase E6AP Using Surface Plasmon Resonance. *Journal of Molecular Biology* *349*, 401 - 412.
- Zanier, K.,ould M'hamed ould Sidi, A., Boulade-Ladame, C., Rybin, V., Chappelle, A., Atkinson, A., Kieffer, B., and Trave, G. (2012). Solution structure analysis of the HPV16 E6 oncoprotein reveals a self-association mechanism required for E6-mediated degradation of p53. *Structure* *20*, 604-617.
- Zaratiegui, M., Irvine, D. V., and Martienssen, R. A. (2007). Noncoding RNAs and gene silencing. *Cell* *128*, 763-776.
- Zavodszky, M. I., Sanschagrin, P. C., Korde, R. S., and Kuhn, L. A. (2002). Distilling the essential features of a protein surface for improving protein-ligand docking, scoring, and virtual screening. *J Comput Aided Mol Des* *16*, 883-902.
- Zhang, J. H., Chung, T. D., and Oldenburg, K. R. (1999). A Simple Statistical Parameter for Use in Evaluation and Validation of High Throughput Screening Assays. *J Biomol Screen* *4*, 67-73.

Zhang, Y., Xiong, Y., and Yarbrough, W. G. (1998). ARF promotes MDM2 degradation and stabilizes p53: ARF-INK4a locus deletion impairs both the Rb and p53 tumor suppression pathways. *Cell* 92, 725-734.

Zheng, Z. M., and Baker, C. C. (2006). Papillomavirus genome structure, expression, and post-transcriptional regulation. *Front Biosci* 11, 2286-2302.

Zhou, Z., Felts, A. K., Friesner, R. A., and Levy, R. M. (2007). Comparative performance of several flexible docking programs and scoring functions: enrichment studies for a diverse set of pharmaceutically relevant targets. *J Chem Inf Model* 47, 1599-1608.

Zuckerman, V., Wolyniec, K., Sionov, R. V., Haupt, S., and Haupt, Y. (2009). Tumour suppression by p53: the importance of apoptosis and cellular senescence. *J Pathol* 219, 3-15.

zur Hausen, H. (1977). Human papillomaviruses and their possible role in squamous cell carcinomas. *Curr Top Microbiol Immunol* 78, 1-30.

zur Hausen, H., Gissmann, L., Steiner, W., Dippold, W., and Dreger, I. (1975). Human papilloma viruses and cancer. *Bibl Haematol*, 569-571.

zur Hausen, H., Schulte-Holthausen, H., Wolf, H., Dorries, K., and Egger, H. (1974). Attempts to detect virus-specific DNA in human tumors. II. Nucleic acid hybridizations with complementary RNA of human herpes group viruses. *Int J Cancer* 13, 657-664.